Ciesielski, P. F., Kristoffersen, Y., et al., 1988
Proceedings of the Ocean Drilling Program, Initial Reports, Vol. 114

6. SITE 699[1]

Shipboard Scientific Party[2]

HOLE 699A

Date occupied: 20 March 1987

Date departed: 26 March 1987

Time on hole: 6 days, 11 hr

Position: 51°32.537′S, 30°40.619′W

Bottom felt (rig floor; m; drill-pipe measurement): 3716.0

Distance between rig floor and sea level (m): 10.50

Water depth (drill-pipe measurement from sea level; corrected m): 3705.5

Total depth (rig floor; corrected m): 4234.1

Penetration (m): 518.1

Number of cores: 56

Total length of cored section (m): 518.1

Total core recovered (m): 356.52

Core recovery (%): 68

Oldest sediment cored:
Depth sub-bottom (m): 518.1
Nature: volcanic sand
Age: early Paleocene
Measured velocity (km/s): 1.95 at 468 mbsf

Principal results: Site 699 is on the northeastern slope of the Northeast Georgia Rise (51°32.537′S, 30°40.619′W) in a water depth of 3705.5 m. This site was selected to obtain a high-quality, continuously cored sequence of Late Cretaceous to Neogene age sediments recording the history of deep-water communication between the Weddell and Georgia basins and the South Atlantic Basin. Site 699 overlies crust that predates the formation of Islas Orcadas Rise, Meteor Rise, and the deep-water gateway that formed between these features. Comparison of the sedimentary record of Site 699 with that of Site 701 (within the early gateway) provides a means of interpreting the influence of the gateway opening on the environment in the subantarctic and other regions south and north of the gateway. Other objectives are to document the development of the Antarctic Circumpolar Current (ACC) and the southern high-latitude biosiliceous province. Carbonate-bearing sequences of Late Cretaceous and Paleogene age from Site 699 and other Leg 114 sites document the evolution of vertical water-mass structure in the subantarctic.

Site 699 consists of a single hole from which 22 cores were obtained with the advanced hydraulic piston corer (APC) to a depth of 205.1 m below seafloor (mbsf) and 34 cores were obtained with the extended core barrel (XCB) system to a depth of 518.1 mbsf, where the core barrel became jammed with sand. In consideration of the hole condition and danger to the drill string, drilling was terminated without logging. The sediment recovery rate varied, averaging 81% above 224.1 mbsf but 54% below this depth because of the presence of gravel. The overall recovery for Hole 699A was 68.8%. The site was occupied between 20 and 26 March 1987 in generally moderate to rough seas. Drilling was hampered by 18 hr waiting on weather with the drill string in the hole.

Site 699 consists a thick pelagic section with an upper unit of siliceous ooze overlying nannofossil ooze with numerous variations of clay and biosiliceous content. The lower part of the sequence is calcareous nannofossil chalk grading into a basal unit of zeolite-bearing claystone and clay-bearing micritic calcareous nannofossil chalk. The dominant lithologies and ages of the stratigraphic sequence are as follows:

0–85.7 mbsf: diatom clay and clayey diatom ooze of early Miocene to Quaternary age

85.7–233.6 mbsf: siliceous nannofossil ooze and nannofossil siliceous ooze with high-frequency variations in clay and biogenic constituents; early Oligocene to early Miocene age

233.6–235.6 mbsf: graded gravel bed of poorly sorted subangular to subround material containing fragments of basalt, andesite, quartz arenite, granite, quartz diorite, schists, and other metamorphic rocks; deposited in the early Oligocene

235.7–243.1 mbsf: no recovery

243.1–335.4 mbsf: a siliceous nannofossil ooze grading downward into a nannofossil ooze of middle/late Eocene to early Oligocene age

335.4–487.9 mbsf: nannofossil chalk and nannofossil micritic chalk of early to middle/late Eocene age

487.9–496.6 mbsf: no recovery

496.6–516.3 mbsf: zeolite-bearing claystone and clay-bearing micritic nannofossil chalk of late Paleocene age

516.3–518.1 mbsf: granitic gravel and redeposited volcanic-rich quartz sand of unknown age.

Hole 699A contains a remarkably complete Paleogene pelagic sedimentary sequence (~426 m thick) representing a 37-m.y. period, overlying basal sediments assigned to foraminifer Zone P4 (58.7–61.0 Ma). In contrast, only ~90 m of Neogene biosiliceous sediments, punctuated by numerous hiatuses, were cored. Only one significant hiatus was noted in the Paleogene (upper middle to lower upper Eocene), although there is some evidence of a minor hiatus within the lowermost Eocene (NP10). A major hiatus of regional significance is noted between the lower Miocene and the uppermost middle Miocene (~9 m.y. duration; ~69 mbsf).

Other Neogene hiatuses bracket the uppermost Miocene to lowermost Pliocene (~8.5–4.5 Ma, between 62.15 and 54.33 mbsf) and the lower/upper Miocene contact (~3.0–3.9 Ma, between 39.03 and 40.37 mbsf). An additional minor hiatus may occur within the upper Pliocene (2.5–2.8 Ma, between 32.20 and 31.0 mbsf).

Sedimentation rates were 3 m/m.y. for the late Paleocene and most of the early Eocene (<61.0 to 53.7 Ma), but averaged 14 m/m.y. during the late early Eocene and middle Eocene, from 53.7 to 45.0 Ma. After the period of nondeposition or erosion that formed the upper middle to lower upper Eocene hiatus, sedimentation rates were 25 m/m.y. during the late Eocene to earliest Oligocene (39–34.6 Ma). Throughout the remainder of the Oligocene to earliest Miocene (34.6 to 20 or 21.0 Ma), sedimentation rates were 12 m/m.y. The mean sedimentation rate for the late Eocene to earliest Miocene was 15 m/m.y. Neogene sedimentation rates are more difficult to evaluate because the Neogene record is more fragmentary and attenuated by erosion and periods of nondeposition. Sedimentation appears to have been most continuous during the last 2.5 m.y., with an average sedimentation rate of 12 m/m.y.

Calcareous nannofossils provide a high degree of biostratigraphic resolution for most of the Paleogene, whereas diatoms provide excellent stratigraphic control for the upper Paleogene and Neogene. A good quality paleomagnetic record was obtained for the upper Oligocene, Pliocene, and Quaternary. Analysis of the 200-m-thick upper Oligocene will provide the first southern high-latitude calibra-

[1] Ciesielski, P. F., Kristoffersen, Y., et al., 1988. *Proc. ODP, Init. Repts.*, 114: College Station, TX (Ocean Drilling Program).

[2] Shipboard Scientific Party is as given in the list of Participants preceding the contents.

tion of biosiliceous stratigraphy to the geomagnetic polarity time scale (GPTS).

The sedimentologic, micropaleontologic, and erosional history of Site 699 provides the most detailed record to date of large-scale Paleogene–early Neogene paleoenvironmental changes in the Southern Ocean. Warm-water foraminifers (including some *Morozovella* spp.) and calcareous nannofossils (discoasters and sphenoliths) indicate that the maximum surface-water temperatures occurred during the late Paleocene–early middle Eocene. Progressive cooling eliminated warm-water calcareous nannofossils by the early late Eocene (NP18), leaving a low-diversity assemblage of cool-water species that lingered into the earliest Miocene. No major change in lithology or assemblages was noted across the Eocene/Oligocene boundary. Diatoms with lower latitude affinities persisted into the early Oligocene. Changes in the deposition of clay, biogenic silica, and carbonate occurred with high frequency during the late early to late Oligocene.

A dramatic decrease in carbonate sedimentation during the late Oligocene culminated in the complete disappearance of carbonate just after the Oligocene/Miocene boundary (~23 Ma). The latest Oligocene–earliest Miocene decrease and disappearance of carbonate is interpreted to reflect the northward advance of the Antarctic Convergence (polar front) and high-latitude biosiliceous province to near its modern-day position.

The earliest Miocene advance of the polar front and biosiliceous province appears to have been intimately related to the early phase of the opening of the Drake Passage and the advent of a less-restricted ACC. Much more vigorous circulation of deep and bottom waters immediately followed the opening of a deep-water passage between Antarctica and South America, resulting in lower sedimentation rates at Site 699 and the formation of a series of regional hiatuses, which were influenced by Antarctic Circumpolar Deep Water (CPDW) and Antarctic Bottom Water (AABW). An evaluation of the changes in Paleogene deep-water circulation through the Georgia Basin, as a consequence of formation of the Meteor Rise–Islas Orcadas Rise gateway, is presented in the "Site 700" chapter (this volume).

Multiple disconformities and the thin (85-m) upper Miocene–Quaternary section are a testimony to the vigor of Neogene circumantarctic circulation. The first ice rafting of detritus to Site 699 occurred during the late Miocene and increased significantly during the Gauss Chron.

The provenance of granitic and quartz diorite cobbles in the gravel deposited during the early Oligocene is intriguing. Several lines of evidence indicate that this gravel may be in place, in which case a crustal fragment of continental nature must be part of the structural framework that forms the Northeast Georgia Rise.

BACKGROUND AND OBJECTIVES

Site 699 (Fig. 1) is in the western region of the West Georgia Basin (51°32.537′S, 30°40.619′W) on the northeastern slope of Northeast Georgia Rise in a water depth of 3705.5 m. The site is 150 km east of Site 698 along the same *Islas Orcadas* single-channel seismic-reflection line (Fig. 2). This site was selected to obtain a high-quality (with the use of APC and XCB systems), continuously cored sequence of Late Cretaceous to Neogene age, recording the history of deep-water communication between the Weddell and Georgia basins with the South Atlantic Basin. Site 699 overlies crust that predates the opening of the formation of the Islas Orcadas Rise, the Meteor Rise, and the deep-water gateway that formed between them. Comparison of the sedimentary record of Site 699 with that of Site 701, which is on crust within the early gateway between the Islas Orcadas Rise and Meteor Rise, will provide a means of interpreting the paleoenvironmental influence of gateway opening in the subantarctic and other regions north and south of the gateway. Post-cruise work to correlate the carbonate-bearing sequences of Late Cretaceous and Paleogene age at a variety of depths from Site 699 and other Leg 114 sites will document how vertical water-mass temperature gradients evolved through time.

Single-channel seismic-reflection data show an 0.8-s-thick (two-way traveltime—TWT) section consisting of three acoustic units. A 400-m-thick upper unit with acoustic stratification overlies a more transparent, but weakly bedded, 300-m-thick section (300 ms thick). An approximately 80-m-thick basal unit defined by a few distinct reflections occurs above basement. The acoustic expression of basement/sediment contact is not clear in the available data.

Based upon the results from nearby deep-basin Sites 328 and 513 of the Deep Sea Drilling Project (DSDP), the upper unit with acoustic stratification is inferred to include Miocene and Oligocene siliceous and calcareous oozes, biosiliceous clays, and Miocene-Quaternary diatomaceous ooze. Within this unit a disconformity is expected between the upper Miocene and the lowermost Miocene. Eocene to Upper Cretaceous zeolitic clays and claystones with some biogenic components are expected in the middle acoustic unit, which is above a basal chalk. Basement at the site is considered to be oceanic crust formed in the Late Cretaceous.

The position of Site 699 in respect to the present-day interaction of antarctic and subantarctic water masses at the Antarctic Convergence Zone (ACZ) is similar to that previously described for Site 698 (see "Background and Objectives" section, "Site 698" chapter, this volume). Seasonal variations of the ACZ are thought to occur presently at this site. The seafloor at Site 699 is deeper relative to that at Site 698 (3705.5 and 2128 m below sea level (mbsl), respectively), which places it within lower CPDW, as opposed to the upper CPDW position of Site 698. According to Reid et al. (1977), the seafloor is within the low-oxygen core of CPDW. Callahan (1972) and Carmack and Foster (1975) have shown that CPDW in this region does not originate from the Atlantic subequatorial oxygen minimum but from the Indo-Pacific CPDW that passes through the Drake Passage. Immediately to the east of the site, AABW flows north through the West Georgia Basin along the eastern margin of the Northeast Georgia Rise at depths greater than 4000 m (Ledbetter, 1986).

Throughout the Late Cretaceous to late Miocene, the environment at Site 699 was influenced significantly by the tectonic framework of the region. During the Late Cretaceous, the East Georgia Basin was separated from deep-water interchange with the Indian Ocean and Weddell Sea by surrounding fracture zones, spreading centers, the Agulhas Plateau, and the South American–Antarctic margin, which has remained contiguous (Fig. 9, "Site 698" chapter). Major changes in intermediate- to deep-water circulation are expected to have accompanied the major regional tectonic events of the latest Oligocene-Neogene, which include the opening of the Drake Passage (23.5 Ma ± 2.5 Ma; Barker and Burrell, 1982), north-south extension of the Central Scotia Sea (21 to 6 Ma; Hill and Barker, 1980), dispersal of the North Scotia Ridge (late Oligocene–late Miocene; Barker et al., 1984), and the development of back-arc extension in the East Scotia Sea and eastward migration of the Scotia Arc (8 Ma to the present; Barker and Hill, 1981).

It is commonly assumed that unrestricted flow of ACC began with the opening of the Drake Passage at approximately the Oligocene/Miocene boundary. This assumption may be incorrect because the arrangement of continental fragments and the ancestral South Sandwich Island Arc may have restricted deep-water flow after the opening of the Drake Passage. The arrangement of obstructions to deep-water circulation following opening of the Drake Passage is illustrated in Figure 3, which shows the tectonic setting for the important oceanic passageway between the Pacific and the Atlantic for 20 and 10 Ma and the present-day configuration. A major objective at Site 699 was to infer Neogene changes in deep-water communication from the Pacific and Weddell Sea to the Georgia Basin and South Atlantic as a consequence of these tectonic events.

Site 699 lies on the northeastern slope of the Northeast Georgia Rise on crust that structurally must be considered to be

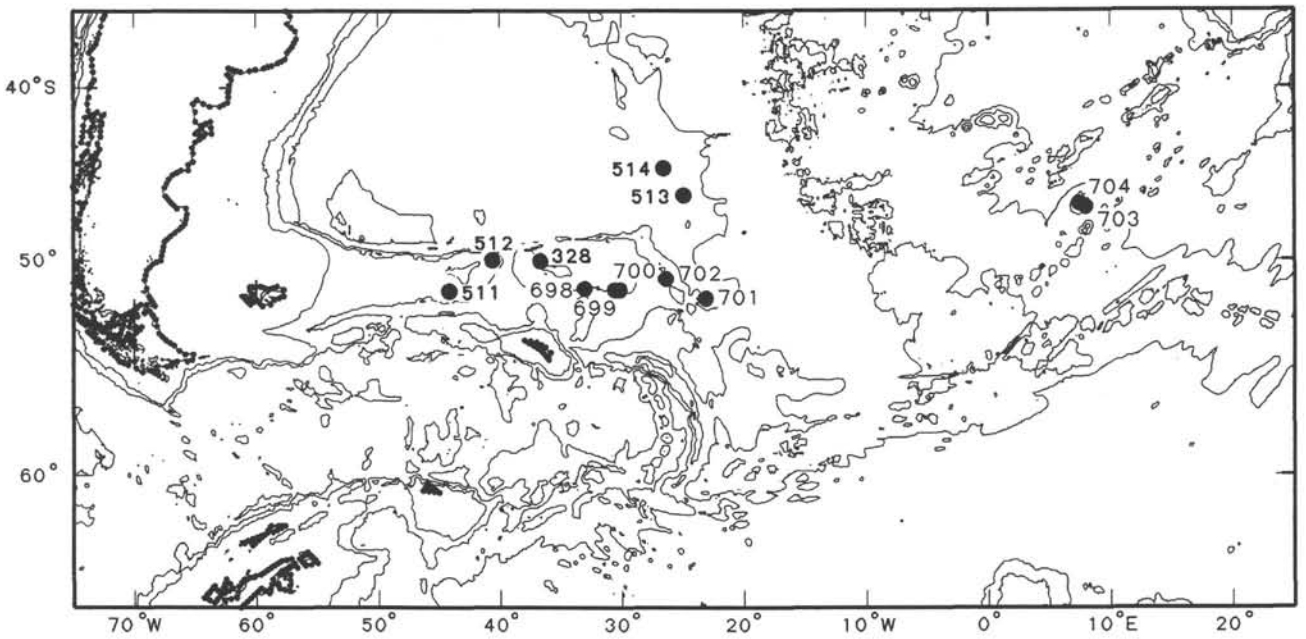

Figure 1. Bathymetric chart of the subantarctic South Atlantic showing the location of Site 699 and other Leg 114 sites. Contour interval 1500 m.

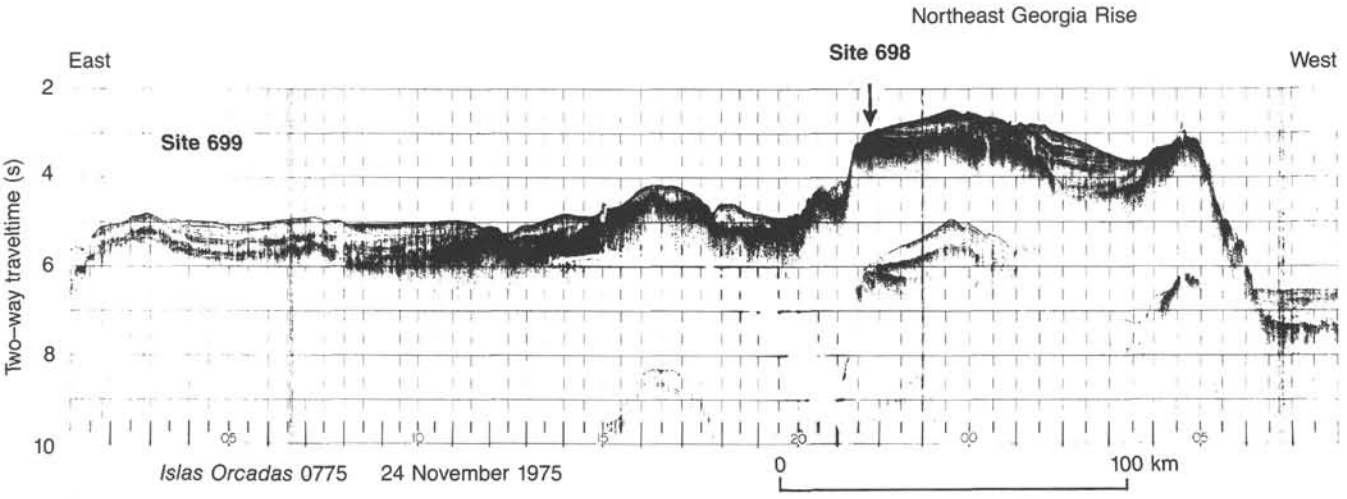

Figure 2. *Islas Orcadas* cruise 0775 single-channel seismic-reflection profile (Fig. 1) showing positions of Sites 698 and 699.

part of the rise itself (Figs. 1 and 2). Basement recovered at Site 698 is Campanian, weakly differentiated, iron-rich oceanic basalt that had been subject to subaerial weathering. In a plate tectonic framework, the rise lies between oceanic crust older than Campanian (Chron 34) to the east and younger than Aptian to the west (LaBrecque and Hayes, 1979). Formation of the rise is considered to have resulted from intraplate deformation in response to rotation of the Malvinas plate against the Falkland Plateau during the Campanian-Eocene. However, the depositional environment at Site 698 during this time interval does not reflect any tectonic activity. Therefore, any incipient subduction to form a fossil island arc must be of pre-Campanian age. The Upper Cretaceous to Paleogene strata on the western ridge of Northeast Georgia Rise were dissected by major faults that have been tentatively related to late Miocene interaction with the advancing South Georgia block (Barker et al., 1984). Thus, the origin of the Northeast Georgia Rise remains an enigma. By drilling into basement at Site 699 on crust at the present-day deepest part of the rise, we endeavored to obtain further constraints on its age, nature, and subsidence history.

The specific objectives for Site 699 were

1. To obtain a sediment record that both pre- and postdates the formation of a gateway for deep-water exchange between antarctic and lower latitude water masses of the Atlantic for interpretation of the influence of gateway formation on the Atlantic paleoenvironment;
2. To document the development of the southern high-latitude biosiliceous province of ACC;
3. To document the influence of the Drake Passage opening on the paleoceanography of the South Atlantic sector of the Southern Ocean;
4. To determine what influence Neogene tectonic events in the Scotia Sea region had on deep-water circulation from the

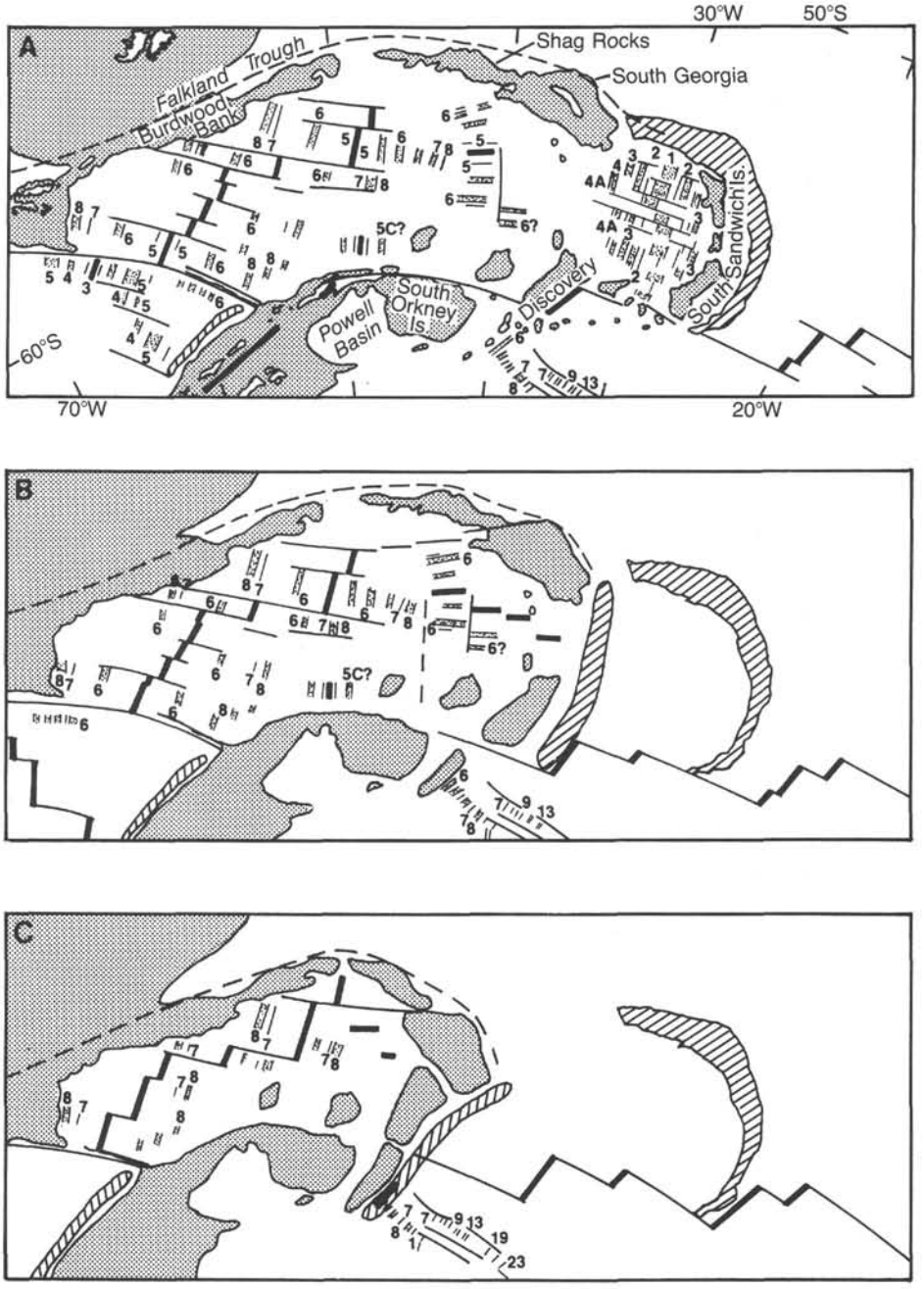

Figure 3. Tectonic evolution of the Scotia Sea region, which influenced deep-water circulation from the Pacific into the Atlantic after the opening of the Drake Passage and changed AABW pathways from the Weddell Sea to the Atlantic. Lightly shaded areas represent shallow areas (continental and island arc) above the 2000-m isobath. Magnetic anomalies are after Barker and Hill (1981) and Barker et al. (1984). **A.** Present-day tectonic setting. **B.** Anomaly 5 (~ 10 Ma) reconstruction. **C.** Anomaly 6 (~ 20 Ma) reconstruction. In Figures 3B and 3C, the present-day position of the South Sandwich trench is hachured to illustrate back-arc extensional development (from Barker et al., 1984).

Weddell Sea and Pacific to the Georgia Basin and South Atlantic;

5. To evaluate the Cenozoic evolution of latitudinal surface-water mass temperature gradients and their influence on the migration and evolution of planktonic biota;

6. To interpret the evolution of vertical water-mass structure during the Paleogene;

7. To calibrate subantarctic microfossil zonal schemes and datums with the GPTS;

8. To investigate the nature and age of basement for establishing the origin of the crust and the subsidence history of the eastern part of Northeast Georgia Rise.

The drilling plan for Site 699 was to recover two APC sections to refusal and then to use the XCB system to core continuously through the remainder of the section to basement. Once basement was reached or upon XCB refusal, the redesigned Navidrill was to be deployed to drill 50 m into basement or up

to the maximum time alloted for the site. Unfortunately, drilling problems resulted in termination of the hole above basement (see "Operations" section, this chapter), and the site was abandoned with insufficient time for a second APC hole.

OPERATIONS

Upon dropping the beacon at 1045 hr on 17 March 1987, Site 699 was established. Arrival was 4 hr ahead of schedule, and within 3 hr, the vessel was dynamically positioned over the beacon. The operating plan for this site was to use the APC/XCB systems to core to basement and then to use the prototype Navidrill core barrel (NCB2) to core into basement. Prior to running the bottom-hole assembly (BHA), we tested the Navidrill system with the intent of verifying that the tool would not unlatch upon impact following deployment of the go-devil and also to ensure that the NCB2 would fit within the BHA without jamming. However, when the tool was dropped inside the outer core barrel/nonmagnetic drill collar assembly, the impact caused the tool to unlatch and telescope out, and the lower assembly fell to the seafloor because a pin thread failed. A second tool was available for use if required; however, deployment would have been on a sand line rather than by freefall to a latched position.

Weather conditions deteriorated and climaxed in a force 10 storm as the drill string was tripped into the hole. Fortunately the pipe was not in the hole as the thrust from the main screws occasionally reached 100% of available power and the vessel continued to lose ground.

The weather improved by morning, and Hole 699A was spudded at 0630 hr on 21 March 1987. The first APC core recovered 8.66 m, including mud-line chert, and established the mud line at 3705.5 m (Table 1). Piston-coring operations continued until 205.1 mbsf, where refusal occurred with a 90,000-lb pullout recorded for Core 114-699A-22H. Recovery was substandard to the average for piston coring because of several conditions. The cored formation was infiltrated with glacial erratics and dropstones that jammed the core catcher and prevented any additional recovery. From the mud line down, the formation was laced with chert stringers that also tended to fracture and lodge in the core catchers, inhibiting core entry. The weather conditions caused a considerable amount of heave and bit motion, even with the heave compensation system in use. Piston coring on the "up heave" or "down heave" is known to influence both the quantity and quality of the cores. In spite of these factors, the APC managed a respectable 80.3% recovery of good quality core.

Coring continued with the XCB system did not fare as well as with the APC system. The XCB system had to deal with the same conditions and in addition, had to constantly be adjusted for flow rate, weight on bit, and rpm in response to the varying degrees of hardness in the chalk formation. The XCB system finished the hole with a 61.2% recovery.

Several gravel layers and sand layers were encountered in the hole but gave surprisingly little trouble. We circulated several high-viscosity mud pills as insurance against future problems, because this hole was to be terminated fairly deep in the section and then logged. After penetrating a particularly auspicious gravel layer, we made a short wiper trip to check, clean, and condition the hole.

By 2200 hr on 23 March, deteriorating weather conditions caused coring operations to be suspended. The real "fall" in the South Atlantic weather was beginning to manifest itself. The drill string was secured with 3 knobby pipe joints through the horn of the ship, and we began waiting on weather. Winds gusted to 55 kt that evening, leading to sea and swell conditions that resulted in a maximum roll condition of 9°. By early the following morning conditions had deteriorated even further. Because of a significant wind shift of nearly 90°, two predominant swells existed. Automated station-keeping requirements dictated that the vessel's nose be kept nearly into the wind, which put us virtually broadside into the large secondary swell. The geometry of the situation resulted in average rolls of 10°–12° with several 15° to 18° rolls. After 17 hr of waiting on weather, conditions improved and XCB coring resumed.

Coring ceased at 0115 hr on 26 March when Core 114-699A-56X could not be retrieved. After 1 hr of retrieval attempts we decided to jar off (sever the overshot shear pin) and try to dislodge the barrel with another core barrel. The overshot pin refused to shear, however, and another couple of anxious hours

Table 1. Site 699 coring summary.

Core no.	Date (Mar. 1987)	Local time (hr)	Depths (mbsf)	Cored (m)	Recovered (m)	Recovery (%)
Hole 699A-						
1H	21	0730	0–8.6	8.6	8.66	100.0
2H	21	0830	8.6–18.1	9.5	6.53	68.7
3H	21	1030	18.1–27.6	9.5	6.16	64.8
4H	21	1245	27.6–37.1	9.5	7.27	76.5
5H	21	1330	37.1–46.6	9.5	7.37	77.6
6H	21	1440	46.6–56.1	9.5	8.43	88.7
7H	21	1540	56.1–65.6	9.5	7.18	75.6
8H	21	1640	65.6–75.1	9.5	8.04	84.6
9H	21	1755	75.1–84.6	9.5	9.30	97.9
10H	21	1930	84.6–94.1	9.5	8.50	89.5
11H	21	2040	94.1–103.6	9.5	7.06	74.3
12H	21	2130	103.6–113.1	9.5	7.69	80.9
13H	21	2230	113.1–122.6	9.5	6.92	72.8
14H	21	2325	122.6–132.1	9.5	6.14	64.6
15H	22	0025	132.1–141.6	9.5	7.37	77.6
16H	22	0125	141.6–151.1	9.5	7.53	79.2
17H	22	0225	151.1–160.6	9.5	7.41	78.0
18H	22	0325	160.6–170.1	9.5	8.41	88.5
19H	22	0425	170.1–179.6	9.5	6.14	64.6
20H	22	0525	179.6–189.1	9.5	8.12	85.5
21H	22	0640	189.1–198.6	9.5	8.33	87.7
22H	22	0750	198.6–205.1	6.5	6.50	100.0
23X	22	0940	205.1–214.6	9.5	7.36	77.5
24X	22	1115	214.6–224.1	9.5	9.37	98.6
25X	22	1300	224.1–233.6	9.5	2.12	22.3
26X	22	1530	233.6–243.1	9.5	2.06	21.7
27X	22	1700	243.1–252.6	9.5	9.74	102.0
28X	22	1815	252.6–259.1	6.5	1.73	26.6
29X	22	1945	259.1–268.6	9.5	3.90	41.0
30X	22	2145	268.6–278.1	9.5	6.09	64.1
31X	23	0020	278.1–287.6	9.5	9.24	97.2
32X	23	0210	287.6–297.1	9.5	9.57	101.0
33X	23	0355	297.1–306.6	9.5	9.38	98.7
34X	23	0530	306.6–316.1	9.5	0.24	2.5
35X	23	0745	316.1–325.6	9.5	9.04	95.1
36X	23	0915	325.6–335.1	9.5	9.83	103.0
37X	23	1030	335.1–344.6	9.5	8.04	84.6
38X	23	1215	344.6–354.1	9.5	5.96	62.7
39X	23	1753	354.1–363.6	9.5	3.14	33.0
40X	23	1940	363.6–373.1	9.5	9.50	100.0
41X	23	2148	373.1–382.6	9.5	2.09	22.0
42X	24	2000	382.6–392.1	9.5	9.79	103.0
43X	24	2210	392.1–401.6	9.5	8.46	89.0
44X	25	0010	401.6–411.1	9.5	0.05	0.5
45X	25	0155	411.1–420.6	9.5	9.73	102.0
46X	25	0320	420.6–430.1	9.5	0	0
47X	25	0500	430.1–439.6	9.5	9.38	98.7
48X	25	0645	439.6–449.1	9.5	7.37	77.6
49X	25	0840	449.1–458.6	9.5	8.64	90.9
50X	25	1015	458.6–468.1	9.5	9.26	97.5
51X	25	1150	468.1–477.6	9.5	0.20	2.1
52X	25	1342	477.6–487.1	9.5	0.25	2.6
53X	25	1703	487.1–496.6	9.5	0.81	8.5
54X	25	2010	496.6–506.1	9.5	3.50	36.8
55X	25	2310	506.1–508.6	2.5	1.45	58.0
56X	26	0000	508.6–518.1	9.5	4.17	43.9
				518.1	356.52	

passed with the status of the drill string in the hole now a serious concern. All circulation ability was lost immediately upon sticking the core barrel. With the sand line attached to the barrel we did not have the ability to rotate the string, and we decided to deploy the Kinley line-severing tool, sever the sand line, and retrieve the remaining line.

The core barrel remained stuck in the pipe preventing the deployment of logging tools. The inability to circulate coupled with drill-string drag and torquing indicated that attempts at logging through the pipe would have constituted an extreme risk of drill string or BHA loss. The poor condition of the hole at the surface was suspected to be a result of the earlier waiting on weather delay. This fact, in addition to the frequent recurrence of poor weather conditions, made deployment of a minicone risky. We decided to terminate the hole without logging and move approximately 8 nmi to Site 700. This site was nearly identical to Hole 699A except that the upper, younger facies were thinner. Reaching basement at this site in the existing time frame was thought possible because troublesome sand layers were less likely to be encountered.

The occupation of Site 699 did not end in the usual manner upon clearing the rotary table with the drill bit because an additional 4.5 hr were expended for refueling prior to departure. This was the first of two refuelings required by the vessel before the transit to Mauritius. The tanker originally contracted to refuel the ship in port at the Falkland Islands would have arrived more than a week late, and by choosing to attempt refueling at sea later in the leg, the ship was able to depart nearly two days early from port. The support vessel *Maersk Master* took on the first load of fuel from the tanker *Sunny Trader* in King Edward Cove, South Georgia Island, and then, using her unique dynamic positioning capabilities, transferred the load to *JOIDES Resolution* while she was on station. The vessel departed Site 699 at 2000 hr on 26 March 1987.

LITHOSTRATIGRAPHY

The sediments drilled at Site 699 are predominantly pelagic in origin. The recovered section is divided into six lithostratigraphic units (Fig. 4), based on composition (Fig. 5), carbonate content (Fig. 6), and diagenetic maturity. Generally, a decrease in siliceous microfossils (diatoms, radiolarians, and silicoflagellates) and an increase in calcareous components (nannofossils and micrite) occur with depth.

Lithostratigraphic Unit I, early Miocene to Quaternary in age, is represented by diatom clay and diatom mud, containing dropstones and ash at the top and manganese nodules toward the bottom. Unit II, early Oligocene to early Miocene in age, is a transitional unit marked by the first appearance of nannofossils that almost exclusively dominate the calcareous component of the sediment. Unit II is further divided into two subunits. Subunit IIA consists of alternating diatom nannofossil ooze and diatom mud to nannofossil diatom mud. Subunit IIB is characterized by siliceous-bearing nannofossil ooze and nannofossil siliceous ooze. A 2-m-thick gravel horizon showing graded bedding is designated as Unit III. In transitional Unit IV of early/middle Eocene to early Oligocene age, the siliceous biogenic components become less important and nannofossil oozes predominate. Unit V, early to late Eocene in age, is carbonate-rich and is divided into Subunit VA of nannofossil chalk and Subunit VB of dominantly micrite-bearing to micritic nannofossil chalk. Unit VI, late Paleocene in age, is represented by zeolite-bearing claystone and clay-bearing micritic nannofossil chalk. The lithostratigraphic units are summarized in Table 2.

In the upper 30 cores of Hole 699A, only the first sections of Cores 114-699A-4H to 114-699A-7H show soupy drilling disturbance. In the lower half of the section, the disturbance increases below Core 114-699A-31X, and Cores 114-699A-41X to 114-699A-50X are moderately disturbed to brecciated. This disturbance probably results from the downhole occurrence of pebbles derived from the gravel bed of Unit III or other unrecovered clastic intervals. Unfortunately, core recovery became more irregular below Core 114-699A-26X (Fig. 4).

Unit I: Core 114-699A-1H to Sample 114-699A-10H-1, 110 cm; Depth: 0–85.7 mbsf; Age: early Miocene to Quaternary.

Unit I consists of siliceous and clayey siliceous sediments. The major lithologies are diatom clay (gray, 5Y 5/1, to light gray, 10YR 6/1, to greenish gray, 5GY 5/1), clayey diatom ooze (olive gray, 5Y 5/1, 5Y 5/2), and diatom ooze (light brownish gray, 2.5Y 6/4, to light yellowish gray, 2.5Y 6/4). Of these, diatom ooze is the most important lithology.

These lithologies occur in alternating sequences, about 10–30 cm thick, in Cores 114-699A-2H to 114-699A-7H, with some occurrences as thin, 2-cm laminae at 15–25 cm in Section 114-699A-2H-2. The lithologic boundaries are gradual to sharp and may be bioturbated. Horizons grading from diatom ooze to diatom clay over 20–30 cm are observed in Section 114-669A-5H-3, from 50–150 cm.

The occurrence of ash was noted from the top of the unit to Sample 114-699A-8H-1, 150 cm (upper Miocene).

Little of the original sediment structure is observed in this unit because of moderate to intense bioturbation. Fine color laminations from pale gray (5Y 7/1) to gray (5Y 6/3) occur in Section 114-669A-1H-5. Mottling and burrowing occur throughout the unit but are most prominent in Cores 114-699A-3H to 114-699A-9H. The ichnofacies is dominated by *Planolites*, with occasional *Thalassinoides*. *Planolites* is more commonly observed in the diatom ooze horizons.

Sand- and silt-sized lithic fragments occur throughout the upper Miocene–Quaternary of this unit (0–65 mbsf) in quantities sufficient to result in a silty-sandy-gritty texture. This component is identified as ice-rafted debris. Dropstones, ranging in size from 1–6 cm and of varying compositions (basalts, metamorphic schists, and quartz arenites), are also found throughout Core 114-699A-8H-2. In Cores 114-699A-1H through 114-699A-3H, the dropstones seem to occur mainly in the diatom ooze horizons, whereas in Cores 114-699A-4H to 114-699A-9H they occur in both diatom oozes and diatom clays.

Manganese nodule occurrences are confined to Cores 114-699A-8H and 114-699A-9H near the base of lithostratigraphic Unit I. In Core 114-699A-8H the nodules occur above and below the lower Miocene–upper middle Miocene hiatus. They range in size from sand-sized micronodules to large 6–9-cm concretions that fill the core liner. Postdepositional remobilization of iron and manganese appears to have occurred in Sample 114-699A-8H-1, 106-117 cm, where framboidal structures radiate out from a nodule crust into and incorporating the surrounding sediment (Fig. 7).

Drilling disturbance in Unit I is minimal and is limited to soupy deformation in the top sections of Cores 114-699A-4H to 114-699A-7H.

Unit II: Sample 114-699A-10H-1, 110 cm, to Section 114-699A-25X, CC; Depth: 85.7–233.6 mbsf; Age: early Oligocene–early Miocene.

Unit II is marked by the first downcore appearance of nannofossils in the sequence. This lithologic change is also documented by an increase in percent $CaCO_3$ from nearly 0% to 20%–30% (Fig. 6). The unit has been divided into two subunits based on the composition and frequency of rhythmic lithologic changes. Subunit IIA tends to be more muddy and consists of thickly alternating horizons of nannofossil siliceous ooze and clayey nannofossil siliceous oozes. Subunit IIB is composed of

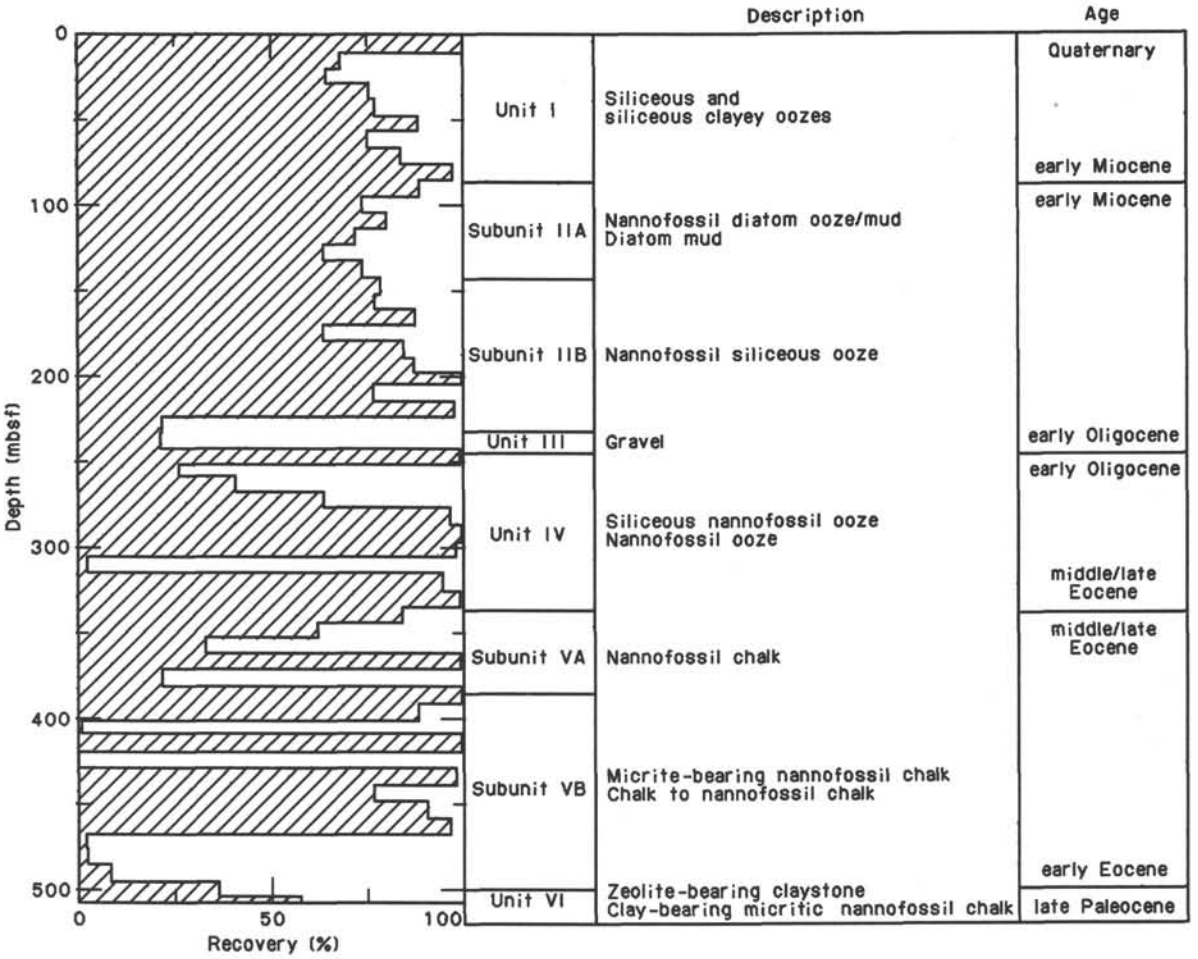

Figure 4. Recovery, description, and ages of Site 699 lithostratigraphic units.

thinner, rhythmical alternations of nannofossil siliceous oozes with less mud and nannofossil ooze.

Subunit IIA: Sample 114-699A-10H-1, 110 cm, to Section 114-699A-15H, CC; Depth: 85.7–142 mbsf; Age: late Oligocene–early Miocene.

The major lithologies in this subunit are nannofossil siliceous ooze, light brown gray (2.5Y 6/2) to light gray (5Y 7/1) to olive gray (5Y 7/1), and clay-bearing nannofossil siliceous ooze, light gray (5Y 7/1) to greenish gray (5Y 6/1). Minor lithologies are greenish gray (5GY 5/1) diatom mud, white (2.5Y 8/1) to light gray (2.5Y 7/2) nannofossil ooze, and greenish gray (5GY 6/1) diatom ooze. These lithologies form alternating units 0.5–3 m thick. Carbonate contents for Subunit IIA range from 0%–30%, reflecting alternating horizons of nannofossil-poor and -rich intervals.

Sedimentary structures are not visible, although Core 114-699A-10H exhibits some color laminae (0.1–0.5 mm thick) at 10 and 110 cm in Section 114-699A-10H-2 (pale olive 5Y 6/3) and at 68 and 125 cm in Section 114-699A-10H-5 (dusky yellow green, 5GY 5/2). This subunit is moderately to strongly bioturbated (Cores 114-699A-10H to 114-699A-13H and 114-699A-15H), with well-preserved burrows, especially in the transition zone between different lithofacies. Mottling is common. The ichnofacies identified consists of *Planolites*, *Thalassinoides*, *Zoophycos*, and *Chondrites*.

Pebbles were found throughout Unit II. Their occurrence is concentrated in the first section of each core. These lithic components probably represent downhole contamination from dropstones in the overlying lithologic unit.

Drilling disturbance in Subunit IIA is minor. Apart from the displaced dropstones, the upper part of the first sections of Cores 114-699A-10H and 114-699A-12H are soupy. Fracturing of the sediments has also occurred in Sections 114-699A-12H-2 and 114-699A-14H-3.

Subunit IIB: Sample 114-699A-16H-1, 0 cm, to Section 114-699A-25X, CC; Depth: 142–233.6 mbsf; Age: early Oligocene to late Oligocene.

Subunit IIB is characterized by thin, 10–20 cm and rarely up to 70 cm, rhythmically alternating sequences of nannofossil-bearing siliceous clay (gray, 5Y 7/1, 5Y 6/1) and nannofossil-bearing clayey siliceous ooze (light gray, 5Y 7/1) in Cores 114-669A-16H and 114-669A-17H. Cores 114-669A-18H to 114-669A-25X consist of alternating siliceous-bearing nannofossil ooze (white 5Y 8/1), nannofossil siliceous ooze (light gray, 5Y 7/1), and siliceous-bearing nannofossil ooze (light gray, 5Y 7/1). This subunit is distinguished from Subunit IIA by a lower clay content, thinner alternating sequences of lithofacies, and carbonate contents ranging up to 50% (Fig. 6). The many changes in lithofacies are reflected by the high frequency of fluctuations in the carbonate content.

No original sediment structures are visible, but lamination is present in Sample 114-669A-18H-5, 25–40 cm. Bioturbation in Cores 114-699A-16H to 114-699A-22H is generally intense, with biodeformational structures occurring at a number of horizons

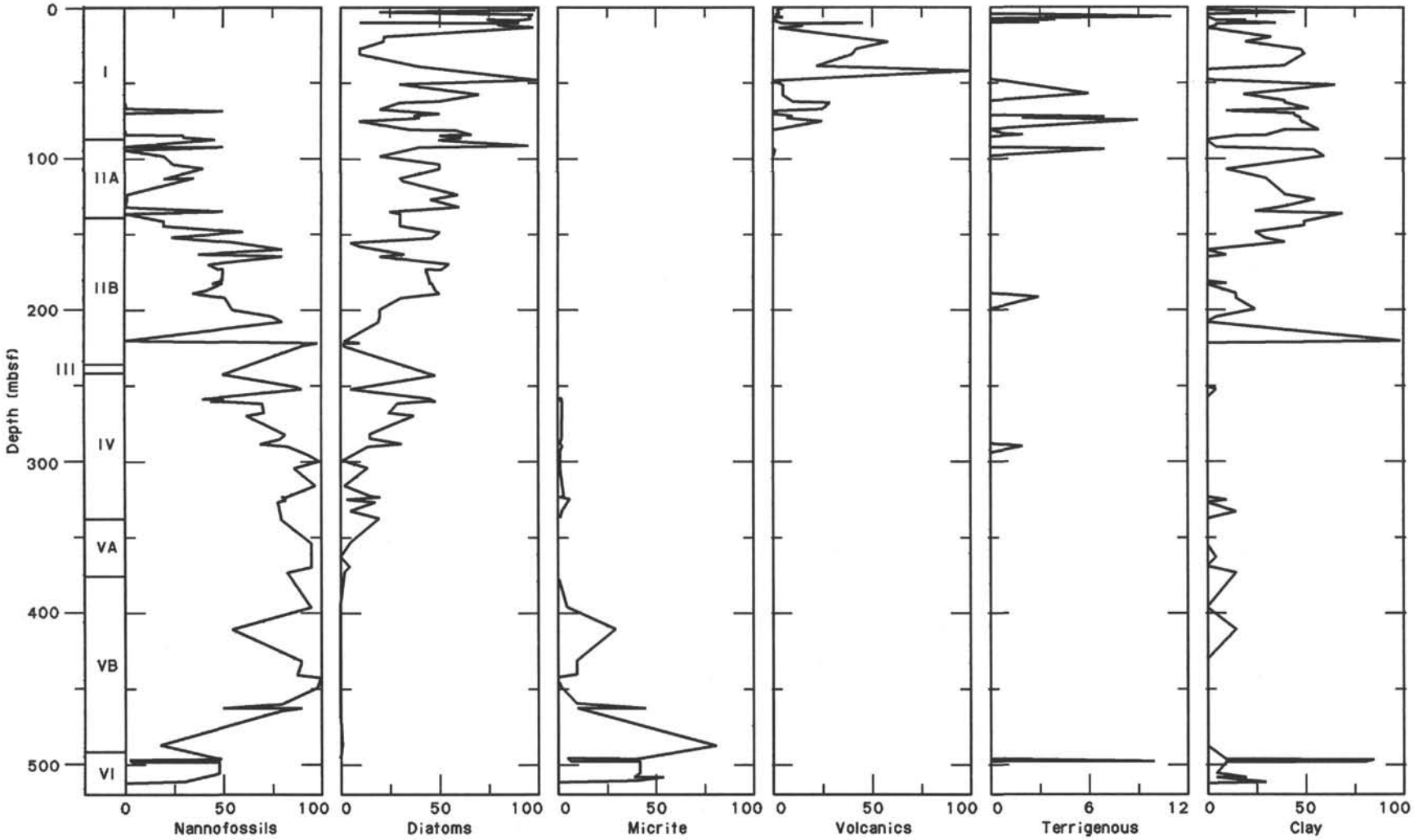

Figure 5. Relative abundances of smear slide components from Hole 699A.

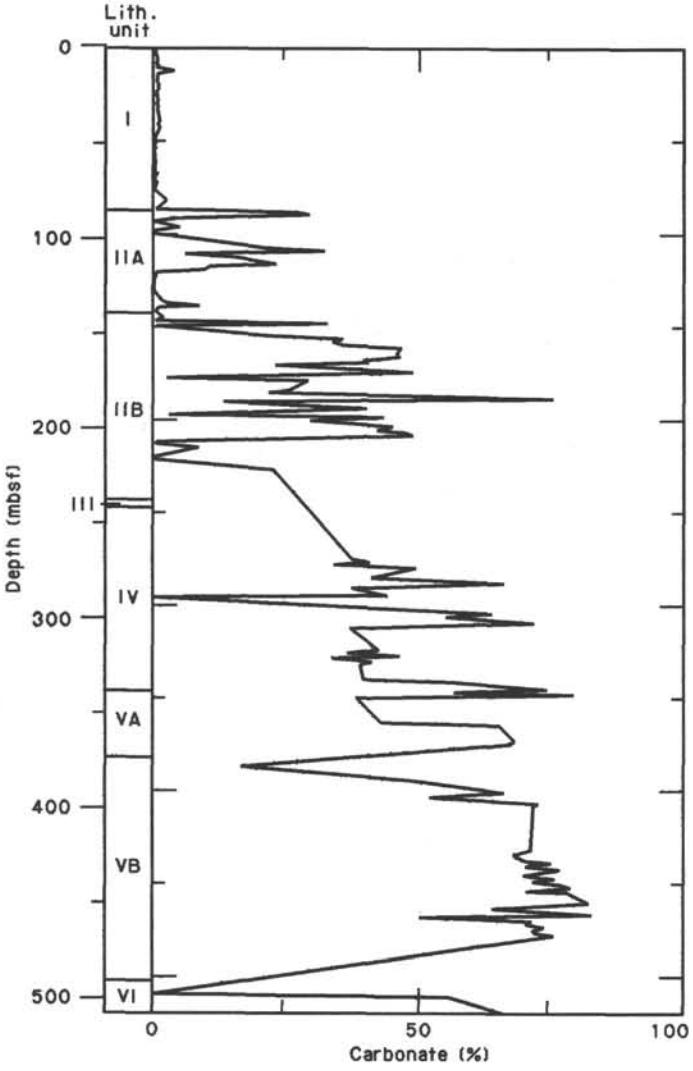

Figure 6. Carbonate content of Hole 699A lithostratigraphic units.

(Samples 114-699A-18H-5, 94–114 cm, 114-699A-20H-1, 110–130 cm, 114-699A-20H-3, 125–135 cm, and 114-699A-20H-5, 87–100 cm). Extensive mottling occurs in this subunit. *Zoophycos*, *Planolites*, *Thalassinoides*, and *Chondrites* burrows are very common. Manganese staining in a *Planolites* burrow was observed in Sample 114-699A-18H-2, 104–105 cm.

The few pebbles that were found (Samples 114-699A-19H-1, 5–10 cm, and 114-699A-23X-1, 0–5 cm) probably originated uphole.

Drilling disturbance in Subunit IIB (Cores 114-699A-21H and 114-699A-23X to 114-699A-25X) is more intense than in the other units. Recovery was discontinuous in Cores 114-699A-21H and 114-699A-23X through 114-699A-25X. Moderate sediment disturbance occurs in Samples 114-699A-21H-1, 0–90 cm, 114-699A-23X-1, 6–20 cm, 114-699A-23X-4, 60–90 cm, 114-699A-23X-5, 60–110 cm, 114-699A-24X-1, 0–50 and 60–70 cm, 114-699A-24X-5, 70–110 cm, 114-699A-25X-1, 0–150 cm, and 114-699A-25X-2, 20–50 cm.

Unit III: Sample 114-699A-26X-1, 0 cm, to Section 114-699A-26X, CC; Depth: 233.6–235.66 mbsf; Age: deposited in the early Oligocene, but the age of the pebbles is unknown.

The thin but distinctive Unit III consists of a normally graded gravel bed with large pebbles (>5 cm) at the base (Sample 114-699A-26X-3, 0–20 cm). The mean diameter of the gravel decreases to 1 cm toward the top of the unit. Section 114-699A-26X-1 is represented by poorly sorted, subangular to subrounded gravels. The lithologic components include manganese nodules, quartz (smokey, rose, and milky white), schists and other metamorphic fragments, basalt, andesite, quartz arenite, granite, oligomict and polymict conglomerates, quartz diorite, and clasts of indurated sediments.

The precise position of this gravel unit is not known because of poor recovery in the preceding core (114-699A-25X), and the subsequent core (114-699A-26X) recovered only 2.1 m of the underlying 9.7 m of sediment cored.

The origin of this unit is controversial. Because of the lack of stratigraphic continuity and absence of lateral control on the spatial distribution of the gravel, we present two alternative hypotheses for its emplacement:

1. The gravel may represent material that originated uphole and fell down during the exchange of the core barrel.
2. The gravel is allochthonous and has been transported by mass flow.

The first hypothesis is supported by the following observations:

- The composition of the pebbles (granites, schists, quartz, and quartz arenites) suggests a continental source and, to date, there is no known continental source in the vicinity of Site 699. The gravel could therefore represent ice-rafted debris from the younger sediments upcore. Pebbles with similar compositions were recovered in piston cores from the Northeast Georgia Rise, where they are clearly a lag deposit of ice-rafted detritus concentrated in Pliocene-Pleistocene sediments (P. Ciesielski, pers. comm., 1987).
- Large pebbles occur in other parts of the unit (Core 114-699A-42X) and can also be interpreted as drilling contamination.
- The gravel is not set within a finer matrix, which implies that the deposit is a washed-out, well-sorted sediment.
- The observed grading may have been artificially induced by the coring process.

Table 2. Lithostratigraphic units at Site 699.

Lithostratigraphic unit/subunit	Lithology	Depth (mbsf)	Age
I	Siliceous and siliceous clayey oozes	0–85.7	early Miocene–Quarternary
IIA	Nannofossil diatom ooze and diatom mud	85.7–142	late Oligocene–early Miocene
IIB	Nanofossil siliceous ooze	142–233.6	early Oligocene–late Oligocene
III	Gravel	233.6–235.6	early Oligocene
IV	Siliceous nanofossil ooze and nannofossil ooze	243.1–335.4	middle/late Eocene–early Oligocene
VA	Nannofossil chalk	335.4–375.2	middle/late Eocene
VB	Nannofossil chalk	382.6–487.9	early Eocene–middle Eocene
VI	Claystone and nannofossil chalk	496.6–516.3	late Paleocene

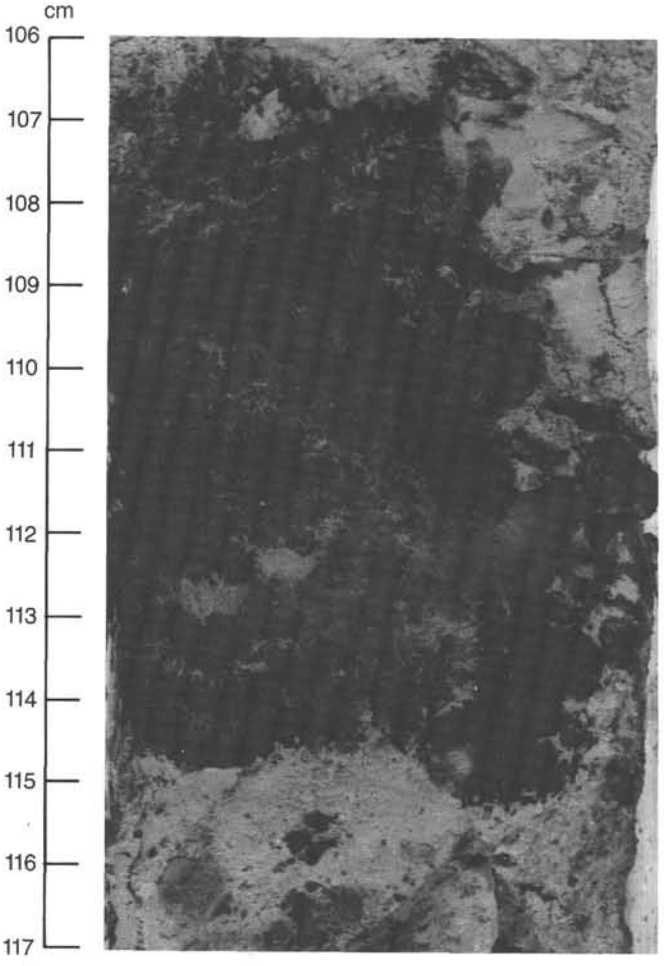

Figure 7. Manganese nodule of early Miocene age, showing postburial mobilization of the iron and manganese in the nodule, as indicated by framboidal structures radiating into the sediment (Sample 114-699A-8H, 106–117 cm).

On the other hand are the observations that support a mass flow origin:

- No strong drilling disturbance or poor core recovery (Fig. 4) occurred prior to Core 114-699A-26X.
- According to the drilling superintendent, the possibility of 2 m of downhole gravel contamination is highly improbable.
- The gravel is graded, which may indicate gravity sedimentation.
- Probable mass flows can be distinguished on seismic profiles from the region (see "Seismic Stratigraphy" section, this chapter).
- The pebbles, which caused most of the subsequent drilling disturbance and in part, the poor recovery in Units IV to VI, seem to have originated from Unit III at 235 mbsf.
- Diagenesis of the sediment, indicated by the occurrence of micrite, starts below Unit III, in Core 114-699A-27X, and increases downhole. The low porosity of the gravel bed might have made it a preferred horizon for lateral water movements.
- Miliolid and hyaline benthic foraminifers are common in Unit III but were not noted anywhere else in Hole 699A (see "Biostratigraphy," this chapter).
- Reworked (transported) shallow-water benthic foraminifers were noted above Unit III (Cores 114-699A-22H and 114-699A-23H), which attests to other episodes of downslope transport.

Unit IV: Sample 114-699A-27X-1, 0 cm, to Section 114-699A-36X, CC; Depth: 243.1–335.43 mbsf; Age: middle/late Eocene–early Oligocene.

Lithostratigraphic Unit IV is a transitional unit, with decreasing siliceous biogenic material downhole. It is characterized by gray (5Y 5/1 to 5Y 6/1) to greenish gray (5GY 6/1) siliceous nannofossil oozes, light greenish gray (5GY 7/1) to light gray (5Y 6/1) siliceous-bearing nannofossil oozes, and light greenish gray (5GY 7/1) to light gray (5Y 7/1) nannofossil oozes.

In Core 114-699A-35X, regular alternations of nannofossil chalk and greenish gray (5GY 6/1) siliceous-bearing nannofossil ooze are separated by gradational contacts. Toward the bottom of the unit (Core 114-699A-36X) the ooze grades into chalk. The boundaries between lithologies and color changes are gradational. In most of the first sections of the cores, gravel is a downhole contaminant, possibly originating from the gravel layer of Unit III.

Bioturbation is abundant in Sections 114-699A-31X-4 and 114-699A-31X-5, 114-699A-32X-2 and 114-699A-32X-3, 114-699A-33X-2, 114-699A-33X-3, and 114-699A-33X-6, 114-699A-35X-4 to 114-699A-35X-6, and 114-699A-36X. In these sections a lighter greenish mottling of the dominantly gray oozes is common. The ichnofacies (see "Ichnology," this section) consists mainly of *Zoophycos* (from 30–150 cm in Section 114-699A-32X-2; Sections 114-699A-35X and 114-699A-36X), *Planolites* (Sections 114-699A-32X-2 to 114-699A-32X-3 and Cores 114-699A-35X and 114-699A-36X), and *Chondrites* and *Thalassinoides* (Cores 114-699A-35X and 114-699A-36X).

Unit V: Sample 114-699A-37X-1, 0 cm, to Section 114-699A-53X, CC; Depth: 335.43–487.91 mbsf; Age: early to middle/late Eocene.

Lithostratigraphic Unit V is characterized by the dominance of carbonate sediments, specifically nannofossil chalk. Its division into two subunits is based mainly on the relative abundance of micrite in the lower part.

Subunit VA: Sample 114-699A-37X-1, 0 cm, to Section 114-699A-41X, CC; Depth: 335.4–375.19 mbsf; Age: middle to late Eocene.

This subunit is represented by nearly pure, light greenish gray (5GY 7/1) to white (5Y 8/1) nannofossil chalk. Clay is an abundant component toward the bottom of the subunit (Core 114-699A-41X). Zeolites (clinoptilolite) occur in the nannofossil chalk below Core 114-699A-39X.

In Sample 114-699A-37X-3, 112–125 cm, a claystone with well-defined upper and lower boundaries represents a minor lithology. In the same core and in Core 114-699A-37X-2, at 56 and 79 cm, finely disseminated manganese nodules stain the nannofossil chalk, producing black spots.

Additional minor lithologies are two gravel and sand layers in Section 114-699A-39X-2, from 91 to 114 cm (layer A) and from 124 to 141 cm (layer B). Layer A is ungraded, and the subrounded components are poorly sorted and consist of quartzite, basalt, greenschist, and quartz. The contact with the overlying nannofossil chalk is sharp and was produced by the coring technique. Layer B has a composition similar to that of layer A (i.e., it is poorly sorted), but the subrounded gravel- to sand-sized grains are not graded. Downhole-washed gravels (basalt, greenschist, granite, and quartzite) were found within the first 30 cm of the first sections of Cores 114-699A-38X through 114-699A-41X.

Strong to moderate bioturbation exhibiting mottling of the darker colored sediment is abundant in this subunit, occurring mainly in Cores 114-699A-37X, 114-699A-38X (Sections 3 and 4), and 114-699A-40X. The ichnofacies includes *Chondrites*, *Planolites*, and *Zoophycos* (see "Ichnology," this section).

Subunit VB: Sample 114-699A-42X-1, 0 cm, to Section 114-699A-53X, CC; Depth: 382.6–487.91 mbsf; Age: early to middle/late Eocene.

Subunit VB contains pale yellow (2.5Y 7/4), yellowish brown (2.5Y 6/4), and brownish gray (2.5Y 6/2) to white (5Y 8/1) nannofossil micritic chalk to nannofossil chalk. Light gray (5Y 7/1) clay-bearing nannofossil micritic chalk is found mainly in Core 114-699A-45X. The boundaries between the nannofossil chalk and nannofossil micritic chalk in Core 114-699A-42X are gradational and may vary slightly in color, ranging from pale yellow (2.5Y 7/4) to white (2.5Y 8/2).

Subrounded pebbles occur within the very disturbed nannofossil micritic chalk at the following horizons:

114-699A-42X-1, 35 to 47 and 50 to 60 cm
42X-2, 8 to 12 cm (rounded granodiorite)
42X-2, 80 to 83 cm (angular basalt and two granodiorites)
43X-1, 21 cm (subrounded greenschist)
43X-2, 10 cm (amphibolite)
43X-2, 55 cm (basalt with hematite)
43X-2, 146 cm (subrounded amphibolite)
43X-4, 60 cm (fine-grained quartzite)

These pebbles are probably not in place, and we prefer to explain their occurrence as downhole contamination resulting from drilling disturbance. Pebbles of similar composition were found higher in the section (Core 114-699A-26X), although smaller in size. In addition, the sediments associated with these pebbles (Core 114-699A-42X and Sections 114-699A-43X-1 to 114-699A-43X-3) are highly disturbed and show flow structures.

In sections with only minor disturbance, we noted moderate to strong bioturbation, which was ascribed to *Zoophycos*, *Planolites*, *Chondrites*, *Thalassinoides*, and *Mycellia*(?) (Cores 114-699A-42X, 114-699A-45X, 114-699A-47X, 114-699A-48X (Sections 2 and 3), 114-699A-49X, and 114-699A-50X).

Unit VI: Samples 114-699A-54X-1, 0 cm, to 114-699A-56X-6, 20 cm; Depth: 496.6–516.3 mbsf; Age: late Paleocene.

This bottom unit is represented by dark brown (7.5YR 4/4) zeolite-bearing claystone, pale brown (10YR 6/3) clay-bearing micritic nannofossil chalk, and light gray (10YR 7/1) clay-bearing micritic nannofossil chalk to clay-bearing nannofossil micritic chalk.

Zeolites increase in abundance within the dark brown claystone (Section 114-699A-54X-1), indicating increased diagenetic alteration of the sediment. The increased clay content may mark an environmental change at the Paleocene/Eocene boundary.

Granitic gravels (Fig. 8) occur in Sample 114-699A-56X-5, 0–10 cm, and may represent downhole contamination. The quartz grains are subangular to subrounded and the presence of an ash component may indicate a redeposited volcanic sand at the bottom of this unit (Fig. 9). The gravels (Sample 114-699A-56X-5, 0–10 cm) and the volcanic sand (Sample 114-699A-56X-6, 0–20 cm) caused the core barrel to become jammed, which forced us to abandon Hole 699A.

Slight bioturbation consisting of *Zoophycos* and *Planolites* burrows is evident in Sample 114-699A-54X-1, 30 cm.

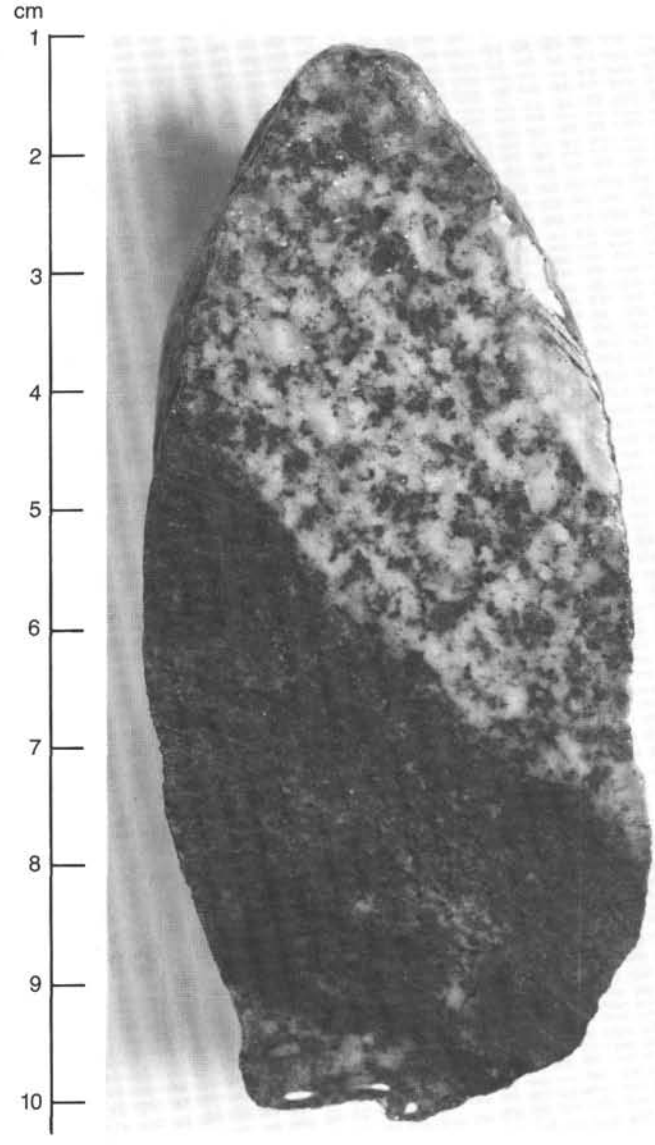

Figure 8. Granitic pebble (Sample 114-699A-56X-5, 1–10 cm).

Ichnology

The soft sediments of the cored section are generally moderately to intensely bioturbated, obliterating any original primary sedimentary structures. Rhythmical lithologic alternations and their contacts were also affected by bioturbation. However, progressive changes in colors and uniform bioturbation imply long intervals of continuous sedimentation. Bioturbation was noted in the following intervals:

114-699A-2H-2, 100–111 cm: *Planolites* showing a slight internal grading at the base of the tube (Fig. 10). *Planolites* is ubiquitous at this site, and only the most outstanding ichnofacies are noted.

114-699A-8H-3, 67–76 cm: the uppermost clear occurrence of a single *Zoophycos* (Fig. 11), about 5 mm wide.

114-699A-9H-2 and 114-699A-9H-4: *Planolites* is present throughout this interval.

114-699A-10H-2, 5–15 cm: youngest age observable *Chondrites*. Within the same core, *Chondrites* occurs with

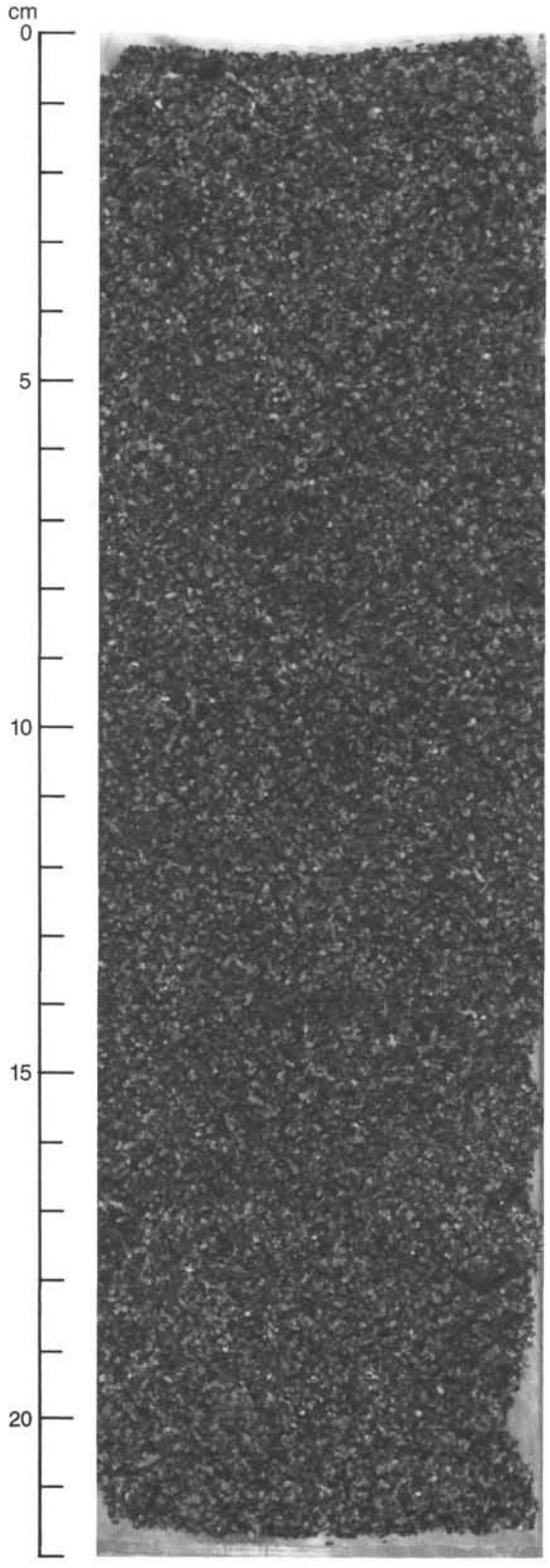

Figure 9. Poorly sorted ash sand (Sample 114-699A-56X-6, 0–22 cm).

Zoophycos and possibly *Thalassinoides* and *Helminthopsis* (at 50 cm in Section 2) and with *Zoophycos* in Section 114-699A-10H-3, at 65, 75, and 90 cm.

Zoophycos also occurs in the following sections:

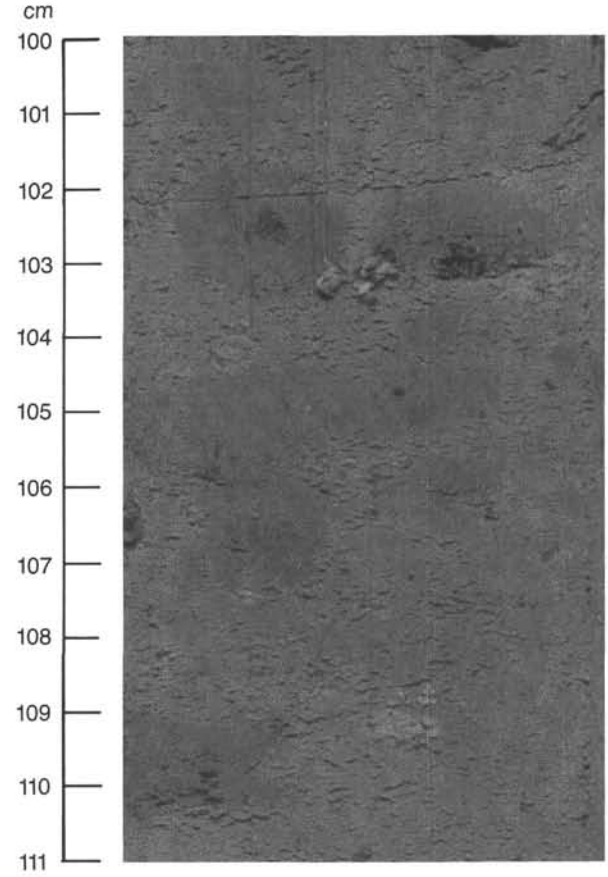

Figure 10. *Planolites* showing internal grading at 103 and 104 cm within Sample 114-699A-2H-2, 100–111 cm.

114-699A-15H-1: irregular occurrences between 18 and 103 cm
16H-5: well-developed between 7–25 and 71–87 cm
17H-2: well-developed at 80–95, 105–115, and 130 cm
17H-3: 73, 110, and 120–150 cm
18H-1: 51, 61, and 72 cm
18H-5: 85 cm 19H-4: sporadic

Bioturbation is very well developed, with clear *Zoophycos*, in Sections 114-699A-32X-2 (Fig. 12) through 114-699A-36X-5, 114-699A-37X-2, 114-699A-37X, CC, 114-699A-40X-2, 114-699A-40X-3, 114-699A-47X-2, and 114-699A-47X-5.

Planar ichnocommunities (i.e., parallel to bedding or *Epichnia*) are not well developed in these cores. On the contrary, vertical bioturbation dominates, probably indicating a low rate of sedimentation on a generally oxygenated seafloor, as suggested by the absence of the low-oxygen indicator *Chondrites*.

Zoophycos is conspicuous because it is one of the last-formed structures and generally cuts the preceding traces; it thus has a better chance of being preserved than other burrows.

As is the case with *Dictyodora liebeana* Geinitz, which is well known in the Carboniferous, *Zoophycos* is considered to be a helicoidal, upward-growing, feeding trace. The organism(s) responsible for this trace is unknown. It is always found in sediments that are quite homogeneous.

As noted previously, *Zoophycos* is one of the last traces to be formed in the sediment. The previous burrowers have already exploited part of the sedimentary organic carbon and also part of the oxygen content. Thus, it seems that *Zoophycos* is a rela-

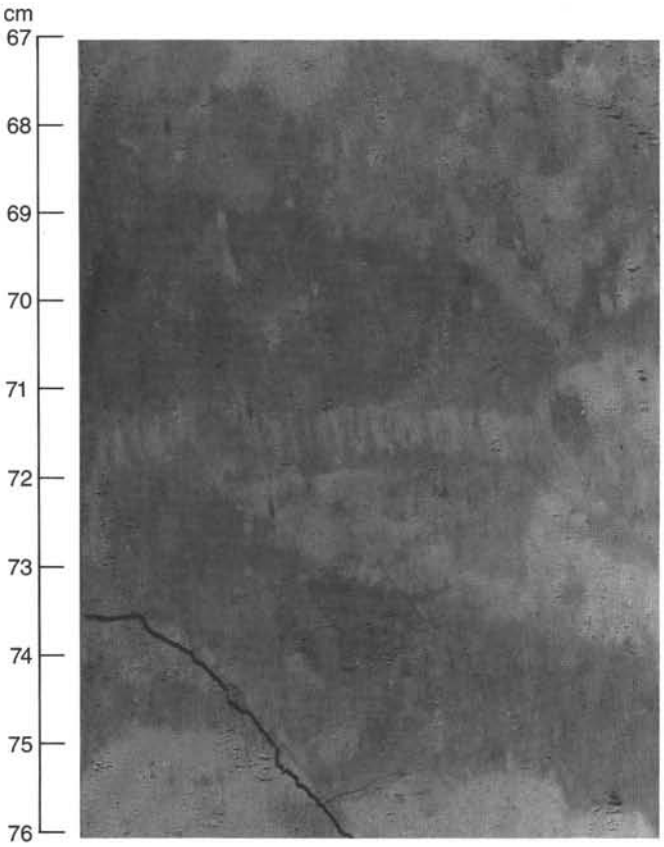

Figure 11. Isolated, 5-mm-thick *Zoophycos* (Sample 114-699A-8H-3, 67–76 cm).

tively good indicator of stable sedimentary conditions, and perhaps suboxic conditions (Eagar et al., 1985). However, significant occurrences of *Chondrites* indicate an even more anoxic environment (Bromley and Ekdale, 1984). *Zoophycos* is common in intermediate or even bathyal environments (Seilacher, 1967, 1975).

Summary and Conclusions

Hole 699A was continuously cored to 516.3 mbsf and obtained a thick sedimentary sequence ranging in age from late Paleocene to Quaternary. The core recovery for the top 224.1 m was high, averaging 81%, but recovery was significantly reduced to 54% below 224.1 mbsf, owing to apparent contamination from a gravel deposit (Unit III), which hampered recovery throughout the remainder of the section. Six lithologic units were recognized at Site 699A:

Unit I. This unit consists of 85.7 m of predominantly biogenic siliceous sediments with moderate interlayering of diatomaceous clays. Angular to subangular lithic fragments occur between 68–0 mbsf (upper Miocene–Quaternary) and are interpreted as dropstones of ice-rafted origin. Unit I spans the lower Miocene to Quaternary.

Unit II. The top of Unit II marks the boundary between predominantly biogenic siliceous sediments above (Unit I) and carbonate biogenic siliceous sediments below. This transition from carbonate to siliceous lithology occurs immediately above the Oligocene/Miocene boundary. Unit II consists of 147.9 m of siliceous and clayey nannofossil siliceous ooze with interbedded horizons of calcareous nannofossil ooze. The carbonate fraction is almost exclusively composed of nannofossils, and foraminifers are rare to absent.

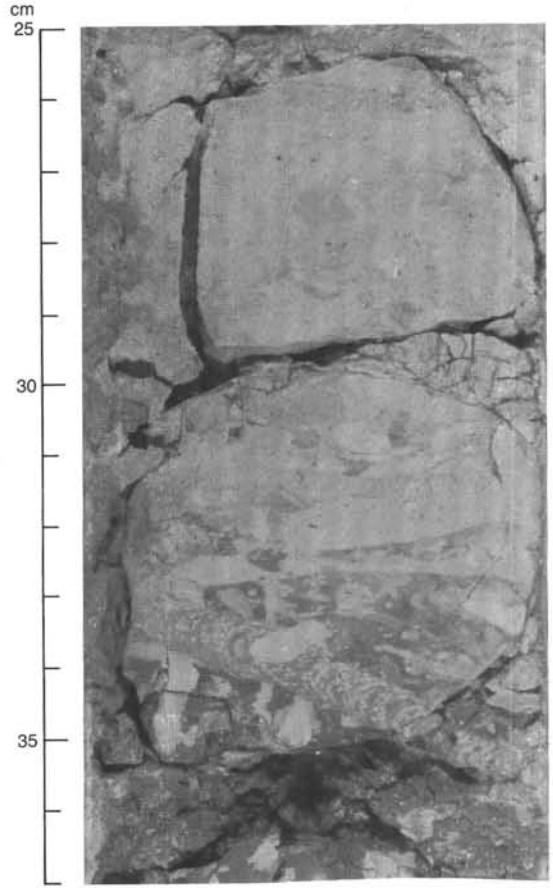

Figure 12. Isolated, 6-mm-thick *Zoophycos* showing internal alternation of lighter color fecal pellets within darker less-bioturbated sediment (Sample 114-699A-32X-2, 25–37 cm).

Unit III. This unit is composed of 2.06 m of normally graded gravels of diverse lithologies: manganese nodules, quartz, schist, basalt, andesite, quartz arenite, granite, oligomict and polymict conglomerates, quartz diorite, and clasts of indurated sediment. The gravel is coarse, ranging in diameter from 1 to 5 cm, and is embedded among nannofossil oozes of early Oligocene age.

Unit IV. This unit is a 92.3-m-thick nannofossil ooze that grades into a nannofossil chalk toward the base of the section. The relative importance of biogenic silica decreases with depth. Lithic fragments, interpreted to be downhole contaminants from the gravel layer above, are found almost exclusively in the first section of each core. The age of Unit IV spans the late Eocene to early Oligocene.

Unit V. This unit consists of 152.5 m of nannofossil chalk with increased diagenesis and formation of micrite downhole. Two gravel and/or sand layers were found at 356.4 and 356.7 mbsf. The age of Unit V is early to late Eocene.

Unit VI. This lowermost unit is composed of claystones and clay-bearing micritic nannofossil chalks. Authigenic zeolites occur within the dark brown claystones. The base consists of a volcanic sand. The unit is late Paleocene in age.

The sedimentary sequence recovered at Site 699 can be broadly interpreted as reflecting large-scale paleoenvironmental changes in the Southern Ocean. Site 699 (51°32.531′S, 30°40.603′W) is presently located near the ACZ (polar front), and its sedimentary history is linked to the development of the polar front during the Cenozoic. In turn, the evolution of the polar front was closely related to the opening of the Drake Passage and the advent of the ACC. In addition, Site 699 is in the East Georgia Basin, which is an important present-day conduit for deep-water flow from the Weddell Sea to the Argentine Basin. Prior to seafloor spreading and the formation of deep ocean floor between the Islas Orcadas Rise and Mid-Atlantic Ridge, the Georgia Basin may have been the principal pathway for deep-water flow between the Antarctic and western South Atlantic basins.

The top 85.7 m (Unit I) at Site 699 is completely dominated by biogenic siliceous sedimentation. An important erosional event occurred in the early to latest middle Miocene and is marked by the preservation of manganese nodules in Cores 114-699A-8H and 114-699A-9H. The occurrence of manganese nodules downcore implies oxidizing conditions (low organic carbon reactivity) because manganese and iron are very soluble in the reduced state. Manganese nodules in the Southern Ocean have been associated typically with areas of nondeposition or erosion by bottom-water currents (Kennett and Watkins, 1975). The combined evidence of the hiatus and manganese nodule preservation suggests that strong currents, probably associated with CPDW, were responsible for erosion during the early to middle Miocene (about 19.5–~11 Ma). This lower to middle Miocene hiatus is regional in extent throughout the subantarctic South Atlantic. At Site 513, for example, a hiatus separates a continuous sequence of early Oligocene–early Miocene age from sediments of late Miocene age.

At Site 699, a sharp change in sedimentation occurs just above the Oligocene/Miocene boundary (85.7 mbsf), marking a shift from dominantly siliceous sedimentation during the Neogene to carbonate deposition during the Paleogene. This facies change from carbonate to siliceous sedimentation near the Paleogene/Neogene boundary has been well documented in previous Southern Ocean drilling, for example, Sites 278 (Kennett, Houtz, et al., 1975) and 513 (Ludwig, Krasheninnikov, et al., 1980). The switch to siliceous Neogene sedimentation undoubtedly reflects a northward expansion of the antarctic biosiliceous sediment province. In the modern ocean, the ACZ (polar front) roughly coincides with the boundary of deposition of calcareous biogenic ooze to the north and siliceous biogenic ooze to the south (Kennett, 1982). By inference, we suggest that the polar front first migrated north of Site 699 during the earliest Miocene. This northward migration of the polar front was probably linked to the opening of the Drake Passage and full development of the ACC.

An apparently complete Eocene/Oligocene contact (between Sections 114-699A-34X, CC, and 114-699A-31X, CC) was recovered at Site 699, occurring in Core 114-699A-33X between 297.1 and 306.6 mbsf, but no lithologic break or change in percent carbonate was observed at the contact. The Eocene extends from Sections 114-699A-35X, CC (325.6 mbsf) to 114-699A-53X, CC (496.6 mbsf). The carbonate sediment becomes more indurated with depth, and the ooze/chalk transition is gradational, occurring approximately in Section 114-699A-36X (325.6 to 335.1 mbsf). The transition corresponds with a decrease in water content and porosity and an increase in density and velocity (see "Physical Properties" section, this chapter). In addition, planktonic foraminifers became increasingly abundant for the first time during the Eocene. The Eocene also marks the first appearance of zeolites (clinoptilolite), which occur within the nannofossil chalks, beginning at about 360 mbsf (Section 114-699A-39X).

Another gravel and/or sand layer occurs at 356.4 and 356.7 mbsf and consists of quartz, basalt, greenschist, and quartz arenite. It probably represents material that washed downhole.

Toward the bottom of the hole, increasing diagenesis results in the recrystallization of nannofossils to form micrite. The boundary between the nannofossil chalk and nannofossil micritic chalk is gradational in Section 114-699A-42X. The Paleocene/Eocene boundary occurs between Sections 114-699A-53X and 114-699A-54X, but core recovery was poor in this interval (8.5% and 36.8%, respectively). Paleocene sediments are marked by a lithologic change to dark brown claystones containing zeolites.

BIOSTRATIGRAPHY

Biostratigraphic Synthesis

Biostratigraphy

The upper part of the section at Site 699 (above Core 114-699A-9H) yielded only siliceous fossils; at and below Core 114-699A-9H calcareous nannofossils were recovered regularly with foraminifers present sporadically. The biostratigraphic division of the hole is thus based mainly on siliceous microfossils for the first 10 cores. Calcareous nannofossils become increasingly important through the underlying Oligocene sequence, with supporting biostratigraphic evidence provided by diatoms in the Oligocene and planktonic foraminifers in the Eocene and upper Paleocene section.

Regional and worldwide biozonation schemes have been applied to the fossiliferous records of the different groups wherever possible (see "Explanatory Notes" chapter, this volume). Zonal assignments are described in detail in the individual fossil sections and graphically summarized and compared in Figure 13. Figure 14 reveals the age vs. depth record of the hole (based on Table 3), for which the last- and first-occurrence ages for the diatom species given by Ciesielski (1983, 1986) were strictly applied. The following is a synthesis of the biostratigraphic divisions of Hole 699A:

Age	Interval
Quaternary	1H-1, 1 cm, to 2H, CC
late Pliocene	3H, CC, to 4H, CC
early Pliocene	5H-2, 4 cm, to 6H-6, 43 cm
late Miocene to latest middle Miocene	7H-5, 5 cm, to 8H-2, 42 cm
early Miocene	8H-3, 60 cm, to 10H-5, 4 cm
late Oligocene	10H, CC, to 21H, 1.95 cm
early Oligocene	21H-1, 125 cm, to 32X, CC
late Eocene–middle Eocene	34X, CC, to 47X-1, 117 cm
early Eocene	47X-7, 38 cm, to 52X, CC
late Paleocene	54X, CC, to 55X, CC

All biostratigraphic boundaries younger than late Oligocene in age are defined by diatom datums. The oldest, definite late Oligocene datum is defined by the base of the silicoflagellate *Corbisema archangelskiana* Zone. All older biostratigraphic boundaries are defined by nannofossil datums. The Paleocene/Eocene boundary is drawn at the top of nannofossil Zone NP9. A list of all identified microfossil datums is given in Table 3.

Paleoenvironment

In Hole 699A siliceous microfossils occur from the upper Eocene (Core 114-699A-36X) upward (Fig. 15). Calcareous microfossils are present through the Paleocene, Eocene, lower Oligocene, and decrease in the upper Oligocene, with sporadic occurrences in the lower Miocene. Benthic foraminifers reflect water depths of 2000–3000 m in the Paleocene, 2500–3000 m in the Eocene, and abyssal (>3000 m) in the Oligocene.

In the Paleocene and lower Eocene, warm-water planktonic foraminifers (several species of the genera *Acarinina* and *Moro-*

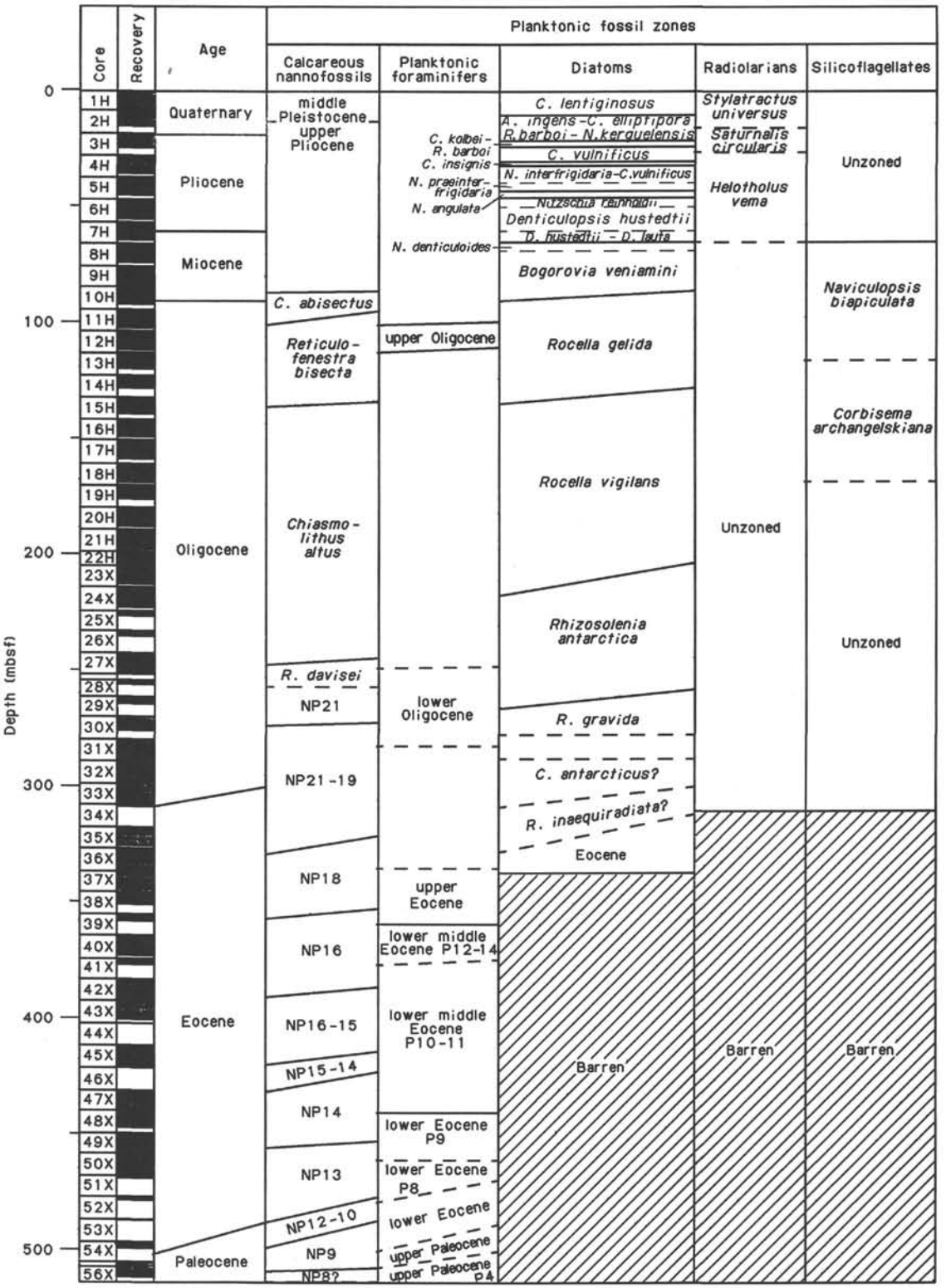

Figure 13. Planktonic fossil zones of the Paleocene to Quaternary in Hole 699A.

zovella) and warm-water calcareous nannofossils (*Discoaster* spp., *Sphenolithus* spp., and *Zygrhablithus bijugatus*) are common.

Planktonic foraminifers decrease in abundance and diversity through the middle Eocene, and the fauna exhibits a cooler character, as do the calcareous nannofossils.

In the upper Eocene, both the calcareous nannofossils and the planktonic foraminifers have only sporadic occurrences, which become more sporadic in the lowest Oligocene. The occurrence of *Discoaster* spp. seems to be always correlated with an increase in the carbonate content of the sediment, probably reflecting an increase in productivity. In this interval a relatively

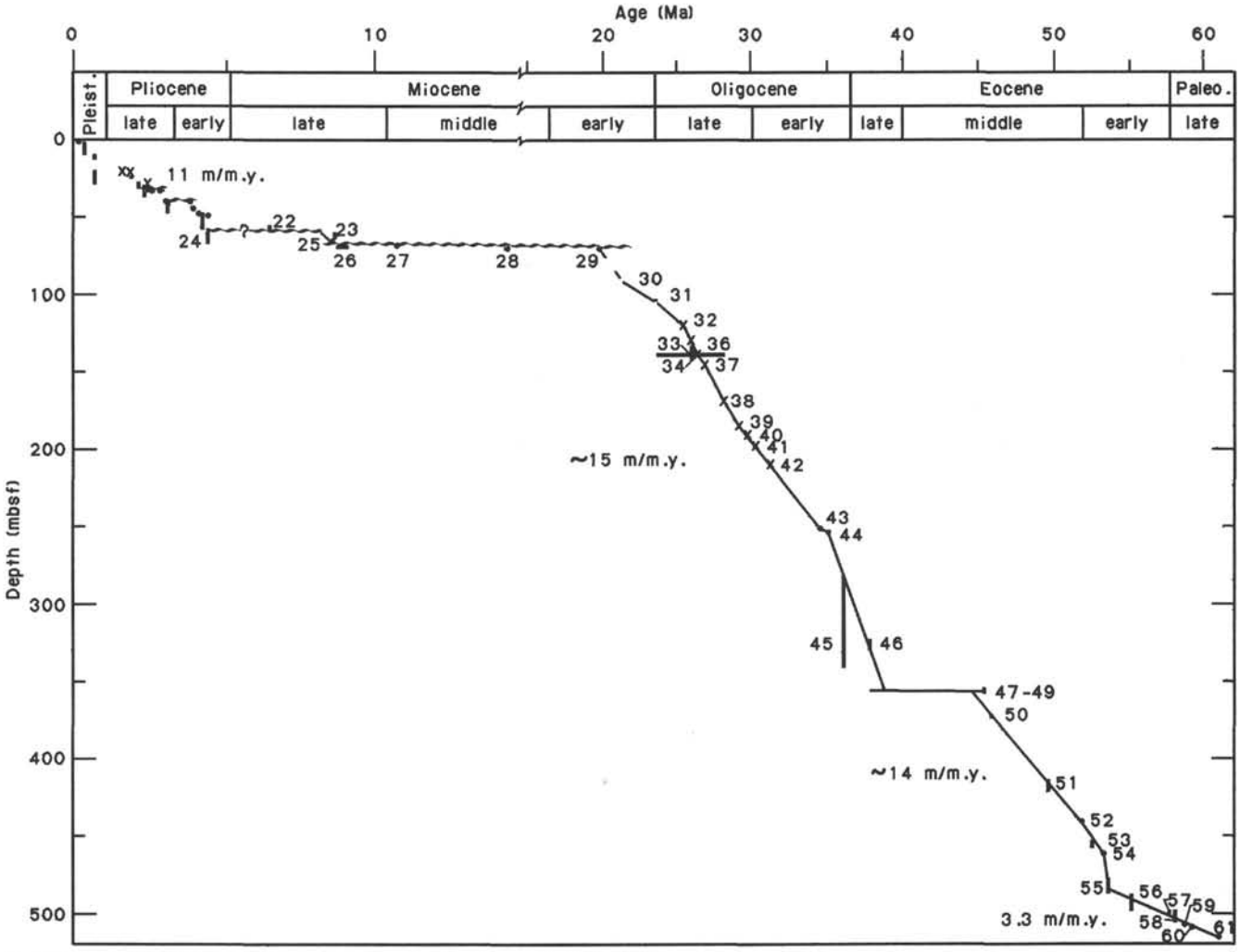

Figure 14. Sedimentation rates based on nannofossils datums for Hole 699A.

high percentage (about 10%) of low-latitude diatom species is still present (e.g., *Cestodiscus reticulatus*, *Cestodiscus gemmifer*, and *Skeletonema barbadiense*), which disappears completely above Core 114-699A-26X.

In the upper lower Oligocene the abundance of siliceous microfossils drops and the diatom flora is dominated by cosmopolitan species. Furthermore, a few high-latitude species (e.g., *Hemiaulus taurus*, *Rhizosolenia antarctica*) appear. Calcareous nannofossils are abundant but reflect a typical high-latitude flora with *Reticulofenestra* spp., *Chiasmolithus* spp., and *Isthmolithus recurvus* dominating. Planktonic foraminifers are totally absent. This continues into the lower upper Oligocene, where diatoms become common to abundant again. The diatom assemblages remain characterized by the presence of predominantly cosmopolitan species and a few high-latitude species.

This picture does not change for the diatoms in the uppermost Oligocene, but the abundance of calcareous nannofossils drops dramatically above Core 114-699A-16H, with a smaller nannofossil occurrence and planktonic foraminifers in the upper Oligocene (Cores 114-699A-11 and 114-699A-12H), in which a few discoasters were also found, indicating a short-lived return to stronger warm-water influence at this time. Another small occurrence of calcareous nannofossils is found in the lowermost Miocene (Core 114-699A-9H), where their diversity is very low. The sediments above are practically free of calcium carbonate and are dominated by biosiliceous components. In this Neogene section the diatom flora reveals a highly endemic character and the low- to midlatitude silicoflagellate zonal scheme can no longer be applied. The Neogene section at this site has several hiatuses (compare Fig. 14).

The environmental changes downhole reflect the gradual cooling of the water masses over this site and the development of the ACC. Major steps in this development have been used to divide the sediment profile at this site into units. The onset of siliceous microfossils in Core 114-699A-36X was not used for defining paleoenvironmental units because their first occurrence is controlled primarily by diagenetic factors (compare Fig. 15).

Unit V represents relatively warm-water conditions. In Unit IV after about 50 Ma, the warm-water species retreated from this area and a southern high-latitude province seems to have developed, which might have been caused by the initiation of a "small circle" shallow ACC flowing through the West Antarctic Passage and passing between Australia and Antarctica. The Eocene/Oligocene boundary, which falls within this unit, is not marked by a dramatic change in lithology.

After about 35 Ma (Unit III to Unit I) no warm-water species are present. Subunit IIB was apparently deposited during a period of relatively low biosiliceous input into the sediments, while during deposition of Subunit IIA the biosiliceous input was higher and the biocalcareous input decreased upcore.

At about 26 Ma the abundance of calcareous nannofossils drops to zero with one smaller abundance peak, including some

Table 3. Identified microfossil and magnetostratigraphic datums, Site 699.

Microfossil and paleomagnetic datums[a]	Age[a] (Ma)	Reference[b]	Interval in Hole 699A	Depth (mbsf)	Mean position (mbsf)
1. LAD *Hemidiscus karstenii* (D)	0.195	19	1H-1, 2 cm, to 1H-1, 40 cm	0.02–0.40	0.21
2. LAD *Stylatractus universus* (R)	+0.40	11	1H, 0 cm, to 1H,CC	0.00–8.66	4.33
3. Brunhes/Matuyama boundary	0.73	4	2H-2, 25 cm, to 2H-2, 132 cm	10.35–11.42	10.86
4. Top Olduvai Subchron	1.66	4	3H-1, 120 cm, to 3H-2, 36 cm	19.35–19.96	19.63
5. Base Olduvai Subchron	1.88	4	3H-2, 121 cm, to 3H-3, 36 cm	20.81–21.46	21.14
6. LAD *Saturnalis circularis* (R)	+0.70	11	2H, CC, to 3H, CC	18.10–27.60	22.85
7. LAD *Coscinodiscus kolbei* (D)	+1.89	10	3H-3, 60 cm, to 3H-4, 110 cm	21.70–23.70	22.70
8. Matuyama/Gauss boundary	2.47	4	3H-4, 121 cm, to 4H-2, 139 cm	23.81–30.49	27.15
9. LAD *Coscinodiscus vulnificus* (D)	+2.20	10	3H, CC, to 4H-1, 124 cm	27.60–28.84	28.22
10. LAD *Coscinodiscus insignus* (D)	+2.49	10	4H-2, 143 cm, to 4H-3, 40 cm	30.53–31.00	30.77
Possible hiatus ~0.3 m.y. duration (~2.5–2.8 Ma)				32.20–31.00	
*11. LAD *Nitzschia weaveri* (D)	+2.64	10	4H-3, 40 cm, to 4H-4, 10 cm	31.00–32.20	31.60
*12. LAD *Nitzschia interfrigidaria* (D)	+2.81	10	4H-3, 40 cm, to 4H-4, 9 cm	31.00–32.20	31.60
13. LAD *Helotholus vema* (R)	+2.43	11	3H, CC, to 4H, CC	27.60–37.10	32.35
14. LAD *Desmospyris spongiosa* (R)	+2.43	11	3H, CC, to 4H, CC	27.60–37.10	32.35
Hiatus ~0.9 m.y. duration (~3.0–3.9 Ma)				39.03–40.37	
*15. First concurrent *C. insignus* and *C. vulnificus* (D)	+3.10	10	5H-2, 43 cm, to 5H-3, 27 cm	39.03–40.37	39.70
*16. FAD *N. weaveri* (D)	+3.88	10	5H-2, 41 cm, to 5H-3, 27 cm	39.03–40.37	39.70
*17. LAD *Prunopyle titan* (R)	+3.20	12	4H, CC, to 5H, CC	37.10–46.60	41.85
18. FAD *N. interfrigidaria* (D)	+4.02	10	5H-4, 43 cm, to 5H-5, 50 cm	42.03–43.60	42.82
19. FAD *Nitzschia angulata* (D)	+4.22	10	5H, CC, to 6H-1, 3 cm	46.60–46.63	46.62
20. LAD *Denticulopsis hustedtii* (D)	+4.48	10	6H-1, 42 cm, to 6H-2, 6 cm	47.02–48.16	47.59
21. LAD *Amphomerium challengerae* (R)	+4.35	12	5H, CC, to 6H, CC	46.60–56.10	51.55
*22. FAD *Nitzschia reinholdii* (D)	+6.50	10	6H-6, 43 cm, to 7H-2, 44 cm	54.53–58.04	56.29
Hiatus 4.50 m.y. duration (~4.5–8.5 Ma)				62.15–54.53	
*23. LAD *Denticulopsis lauta* (D)	#8.70	10	7H-3, 5 cm, to 7H-5, 5 cm	59.15–62.15	60.65
*24. LAD *Stichocorys peregrina* (R)	+4.50	12	6H, CC, to 7H, CC	56.10–65.60	60.85
25. LAD *Denticulopsis dimorpha* (D)	8.6–8.7	14, 15	7H, CC, to 8H-1, 40 cm	65.60–66.00	65.80
26. LAD *Nitzschia denticuloides* (D)	8.7–9.1	10	8H-1, 55 cm, to 8H-1, 142 cm	66.15–67.02	66.59
27. LAD *Craspedodiscus costinodiscus* (D)	+10.70	14	8H-1, 70 cm, to 8H-2, 40 cm	66.30–67.52	66.91
*28. FAD *N. denticuloides* (D)	~14.40	18	8H-2, 42 cm, to 8H-3, 60 cm	67.52–69.20	68.36
Hiatus 5.5–9.0 m.y. duration				69.20–67.52	
*29. LAD *Bogorovia veniamini* (D)	+19.90	13	8H-2, 42 cm, to 8H-3, 60 cm	67.52–69.20	68.36
30. LAD *Rocella gelida* (D)	~21.50	16	10H-3, 143 cm, to 10H-5, 4 cm	89.02–90.64	89.84
31. Top *Reticulofenestra bisecta* Zone (N)	23.70	1, 4	11H-5, 8–9 cm, to 11H, CC	100.19–103.60	100.90
32. Top Chron C7N	25.50	4	13H-4, 45 cm, to 13H-4, 55 cm	118.05–118.15	118.10
33. Base Chron C7N	25.97	4	14H-4, 55 cm, to 14H-4, 65 cm	127.65–127.75	127.75
34. Top *Chiasmolithus altus* Zone (N)	23.7–28.1	2, 4	15H-2, 23 cm, to 15H-4, 23 cm	133.83–136.83	135.33
35. FAD *R. gelida* (D)	~26.00	16, 17	14H, CC, to 15H, CC	132.10–141.60	136.85
36. Top Chron C7AN	26.40	4	15H-4, 45 cm, to 15H-4, 55 cm	137.05–137.15	137.10
37. Top Chron C8N	26.86	4	16H-2, 75 cm, to 16H-2, 85 cm	143.85–143.95	143.90
38. Top Chron C9N	28.15	4	18H-5, 75 cm, to 18H-5, 85 cm	167.35–167.45	167.40
39. Base Chron C9N	29.21	4	20H-3, 5 cm, to 20H-3, 15 cm	182.65–182.75	182.70
40. Top Chron C10N	29.73	4	21H-1, 25 cm, to 21H-1, 35 cm	189.35–189.45	189.40
41. Base Chron C10N	30.33	4	21H-5, 35 cm, to 21H-5, 55 cm	195.45–195.65	195.55
42. Top Chron C11N	31.23	4	23X-2, 145 cm, to 23X-3, 5 cm	208.05–208.15	208.10
43. Top NP22 Zone (N)	34.60	4	27X-5, 61 cm, to 27X-6, 60 cm	249.71–251.20	250.46
44. Top *Clausicoccus subdistichus* acme (N)	35.10	3, 4	27X-7, 1–2 cm, 28X-1, 33 cm	252.60–252.93	252.77
45. Base P18 Zone (F)	36.20	4	31X-2, 122 cm, to 36X-6, 85 cm	280.82–339.95	307.39
46. Top NP18 Zone (N)	37.80	4	35X-5, 26 cm, to 36X-2, 60 cm	322.36–327.71	325.04
Hiatus Maximum duration = 6.0 m.y. (~39–45 Ma) Minimum duration = 2.3 m.y. (40.0–42.3 Ma)				354.78–354.10	
*47. Base NP18 Zone (N)	40.00	4	38X, CC, to 39X-1, 60 cm	354.10–356.30	355.20
*48. Top NP16 Zone (N)	42.30	4	38X, CC, to 39X-1, 60 cm	354.10–356.30	355.20
*49. Base P15 Zone (F)	41.30	7	39X-1, 68 cm, to 39X-2, 66 cm	354.78–356.26	355.52
50. Base P12 Zone (F)	46.00	7	40X-6, 18 cm, to 40X, CC	371.28–373.10	372.19
51. Base NP15 Zone (N)	49.80	4	45X-1, 140 cm, 45X-6, 139 cm	412.50–419.99	416.25
52. Base P10 Zone (F)	52.00	7	47X-7, 29 cm, to 47X, CC	439.60	439.60
53. Base NP14 Zone (N)	52.60	4	49X-3, 56 cm, to 49X-6, 33 cm	452.66–456.93	454.80
54. Base P9 Zone (F)	53.40	4, 6	50X-2, 41 cm, to 50X-3, 10 cm	460.51–461.70	461.11
55. Top NP12 Zone (N)	53.70	4	51X, CC, to 52X, CC	477.60–487.10	482.35
56. Base P8 Zone (F)	55.20	4	52X, CC, to 53X, CC	487.10–496.60	491.85
57. LAD *Fasciculithus* (N)	57.60	4	53X, CC, to 54X-2, 135 cm	496.60–499.45	498.03
58. Base P6 Zone (F)	58.20	4	53X, CC, to 54X, CC	496.60–506.10	501.35
59. Base P5 Zone (F)	58.70	4	54X, CC, to 55X, CC	506.10–508.60	507.35
60. Base NP9 Zone (N)	59.20	4	55X, CC, to 56X-2, 40–41 cm	508.60–510.50	509.55
61. Base P4 Zone (F)	61.00	4	56X-1, 12 cm	>516.22	

[a] + = direct correlation to paleomagnetic stratigraphy; # = absolute age data; * = probable truncation of datum by hiatus; D = diatom; F = planktonic foraminifer; N = carcareous nannofossil.

[b] 1. Wise (1983); 2. Martini and Müller (1986); 3. Perch-Nielsen (1985); 4. Berggren et al. (1985a) (1985b); 6. Jenkins (1985); 7. McGowran (1986); 10. Ciesielski (1983); 11. Chen (1975); 12. Weaver (1983); 13. L. H. Burckle (pers. comm., 1980) in Barron (1985); 14. Barron et al. (1985), Ciesielski (1986); 15. Ciesielski (1986); 16. Gombos (1983); 17. Fenner (1984), 18. Weaver and Gombos (1981), revised based upon Berggren et al. (1985a, 1985b); 19. Hays and Shackleton (1976).

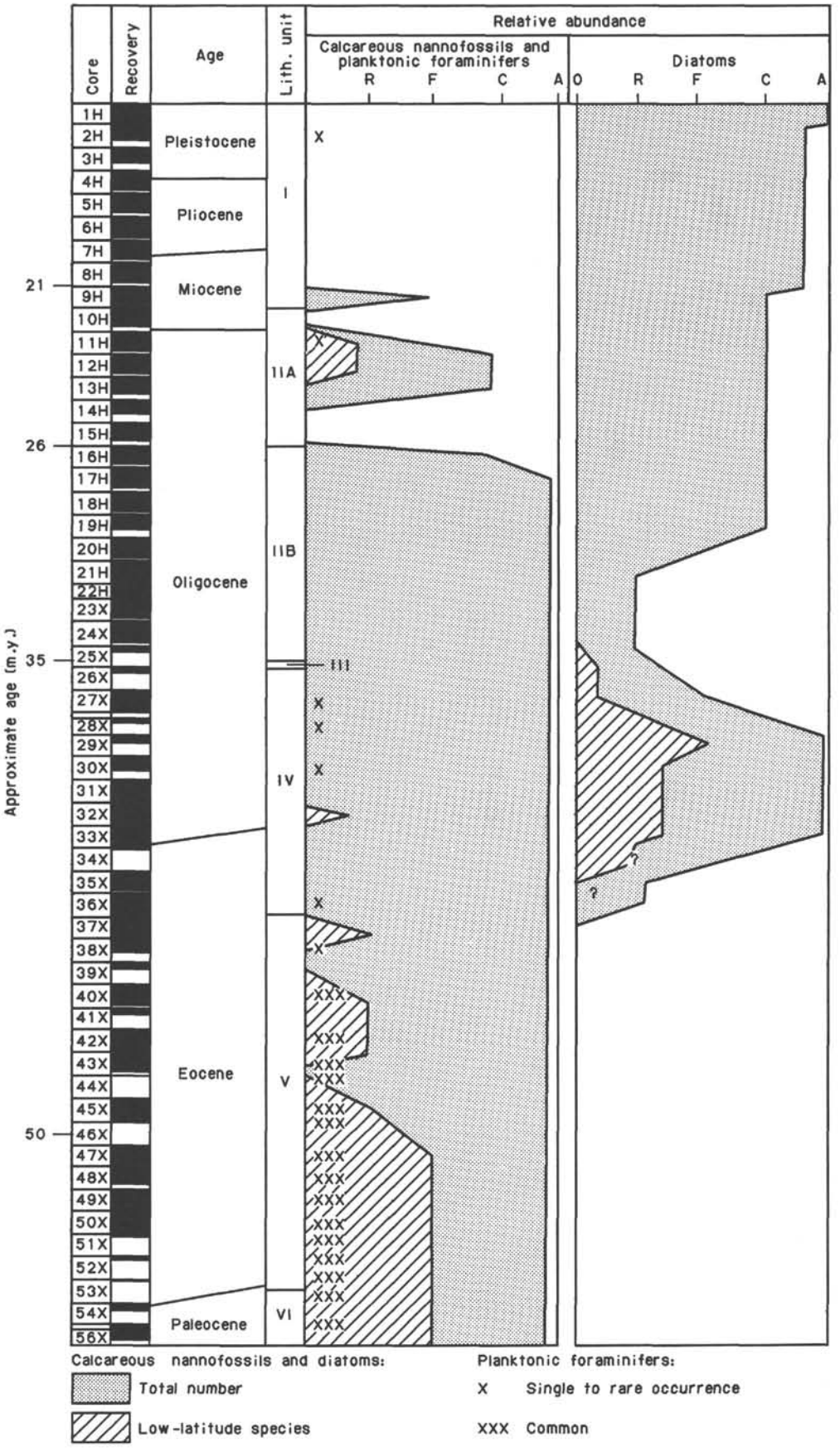

Figure 15. Relative abundance of calcareous microfossils and diatoms through the Tertiary in Hole 699A.

warm-water discoasters, occurring in the uppermost Oligocene. A last, even smaller, peak of a very low-diversity flora occurs in the lowermost Miocene.

Since approximately 21 Ma (the lower Miocene base of lithostratigraphic Unit I), the zone of calcareous productivity was north of this site and biosiliceous accumulation strongly controlled sedimentation rates at Site 699. The cored profile of this unit is characterized by a series of hiatuses. Bulk sedimentation rates (largely biosiliceous and clay) in this unit are high, between 7–25 m/m.y. (Fig. 14).

The highly endemic character of the planktonic siliceous fauna and flora and the number of hiatuses in Unit I suggest that a deep-water connection through the Drake Passage has existed since 21 Ma. The northward migration of the calcareous/siliceous sediment boundary began in the late Oligocene, becoming effective at this site by about 26 Ma. A shallow-water connection with the "large circle" shallow ACC probably existed through the Drake Passage since about 26 Ma, while the "shallow" West Antarctic seaway became gradually closed by glacial ice.

Calcareous Nannofossils

One hundred and four core samples and all the core-catcher samples from Hole 699A were examined for calcareous nannofossils. Most of the samples studied contain rich nannofossil floras. The floras are assigned to the Wise (1983) and Martini (1971) schemes, as described in the "Explanatory Notes" chapter.

Biostratigraphy

Samples 114-699A-1H-2, 60–61 cm, to 114-699A-2H-2, 15–16 cm, are barren of nannofossils. A single sample (114-699A-2H-4, 5–6 cm) yielded a sparse nannofossil flora, which includes *Pseudoemiliania lacunosa* and *Gephyrocapsa* spp.; the co-occurrence of these taxa indicates the presence of middle Pleistocene to upper Pliocene strata. An abundant but non-age-diagnostic flora occurs in Section 114-699A-9H, CC. Samples 114-699A-3H-1, 16–17 cm, through 114-699A-9H-4, 54–55 cm, are either barren or contain rare specimens of *Coccolithus pelagicus*.

Samples 114-699A-10H-2, 9–10 cm, through 114-699A-11H-5, 8–9 cm, are assigned to the *Cyclicarglolithus abisectus* Zone (lower Miocene); those between Section 114-699A-11H, CC, and Sample 114-699A-15H-2, 22–23 cm, are assigned to the *Reticulofenestra bisecta* Zone (lower Miocene–upper Oligocene); and those between Samples 114-699A-15H-4, 23–24 cm, and 114-699A-27X-5, 60–61 cm, are assigned to the *Chiasmolithus altus* Zone (upper lower Oligocene). The tops of all three zones are recognized by the last-appearance datums (LAD) of the nominate taxons.

The *Reticulofenestra davisei* Zone (NP22) (lower Oligocene) is present between Samples 114-699A-27X-6, 60–61 cm, and 114-699A-27X-7, 1–2 cm. The top of this zone is recognized by the LAD of *Reticulofenestra umbilicus*; also present in both samples from this zone is *Isthmolithus recurvus*. Wise (1983) reported that this species did not range above the *Blackites spinosus* zone, its LAD defining the top of that zone. The presence of *B. spinosus* in the *R. davisei* Zone indicates that the lower Oligocene zones of Wise (1983) need to be revised.

The presence of *Clausicoccus subdistichus* in Sample 114-699A-28X-1, 33–34 cm, and its greater abundance in Samples 114-699A-29X-1, 59–60 cm, through 114-699A-30X-1, 146–147 cm, suggest the presence of Zone NP21 (lower Oligocene–upper Eocene). However, the species *Ericsonia formosa* and *Discoaster saipanensis* (the LADs of which, respectively, define the top and base of this zone) were not recorded until much lower in the hole.

Undifferentiated NP21–19 (lower Oligocene–upper Eocene) is inferred below the abundant occurrence of *C. subdistichus* and down to the first-appearance datum (FAD) of *I. recurvus* in Sample 114-699A-30X-3, 87–88 cm, to Section 114-699A-35X, CC. The presence of *D. saipanensis* in the lowest of these samples indicates that at least part of this interval is of Eocene age. The interval between the FAD of *I. recurvus* and the FAD of *Chiasmolithus oamaruensis* defines the NP18 Zone (upper Eocene) in Sample 114-699A-36X-2, 60–61 cm, to Section 114-699A-38X, CC. A possible stratigraphic break occurs between the base of this zone and the top of the underlying NP16 Zone (middle Eocene) at Sample 114-699A-39X-1, 60–61 cm, with NP17 absent.

The NP16 Zone is definitely present between Samples 114-699A-39X-1, 60–61 cm, and 114-699A-42X-4, 4–5 cm, as indicated by the co-occurrence of *Chiasmolithus solitus* and *R. bisecta*. The base of NP16 cannot be defined in most areas outside northwest Europe because of the absence of *Rhabdosphaera gladius*. We use the FAD of *R. bisecta* to define the definite base NP16, with an underlying interval between Samples 114-699A-42X-7, 4–5 cm, and 114-699A-45X-1, 139–140 cm, assigned to NP16–15 (middle Eocene). Supporting evidence for this assignment is provided by the occurrence of *Sphenolithus furcatolithoides* between Samples 114-699A-42X-4, 4–5 cm, and 114-699A-43X-4, 72–73 cm, whereas its base is defined by the occurrence of *Nannotetrina fulgens* in the lowest sample.

Sample 114-699A-45X-6, 139–140 cm, and Section 114-699A-45X, CC, are assigned to NP15–14 (middle lower Eocene) by virtue of their stratigraphic position between NP16–15 and NP14 strata. The presence of NP14 (middle lower Eocene) is inferred from the first downhole occurrence of *Discoaster lodoensis* in Sample 114-699A-47X-1, 116–117 cm. The base of NP14 is defined by the FAD of *Discoaster sublodoensis* and was recorded in Sample 114-699A-49X-3, 55–56 cm.

Sample 114-699A-49X-6, 33–34 cm, through Section 114-699A-51X, CC, are assigned to NP13 (lower Eocene). The interval between Sections 114-699A-52X, CC, and 114-699A-53X, CC, is assigned to NP12–10 (lower Paleocene). The top of NP12 is defined by the LAD of *Tribrachiatus orthostylus*. The index species that mark the base of NP12 and NP11 are absent; thus, NP12 to NP10 are grouped together.

The occurrence of *Fasciculithus tympaniformis* and *Discoaster multiradiatus* between Sample 114-699A-54X-2, 135–136 cm, and Section 114-699A-55X, CC, is taken here to indicate NP9 (upper Paleocene). The true top of NP9 is defined by the FAD of *Tribrachiatus bramlettei*, which is absent in the area of Site 699, so the LAD of *F. tympaniformis* is used to mark the top of the zone. The single sample studied below this interval (Sample 114-699A-56X-2, 40–41 cm) is tentatively assigned to NP8 (upper Paleocene) because it has nannofossil floras similar to those of NP9, but without *D. multiradiatus*.

Paleoenvironment

The dominance of the Oligocene and upper Eocene nannofossil floras by *Reticulofenestra* spp., *Cyclicarglolithus floridanus*, and *Chiasmolithus* spp. is typical of cold-water floras, as is the presence of the high-latitude *I. recurvus*. The absence of the Oligocene *Sphenolithus* spp. and *Discoaster* spp. also support a cold-water environment of deposition. The increasing abundance of discoasters down through the middle lower Eocene probably indicates a warmer water environment of deposition. The absence of *Zygrhablithus bijugatus* from the Oligocene to middle Eocene strata possibly indicates a deeper water environment than that of the lower Eocene to Paleocene where this species is common.

Preservation

The nannofossils recovered from the upper part of the hole above Core 114-699A-27X show etching of the coccoliths. The nannofossil floras are generally well preserved between Cores 114-699A-27X and 114-699A-45X. Below Core 114-699A-45X, the floras show both etching and overgrowth of secondary calcite.

Planktonic Foraminifers

The sediments down to 316 mbsf (Section 114-699A-35X, CC) are mainly siliceous oozes and siliceous nannofossil oozes deposited from the late Eocene/early Oligocene to the Quaternary. Within this stratigraphic interval the samples are almost completely depleted of planktonic foraminifers. In contrast, planktonic foraminifers are present almost continuously from Sections 114-699A-36X, CC, to 114-699A-55X, CC, and offer a discrete stratigraphic resolution for the Eocene and Paleocene part of the section, which is ~175 m thick and composed of nannofossil and micritic nannofossil chalks. In this stratigraphic interval, planktonic foraminifers are the most common microfossils in the >45-μm size fraction.

Biostratigraphy

Sections 114-699A-1H, CC, to 114-699A-26X, CC, are barren, with the exception of Section 114-699A-2H, CC, (few *Neogloboquadrina pachyderma*, <350 μm) and the intervals between Sample 114-699A-12H-1, 131–133 cm, and Section 114-699A-12, CC, where few specimens of "*Globigerina*" *euapertura*, "*Globigerina*" *labiacrassata, Catapsydrax dissimilis*, and *Catapsydrax ciperoensis* occur, indicating a probable late Oligocene age.

Sections 114-699A-27X, CC, 114-699A-28X, CC, and 114-699A-30X, CC, contain a few specimens belonging to *Subbotina angiporoides angiporoides*, "*G.*" *euapertura, Tenuitella insolita, Catapsydrax dissimilis dissimilis, Catapsydrax unicavus, Catapsydrax unicavus primitivus, Catapsydrax martini scandretti*, and *Chiloguembelina linids*.

Section 114-699A-28X, CC, contains only *Catapsydrax* spp. These identified species are indicative of the lower Oligocene *Globigerina brevis* and *Globigerina angiporoides angiporoides* Zones (Jenkins, 1985). This sample is not younger than P19 of the Blow (1969) zonation and is of latest Eocene age. Planktonic foraminifers are absent in Sections 114-699A-32X, CC, to 114-699A-35X, CC, whereas they occur sporadically from Section 114-699A-36X, CC, to Sample 114-699A-39X-1, 66–68 cm. This interval contains few forms belonging to the upper Eocene P17–15 zones.

Sample 114-699A-39X-2, 66–68 cm, is the first sample to contain abundant planktonic foraminifers. Planktonic foraminifers are continuously present and abundant, and therefore, the biostratigraphic resolution is good. Both the zonations of Jenkins (1985) and Berggren et al. (1985a, 1985b) are used to subdivide the underlying section, as follows:

- 114-699A-36X-2, 66–68 cm, to 114-699A-40X, CC: middle Eocene, *Globigerinatheka index* Zone
- 114-699A-41X, 134–136 cm, to 114-699A-44X, CC: middle Eocene, *Acarinina primitiva* Zone (P11)
- 114-699A-45X-1, 103–105 cm, to 114-699A-47X-7, 29–31 cm: middle Eocene, *Acarinina primitiva* Zone (P10–11, lower part)
- 114-699A-47X, CC, to 114-699A-50X-2, 39–41 cm: lower Eocene, *Morozovella crater* Zone (P9)
- 114-699A-50X-3, 10–12 cm, to 114-699A-52X, CC: lower Eocene, *Pseudohastigerina wilcoxensis* Zone (P8)

Section 114-699A-53X, CC, belongs to the lower Eocene because of the presence of *P. wilcoxensis*. The lower Eocene/upper Paleocene boundary is not identifiable. Sample 114-699A-54X, CC, is assigned to upper Paleocene P5 Zone because the marker species of the lower Eocene, *P. wilcoxensis*, is absent. Section 114-699A-55X, CC, through Sample 114-699A-56X-6, 10–12 cm, are assigned to the upper Paleocene Zone P4.

The occurrence and abundance of planktonic foraminifers and their ages are shown in Figure 13. The upper Eocene assemblages are oligotypic with low species diversity, with more than 50% of the specimens belonging to *Globigerinatheka index*, which is the dominant form through the upper middle Eocene and the upper Eocene. *G. index* apparently disappears in Zone P17 according to McGowran (1986). In the upper Eocene, it is associated with *Subbotina angiporoides minima* and *Catapsydrax*, such as *C. unicava, C. globoformis*, and *C. africanus*. Very rare occurrences of *Globorotalia opima nana* are just above the middle Eocene/late Eocene boundary, whereas its occurrences are 25 and 23 m above the boundary at Sites 702 and 703, respectively. This discrepancy could indicate the presence of a hiatus at 354 mbsf. According to the paleomagnetic data of Hole 702B, the *G. index* Zone interval assigned to middle Eocene belongs to Zones P12–14 because although *G. index* is very abundant in Sample 114-699A-40, CC, it is supposed to appear below it. In fact, the FAD of *G. index* falls within the upper part of P11 but is very rare at the beginning of its range.

In the middle Eocene *G. index* Zone, the index fossil is associated with *Subbotina linaperta, Globigerina angiporoides minima*, and several species of *Catapsydrax*.

The *G. index* Zone is characterized by the concurrent range of *G. index* and *A. primitiva*, the LAD of which defines the upper boundary of the zone and the middle Eocene/late Eocene boundary. The upper boundary of the middle Eocene *A. primitiva* Zone is the FAD of *G. index*. In this zone, *A. primitiva* is extremely abundant and associated mainly with low-spired subbotinids such as *Subbotina inaequispira* and the *S. eocaena* group, including a few *S. corpulenta. Globigerinatheka senni* is the only *Globigerinatheka* in this zone. Other acarininids present include *Acarinina pseudotopilensis* and *Acarinina collactea*, but they are rare, and the *Acarinina* assemblage is dominated by *A. primitiva*. In the lower part of this zone there subacute acarininids (with a subangular peripheric margin). Within the *A. primitiva* Zone the *Planorotalites* taxon disappears, and this event has been calibrated to occur in the lower part of P11.

The lower boundary of the *A. primitiva* Zone in this section has been identified because the marker species *Morozovella crater* of the underlying zone disappears in Section 114-699A-47, CC (439.60 mbsf). Within the *M. crater* zone, the characteristic horizon represented by an exceptional abundance of *M. crater* is considered an *M. crater* acme horizon, which was found within Sample 114-699A-49X-4, 32–34 cm, at 453.92 mbsf. The *M. crater* Zone and the FAD of this species is characteristic of Zone P9, according to Blow (1979), and the last occurrence (LO) of *M. crater* (= *Morozovella caucasica*) indicates the early Eocene/middle Eocene boundary (McGowran, 1986).

The upper part of the *P. wilcoxensis* Zone belongs to Zone P8, based on the occurrence of *Acarinina pentacamerata* and *G. senni* in Section 114-699A-51X, CC. The joint occurrence of *Morozovella subbotinae, Morozovella dolabrata*, and *Morozovella lensiformis* in association with *G. senni* of the low- to mid-latitude lower Eocene indicates the presence of the lower part of Zone P8 in Sample 114-699A-52X, CC.

The lower Eocene has a peculiar character in comparison with the younger zones: the greatest species diversity is due to the presence of several species of *Acarinina* common in the low- to midlatitudes, such as *A. pentacamerata, Acarinina wilcoxensis, Acarinina triplex*, and the *Acarinina bullbrooki* group. *Planorotalites pseudoscitulus* and *Planorotalites australiformis* are common. The finding of *M. subbotinae*, a typical warm-water form, is significant, although this species is very rare. Low-

spired subbotinids (*S. patagonica-S. eocaenica* group) are abundant.

The upper Paleocene is characterized by the abundance of *Subbotina triloculinoides* and *Subbotina pseudobulloides*, the LAD of which defines the P4 upper boundary. They are associated with several species of *Planorotalites* and *Acarinina* such as *Planorotalites compressus, Planorotalites chapmani, P. australiformis, Acarinina mckannai, Acarinina convexa, Acarinina nitida, Acarinina esnaensis*, and *Acarinina djanensis*. The typical low-latitude morozovellids of the upper Paleocene are absent.

Paleoenvironment

From the upper Paleocene to the Quaternary, the evolutionary trend of the planktonic foraminiferal content in the sediments shows a maximum abundance through upper Paleocene and lower and middle Eocene, a gradual decrease from the end of middle Eocene to the lower Oligocene, and an almost total disappearance in sediments succeeding the lower Oligocene, where the calcareous plankton are replaced by siliceous ones.

Within the lower Eocene the planktonic foraminifer species diversity is greater than in the younger stages, and the fauna is distinctly diversified with the presence of several species of *Acarinina* and some morozovellids, which are dominant at low and midlatitudes.

In the middle and upper Eocene, the diversity of planktonic foraminifers is low, and the assemblages, dominated by subbotinids, are more characteristic of the high-latitude province with the maximum development of two species: at first *A. primitiva* and, later on, *G. index*, which together dominate with low-spired subbotinids and *Globorotaloides*.

The influx of angular acarininids and few keeled morozovellids, such as *M. subbotinae*, has been noted by Tjalsma (1977) in the lower Eocene at DSDP Site 329 (1519 mbsl) at the eastern end of the Falkland Plateau. According to Tjalsma, the rapid increase in number of species and the invasion by midlatitude angular acarininids and keeled morozovellids during the latest Paleocene and early Eocene indicate a progressive warming trend through most of the early Eocene. Moreover, it must be pointed out that *M. crater*, which is characteristic of lower Eocene in the austral province, can be considered a phenotypic variation of *Morozovella velascoensis*, the dominant tropical form in the upper Paleocene.

A cooling trend is indicated after the early Eocene by the increasing number of *Catapsydrax* and by the great abundance of *G. index*, which is the unique *Globigerinatheka* of the high-latitude late Eocene. This species is the last *Globigerinatheka* to disappear from midlatitudes in regions influenced by a gradual cooling around the Eocene/Oligocene boundary.

The state of preservation of the planktonic foraminifer assemblages indicates deposition above the foraminifer lysocline from the Paleocene to the middle Eocene, but the strong decrease in abundance during the late Eocene and the almost total disappearance of the calcareous plankton through the Oligocene probably results from intense dissolution. Only few dissolution-resistant forms, such as *Catapsydrax* and "*G.*" *labiacrassata* have been found; they are associated with rare but well-preserved benthic foraminifers. Such thanatocoenoses are indicative of sediments deposited below the foraminifer lysocline near the carbonate compensation depth (CCD). Moreover, in more elevated regions such as Site 329, which is at the same approximate latitude as Site 699, planktonic foraminifer assemblages were found in the Oligocene and Neogene; this means that the disappearance of planktonic foraminifers is related partially to the depth of deposition.

Preservation

Planktonic foraminifers are moderately to well-preserved in the Paleocene and lower Eocene. They begin to show signs of strong dissolution in the upper middle Eocene. Within the upper Eocene the assemblages have undergone selective dissolution.

Benthic Foraminifers

Preservation of benthic foraminifers at Hole 699A is generally good below Section 114-699A-15H, CC. Above this, the core catchers are barren or nearly barren and contain, at most, several benthic foraminiferal specimens per sample. There are few or no planktonic foraminifers preserved above Section 114-699A-42X, CC; below this, there is a rapid downhole increase in the planktonic/benthic foraminifer ratio, reflecting a middle middle Eocene shallowing of the CCD/foraminifer lysocline. There is evidence of recrystallization in both planktonic and benthic foraminifers from Section 114-699A-52X, CC, to the bottom of the hole.

Sections 114-699A-1H, CC, to 114-699A-15H, CC, are nearly barren, with rare specimens of *Clavulina* sp., *Cyclammina* sp., *Dentalina* spp., *Martinottiella* sp., *Spirosigmoilinella compressa*, and *Stilostomella* spp. in a few samples. Sections 114-699A-18H, CC, and 114-699A-30X, CC, are barren. The exception is Section 114-699A-11H, CC, which contains a well-preserved assemblage consisting of *Cibicidoides eocaena, Eggerella bradyi, Globocassidulina subglobosa, Oridorsalis* spp., *Pullenia bulloides, S. compressa, Stilostomella* spp., and *Uvigerina* sp. Section 114-699A-16H, CC, contains a well-preserved but sparse fauna of *Gyroidinoides* spp., *Oridorsalis* spp., and pleurostomellids. Well-preserved calcareous faunas are found consistently beginning in Section 114-699A-17H, CC, with the exception of Section 114-699A-18H, CC. Sections 114-699A-17H, CC, 114-699A-19H, CC, and 114-699A-20H, CC, contain *Astrononion pusillum, Laticarinina pauperata, Nuttalides umbonifera, G. subglobosa, Gyroidinoides* spp., *Oridorsalis* spp., *P. bulloides, Pullenia quinqueloba*, and *Stilostomella* spp.

The Oligocene fauna at Hole 699A becomes established downhole beginning in Section 114-699A-21H, CC. The dominant taxa are *C. eocaena, Cibicidoides praemundulus, N. umbonifera, Anomalinoides capitatus, G. subglobosa, P. bulloides*, and *P. quinqueloba. Cibicidoides bradyi, Cibicidoides grimsdalei, Cibicidoides micrus, S. compressa, Plectina* sp., *E. bradyi*, and *Nonion havanensis* are common. Undifferentiated frequent taxa include *Gyroidinoides* spp., *Oridorsalis* spp., *Stilostomella* spp., *Pleurostomella* spp., pleurostomellids, and polymorphinids. The fauna in Section 114-699A-26X, CC, is atypical in that its most abundant taxon is the miliolid *S. compressa*, whereas the hyaline fauna is sparse. This assemblage is clearly inconsistent with surrounding faunas is most likely not *in situ*. Evidence of reworking and contamination in the Oligocene section includes *Nuttalides truempyi* and reworked unrecognizable specimens in Section 114-699A-21H, CC, *N. truempyi* and shallow-water *Cibicidoides incrassatus* (outer neritic through bathyal depths) in Section 114-699A-22H, CC, and *N. truempyi* in Section 114-699A-23X, CC.

The downhole benthic foraminifer assemblage becomes abundant and very diverse from Sections 114-699A-40X, CC, to 114-699A-42X, CC, and remains so throughout the upper Paleocene–lower middle Eocene. The Eocene assemblage is dominated by *N. truempyi, C. eocaena, Cibicidoides praemundulus, P. bulloides, Pullenia eocenica*, and *P. quinqueloba* and is further characterized by common occurrences of *C. grimsdalei, C. havanensis, C. micrus, A. capitatus, Anomalinoides semicribratus, Hanzawaia ammophila, N. havanensis*, and *Spiroplectammina spectabilis*. Agglutinated taxa occur sporadically and include *Cyclammina* sp., *Dorothia trochoides, E. bradyi, Gaudryina laevigata, K. subglabra, Karreriella chapapotensis, Martinottiella* sp., *Plectina* sp., and *Textularia* sp. The buliminids are a consistent component of the fauna in and below Sample 114-699A-42X, CC, and include *Buliminella grata, Bulimina glomarchallengeri, Bulimina jarvisi, Bulimina semicostata*, and *Bulimina*

trinitatensis. *Alabamina dissonata* becomes a dominant contributor to the fauna from Section 114-699A-42X, CC, and below.

The decrease in benthic foraminifer diversity between Sections 114-699A-42X, CC, and 114-699A-39X, CC, coincides with the last abundant planktonic foraminifers. This reflects a relative shallowing of the CCD/foraminiferal lysocline at this time. *Aragonia aragonensis* occurs consistently in and below Section 114-699A-45X, CC. *Clinapertina complanata* and *Osangularia mexicana* are common from Section 114-699A-50X, CC, to the base of the hole. The fauna of Section 114-699A-50X, CC, contains Paleocene or older contaminants, including *Stensioina beccariiformis* and *Anomalinoides rubiginosus*.

A significant faunal change occurs between the Eocene fauna and the Paleocene fauna in Sections 114-699A-54X, CC, and 114-699A-55X, CC. The diverse Paleocene assemblage is dominated by *N. truempyi* and *S. beccariiformis*, with occurrences of *A. capitatus, Anomalinoides praeacuta, Aragonia velascoensis, Bolivinoides delicatulus, Cibicidoides hyphalus, Gyroidinoides globulosus, Neoeponides hildebrandti, Neoeponides lunata, Neoflabellina semireticulata, Osangularia velascoensis, Gaudryina pyramidata, D. trochoides*, and *Tritaxia paleocenica*.

Paleocene and Eocene paleodepth estimates for Hole 699A are based on Tjalsma and Lohmann's (1983) study of paleobathymetric ranges from 27 Atlantic locations in which they delineated two distinct Paleocene benthic foraminiferal assemblages related to paleobathymetry: the bathyal to upper abyssal *S. beccariiformis* assemblage was gradually restricted by the depth range expansion of the deeper *N. truempyi* assemblage through the Paleocene.

The dominance of *N. truempyi* over *S. beccariiformis* along with high abundances of *C. hyphalus* and low abundances of *Lenticulina* spp. in the Paleocene samples at Hole 699A suggest that the paleodepth was 2000–3000 m. An Eocene paleobathymetric estimate of 2500–3000 m is supported by low abundances of *Lenticulina* spp., *Abyssamina* spp., and *Clinapertina* spp. and moderate abundances of *A. dissonata* in an Eocene assemblage that is otherwise typical of abyssal depths. An abyssal paleodepth at Hole 699A is further supported by the lack of the characteristic influx of new bathyal late Eocene and Oligocene *Uvigerina* and *Bolivina* species (Tjalsma and Lohmann, 1983). The Oligocene taxonomic upper depth limits defined by van Morkhoven et al. (1986) for cosmopolitan deep-water benthic foraminifers support evidence for a benthic foraminiferal assemblage from the abyssal (>2000 m) zone.

The Paleogene benthic foraminifer assemblages from Hole 699A are more diverse than those described from DSDP Sites 511 and 512, although Hole 699A includes the dominant taxa found at these other sites. An important component present at Hole 699A that is absent from Sites 511 and 512 is *N. truempyi*, suggesting that this site may be somewhat deeper than the Paleogene lower bathyal depths interpreted at those sites (Basov and Krasheninnikov, 1983). The Oligocene sediments recovered at Hole 699A yield a fauna that is similar but more diverse than that found at DSDP Site 513 (Basov and Krasheninnikov, 1983). Similarly, *N. umbonifera* is common at Hole 699A but absent at Site 513, implying that Hole 699A may have been slightly deeper at this time.

Diatoms

In Hole 699A the entire Neogene section and upper part of the Paleogene through the upper Eocene contain siliceous microfossils. Below Core 114-699A-36X diatoms are dissolved, and below Core 114-699A-40X the authigenic silicate clinoptilolite is dominant in the silt fraction (compare with Fig. 18, "Geochemistry" section, this chapter). In the interval from Cores 114-699A-21H to 114-699A-27X the diatom abundance is reduced to rare and few, and their preservation is poor, which also results in low diversity. Otherwise, their preservation in the diatomaceous sediments is moderate to good, with the number of diatom species per approximately 1000 checked varying between 15 and 30.

For the upper Neogene, the zonation of Ciesielski (1983), which provides the highest stratigraphic resolution, was applied. For the lower Neogene the zonation of Weaver and Gombos (1981) was followed.

Biostratigraphy

Core 114-699A-1H to Sample 114-699A-2H-5, 74 cm, were assigned to the *Coscinodiscus lentiginosus* Zone McCollum (1975). In Sample 114-699A-2H, 15 cm, *Actinocyclus ingens* and *Coscinodiscus elliptipora* are present together with several species of the genus *Rouxia*. *Rhizosolenia barboi* occurs only as single sporadic specimens in the Neogene section below; therefore, its LO was not used as a datum at this site. Thus, the *A. ingens–C. elliptipora* Zone and the *R. barboi–Nitzschia kerguelensis* Zone were not differentiated. Together, both cover the interval from Samples 114-699A-2H-2, 15 cm, to 114-699A-3H-3, 60 cm.

Sample 114-699A-3H-4, 110 cm, to Section 114-699A-3H, CC, were assigned to the *C. kolbei–R. barboi* Zone (1.89–2.22 Ma). The presence of *Coscinodiscus vulnificus* above the last *Cosmiodiscus insignis* places the interval between Samples 114-699A-4H-1, 124 cm, and 114-699A-4H-2, 143 cm, in the lower Matuyama *C. vulnificus* Zone (2.20–2.49 Ma). A single sample, 114-699A-4H-3, 40 cm, is assigned to the *C. insignis* Zone (2.49–2.64 Ma) of the late Gauss Chron.

The presence of a hiatus is indicated between Samples 114-699A-4H-4, 10 cm, and 114-699A-4H-3, 40 cm, by the joint LOs of *Nitzschia weaveri* and *Nitzschia interfrigidaria* in the former sample. The *N. weaveri* Zone and possibly parts of the overlying *C. insignis* Zone and underlying *N. interfrigidaria-C. vulnificus* Zone are missing. The intervening hiatus represents a period between approximately 2.5 and 2.8 to 2.9 Ma.

Between Samples 114-699A-4H-4, 10 cm, and 114-699A-5H-1, 84 cm, diatom floras are characteristic of the *N. interfrigidaria/C. vulnificus* Zone (2.81–3.10 Ma). The FAD of *N. weaveri* and *C. vulnificus* are concurrent in Sample 114-699A-5H-2, 41 cm, indicative of the absence of the *N. interfrigidaria* Zone (3.10–3.88 Ma) and a hiatus between this and the aforementioned sample.

Beneath the lower/upper Pliocene hiatus, the *Nitzschia praeinterfrigidaria* Zone (3.88–4.02 Ma) was encountered down to the FAD of *N. interfrigidaria* in Sample 114-699A-5H-4, 43 cm. Conformable with the overlying zone is the *Nitzschia angulata* Zone (4.02–4.20 Ma) down to the FAD of the nominate species in Section 114-699A-5H, CC. The absence of *N. angulata* and *Denticulopsis hustedtii* is the basis of inferring the presence of the *Nitzschia reinholdii* Zone (4.20–4.88 Ma) in Sample 114-699A-6H-1, 3 cm. The upper Miocene–lower Pliocene *D. hustedtii* Zone was encountered between Samples 114-699A-6H-2, 6 cm, and 114-699A-7H-3, 5 cm.

The LO of *Denticulopsis lauta* (8.7 Ma) occurs in Sample 114-699A-7H-5, 5 cm, representing the top of the *D. hustedtii/D. lauta* Zone. A combination of data from radiolarians and diatoms suggests the presence of a significant hiatus between this datum and a position in the middle to lower part of Core 114-699A-7H, which may represent the uppermost Miocene to lowermost Pliocene (8.5–4.5 Ma: Fig. 14 and Table 3). Further study is required to delineate this hiatus.

The LADs of *Denticulopsis dimorpha* (8.6–8.7 Ma) and *Nitzschia denticuloides* (8.7–9.1 Ma) occur in Sample 114-699A-8H-1, 40 cm, and the LAD of *Craspedodiscus coscinodiscus* (10.7 Ma) occurs in Sample 114-699A-8H-2, 40 cm. The middle/upper Miocene boundary thus falls between these samples, and the in-

terval between Samples 114-699A-7H-5, 5 cm, and 114-699A-8H-2, 40 cm, is latest middle Miocene to early late Miocene in age.

Bogorovia veniamini is found in Sample 114-699A-8H-3, 60 cm, which places the interval down to Sample 114-699A-10H-3, 146 cm, in the *B. veniamini* Zone Weaver and Gombos (1981) and requires a relatively large hiatus in the upper part of Core 114-699A-8H. Sediments representing a time duration of approximately 9.0 m.y. (see Fig. 14) are missing.

Single manganese nodules were found throughout Cores 114-699A-8H and 114-699A-9H.

From about the middle Miocene and downward, the stratigraphic resolution of known planktonic diatom datums decreases, and erosional events of relatively short duration can not be delineated as in the overlying Neogene section.

The stratigraphic zonation of Fenner (1984) was used for the Oligocene–lowermost Miocene because most of the marker species used by Gombos and Ciesielski (1983) are not present at this site.

Rocella gelida occurs from Sample 114-699A-10H-5, 4 cm, to Section 114-699A-14H, CC, placing this interval in the *R. gelida* Zone Fenner (1984). Sections 114-699A-15H, CC, to 114-699A-22H, CC, and possibly 114-699A-23X, CC, are in the *Rocella vigilans* Zone Fenner (1984) as well. But preservation in the latter section is too poor to be certain. The presence of a well-preserved and diverse calcareous nannofossil flora in the Oligocene (compare nannofossil results) makes it possible to estimate the duration of this zone as extending from just above the upper boundary of the *Chiasmolithus altus* Zone Wise (1983), which seems to fall in magnetic Chron C8 (see "Paleomagnetics" section, this chapter), to the lower part of that zone. This is the upper part of the lower Oligocene (equivalent to somewhere in NP22). Above Section 114-699A-23X, CC, *Pyxilla reticulata* (*prolongata* type) becomes very rare.

The presence of *Rhizosolenia antarctica* in Sections 114-699A-24X, CC, to 114-699A-28X, CC, places this interval in the lower Oligocene *R. antarctica* Zone Fenner (1984). This species is absent in the samples below. *Rhizosolenia gravida* is found in Sections 114-699A-29X, CC, and 114-699A-30X, CC, with a number of *Cestodiscus* species characteristic of the lower Oligocene, which place these two cores in the *R. gravida* Zone Fenner (1984).

Dating by planktonic diatoms becomes increasingly difficult below Section 114-699A-32X, CC. Cores 114-699A-32X to 114-699A-34X seem to be close in age to the Eocene/Oligocene boundary. Preservation of diatoms becomes poor in Cores 114-699A-35X and 114-699A-36X, but the fragments found suggest an Eocene age.

The diatom assemblages suggest open-ocean conditions for this site from the late Eocene to Recent, as benthic and meroplanktonic species are rare to very rare. In the uppermost Eocene to lowermost Oligocene (up to Section 114-699A-28X, CC), species that are commonly found in the low latitudes occur with a frequent abundance. Above Section 114-699A-28X, CC, no low-latitude species are found, and the flora becomes increasingly endemic.

Radiolarians

Radiolarians are generally abundant and well preserved from Sections 114-699A-1H, CC, to 114-699A-34X, CC. In Sections 114-699A-1H, CC, and 114-699A-2H CC, *Stylatractus universus* was observed together with modern antarctic forms, indicating that the samples are in the *S. universus* Zone. This suggests that the Recent *Antarctissa denticulatala* Zone is either absent from the site or within Core 114-699A-1H. Section 114-699A-3H, CC, is assigned to *Saturnalis circularis* by the presence of the named species. The joint occurrence of *Helotholus vema* and *Desmospyris spongiosa* suggests the lower Pliocene *H. vema* Zone for Sections 114-699A-4H, CC, and 114-699A-5H, CC; therefore, the upper Pliocene *Eucyrtidium calvertense* Zone is probably within Section 114-699A-4H, CC. The presence of *Amphymenium challengerae* in Section 114-699A-6H, CC, and *Stichocorys peregrina* in Section 144-699A-7H, CC, indicates the *H. vema* Zone of Chen (1975) and the *S. peregrina* Zone of Weaver (1983).

From Sections 114-699A-8H, CC, through 114-699A-34X, CC, of the lower Miocene–Oligocene section, Chen's (1975) scheme could not be followed because his index forms were not observed from Miocene sediments. Numerous new forms were encountered from Oligocene samples, and it is interesting to note that many of these new forms are much larger in size compared with those observed elsewhere from sediments of correlative age.

No radiolarians were observed from Section 114-699A-39X, CC.

Silicoflagellates

Silicoflagellates were observed only from Neogene and Oligocene samples. Because Site 699 is close to Sites 511 and 513 of DSDP Leg 71, the zonation proposed by Shaw and Ciesielski (1983) could be compared directly.

Probable assignment can be made for Sections 114-699A-8R, CC to 114-699A-12R, CC, to the *Naviculopsis biapiculata* Zone and Sections 114-699A-13R, CC, to 114-699A-18R, CC, to the *Corbisema archangelskiana* Zone.

Silicoflagellates were absent from Eocene and Paleocene sections, between Sections 114-699A-35X, CC, to 114-699A-55X, CC, the basal recovery of the hole.

Ebridians

Moderately well-preserved ebridians occur in many samples ranging in age from Pliocene to Oligocene. The LO of *Ammodochium rectagulare* is in the upper Pliocene Section 114-699A-3H, CC, which agrees well with results from the North Pacific (Ling, 1971). Some of the forms recognized from Site 699 are closely related to, if not co-specific, with those reported by Perch-Nielsen (1975) from Oligocene and Eocene sediments of this sector of the antarctic region. The occurrence of ebridians therefore needs close evaluation before their biostratigraphic distribution and zonation can be established.

GEOCHEMISTRY

Pore waters in Hole 699A were squeezed from eighteen 5- or 10-cm whole-round samples taken throughout the section at about 30-m intervals. The results of the pore-water chemistry are reported in Table 4 and in Figures 16 through 18.

Pore-water chemistry reflects primarily alteration reactions with basalt basement below the recovered section and siliceous reactions within the sediment column to produce zeolites.

Headspace samples from every core were analyzed for volatile hydrocarbon gases (Table 5). Sedimentary organic carbon and calcium carbonate were determined for most sections (Table 6).

Salinity and Chloride

Salinity and chloride profiles reflect the salinity of the water column overlying the sediment column. Salinities and chloride concentrations below 10 mbsf are slightly higher than those of present-day seawater at this location and probably reflect diffusional profiles resulting from higher salinities during the last glacial maximum (McDuff, 1985). Low salinities and chloride concentrations below 330 mbsf to the bottom of the hole are difficult to explain. Circulation of surface seawater to the bottom of the hole during drilling operations and subsequent contamination of disturbed cores might dilute salinities somewhat but do not explain values less than about 34.5 per mil. This ex-

Table 4. Interstitial-water chemistry from Hole 699A.

Sample (core, section, cm)	Depth (mbsf)	Volume (mL)	pH	Alkalinity (mmol/L)	Salinity (g/kg)	Magnesium (mmol/L)	Calcium (mmol/L)	Chloride (mmol/L)	SO_4 (mmol/L)	Fluoride (μmol/L)	SiO_2 (μmol/L)	Mg/Ca
1H-4, 145–150	5.95	95	7.73	3.09	34.2	51.48	10.88	554.06	28.30	62.20	822	4.73
3H-3, 145–150	22.55	73	7.46	3.45	35.4	51.24	12.49	569.86	27.90	41.10	730	4.10
6H-5, 145–150	54.05	70	7.83	4.08	35.0	48.89	14.60	568.87	26.80	41.40	872	3.35
9H-4, 145–150	81.05	105	7.78	4.50	35.0	47.85	16.12	565.91	26.30	41.90	984	2.97
12H-4, 145–150	109.55	60	7.76	4.51	35.0	47.47	18.04	566.90	25.10	36.00	950	2.63
15H-3, 145–150	136.55	58	7.46	4.79	35.0	45.80	19.63	559.99	25.10	30.90	997	2.33
18H-4, 145–150	166.55	58	7.22	4.54	34.8	44.73	20.85	560.97	24.80	28.50	1152	2.15
21H-4, 140–150	195.00	120	7.24	4.71	34.8	43.37	22.85	565.94	24.30	25.90	1090	1.90
24X-2, 140–150	217.50	42	8.14	4.94	34.8	43.74	22.84	567.92	24.40	22.20	1073	1.92
30X-3, 140–150	273.00	120	7.25	5.60	35.0	40.59	26.67	568.91	23.90	19.00	1094	1.52
33X-5, 140–150	304.50	80	7.23	5.23	35.0	40.75	26.75	570.89	23.60	19.40	1032	1.52
36X-5, 140–150	333.00	32	7.25	4.98	34.8	38.81	28.85	569.90	23.60	17.50	1146	1.35
39X-1, 140–150	355.50	6	7.85	4.79	34.0	41.18	33.58	536.20	21.00	16.30	655	1.23
42X-5, 140–150	390.00	9			33.7	39.51	36.27	539.18	20.30	19.30	595	1.09
45X-5, 140–150	418.50	4			33.8	37.02	35.36	559.00	22.10	26.10	508	1.05
48X-4, 140–150	445.50	12	7.19	3.56				555.03	25.20	34.50	408	
48X-4, 140–150	445.50	18	7.43	3.71	33.8			551.07		33.80	484	
54X-1, 140–150	498.00	4			32.3	33.60	38.62	531.25	19.40	30.20	577	0.87

planation would also require that the other chemical constituents be diluted by the introduction of surface seawater, which does not seem to be the case. Clay membrane filtration (high-pressure reverse osmosis) might be responsible for separating salts from water near the bottom of this hole.

Calcium and Magnesium

Calcium concentrations increase downhole from a bottom-water concentration of 10 to about 38 mmol/L, whereas magnesium decreases from a bottom-water concentration of 55 mmol/L to about 34 mmol/L at the bottom of the hole. The magnesium/calcium ratio decreases downhole from seawater values of 5.2 to about 1.0. A plot of calcium vs. magnesium demonstrates that the relative changes in their concentrations are linear, i.e., conservative (Fig. 17).

These observations are consistent with simple diffusive exchange of seawater Ca and Mg through the sediment column being driven by low-temperature basalt alteration reactions in the basement (McDuff, 1981; Gieskes and Lawrence, 1981; Gieskes, 1983). Weathering of basalts consumes magnesium in the production of Mg-smectites and Mg-hydroxysilicates and releases calcium from plagioclase dissolution. The nearly linear vertical profiles of calcium and magnesium through the sediment column suggest that any upward and/or downward advection in the past of fluids through the sediments (driven by circulation cells in the underlying basalts) have ceased at this site. A conservative magnesium vs. calcium plot infers that there are no longer significant reactions within the sediment column either producing calcium or consuming magnesium. There are apparently no sedimentary dolomitization, smectite formation, volcanic ash alteration, or calcite recrystallization reactions presently occurring in the upper 500 m of the sediment column at this site. Assuming that this is true of the sediment column below the recovered interval and that the magnesium gradient (about 4 mmol/L/100 m) continues to decrease downward linearly, then the depth at which Mg approaches zero (maximum depth of inferred basement) is over 1000 mbsf at this site.

Alkalinity

Alkalinity increases downhole from bottom-water concentrations of about 2.5 mmol/L to a maximum of about 5.6 mmol/L at 273 mbsf. Below this depth, alkalinity decreases again to about 3.6 mmol/L at 450 mbsf. This profile reflects the increase in alkalinity resulting from slight organic regeneration and carbonate dissolution in the upper 250 m. Dissolution is particularly pronounced where alkalinity is at a maximum (273 mbsf), which may represent a dissolution horizon. The downward linear decrease in alkalinity may reflect alkalinity consumption at or near basement as a result of calcite precipitation reactions related to the weathering of basalts. These deep alkalinity changes are too small to be reflected in the observed calcium concentrations.

Fluoride, Silica, and Sulfate

Fluoride decreases downhole from bottom-water concentrations of 70 μmol/L to a minimum of about 16 μmol/L at 356 mbsf and then increases again to values of 30–35 μmol/L in the bottom 50 m of the hole. This profile requires consumption of fluoride by incorporation into some unidentified mineral phase between about 0–20 mbsf and between 300 and 400 mbsf, perhaps by sorption onto clays or by formation of carbonate fluorapatite (Froelich et al., 1983).

Dissolved silica increases downhole from bottom-water concentrations of about 80 μmol/L to a maximum of about 1100 μmol/L between 170 and 330 mbsf. Below 330 mbsf, dissolved silica concentrations decrease dramatically to levels of about 500 μmol/L. The interval between 333 and 355 mbsf thus displays a dramatic downward silica gradient that requires intense silica dissolution at 330 mbsf and concomitant precipitation of an authigenic siliceous phase at about 355 mbsf. This horizon corresponds to the depth at which the upper diatomaceous-rich unit is replaced by lower diatom-barren and zeolite-rich nannofossil oozes (Fig. 18; also see "Biostratigraphy" section). These data suggest that diatoms at the base of the upper Eocene–lower Oligocene diatomaceous unit are dissolving and providing a diffusive flux of silica downward that precipitates into authigenic silicates presently forming at the top of the zeolite-rich unit. Clinoptilolite was positively identified as the dominant zeolite in this unit both microscopically and by X-ray diffraction. Thus, these data suggest that zeolites are presently forming in Hole 699A from silica derived by the dissolution of diatoms buried higher up in the section.

Sulfate decreases slightly from bottom-water concentrations of 28 mmol/L to a minimum of 19 mmol/L near the bottom of the hole. The entire sediment column above 500 mbsf is thus suboxic (depleted in oxygen) but not strongly anoxic (depleted in sulfate). The presence of intact manganese nodules 11–20 Ma old buried both above and below an unconformity at this site attests to the low organic carbon reactivity and thus the preservation of MnO_2.

Volatile Hydrocarbon Gases

Headspace analyses for volatile hydrocarbon gases in Hole 699A are tabulated in Table 5. Methane (C_1) and ethane (C_2) are both at very low levels. Organic carbon is very low in these sedi-

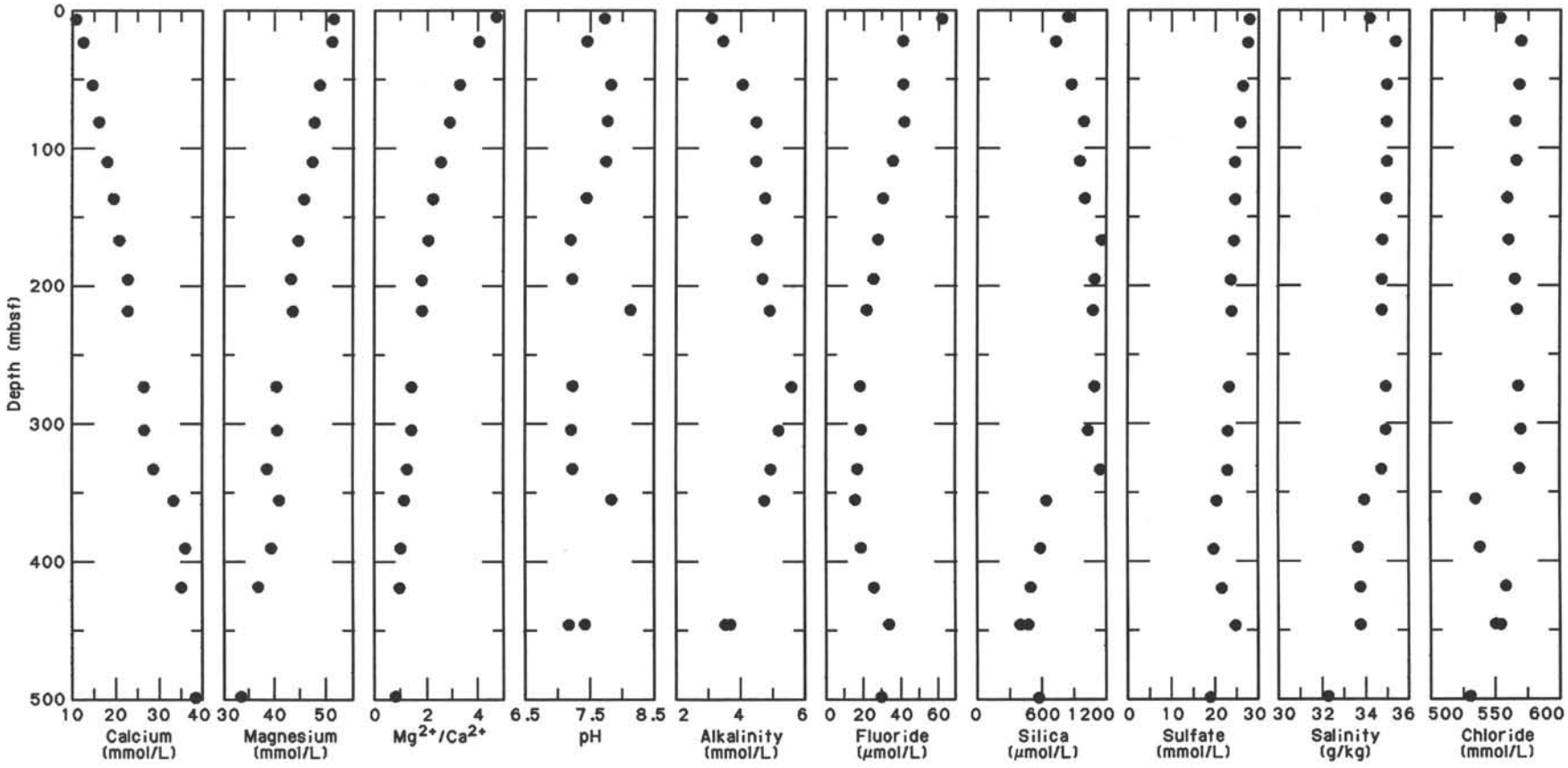

Figure 16. Pore-water calcium, magnesium, Mg/Ca ratio, pH, titration alkalinity, fluoride, sulfate, dissolved silica, salinity, and chloride profiles, Hole 699A.

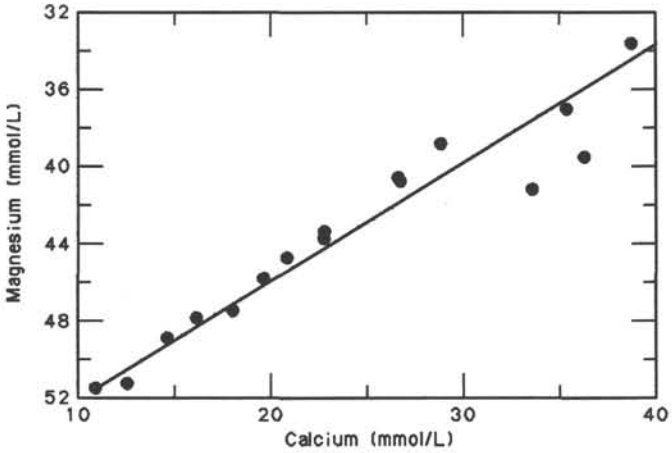

Figure 17. Pore-water calcium vs. magnesium, Hole 699A.

ments (see the following) and sulfate is never depleted. Methanogenesis is not an important process here.

Sedimentary Organic and Inorganic Carbon

In general, calcium carbonate content increases irregularly downhole, reflecting changes coincident with lithostratigraphic unit boundaries. Carbonate content is low (usually less than 5% but never more than 40%) in the upper siliceous clay units and high (60%–80%) in the lower nannofossil oozes. Carbonate is completely lacking in the upper Neogene biosiliceous Unit I (0–85.7 mbsf) and begins occurring sporadically as nannofossil oozes between 85.7 and 233.6 mbsf (Unit II) in the lower Miocene–lower Oligocene. Below the gravel layer (Unit III) at 235 mbsf, carbonate dominates the biogenic component of the sediments in the form of nannofossil oozes and chalk. Carbonate-poor horizons in the lower section are either diatom rich (290.1 mbsf) or clay rich (369.1 and 497.6 mbsf), suggesting short intervals of high siliceous productivity and/or carbonate dissolution during periods dominated by nannofossil deposition.

Organic carbon values in the upper 30 m of the hole are low, ranging from 0% to about 0.4%. Below 30 m, there is virtually no detectable organic carbon. Statistical analysis of the organic carbon data below 30 mbsf suggests that the organic carbon content of these sediments is indistinguishable from zero (less than 0.08%).

PALEOMAGNETICS

Introduction and Procedures

The archive halves of each core section from Hole 699A were measured at 10-cm intervals using the three-axis, pass-through, cryogenic magnetometer. After measuring the natural remanent magnetization (NRM), the archive halves were partially demagnetized with alternating fields of 5 to 9 mT using the in-line alternating field (AF) demagnetizer. Twenty-nine discrete samples were measured using the Molspin spinner magnetometer. Detailed progressive AF demagnetization studies were conducted on representative samples from the section. These samples were partially demagnetized using a Schonstedt AF demagnetizer at increments ranging from 5 to 10 mT up to a maximum of 70 mT. Treatment at peak fields greater than 30 mT occasionally resulted in anomalous behavior, which appears to be the result of intermittent malfunctioning of the demagnetizer.

Magnetic susceptibility measurements were made using the pass-through Bartington susceptibility meter. Whole-core measurements made at 10-cm intervals on all APC-recovered core sections from Hole 699A provide a fairly complete record of

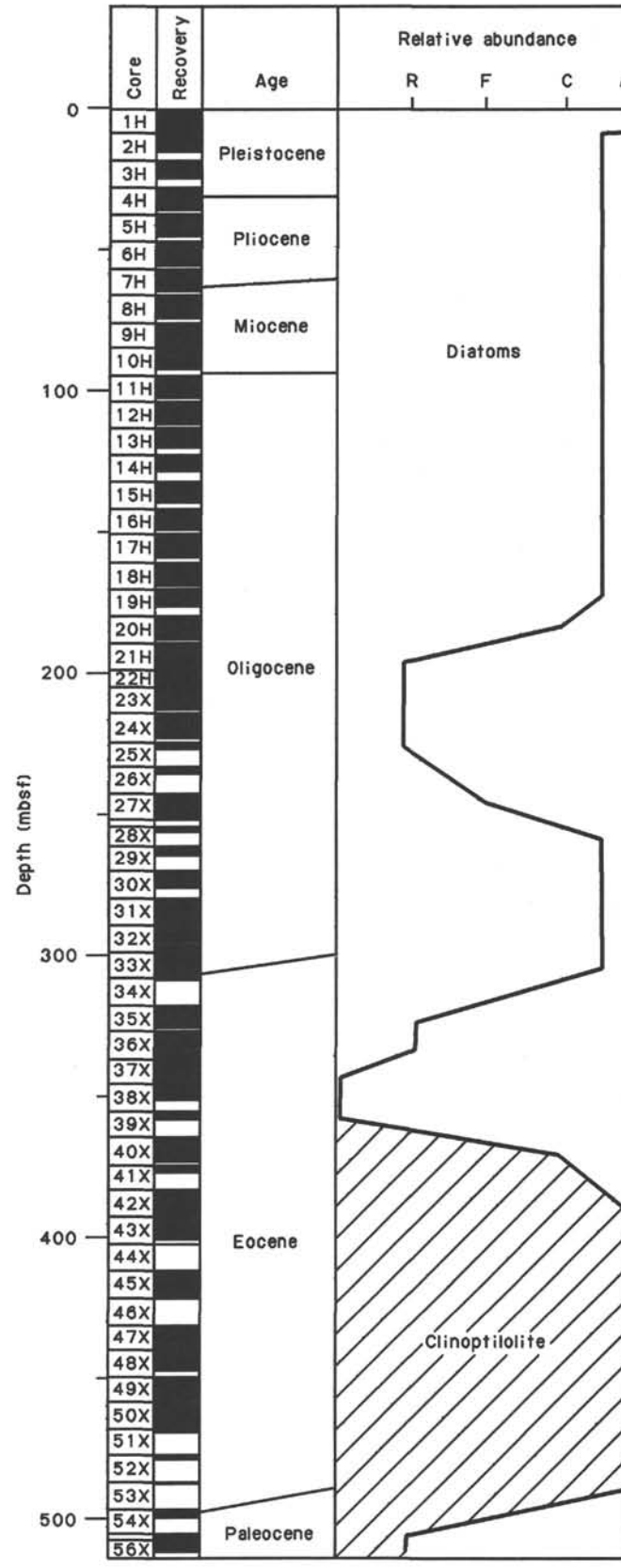

Figure 18. Relative abundance of diatoms and zeolites (clinoptilolite) in Hole 699A.

Table 5. Volatile hydrocarbon gases (methane and ethane) from Hole 699A headspace samples.

Sample (core, section, cm)	Depth (mbsf)	C_1 (ppm)	C_2 (ppm)
1H-3, 148–150	4.48	1.7	0.9
2H-3, 148–150	13.08	3.0	0.0
3H-3, 143–145	22.53	2.7	0.5
4H-3, 145–150	32.05	3.7	0.6
5H-4, 145–150	43.05	5.7	1.0
6H-5, 145–150	54.05	5.3	0.6
7H-4, 145–150	62.05	5.4	0.5
8H-5, 145–150	73.05	5.7	0.0
10H-5, 145–150	92.05	6.2	0.7
11H-4, 145–150	100.05	5.1	0.6
12H-4, 145–150	109.55	5.5	0.8
13H-3, 145–150	117.55	5.6	0.8
14H-3, 145–150	127.05	3.8	0.3
15H-4, 145–150	138.05	5.8	0.0
16H-4, 145–150	147.55	7.1	0.8
17H-4, 145–150	157.05	7.4	0.8
18H-3, 145–150	165.05	6.3	0.5
19H-3, 145–150	174.55	7.0	0.5
20H-3, 145–150	184.05	5.7	0.4
21H-3, 145–150	193.55	6.6	0.6
22H-3, 145–150	203.05	7.1	0.7
23X-3, 145–150	209.55	7.1	0.0
24X-2, 110–115	217.20	7.0	0.5
27X-5, 145–150	250.55	6.8	0.0
28X-1, 140–145	254.00	3.2	0.0
29X-2, 145–150	262.05	1.3	0.0
30X-3, 135–140	272.95	1.3	0.0
31X-4, 145–150	284.05	0.0	0.0
32X-2, 145–150	290.55	4.3	0.0
33X-4, 145–150	303.05	3.0	0.3
35X-4, 145–150	322.05	2.1	0.0
36X-5, 110–115	332.70	3.5	0.0
37X-3, 145–150	339.55	3.9	0.0
38X-3, 145–150	349.05	5.6	0.0
39X-1, 110–115	355.20	6.2	0.4
41X-1, 145–150	374.55	9.3	0.0
42X-5, 110–115	389.70	4.3	0.5
43X-4, 145–150	398.05	8.7	0.8
45X-4, 145–150	417.05	8.7	0.4
48X-4, 145–150	445.55	6.4	0.0
49X-4, 145–150	455.05	5.9	0.7
50X-4, 145–150	464.55	3.3	0.0
54X-1, 110–115	497.70	6.9	1.6

susceptibility variations for the interval from 0 to 200 mbsf (upper Oligocene to Pleistocene). The XCB technique was used for coring beneath this depth, and the resulting higher levels of drilling disturbance and less continuous recovery in the XCB cores limited measurement of whole-core susceptibility data to only isolated sections of pre-Oligocene cores.

NRM Intensity and Magnetic Susceptibility

The variations downcore of NRM intensity and magnetic susceptibility for the interval 0–200 mbsf are shown together with the lithostratigraphic unit boundaries in Figures 19 and 20. Lithostratigraphic Unit I is characterized by considerably higher and more variable values of both these parameters than Unit II. This reflects the higher terrigenous content of the siliceous (diatomaceous) clays of Unit I compared with that of the nannofossil-diatom muds and nannofossil oozes of Unit II. The increase in susceptibility values above approximately 85 mbsf is particularly striking (Fig. 20) and appears to herald the first appearance of ice-rafted debris at the beginning of the Miocene.

The susceptibility values for 0–40 mbsf are shown at an expanded depth scale in Figure 21. A striking feature of this plot is the occurrence of quasicyclical fluctuations in susceptibility values, with a mean wavelength of approximately 0.4 m. The cyclicity becomes less regular in the uppermost core. Using the pa-

Table 6. Sedimentary calcium carbonate content, Hole 699A.

Sample (core, section, cm)	Depth (mbsf)	C_{org} (%)	$CaCO_3$ (%)
1H-1, 100–102	1.00	−0.06	0.58
1H-2, 100–102	2.50	0.38	0.42
1H-3, 98–100	3.98	0.22	0.50
1H-4, 100–102	5.50	0.19	0.67
1H-5, 100–102	7.00	0.25	0.58
1H-6, 90–92	8.40	0.37	0.50
2H-1, 100–102	9.60	0.26	0.83
2H-2, 100–102	11.10	0.11	0.50
2H-3, 100–102	12.60	0.16	3.84
2H-4, 100–102	14.10	0.09	0.75
3H-1, 100–102	19.10	0.85	0.75
3H-2, 100–102	20.60	0.14	0.92
3H-3, 100–102	22.10		0.92
3H-4, 100–102	23.60		0.50
4H-1, 100–102	28.60	0.08	0.75
4H-2, 100–102	30.10		0.58
4H-3, 100–102	31.60		0.75
4H-4, 75–77	32.85		0.67
4H-5, 100–102	34.01		0.83
5H-1, 100–102	38.10	−0.01	1.00
5H-2, 100–102	39.60		1.08
5H-3, 100–102	41.10		0.83
5H-4, 100–102	42.60		1.08
5H-5, 100–102	44.10		0.92
6H-1, 94–96	47.54	0.04	0.33
6H-2, 100–102	49.10		0.25
6H-3, 90–92	50.50		0.33
6H-4, 100–102	52.10		0.17
6H-5, 99–101	53.59		0.42
6H-6, 38–40	54.48	0.07	0.17
7H-2, 100–102	58.60		0.17
7H-3, 100–102	60.10		0.17
7H-4, 100–102	61.60		0.25
7H-5, 80–82	62.90		0.25
8H-1, 100–102	66.60	0.04	0.83
8H-2, 100–102	68.10		0.08
8H-3, 100–102	69.60		0.33
8H-4, 100–102	71.10		0.58
8H-5, 100–102	72.60		0.42
9H-1, 60–62	75.70	0.06	0.25
9H-4, 100–102	80.60		2.50
10H-1, 100–102	85.60	0.11	0.33
10H-2, 100–102	87.10		26.94
10H-3, 100–102	88.60		29.36
10H-4, 100–102	90.10		4.34
10H-5, 100–102	91.60		0.17
10H-6, 40–42	92.50		0.25
11H-1, 103–105	95.13	0.11	4.84
11H-2, 103–105	96.63		0.25
11H-3, 103–105	98.13		0.50
11H-4, 103–105	99.63		5.42
12H-2, 100–102	106.10	0.06	21.68
12H-3, 98–100	107.58		32.11
12H-4, 100–102	109.10		5.92
12H-5, 100–102	110.60		13.26
13H-1, 101–103	114.11	0.09	23.02
13H-2, 98–100	115.58		10.51
13H-3, 100–102	117.10		9.67
13H-4, 100–102	118.60		0.58
14H-1, 100–102	123.60	0.12	0.08
14H-2, 100–102	125.10		0.17
14H-3, 100–102	126.60		0.17
14H-4, 100–102	128.10		0.17
15H-1, 100–102	133.10	−0.02	1.58
15H-2, 98–100	134.58		2.50
15H-3, 100–102	136.10		8.59
15H-4, 100–102	137.60		1.25
15H-5, 98–100	139.40		0.42
16H-1, 98–100	142.58	0.18	2.09
16H-2, 98–100	144.08		0.50
16H-3, 98–100	145.58		32.61
16H-4, 98–100	147.08		0.67
16H-5, 98–100	148.58		6.51
17H-1, 98–100	152.08	0.11	21.60
17H-2, 100–102	153.60		35.36
17H-3, 100–102	155.10		33.69
17H-4, 100–102	156.60		35.70

Table 6 (continued).

Sample (core, section, cm)	Depth (mbsf)	C_{org} (%)	$CaCO_3$ (%)
17H-5, 100–102	158.10		46.45
18H-1, 100–102	161.60	0.00	45.79
18H-2, 100–102	163.10		46.20
18H-3, 100–102	164.60		39.36
18H-4, 100–102	166.10		40.37
18H-5, 100–102	167.60		23.10
19H-1, 100–102	171.10	−0.01	48.71
19H-2, 100–102	172.60		29.19
19H-3, 100–102	174.10		2.75
19H-4, 100–102	175.60		29.19
20H-1, 103–105	180.63	0.05	25.52
20H-2, 102–104	182.12		21.85
20H-3, 102–104	183.62		43.45
20H-4, 102–104	185.12		75.06
20H-5, 102–104	186.62		13.26
21H-1, 103–105	190.13	0.04	40.03
21H-2, 103–105	191.63		15.51
21H-3, 103–105	193.13		3.17
21H-4, 103–105	194.63		3.20
21H-5, 103–105	196.13		29.61
22H-1, 102–104	199.62	−0.04	45.04
22H-2, 102–104	201.12		42.03
22H-3, 102–104	202.62		47.54
22H-4, 102–104	204.12		48.71
23X-2, 100–102	207.60	0.14	0.92
23X-3, 100–102	209.10	0.18	0.75
23X-4, 100–102	210.60		8.59
24X-1, 100–102	215.60	0.11	0.17
24X-2, 100–102	217.10		0.58
24X-6, 100–102	223.10		22.43
30X-1, 100–102	269.60	0.34	37.53
30X-2, 100–102	271.10		40.70
30X-3, 60–62	272.20		34.19
30X-4, 100–102	274.10		49.54
31X-1, 110–112	279.20	0.13	41.12
31X-2, 100–102	280.60		51.79
31X-3, 100–102	282.10		66.05
31X-4, 100–102	283.60		45.70
31X-5, 100–102	285.10		37.45
31X-6, 100–102	286.60		40.03
32X-1, 100–102	288.60	0.11	44.04
32X-2, 100–102	290.10	0.30	0.33
32X-3, 100–102	291.60		15.51
32X-6, 100–102	296.10		54.38
33X-1, 100–102	298.10	−0.06	63.72
33X-2, 101–103	299.61		55.04
33X-3, 103–105	301.13		63.13
33X-4, 100–102	302.60		71.81
33X-5, 100–102	304.10		49.62
33X-6, 108–110	305.68		37.03
35X-1, 100–102	317.10	−0.04	42.62
35X-2, 100–102	318.60		36.61
35X-3, 100–102	320.10		46.54
35X-4, 100–102	321.60		33.78
35X-5, 100–102	323.10		41.28
35X-6, 100–102	324.60		38.95
36X-5, 100–102	332.60	0.03	39.78
36X-6, 100–102	334.10		55.99
37X-2, 100–102	337.60	0.00	74.23
37X-3, 100–102	339.10		56.71
37X-4, 100–102	340.60		79.31
37X-5, 100–102	342.10		38.36
39X-1, 106–108	355.16	−0.08	43.04
39X-2, 90–92	356.50		65.22
40X-1, 105–107	364.65	−0.03	68.30
40X-2, 100–102	366.10		67.22
40X-3, 104–106	367.64		60.21
40X-4, 102–103	369.12		16.68
42X-1, 106–108	383.66	0.03	41.95
42X-2, 104–106	385.14		48.96
42X-5, 101–103	389.61		59.88
42X-7, 32–34	391.92		66.30
43X-2, 100–102	394.60	−0.16	52.12
43X-4, 98–100	397.58		72.72
43X-5, 90–92	399.00		71.81
45X-1, 100–102	412.10	0.03	71.31

Table 6 (continued).

Sample (core, section, cm)	Depth (mbsf)	C_{org} (%)	$CaCO_3$ (%)
45X-3, 99–101	415.09		67.89
45X-5, 99–101	418.09		70.22
45X-6, 99–101	419.59		75.23
47X-1, 53–55	430.63	−0.02	70.31
47X-2, 96–98	432.56		77.23
47X-3, 100–102	434.10		74.56
47X-4, 100–102	435.60		69.72
47X-5, 100–102	437.10		75.89
47X-6, 100–102	438.60		71.47
48X-1, 104–106	440.64	−0.31	76.98
48X-2, 100–102	442.10		78.90
48X-3, 97–99	443.57		70.31
48X-4, 30–32	444.40		78.15
49X-1, 100–102	450.10	−0.11	82.40
49X-2, 100–102	451.60		76.23
49X-3, 96–98	453.06		64.72
49X-4, 100–102	454.60		72.81
49X-5, 100–102	456.10		82.82
49X-6, 70–72	457.30		50.12
50X-1, 100–102	459.60	−0.09	71.56
50X-2, 80–82	460.90		70.39
50X-3, 98–100	462.58		73.98
50X-4, 100–102	464.10		71.89
50X-5, 99–101	465.59		72.14
50X-6, 99–101	467.09		75.06
54X-1, 99–101	497.59	0.00	0.25
54X-2, 99–101	499.09		55.46
55X-1, 102–104	507.12	0.02	66.30

leomagnetically determined mean sedimentation rate of 9.3 m/m.y. for the depth interval 10 to 15 mbsf, the periodicity of these susceptibility fluctuations is approximately 40,000 yr.

Directions of Magnetizations: Evaluation of Data

As a result of various technical problems, the pass-through cryogenic magnetometer was removed from *JOIDES Resolution* at the end of Leg 111 to undergo a number of modifications aimed at improving its reliability and stability. The equipment was reinstalled on the ship at the start of Leg 114, and an important objective of the initial paleomagnetic investigations on this cruise was to assess the reliability of the system.

Measurements were made of the NRM and the magnetization remaining after AF demagnetization at 5 mT for the archive halves of Cores 114-699A-2H through 114-699A-23X, with the exception of Core 114-699A-9H, which was highly disturbed. Sections were also occasionally measured after partial AF demagnetization at peak fields of 9 mT. Cores 114-699A-1H and 114-699A-2H were demagnetized at different fields ranging from 3 to 9 mT during the initial AF demagnetizer and magnetometer tests. Because of excessive drilling disturbance and/or poor recovery, most of the sediments in Cores 114-699A-24X to 114-699A-46X are generally unsuitable for paleomagnetic analysis, and few core sections were measured. A short interval of good recovery in Cores 114-699A-47X and 114-699A-48X provided an opportunity to obtain preliminary information on the stability of the magnetizations of lower Paleocene sediments at this site.

Figure 22 shows the downcore variation of inclination and intensity of remanent magnetization for the depth interval 0–35 mbsf, as determined from pass-through cryogenic magnetometer measurements (continuous lines) and the results of discrete sample measurements (solid circles). Both sets of values are after partial AF demagnetization at peak fields of 5 mT. In general, the two sets of measurements are in good agreement, especially considering that the pass-through magnetometer averages over a volume that is roughly 30 times that of discrete samples.

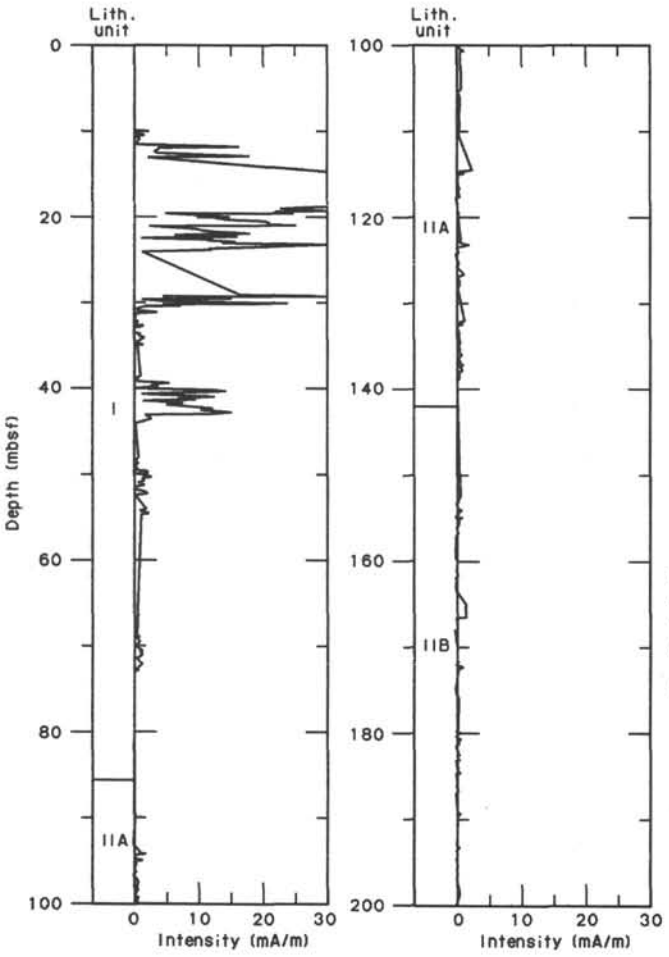

Figure 19. Magnetization (NRM) intensities measured using the three-axis pass-through cryogenic magnetometer in relation to the lithostratigraphic units for the upper 200 m of Hole 699A.

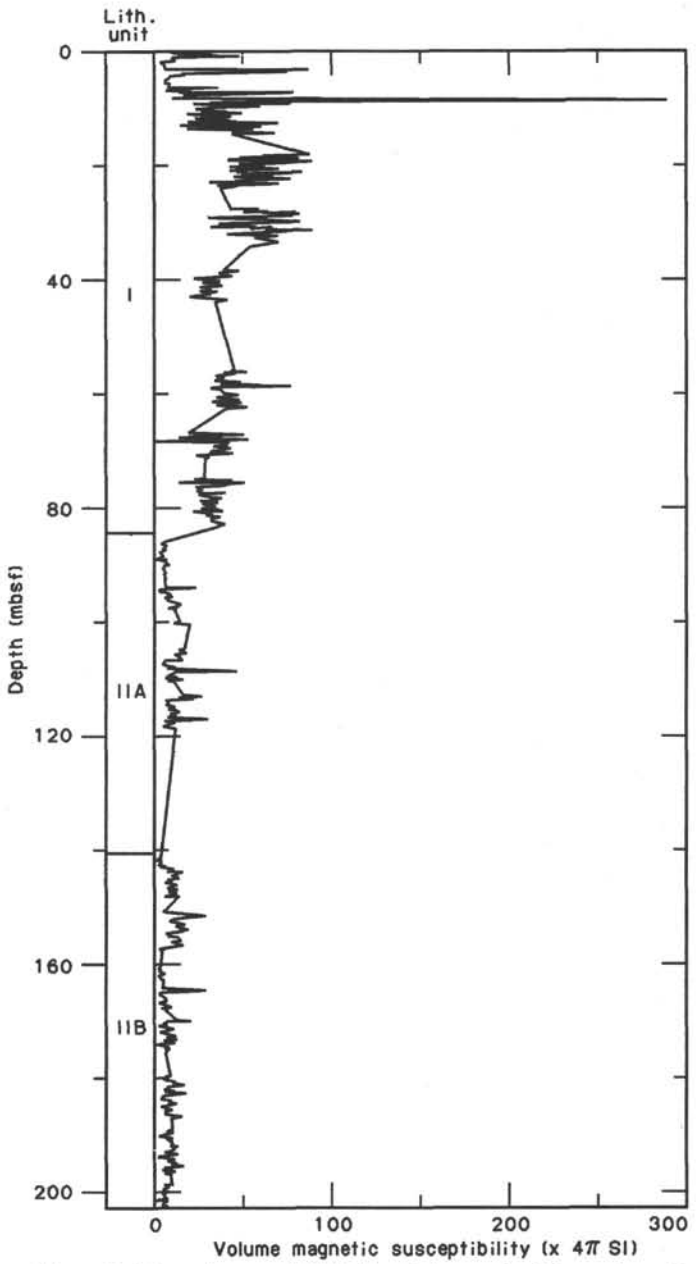

Figure 20. Magnetic suscepibilities in relation to the lithostratigraphic units for the upper 200 m of Hole 699A.

Figure 23 illustrates the response to progressive AF demagnetization of a typical reverse polarity sample from Core 114-699A-12H and a normal polarity sample from Core 114-699A-14H. Both samples are upper Oligocene nannofossil-diatom oozes. Small directional changes occur after demagnetization at 5 mT, consistent with the removal of a weak secondary overprint, but thereafter, the samples display simple univectorial behavior. These results indicate that AF demagnetization of the split-core sections of Oligocene sediment at 5 mT using the in-line AF demagnetizer is likely to remove any magnetic overprints. The corresponding paleomagnetic data from the pass-through magnetometer are believed to provide a reliable determination of the polarity of the characteristic remanent magnetization of these younger sediments, provided that the cores have not suffered significant drilling disturbance.

In contrast, the short section of lower Paleogene sediments recovered from Cores 114-699A-47X to 114-699A-49X possesses a harder magnetic overprint, which requires demagnetization to higher peak field levels for complete removal. Figure 24 shows the inclination of remanent magnetization of Core 114-699A-47X before demagnetization and after treatment at 5 and 9 mT, using the cryogenic magnetometer and the in-line AF demagnetizer. The NRM data are noisy but suggest a dominant normal polarity magnetization through the core. After treatment at 5 mT there is an indication of a reverse polarity interval in the lower half of the core, but this is poorly defined. Treatment at 9 mT improves the definition of this reverse polarity interval but data for the upper part of the core are still very noisy. The AF demagnetization behavior of discrete samples from this interval indicates that although the magnetic polarity can be correctly deduced after AF demagnetization at 9–10 mT, precise definition of the demagnetization stable end point requires fields of 15 mT or possibly higher. These results confirm that the in-line three-axis demagnetizer functions well, up to the maximum field used for these cores (9 mT) and that there is no indication of spurious components of magnetization being induced in the sediment through instrument malfunctions.

Magnetostratigraphic Results

The downhole variation of inclination after 5 mT demagnetization for the upper 200 m of sediment recovered from Hole 699A is shown in Figure 25.

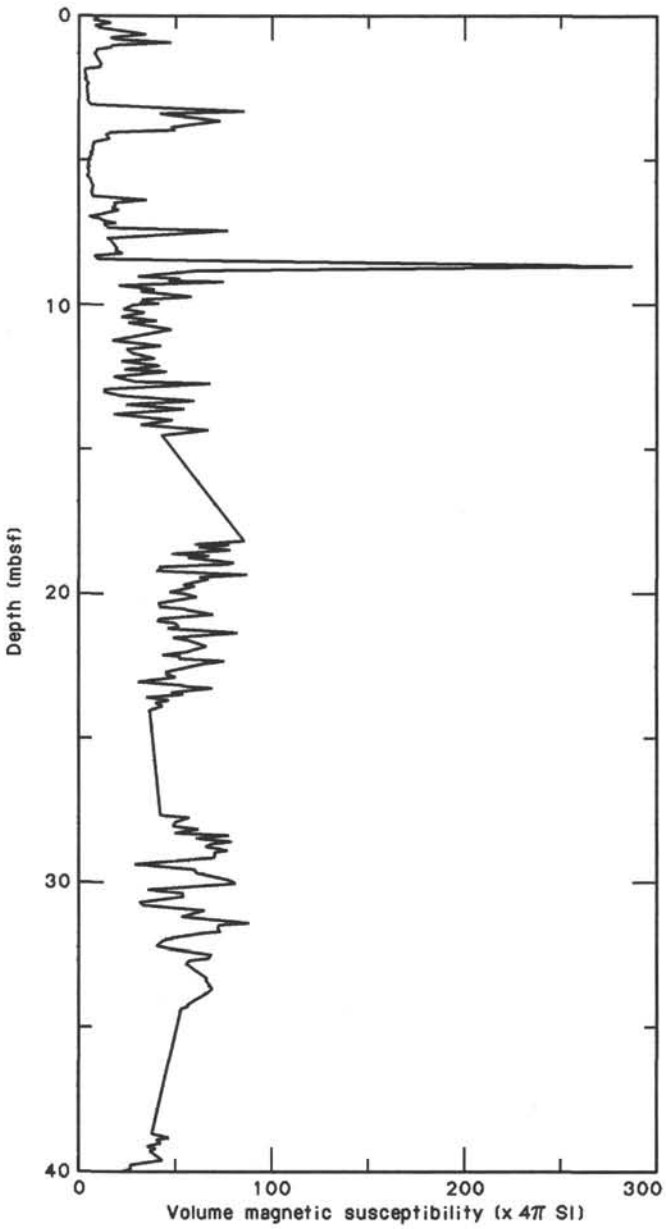

Figure 21. Magnetic susceptibilities for the upper 40 m of Hole 699A. Note the strong cyclicity apparent in the data.

A particularly complete section of Oligocene nannofossil-diatom muds and nannofossil oozes was recovered from Hole 699A. The sequence of normal and reverse polarity magnetozones identified in this section is shown in the vertical column of Figure 26. Using the limited biostratigraphic data currently available from these cores it is possible to make a tentative correlation with the GPTS of Berggren et al. (1985a, 1985b) shown across the top of this figure.

Preliminary diatom zonations indicate that the Oligocene/Miocene boundary lies in the lower part of Core 114-699A-10H. Consequently, the long reverse polarity section in Cores 114-699A-11H and 114-699A-12H can be correlated with the distinctive long reverse interval of Chron C6CR. The FAD of *Rocella gelida*, with an estimated age of 26 Ma (Gombos and Ciesielski, 1983; Fenner, 1984) occurs in the depth range 128 to 139 mbsf, suggesting that the reverse magnetozone in the lower part of Core 114-699A-14H and upper part of Core 114-699A-15H rep-

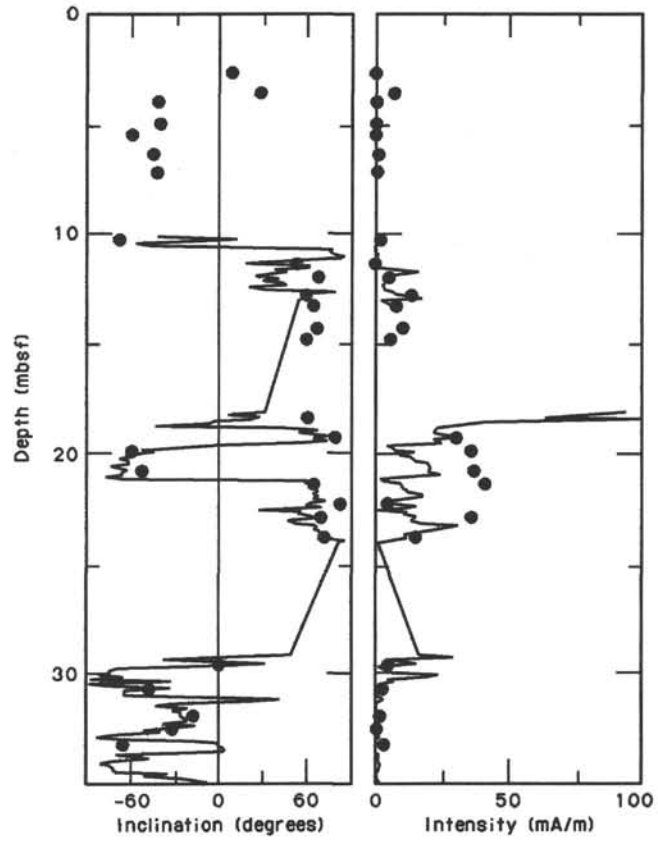

Figure 22. Comparison between the inclination and intensity of remanent magnetization measured using the three-axis pass-through cryogeic magnetometer (solid lines) and the values obtained from discrete samples using the Molspin spinner magnetometer (filled circles). Both sets of data are after demagnetization at 5 mT.

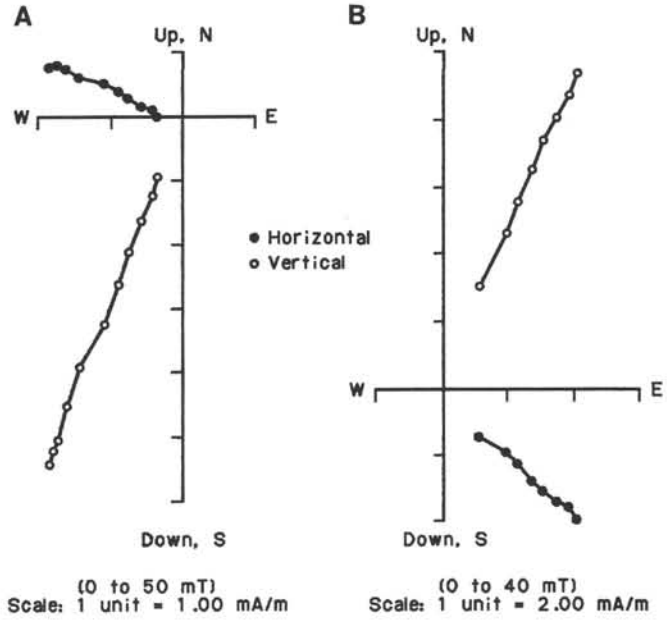

Figure 23. Response to AF demagnetization of (A) a typical sample carrying a reverse polarity stable magnetization (114-699A-12H-2, 120–122 cm) and (B) one carrying a normal polarity magnetization (114-699A-14H-3, 118–120 cm). The results are plotted on vector-end-point diagrams. The data do not have azimuthal orientation, so N, E, S, and W are specified relative to an arbitrary azimuth.

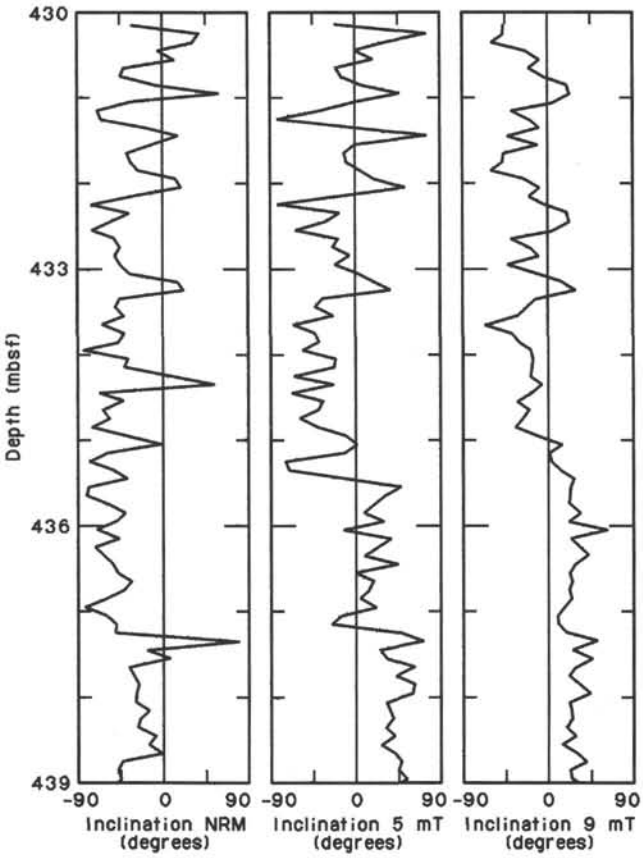

Figure 24. Magnetic inclination records obtained by pass-through measurement of Core 114-199A-47X, before demagnetization (NRM) and after demagnetization at 5 and 9 mT.

resents Chron C7R. No other specific biostratigraphic tie-point is currently available from Cores 114-699A-10H to 114-699A-23X, but the top of nannofossil Zone NP22 of early Oligocene age (early Chron C12R) has been identified in Core 114-699A-27X. Thus, the normal polarity zone in Core 114-699A-23X must represent part or all of either Chrons C12N or C11N. The latter assignment is preferred, because the distinctive polarity signature of Cores 114-699A-22H to 114-699A-20H then provides a good correlation with Chrons C10R to C9R inclusive.

The correlation tie-points indicated in Figure 26 all lie on two linear correlation lines. The only magnetozone of significant duration that does not have a counterpart in the GPTS is the short reverse polarity interval in Core 114-699A-17H.

In conclusion, a good quality magnetostratigraphic record appears to be present in the upper Neogene and Oligocene sediments recovered from Hole 699A. Post-cruise studies should help to refine the very tentative magnetostratigraphic correlation proposed in Figure 26, and these data hold considerable promise for making a significant contribution to the chronometric calibration of high-latitude diatom and nannofossil zonation schemes. Such a calibration will be of importance to the interpretation of the detailed chronology of paleoceanographic events during this time.

PHYSICAL PROPERTIES

Physical-property measurements at Site 699 serve two main purposes: to determine how changes in the physical properties

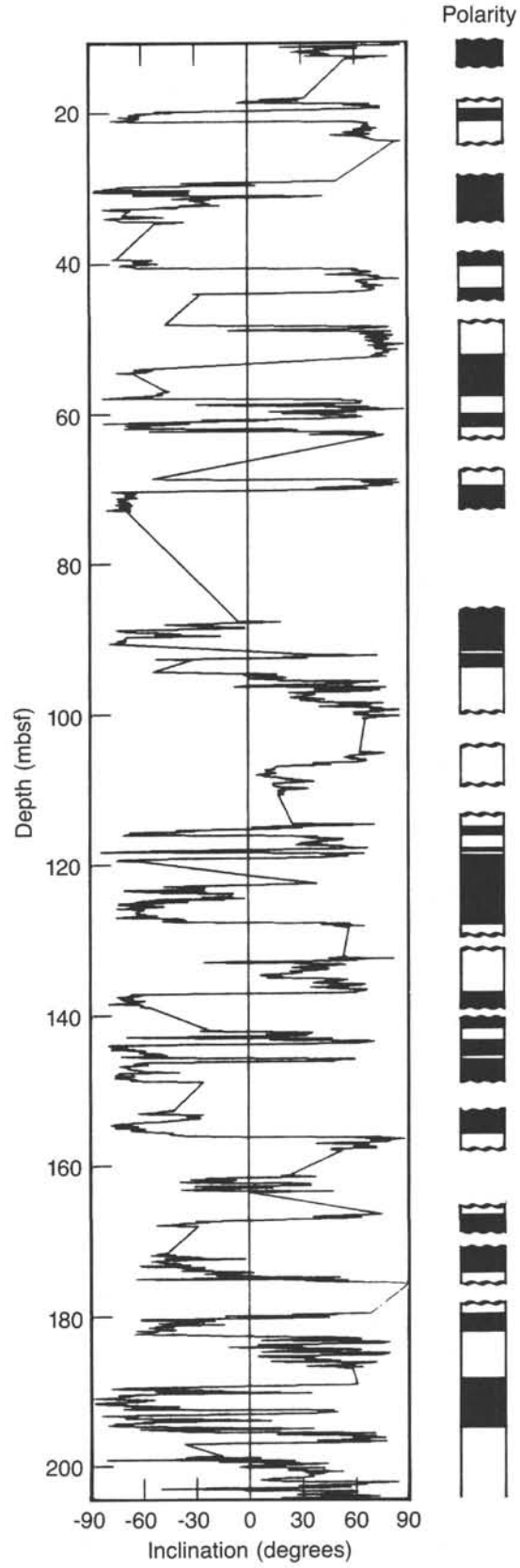

Figure 25. Results of pass-through measurements of the archive halves of cores from Hole 699A after partial AF demagnetization at 5 mT, plotted as inclination vs. depth (mbsf).

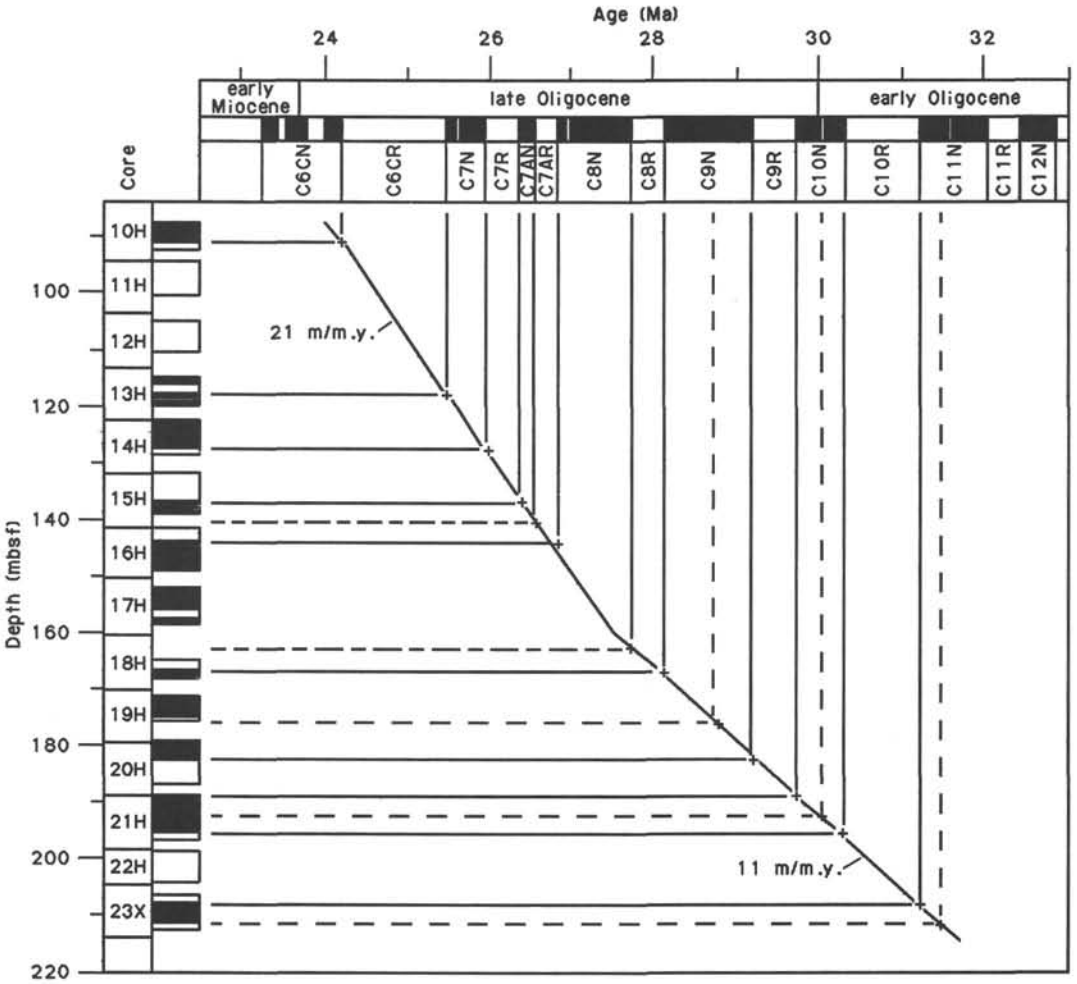

Figure 26. Tentative correlation of magnetic polarity zonations observed in Hole 699A with the geomagnetic polarity time scale of Berggren et al. (1985a, 1985b). Correlation is based on available shipboard biostratigraphic data.

correspond to changes in the biogenic and terrigenous sediments of the Atlantic part of the Southern Oceans and to investigate whether these changes correlate to individual reflectors or seismic sequences in order to establish a detailed seismic stratigraphy for the area under investigation. Furthermore, we investigated whether hiatuses (see "Biostratigraphy" section) caused changes in the sedimentary record large enough to be detected in the physical-property and seismic record, and we examined the apparent cyclical nature of the physical-property record.

The methodology of physical-property measurements is described in the "Explanatory Notes" chapter. Four sets of measurements were obtained: (1) index properties (bulk density, porosity, water content, and grain density); (2) compressional-wave (*P*-wave) velocity; (3) vane shear strength; and (4) thermal conductivity. The carbonate content (see "Geochemistry" section) is shown for comparison with the physical-property data. The data are presented unfiltered for any bad data points. Physical-property measurements were made on sediments cored with the APC system (Cores 114-699A-1H to 114-699A-22H, 0–205.1 mbsf) and with the XCB system (Cores 114-699A-23X to 114-699A-56X, 205.1–518.1 mbsf). Thus, any changes observed in the physical properties at the depth of 205.1 mbsf may result from a change in the coring method. The degree of coring disturbance was significant in the upper XCB cores, especially in Cores 114-699A-25X through 114-699A-29X, which were not sampled.

Physical-Property Summary and Lithostratigraphic Correlation

Values for the index properties and carbonate content, vane shear strength, *P*-wave velocity, and thermal conductivity are listed in Tables 7 through 10. Downcore profiles of wet-bulk density, porosity, water content, grain density, carbonate content, *P*-wave velocity, shear strength, and thermal conductivity are illustrated in Figure 27. The changes in these parameters generally correlate quite well with the six lithostratigraphic units (see "Lithostratigraphy" section, this chapter). For comparison, the properties of the six lithostratigraphic units are summarized as follows:

Lithostratigraphic Unit I (0–85.7 mbsf) is characterized by a lack of carbonate and an abundance of siliceous sediments, which is evident in a comparison of the records of carbonate content and grain density (Fig. 27). Siliceous sediments have a grain density of 1.6 to 2.6 g/cm^3. In contrast, both carbonate and terrigenous sediments have an average grain density of 2.65 to 2.75 g/cm^3. Thus, the low grain densities (less than 2.6 g/cm^3) and the low carbonate content clearly indicate high concentrations of siliceous material. In contrast, dilution of carbonate by terrigenous material should show no distinct changes in grain density, but merely changes in the carbonate content. Thus, the increase in grain density without an associated increase in carbonate content at the base of Unit I, in Cores 114-

Table 7. Index properties and carbon content, Hole 699A.

Sample (core, section, cm)	Depth (mbsf)	Water content (%)	Porosity (%)	Densities: Wet bulk (g/cm^3)	Densities: Grain (g/cm^3)	Densities: Dry bulk (g/cm^3)	Carbonate content (%)
1H-1, 100–102	1.00	79.58	92.15	1.19	2.21	0.24	0.58
1H-2, 100–102	2.50	74.21	87.82	1.21	2.36	0.31	0.42
1H-3, 98–100	3.98	57.85	79.58	1.41	2.62	0.59	0.50
1H-4, 100–102	5.50	73.53	88.23	1.23	2.39	0.33	0.67
1H-5, 100–102	7.00	71.17	85.68	1.23	2.37	0.36	0.58
1H-6, 90–92	8.40	59.93	79.19	1.35	2.47	0.54	0.50
2H-1, 100–102	9.60	53.37	77.01	1.48	2.56	0.69	0.83
2H-2, 100–102	11.10	60.10	80.95	1.38	2.80	0.55	0.50
2H-3, 100–102	12.60	55.48	77.56	1.43	2.61	0.64	3.84
2H-4, 100–102	14.10	50.50	72.94	1.48	2.82	0.73	0.75
3H-1, 100–102	19.10	52.16	74.04	1.45	2.57	0.70	0.75
3H-2, 100–102	20.60	47.76	72.04	1.55	2.79	0.81	0.92
3H-3, 100–102	22.10	49.92	72.91	1.50	2.73	0.75	0.92
3H-4, 100–102	23.60	58.10	78.98	1.39	2.57	0.58	0.50
4H-1, 100–102	28.60	56.43	78.70	1.43	2.73	0.62	0.75
4H-2, 100–102	30.10	52.60	74.87	1.46	2.75	0.69	0.58
4H-3, 100–102	31.60	49.07	72.92	1.52	2.73	0.78	0.75
4H-4, 75–77	32.85	51.71	74.09	1.47	2.49	0.71	0.67
4H-5, 100–102	34.01	51.46	75.14	1.50	2.82	0.73	0.83
5H-1, 100–102	38.10	58.16	79.21	1.40	2.73	0.58	1.00
5H-2, 100–102	39.60	51.39	73.00	1.46	2.70	0.71	1.08
5H-3, 100–102	41.10	57.71	78.32	1.39	2.54	0.59	0.83
5H-4, 100–102	42.60	52.43	73.60	1.44	2.47	0.68	1.08
5H-5, 100–102	44.10	51.21	73.47	1.47	2.45	0.72	0.92
6H-1, 94–96	47.54	51.43	72.00	1.43	2.60	0.70	0.33
6H-2, 100–102	49.10	54.65	77.05	1.44	2.59	0.66	0.25
6H-3, 90–92	50.50	55.78	77.56	1.42	2.59	0.63	0.33
6H-4, 100–102	52.10	50.55	73.60	1.49	2.72	0.74	0.17
6H-5, 99–101	53.59	52.22	75.05	1.47	2.71	0.70	0.42
6H-6, 38–40	54.48	52.16	75.15	1.48	2.82	0.71	0.17
7H-2, 100–102	58.60	54.70	77.50	1.45	2.48	0.66	0.17
7H-3, 100–102	60.10	50.73	73.93	1.49	2.62	0.74	0.17
7H-4, 100–102	61.60	50.10	73.01	1.49	2.65	0.75	0.25
7H-5, 80–82	62.90	53.10	76.01	1.47	2.77	0.69	0.25
8H-1, 100–102	66.60	51.81	71.84	1.42	2.44	0.68	0.83
8H-2, 100–102	68.10	49.49	73.75	1.53	2.81	0.77	0.08
8H-3, 100–102	69.60	62.04	83.36	1.38	2.72	0.52	0.33
8H-4, 100–102	71.10	63.40	85.32	1.38	3.05	0.50	0.58
8H-5, 100–102	72.60	67.57	85.11	1.29	2.80	0.42	0.42
9H-1, 60–62	75.70	51.96	74.93	1.48	2.66	0.71	0.25
9H-4, 100–102	80.60	62.04	83.54	1.38	2.81	0.52	2.50
10H-1, 100–102	85.60	63.36	84.40	1.36	2.87	0.50	0.33
10H-2, 100–102	87.10	62.31	82.43	1.36	2.45	0.51	26.94
10H-3, 100–102	88.60	61.80	81.50	1.35	2.68	0.52	29.36
10H-4, 100–102	90.10	65.45	86.09	1.35	2.45	0.47	4.34
10H-5, 100–102	91.60	68.56	85.51	1.28	2.41	0.40	0.17
10H-6, 40–42	92.50	69.53	86.80	1.28	2.33	0.39	0.25
11H-1, 103–105	95.13	67.98	85.14	1.28	2.49	0.41	4.84
11H-2, 103–105	96.63	66.18	84.45	1.31	2.71	0.44	0.25
11H-3, 103–105	98.13	63.59	83.26	1.34	2.69	0.49	0.50
11H-4, 103–105	99.63	65.19	86.36	1.36	2.37	0.47	5.42
12H-2, 100–102	106.10	64.25	83.25	1.33	2.47	0.47	21.68
12H-3, 98–100	107.58	60.71	80.99	1.37	2.59	0.54	32.11
12H-4, 100–102	109.10	64.46	83.55	1.33	2.65	0.47	5.92
12H-5, 100–102	110.60	64.01	81.16	1.30	2.43	0.47	13.26
13H-1, 101–103	114.11	66.19	84.88	1.31	2.44	0.44	23.02
13H-2, 98–100	115.58	66.08	83.55	1.30	2.50	0.44	10.51
13H-3, 100–102	117.10	65.74	83.07	1.29	2.29	0.44	9.67
13H-4, 100–102	118.60	66.91	82.74	1.27	2.34	0.42	0.58
14H-1, 100–102	123.60	68.59	84.72	1.27	2.58	0.40	0.08
14H-2, 100–102	125.10	64.62	83.36	1.32	2.67	0.47	0.17
14H-3, 100–102	126.00	62.36	80.68	1.33	2.45	0.50	0.17
14H-4, 100–102	128.10	62.85	80.67	1.32	2.54	0.49	0.17
15H-1, 100–102	133.10	66.77	80.23	1.23	2.65	0.41	1.58
15H-2, 98–100	134.58	64.12	82.56	1.32	2.51	0.47	2.50
15H-3, 100–102	136.10	61.94	80.89	1.34	2.48	0.51	8.59
15H-4, 100–102	137.60	62.73	83.29	1.36	2.49	0.51	1.25
15H-5, 98–100	139.08	61.21	80.65	1.35	2.68	0.52	0.42
16H-1, 98–100	142.58	60.36	79.75	1.35	2.56	0.54	2.09
16H-2, 98–100	144.08	61.54	82.19	1.37	2.58	0.53	0.50
16H-3, 98–100	145.58	52.71	74.53	1.45	2.67	0.69	32.61
16H-4, 98–100	147.08	55.86	75.76	1.39	2.50	0.61	0.67
16H-5, 98–100	148.58	59.50	80.31	1.38	2.82	0.56	6.51
17H-1, 98–100	152.08	48.53	72.70	1.53	2.96	0.79	21.60
17H-2, 100–102	153.60	51.58	76.16	1.51	2.88	0.73	35.36

Table 7 (continued).

Sample (core, section, cm)	Depth (mbsf)	Water content (%)	Porosity (%)	Densities: Wet bulk (g/cm^3)	Densities: Grain (g/cm^3)	Densities: Dry bulk (g/cm^3)	Carbonate content (%)
17H-3, 100–102	155.10	47.14	70.66	1.54	2.71	0.81	33.69
17H-4, 100–102	156.60	50.04	75.84	1.55	2.71	0.78	35.70
17H-5, 100–102	158.10	52.17	76.35	1.50	2.73	0.72	46.45
18H-1, 100–102	161.60	55.98	81.26	1.49	2.67	0.65	45.79
18H-2, 100–102	163.10	52.77	77.94	1.51	2.46	0.71	46.20
18H-3, 100–102	164.60	50.03	74.30	1.52	2.79	0.76	39.36
18H-4, 100–102	166.10	49.72	76.35	1.57	2.79	0.79	40.37
18H-5, 100–102	167.60	52.86	77.95	1.51	2.87	0.71	23.10
19H-1, 102–104	171.12	46.70	74.73	1.64	2.97	0.87	48.71
19H-2, 102–104	172.62	49.71	73.21	1.51	2.66	0.76	29.19
19H-3, 102–104	174.12	55.27	77.64	1.44	2.74	0.64	2.75
19H-4, 102–104	175.62	52.84	76.55	1.48	2.51	0.70	29.19
20H-1, 103–105	180.63	49.75	73.39	1.51	2.79	0.76	25.52
20H-2, 102–104	182.12	54.50	76.66	1.44	2.72	0.66	21.85
20H-3, 102–104	183.62	48.34	71.30	1.51	2.56	0.78	43.45
20H-4, 102–104	185.12	41.17	66.54	1.66	2.64	0.97	75.06
20H-5, 102–104	186.62	49.98	73.83	1.51	2.73	0.76	13.26
21H-1, 103–105	190.13	50.89	76.01	1.53	2.63	0.75	40.03
21H-2, 103–105	191.63	51.35	75.72	1.51	2.90	0.79	15.51
21H-3, 103–105	193.13	54.89	77.49	1.45	2.80	0.65	3.17
21H-4, 103–105	194.63	50.01	73.77	1.51	2.72	0.76	3.20
21H-5, 103–105	196.13	47.89	70.76	1.51	2.58	0.79	29.61
22H-1, 102–104	199.62	46.82	71.09	1.56	2.90	0.83	45.04
22H-2, 102–104	201.12	40.62	66.30	1.67	2.95	0.99	42.03
22H-3, 102–104	202.62	41.09	65.80	1.64	2.72	0.97	47.54
22H-4, 102–104	204.12	45.98	73.61	1.64	2.98	0.89	48.71
23X-2, 100–102	207.60	54.82	79.46	1.49	3.22	0.67	0.92
23X-3, 100–102	209.10	49.57	75.54	1.56	2.90	0.79	0.75
23X-4, 100–102	210.60	50.74	74.95	1.51	2.79	0.75	8.59
24X-1, 100–102	215.60	53.31	76.46	1.47	2.94	0.69	0.17
24X-2, 100–102	217.10	51.43	75.40	1.50	2.91	0.73	0.58
24X-6, 100–102	223.10	49.40	72.51	1.50	2.97	0.76	22.43
30X-1, 100–102	269.60	45.34	70.47	1.59	2.72	0.87	37.53
30X-2, 100–102	271.10	50.57	73.83	1.50	2.52	0.74	40.70
30X-3, 60–62	272.20	53.33	76.41	1.47	2.47	0.69	34.19
30X-4, 100–102	274.10	48.37	73.31	1.55	2.78	0.80	49.54
31X-1, 110–112	279.20	49.78	73.26	1.51	2.59	0.76	41.12
31X-2, 100–102	280.60	48.30	70.98	1.51	2.54	0.78	51.79
31X-3, 100–102	282.10	43.66	68.84	1.62	2.59	0.91	66.05
31X-4, 100–102	283.60	48.46	71.63	1.51	2.63	0.78	45.70
31X-5, 100–102	285.10	25.98	27.22	1.07	2.65	0.79	37.45
31X-6, 100–102	286.60	47.50	72.35	1.56	2.82	0.82	40.03
32X-1, 100–102	288.60	60.21	80.05	1.36	2.57	0.54	44.04
32X-2, 100–102	290.10	68.68	84.76	1.26	2.47	0.40	0.33
32X-3, 100–102	291.60	60.15	81.10	1.38	2.93	0.55	15.51
32X-6, 100–102	296.10	49.25	76.77	1.60	2.72	0.81	54.38
33X-1, 100–102	298.10	40.05	64.40	1.65	2.73	0.99	63.72
33X-2, 101–103	299.61	44.24	67.47	1.56	2.79	0.87	55.04
33X-3, 103–105	301.13	42.97	66.99	1.60	2.66	0.91	63.13
33X-4, 100–102	302.60	46.75	70.72	1.55	2.71	0.83	71.81
33X-5, 100–102	304.10	48.86	73.15	1.53	2.82	0.78	49.62
33X-6, 108–110	305.68	52.70	75.59	1.47	2.55	0.70	37.03
35X-1, 100–102	317.10	49.70	76.40	1.58	2.83	0.79	42.62
35X-2, 100–102	318.60	48.10	72.81	1.55	2.76	0.81	36.61
35X-3, 100–102	320.10	45.14	68.02	1.54	2.58	0.85	46.54
35X-4, 100–102	321.60	48.85	73.76	1.55	2.73	0.79	33.78
35X-5, 100–102	323.10	44.22	69.24	1.60	2.76	0.89	41.28
35X-6, 100–102	324.60	48.26	71.41	1.52	2.74	0.78	38.95
36X-5, 100–102	332.60	48.56	71.87	1.52	2.66	0.78	39.78
36X-6, 100–102	334.10	48.26	71.41	1.52	2.74	0.78	55.99
37X-2, 100–102	337.60	28.29	54.07	1.96	2.75	1.40	74.23
37X-3, 100–102	339.10	30.72	56.82	1.89	2.78	1.31	56.71
37X-4, 100–102	340.60	27.31	53.37	2.00	2.77	1.45	79.31
37X-5, 100–102	342.10	32.38	58.41	1.85	2.85	1.25	38.36
39X-1, 106–108	355.16	31.92	58.40	1.87	2.80	1.28	43.04
39X-2, 90–92	356.50	24.40	48.36	2.03	2.79	1.54	65.22
40X-1, 105–107	364.65	23.21	46.44	2.05	2.82	1.57	68.30
40X-2, 100–102	366.10	23.38	46.32	2.03	2.84	1.55	67.22
40X-3, 104–106	367.64	25.85	49.78	1.97	2.77	1.46	60.21
40X-4, 102–104	369.12	36.92	63.08	1.75	2.79	1.10	16.68
42X-1, 106–108	383.66	24.82	48.19	1.99	2.76	1.50	41.95
42X-2, 104–106	385.14	24.11	47.52	2.02	2.84	1.53	48.96
42X-5, 101–103	389.61	22.97	44.87	2.00	2.78	1.54	59.88
42X-7, 32–34	391.92	22.92	47.20	2.11	2.81	1.63	66.30
43X-2, 100–102	394.60	25.33	48.27	1.95	2.83	1.46	52.12

Table 7 (continued).

Sample (core, section, cm)	Depth (mbsf)	Water content (%)	Porosity (%)	Densities: Wet bulk (g/cm^3)	Densities: Grain (g/cm^3)	Densities: Dry bulk (g/cm^3)	Carbonate content (%)
43X-4, 98–100	397.58	22.97	46.37	2.07	2.75	1.59	72.72
43X-5, 90–92	399.00	23.70	45.79	1.98	2.76	1.51	71.81
45X-1, 100–101	412.10	23.68	45.85	1.98	2.73	1.51	71.31
45X-3, 99–101	415.09	22.80	44.31	1.99	2.77	1.54	67.89
45X-5, 99–101	418.09	22.28	43.46	2.00	2.81	1.55	70.22
45X-6, 99–101	419.59	22.79	44.76	2.01	2.73	1.55	75.23
47X-1, 53–55	430.63	21.17	42.76	2.07	2.76	1.63	70.31
47X-2, 96–98	432.56	29.30	55.32	1.93	2.59	1.37	77.23
47X-3, 100–102	434.10	21.31	42.31	2.03	2.66	1.60	74.56
47X-4, 100–102	435.60	21.55	43.11	2.05	2.75	1.61	69.72
47X-5, 99–101	437.09	20.83	41.38	2.04	2.68	1.61	75.89
47X-6, 99–101	438.59	19.60	40.26	2.10	2.71	1.69	71.47
48X-1, 104–106	440.64	19.81	40.28	2.08	2.67	1.67	76.98
48X-2, 100–102	442.10	24.25	47.96	2.03	2.79	1.53	78.90
48X-3, 97–99	443.57	21.74	45.60	2.15	2.88	1.68	70.31
48X-4, 30–32	444.40	20.80	41.91	2.06	2.64	1.63	78.15
49X-1, 100–102	450.10	21.53	44.77	2.13	2.80	1.67	82.40
49X-2, 101–103	451.61	19.59	39.59	2.07	2.69	1.66	76.23
49X-3, 96–98	453.06	19.93	40.05	2.06	2.68	1.65	64.72
49X-4, 100–102	454.60	19.64	39.89	2.08	2.77	1.67	72.81
49X-5, 100–102	456.10	22.18	44.43	2.05	2.70	1.60	82.82
49X-6, 70–72	457.30	20.45	42.67	2.14	2.64	1.70	50.12
50X-1, 100–102	459.60	21.31	42.91	2.06	2.71	1.62	71.56
50X-2, 80–82	460.90	21.23	42.72	2.06	2.73	1.62	70.39
50X-3, 98–100	462.58	19.90	40.59	2.09	2.73	1.67	73.98
50X-4, 100–102	464.10	20.39	41.46	2.08	2.67	1.66	71.89
50X-5, 99–101	465.59	19.51	41.05	2.16	2.79	1.73	72.14
50X-6, 99–101	467.09	19.68	40.85	2.13	2.68	1.71	75.06
54X-1, 99–101	497.59	26.51	51.69	2.00	3.00	1.47	0.25
54X-2, 99–101	499.09	19.84	43.32	2.24	3.09	1.79	55.46
55X-1, 102–104	507.12	19.33	40.87	2.17	2.65	1.75	66.30

699A-8H and 114-699A-9H, results from an increase in terrigenous material.

Unit I (0–85.7 mbsf, lower Miocene to Quaternary)

		Mean	Minimum	Maximum
Wet-bulk density	(g/cm^3)	1.42	1.19	1.55
Dry-bulk density	(g/cm^3)	0.63	0.24	0.81
Grain density	(g/cm^3)	2.64	2.21	3.05
Porosity	(%)	77.75	71.80	92.20
Water content	(%)	56.50	47.80	79.60
Carbonate content	(%)	0.44	0.08	2.50
Shear strength	(kPa)	56.3	3.5	190.8
Thermal conductivity	(W/m/K)	1.0162	0.7850	1.6760
P-wave velocity	(m/s)	1627	1478	2115

Lithostratigraphic Unit II (85.7–233.6 mbsf) is subdivided into two subunits, which are readily apparent in the physical properties. The carbonate content starts to become appreciable in this unit, although siliceous matter still dominates in Subunit IIA, as seen in the grain density (Fig. 27). The carbonate content is markedly higher in Subunit IIB; this is reflected in the physical properties by increases in wet- and dry-bulk densities, grain density, shear strength, *P*-wave velocity, and thermal conductivity, and by decreases in porosity and water content from Subunits IIA to IIB.

Unit II (85.7–233.6 mbsf, lower Oligocene to lower Miocene)

		Mean	Minimum	Maximum
Wet-bulk density	(g/cm^3)	1.43	1.23	1.67
Dry-bulk density	(g/cm^3)	0.63	0.39	0.99
Grain density	(g/cm^3)	2.67	2.29	3.22
Porosity	(%)	78.19	65.80	86.80
Water content	(%)	56.49	40.60	69.50
Carbonate content	(%)	19.25	0.08	75.06
Shear strength	(kPa)	167.7	37.7	391.0
Thermal conductivity	(W/m/K)	1.0082	0.7120	1.2890
P-wave velocity	(m/s)	1628	1547	1704

Subunit IIA (85.7–142 mbsf)

		Mean	Minimum	Maximum
Wet-bulk density	(g/cm^3)	1.32	1.23	1.37
Dry-bulk density	(g/cm^3)	0.46	0.39	0.54
Grain density	(g/cm^3)	2.51	2.29	2.71
Porosity	(%)	83.15	80.20	86.80
Water content	(%)	64.77	61.20	69.50
Carbonate content	(%)	7.84	0.08	32.11
Shear strength	(kPa)	108.6	37.7	186.2
Thermal conductivity	(W/m/K)	0.8826	0.7400	0.9640
P-wave velocity	(m/s)	1614	1547	1668

Subunit IIB (142–233.6 mbsf)

		Mean	Minimum	Maximum
Wet-bulk density	(g/cm^3)	1.51	1.35	1.67
Dry-bulk density	(g/cm^3)	0.74	0.53	0.99
Grain density	(g/cm^3)	2.77	2.46	3.22
Porosity	(%)	74.89	65.80	82.20
Water content	(%)	50.97	40.60	61.50
Carbonate content	(%)	26.85	0.17	75.06
Shear strength	(kPa)	209.3	78.0	391.0
Thermal conductivity	(W/m/K)	1.0815	0.7120	1.2890
P-wave velocity	(m/s)	1644	1572	1704

Lithostratigraphic Unit IV (243.1–335.43 mbsf) is fairly uniform in its properties, except for one sample from a diatom-rich layer that has essentially no carbonate and a grain density of 2.47 g/cm^3. We restricted sampling of Unit IV to the lower part because of drilling disturbance down to Core 114-699A-29X. As mentioned in "Lithostratigraphy" section, there was some contamination from Unit III in the cores of Unit IV, and as much as was possible, our sampling avoided the contaminated segments.

The transition from the nannofossil ooze of Unit IV to the nannofossil chalk of lithostratigraphic Unit V (335.4–487.9 mbsf) yields the most dramatic changes in the physical properties. Water content and porosity decrease from 48.26% to 28.29% and

Table 8. Vane shear strength, Hole 699A.

Sample (core, section, cm)	Depth (mbsf)	Shear strength (kPa)
1H-1, 100–102	1.00	5.8
1H-2, 100–102	2.50	5.8
1H-3, 98–100	3.98	5.1
1H-4, 100–102	5.50	4.7
1H-5, 100–102	7.00	13.3
1H-6, 90–92	8.40	12.6
2H-1, 100–102	9.60	6.5
2H-2, 100–102	11.10	48.4
2H-3, 100–102	12.60	41.9
2H-4, 100–102	14.10	60.0
3H-1, 100–102	19.10	41.4
3H-2, 100–102	20.60	63.3
3H-3, 100–102	22.10	74.0
3H-4, 100–102	23.60	63.3
4H-1, 100–102	28.60	10.0
4H-2, 100–102	30.10	29.1
4H-3, 100–102	31.60	17.5
4H-4, 75–77	32.85	10.5
4H-5, 100–102	34.01	8.6
5H-1, 100–102	38.10	3.5
5H-2, 100–102	39.60	48.4
5H-3, 100–102	41.10	69.3
5H-4, 100–102	42.60	100.1
5H-5, 100–102	44.10	93.1
6H-1, 95–97	47.55	20.9
6H-2, 100–102	49.10	51.2
6H-3, 90–92	50.50	60.5
6H-4, 100–102	52.10	53.5
6H-5, 100–102	53.60	90.8
6H-6, 38–40	54.48	97.7
7H-2, 100–102	58.60	74.5
7H-3, 100–102	60.10	76.8
7H-4, 100–102	61.60	90.8
7H-5, 80–82	62.90	104.7
8H-1, 100–102	66.60	90.8
8H-2, 100–102	68.10	83.8
8H-3, 100–102	69.60	107.0
8H-4, 100–102	71.10	190.8
8H-5, 100–102	72.60	142.0
9H-4, 100–102	80.60	79.1
10H-1, 100–102	85.60	55.9
10H-2, 98–100	87.08	55.9
10H-3, 100–102	88.60	104.7
10H-4, 100–102	90.10	111.7
10H-5, 100–102	91.60	130.3
10H-6, 50–52	92.60	153.6
11H-1, 100–102	95.10	83.8
11H-2, 100–102	96.60	83.8
11H-3, 100–102	98.10	158.2
11H-4, 100–102	99.60	186.2
12H-2, 100–102	106.10	51.2
12H-3, 100–102	107.60	161.0
12H-4, 100–102	109.10	147.8
12H-5, 100–102	110.60	122.2
13H-1, 100–102	114.10	48.9
13H-2, 100–102	115.60	120.5
13H-3, 100–102	117.10	154.1
13H-4, 100–102	118.60	124.5
14H-1, 100–102	123.60	37.7
14H-2, 100–102	125.10	79.6
14H-3, 100–102	126.60	124.5
14H-4, 100–102	128.10	93.8
15H-1, 100–102	133.10	66.8
15H-2, 100–102	134.60	59.3
15H-3, 100–102	136.10	109.4
15H-4, 100–102	137.60	183.1
15H-5, 100–102	139.10	70.3
16H-1, 100–102	142.60	78.0
16H-2, 101–103	144.11	108.9
16H-3, 100–102	145.60	174.5
16H-4, 100–102	147.10	204.3
16H-5, 100–102	148.60	144.3
17H-2, 100–102	153.60	143.1
17H-3, 99–101	155.09	179.2

Table 8 (continued).

Sample (core, section, cm)	Depth (mbsf)	Shear strength (kPa)
17H-4, 100–102	156.60	195.5
17H-5, 100–102	158.10	158.2
18H-1, 100–102	161.60	83.8
18H-2, 100–102	163.10	93.1
18H-3, 100–102	164.60	190.8
18H-4, 100–102	166.10	193.2
19H-1, 100–102	171.10	388.6
19H-2, 100–102	172.60	297.9
19H-3, 100–102	174.10	288.6
19H-3, 125–127	174.35	391.0
19H-4, 100–102	175.60	286.2
20H-1, 100–102	180.60	128.0
20H-2, 100–102	182.10	342.1
20H-3, 100–102	183.60	314.2
20H-4, 100–102	185.10	228.1
20H-5, 100–102	186.60	288.6
21H-1, 100–102	190.10	93.1
21H-2, 100–102	191.60	279.3
21H-3, 100–102	193.10	321.1
21H-4, 100–102	194.60	283.9
21H-5, 100–102	196.10	209.4
22H-1, 100–102	199.60	246.7
22H-2, 96–98	201.06	323.5
22H-3, 100–102	202.60	321.1
22H-4, 100–102	204.10	256.0
23X-1, 90–92	206.00	90.8
23X-2, 103–105	207.63	97.7
23X-3, 100–102	209.10	123.3
24X-2, 85–87	216.95	81.4
24X-3, 30–32	217.90	116.4
30X-1, 100–102	269.60	97.7
30X-2, 100–102	271.10	75.6
30X-3, 100–102	272.60	42.4
30X-4, 100–102	274.10	60.5
31X-1, 110–112	279.20	52.4
31X-2, 100–102	280.60	87.3
31X-4, 100–102	283.60	122.9
31X-5, 100–102	285.10	113.3
33X-1, 100–102	298.10	104.7
33X-2, 100–102	299.60	153.6
33X-3, 102–104	301.12	87.3
33X-4, 102–104	302.60	74.0
33X-5, 100–102	304.10	58.2
33X-6, 108–110	305.68	108.9
35X-2, 100–102	318.60	111.7

from 71.41% to 54.07%, respectively, and the density and velocity correspondingly increase from 1.52 to 1.96 g/cm^3 and from 1590 to 1840 m/s, respectively. The overall physical properties for Unit IV are summarized as follows:

Unit IV (243.1–335.43 mbsf, upper Eocene to lower Oligocene)

		Mean	Minimum	Maximum
Wet-bulk density	(g/cm^3)	1.51	1.07	1.65
Dry-bulk density	(g/cm^3)	0.78	0.40	0.99
Grain density	(g/cm^3)	2.72	2.47	2.93
Porosity	(%)	71.22	27.20	84.80
Water content	(%)	48.40	26.00	68.70
Carbonate content	(%)	44.08	0.33	71.81
Shear strength	(kPa)	90.0	42.4	122.9
Thermal conductivity	(W/m/K)	1.1987	0.7500	1.7200
P-wave velocity	(m/s)	1629	1545	1738

Unit V is subdivided into Subunits VA (335.44–375.2 mbsf) and VB (382.6–487.91 mbsf) based on the relative abundance of chalk and diagenetic micrite, but the subunits are not evident in the physical properties. The brittle nature of the cores precluded vane-shear-strength measurements. The physical properties for Unit V are as follows:

Table 9. Sonic velocity, Hole 699A.

Sample (core, section, cm)	Depth (mbsf)	Direction[a]	Velocity (m/s)
2H-2, 100–102	11.10	C	1472
2H-4, 100–102	14.10	C	1500
3H-1, 100–102	19.10	C	1473
3H-3, 100–102	22.10	C	1511
5H-2, 100–102	39.60	C	1398
5H-3, 100–102	41.10	C	1474
5H-4, 100–102	42.60	C	1441
5H-5, 100–102	44.10	C	1473
7H-4, 3–5	60.63	C	2031
8H-1, 50–52	66.10	C	1612
8H-3, 30–32	68.90	C	1568
8H-4, 50–52	70.60	C	1581
10H-2, 94–96	87.04	C	1569
10H-3, 50–52	88.10	C	1563
10H-4, 30–32	89.40	C	1589
11H-1, 97–99	95.07	C	1500
11H-2, 48–50	96.08	C	1546
11H-4, 48–50	99.08	C	1575
12H-2, 100–102	106.10	C	1463
12H-3, 100–102	107.60	C	1570
12H-4, 100–102	109.10	C	1583
12H-5, 100–102	110.60	C	1462
13H-2, 98–100	115.58	C	1556
13H-4, 99–101	118.59	C	1488
14H-2, 100–102	125.10	C	1512
15H-1, 100–102	133.10	C	1486
15H-2, 99–101	134.59	C	1474
15H-3, 99–101	136.09	C	1568
15H-4, 99–101	137.59	C	1559
15H-5, 99–101	139.09	C	1507
16H-1, 99–101	142.59	C	1568
16H-3, 98–100	145.58	C	1589
16H-4, 99–101	147.09	C	1525
16H-5, 99–101	148.59	C	1552
17H-2, 99–101	153.59	C	1498
17H-3, 99–101	155.09	C	1566
17H-4, 99–101	156.59	C	1505
17H-5, 99–101	158.09	C	1555
18H-1, 99–101	161.59	C	1499
18H-2, 100–102	163.10	C	1507
19H-1, 70–72	170.80	C	1612
19H-2, 70–72	172.30	C	1626
20H-1, 48–50	180.08	C	1596
20H-3, 100–102	183.60	C	1605
21H-5, 50–52	195.60	C	1583
22H-4, 58–60	203.68	C	1600
30X-2, 100–102	271.10	C	1526
30X-4, 100–102	274.10	C	1584
31X-1, 110–112	279.20	C	1587
31X-2, 100–102	280.60	C	1575
31X-4, 100–102	283.60	C	1488
33X-1, 100–102	298.10	C	1594
33X-2, 100–102	299.60	C	1511
33X-3, 102–104	301.12	C	1461
33X-6, 108–110	305.68	C	1483
35X-4, 48–50	321.08	C	1590
36X-7, 23–25	334.83	C	1642
37X-2, 78–80	337.38	C	1754
40X-1, 100–102	364.60	C	1840
47X-1, 48–50	430.58	C	1769
47X-4, 48–50	435.08	C	1943
48X-1, 106–108	440.66	C	1841
48X-2, 100–102	442.10	C	1770
48X-3, 99–101	443.59	C	1787
48X-4, 30–32	444.40	C	1875
48X-4, 86–88	444.96	C	1658
49X-1, 100–102	450.10	C	1981
49X-2, 102–104	451.62	C	1940
49X-3, 97–99	453.07	C	1966
49X-4, 100–102	454.60	C	1894
49X-5, 100–102	456.10	C	1976
49X-6, 70–72	457.30	C	1876
50X-1, 100–102	459.60	C	1872
50X-2, 80–82	460.90	C	1730
50X-3, 101–103	462.61	C	1804
50X-5, 101–103	465.61	C	1954
50X-6, 100–102	467.10	C	1866

[a] A = perpendicular to split-core surface; B = parallel to split-core surface; C = axial.

Table 10. Thermal conductivity, Hole 699A.

Sample (core, section, cm)	Depth (mbsf)	Thermal conductivity (W/m/K)
1H-2, 100–102	2.50	0.8290
1H-3, 100–102	4.00	0.7850
1H-4, 100–102	5.50	0.8860
1H-5, 100–102	7.00	0.7850
1H-6, 90–92	8.40	0.9450
2H-1, 100–102	9.60	0.9880
2H-2, 100–102	11.10	0.9240
2H-3, 100–102	12.60	0.9880
2H-4, 100–102	14.10	1.0090
3H-1, 100–102	19.10	1.4450
3H-2, 100–102	20.60	1.0370
3H-3, 100–102	22.10	1.0740
3H-4, 100–102	23.60	0.9350
4H-1, 100–102	28.60	0.9630
4H-2, 100–102	30.10	1.0080
4H-3, 100–102	31.60	1.0060
4H-4, 75–77	32.85	1.0590
4H-5, 100–102	34.01	0.9540
5H-1, 100–102	38.10	0.9120
5H-2, 100–102	39.60	1.0650
5H-3, 100–102	41.10	0.9650
5H-4, 100–102	42.60	1.0450
5H-5, 100–102	44.10	1.0190
6H-1, 100–102	47.60	0.2640
6H-2, 100–102	49.10	0.2540
6H-3, 100–102	50.60	0.2390
6H-4, 100–102	52.10	0.2390
6H-5, 100–102	53.60	1.6760
6H-6, 60–62	54.70	0.9930
7H-1, 100–102	57.10	0.9560
7H-2, 100–102	58.60	1.0270
7H-3, 100–102	60.10	1.1160
7H-4, 100–102	61.60	1.1240
8H-1, 100–102	66.60	0.9560
8H-2, 100–102	68.10	1.1240
8H-3, 100–102	69.60	1.0260
8H-4, 100–102	71.10	1.1160
10H-3, 100–102	88.60	0.9640
11H-1, 100–102	95.10	0.8550
11H-2, 100–102	96.60	0.8470
11H-3, 100–102	98.10	0.9090
11H-4, 100–102	99.60	0.8910
12H-2, 100–102	106.10	0.9340
12H-3, 100–102	107.60	0.9030
12H-4, 100–102	109.10	0.8800
12H-5, 100–102	110.60	0.8950
13H-2, 100–102	115.60	0.8570
13H-3, 100–102	117.10	0.8640
13H-4, 100–102	118.60	0.8770
14H-1, 100–102	123.60	0.7910
14H-2, 100–102	125.10	0.8900
14H-3, 100–102	126.60	0.8920
14H-4, 100–102	128.10	0.8910
15H-1, 100–102	133.10	0.7400
15H-2, 100–102	134.60	0.9310
15H-3, 100–102	136.10	0.9390
15H-4, 100–102	137.60	0.9420
15H-5, 100–102	139.10	0.8420
16H-1, 100–102	142.60	0.8430
16H-2, 100–102	144.10	0.9840
16H-3, 100–102	145.60	1.0180
16H-4, 100–102	147.10	0.9200
16H-5, 100–102	148.60	0.9700
17H-1, 100–102	152.10	1.0930
17H-2, 100–102	153.60	1.1890
17H-3, 100–102	155.10	0.7710
17H-4, 100–102	156.60	1.1300
17H-5, 100–102	158.10	1.1900
18H-1, 100–102	161.60	0.5560
18H-2, 100–102	163.10	0.9960
18H-3, 100–102	164.60	1.1500
18H-4, 100–102	166.10	1.1290
18H-5, 100–102	167.60	1.0290
18H-6, 40–42	168.50	1.0860
19H-1, 100–102	171.10	1.2520
19H-2, 100–102	172.60	1.0940

Table 10 (continued).

Sample (core, section, cm)	Depth (mbsf)	Thermal conductivity (W/m/K)
19H-4, 100–102	175.60	1.0670
20H-1, 100–102	180.60	1.1390
20H-2, 100–102	182.10	1.1150
20H-3, 100–102	183.60	0.7120
20H-4, 100–102	185.10	1.0990
20H-5, 100–102	186.60	1.2890
21H-1, 100–102	190.10	1.1751
21H-2, 100–102	191.60	1.1200
21H-3, 100–102	193.10	1.0440
21H-4, 100–102	194.60	1.1840
21H-5, 100–102	196.10	1.1450
21H-6, 40–42	197.20	1.2600
22H-1, 100–102	199.60	1.2000
22H-2, 100–102	201.10	1.2030
22H-3, 100–102	202.60	1.2750
23X-2, 100–102	207.60	0.9980
23X-3, 100–102	209.10	1.0370
23X-4, 100–102	210.60	1.0000
24X-1, 100–102	215.60	1.0280
30X-1, 110–112	269.70	1.1020
30X-2, 100–102	271.10	1.0320
30X-3, 60–62	272.20	1.0420
30X-4, 100–102	274.10	1.2600
31X-1, 110–112	279.20	1.2040
31X-2, 100–102	280.60	1.0990
31X-3, 100–102	282.10	1.3640
31X-4, 100–102	283.60	1.1970
31X-5, 100–102	285.10	1.1480
31X-6, 100–102	286.60	1.1210
32X-1, 100–102	288.60	0.8760
32X-2, 100–102	290.10	0.7500
32X-3, 100–102	291.60	1.5780
32X-6, 100–102	296.10	1.1300
33X-1, 100–102	298.10	1.3240
33X-2, 100–102	299.60	1.3360
33X-3, 100–102	301.10	1.2270
33X-4, 100–102	302.60	1.4530
33X-5, 100–102	304.10	1.2570
33X-6, 100–102	305.60	1.1350
35X-1, 100–102	317.10	1.1390
35X-2, 100–102	318.60	1.1550
35X-3, 100–102	320.10	1.3240
35X-4, 100–102	321.60	1.1320
35X-5, 100–102	323.10	1.0940
35X-6, 100–102	324.60	1.1270
36X-1, 100–102	326.60	1.7200
36X-2, 100–102	328.10	1.0960
36X-3, 100–102	329.60	1.1640
36X-4, 100–102	331.10	1.1890
36X-5, 100–102	332.60	1.2720
36X-6, 100–102	334.10	1.3110
37X-1, 100–102	336.10	1.5570
37X-2, 100–102	337.60	1.4330
37X-3, 100–102	339.10	1.4740
39X-2, 100–102	356.60	1.5130
40X-1, 100–102	364.60	1.6780
42X-1, 100–102	383.60	1.4920
42X-2, 100–102	385.10	1.5780
42X-3, 100–102	386.60	1.5210
42X-4, 100–102	388.10	1.3700
43X-2, 100–102	394.60	1.5270
43X-3, 100–102	396.10	1.3290
43X-4, 100–102	397.60	1.5490
43X-5, 100–102	399.10	1.4910

Unit V (335.4–487.9 mbsf, lower to upper Eocene)

		Mean	Minimum	Maximum
Wet-bulk density	(g/cm^3)	2.03	1.75	2.16
Dry-bulk density	(g/cm^3)	1.55	1.10	1.73
Grain density	(g/cm^3)	2.75	2.59	2.88
Porosity	(%)	46.13	39.60	63.10
Water content	(%)	23.45	19.50	36.90
Carbonate content	(%)	66.87	16.68	82.82
Thermal conductivity	(W/m/K)	1.5093	1.3290	1.6780
P-wave velocity	(m/s)	1959	1744	2074

The bottom lithostratigraphic Unit VI (496.6–516.3 mbsf) was only sparsely sampled for physical properties. Nonetheless, based on the few samples that we have, there appears to be little change in the physical properties across the unit boundary. The properties of Unit VI are as follows:

Unit VI (496.6–516.3 mbsf, upper Paleocene)

		Mean	Minimum	Maximum
Wet-bulk density	(g/cm^3)	2.14	2.00	2.24
Dry-bulk density	(g/cm^3)	1.67	1.47	1.79
Grain density	(g/cm^3)	2.91	2.65	3.09
Porosity	(%)	45.30	40.90	51.70
Water content	(%)	21.87	19.30	26.50
Carbonate content	(%)	40.67	0.25	66.30

Cyclicity in Physical Properties

In the lithologic descriptions, there is evidence for cyclicity in the depositional record. The physical-property sampling shows cyclicity as well, but our sampling procedure was not capable of recording the fine-scale variations apparent in the core. As many as 10 samples per section would be required to properly define some of the cycles, instead of the current practice of one sample per section. The *P*-wave logger (PWL) records have sufficient sample density to provide evidence of apparent cyclicity in the physical properties. Unfortunately, the GRAPE data are plotted on too coarse a scale to be useful for such a purpose, and at the moment there is no shipboard capability to replot the GRAPE data. The PWL data, however, show definite apparent cyclicity, as does the magnetic susceptibility (Fig. 28).

For comparison, the PWL and volume magnetic susceptibility data have been plotted on the same depth scale for Core 114-699A-2H (Fig. 28). There appears to be an 180° phase shift between the PWL and susceptibility curves, and the PWL data display both short and long spatial wavelengths that are not apparent in the susceptibility record. The PWL data from other cores have also been plotted to compare any apparent cyclicity observed in the *P*-wave velocity in sections representing different time periods: the Quaternary (Core 114-699A-2H), the early Miocene (Core 114-699A-9H), the late Oligocene (Core 114-699A-18H), and the late Eocene (Core 114-699A-33X) (Fig. 29). The general pattern does appear to be present, but as might be expected, the spatial cyclicity becomes compressed in the deeper sections because of the process of compaction. However, differences could also arise from changes in sedimentation rates and the presence of hiatuses. A more detailed quantitative analysis will be carried out on shore using the detailed time-depth scale constructed from the "Biostratigraphy" and "Paleomagnetics" sections.

Hiatuses and Physical Properties

The overall pattern at Site 699 shows that the observed changes in physical properties correspond to both changes in the sediment facies and an increase in sediment compaction and diagenetic alteration of the sediment with depth. These changes dominate the record. To investigate whether hiatuses, as documented in the diatom biostratigraphic record (see "Biostratigraphy" section), also cause distinct changes in physical properties, we will concentrate on the sections just above and below three hiatuses. The sediments of Neogene age in lithostratigraphic Unit I show three major hiatuses (see "Lithostratigraphy" and "Biostratigraphy" sections), which are compared with the record of physical properties. The approximate lengths of the missing sediment sections are calculated by drawing a line parallel to the sedimentation rate just below the hiatus, which is connected to the top of the hiatus, and then picking the intercept between that line and the isochron for the age of the bottom of the hiatus. The difference between the actual sediment depth at the bottom of the hiatus and the intercept depth is approximately equal to the amount of missing sediment.

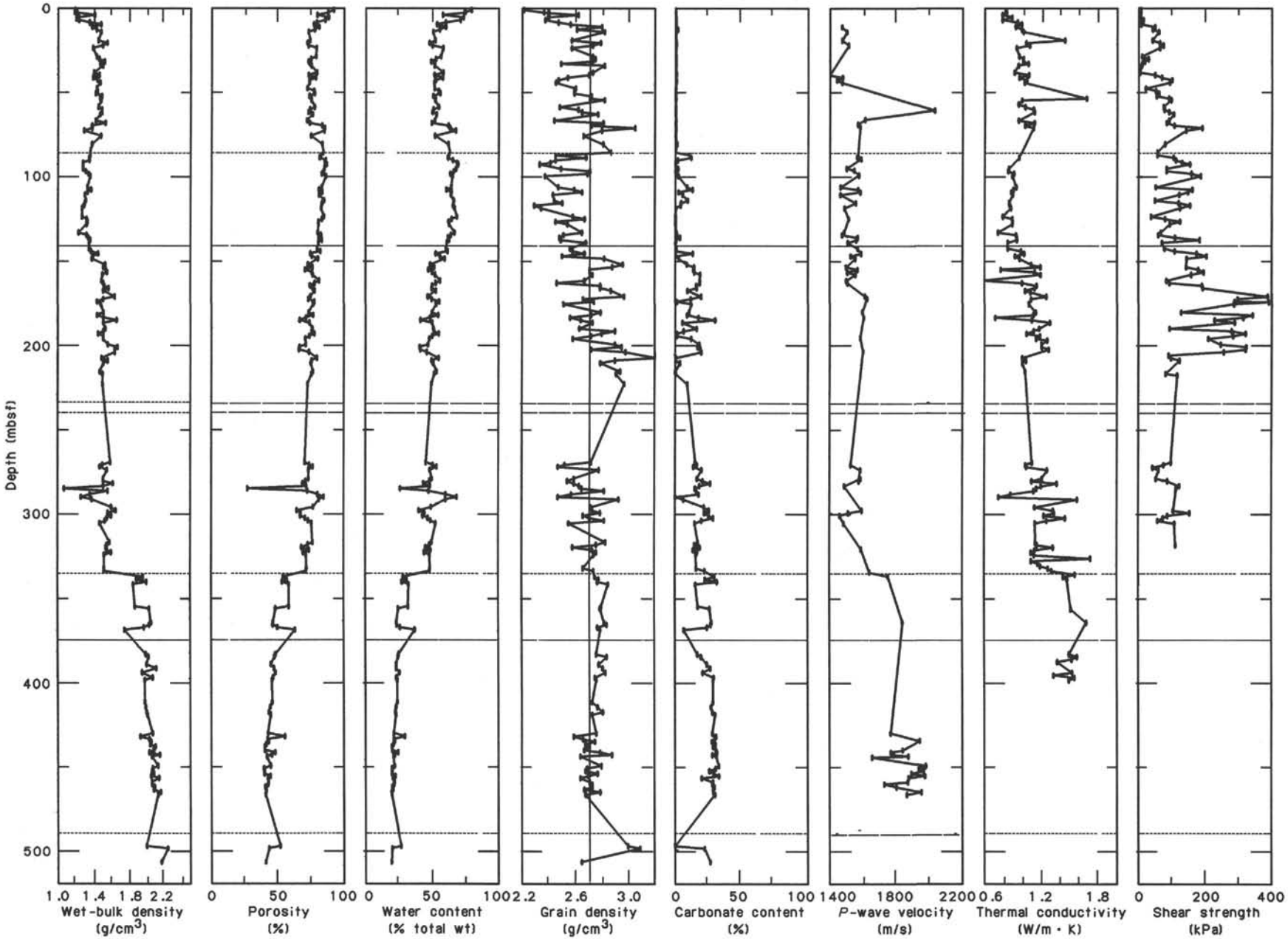

Figure 27. Wet-bulk density, porosity, water content, grain density, carbonate content, *P*-wave velocity, vane shear strength, and thermal conductivity profiles for Hole 699A. The boundaries between the lithostratigraphic units are indicated by the long dashed lines, the subunit divisions are shown by the short dashed lines. Note thin Unit III at a depth of about 234 mbsf. In the grain density plot, the vertical line marks a grain density of 2.70 g/cm^3, and areas to the left of the line represent samples where the siliceous content may be higher.

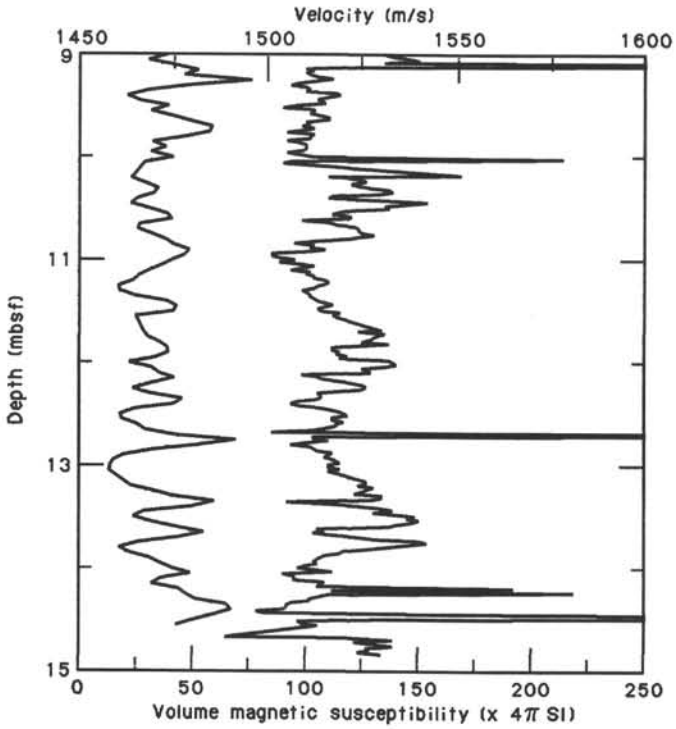

Figure 28. Comparative plot of *P*-wave logger (curve on right) and volume magnetic susceptibility data (curve on left) for Core 114-699A-2H. Note the apparent correlation between magnetic susceptibility highs and *P*-wave velocity lows except for scattered dropstones, as indicated by the sharp velocity peaks.

Hiatus I
(Approximate depth = 31 mbsf; Age of missing section = 2.5–2.8 m.y.;
Approximate thickness of missing section = 5–10 m)

Relationship to hiatus	Depth (mbsf)	Water content (%)	Porosity (%)	Wet-bulk density (g/cm^3)	Dry-bulk density (g/cm^3)	$CaCO_3$ content (%)	Grain density (g/cm^3)	Shear strength (kPa)	Velocity (m/s)
Above	28.6	56.43	78.70	1.43	0.62	0.75	2.73	10.0	
Above	30.1	52.60	74.87	1.46	0.69	0.58	2.75	29.1	
At	31.6	49.07	72.92	1.52	0.78	0.75	2.73	17.5	
Below	32.9	51.71	74.09	1.47	0.71	0.67	2.49	10.5	
Below	34.0	51.46	75.14	1.50	0.73	0.83	2.82	8.6	

Hiatus III
(Approximate depth = 54 mbsf; Age of missing section = 4.5–8.5 m.y.;
Approximate thickness of missing section = 5–12 m)

Relationship to hiatus	Depth (mbsf)	Water content (%)	Porosity (%)	Wet-bulk density (g/cm^3)	Dry-bulk density (g/cm^3)	$CaCO_3$ content (%)	Grain density (g/cm^3)	Shear strength (kPa)	Velocity (m/s)
Above	52.1	50.55	73.60	1.49	0.74	0.17	2.72	53.5	
Above	53.6	52.22	75.05	1.47	0.70	0.42	2.71	90.8	
At	54.48	52.16	75.15	1.48	0.71	0.17	2.82	97.7	
Below	58.6	54.70	77.50	1.45	0.66	0.17	2.48	74.5	

Hiatus IV
(Approximate depth = 68 mbsf; Age of missing section = 9.5–19.9 m.y.;
Approximate thickness of missing section = 65 m)

Relationship to hiatus	Depth (mbsf)	Water content (%)	Porosity (%)	Wet-bulk density (g/cm^3)	Dry-bulk density (g/cm^3)	$CaCO_3$ content (%)	Grain density (g/cm^3)	Shear strength (kPa)	Velocity (m/s)
Above	66.6	51.81	71.84	1.42	0.68	0.83	2.44	90.8	1612
Above	68.1	49.43	73.75	1.53	0.77	0.08	2.81	83.8	1568
At	69.6	62.04	83.36	1.38	0.52	0.33	2.72	107.0	
Below	71.1	63.40	85.32	1.38	0.50	0.58	3.05	190.8	1581
Below	72.6	67.57	85.11	1.29	0.42	0.42	2.80	142.0	

The correlation between changes in physical properties and hiatuses is present but weaker for hiatuses I and III, where the approximate length of the missing sediments is 5–10 m. The apparent correlation is distinct at hiatus IV, where the approximate thickness of the missing sediment is 65 m.

Normally, we would expect to see a decrease in water content and porosity and an associated increase in bulk density across a hiatus because of the removal of the top section of sediments. Hiatus IV, instead, displays increased water content and porosity across the hiatus. This observation may be related to increased clay content just below the hiatus, as has been documented in the lower part of lithostratigraphic Unit I (see "Lithostratigraphy" section). In addition, manganese nodules were found at or very near the top of the hiatus. This information, taken as a whole, leads us to suggest a model of sediment nondeposition, as opposed to sediment removal, to explain hiatus IV.

SEISMIC STRATIGRAPHY

JOIDES Resolution approached Site 699 following the track of *Islas Orcadas* (Fig. 30) and started acquiring seismic-reflection data at a survey speed of 5.5 kt about 1.5 nmi before and continued 3 nmi beyond the site location. Two 80-in.^{3} water guns were used as the seismic source. The beacon was dropped on the first pass. The 3.5-kHz echo-sounder showed a penetration of about 20 m along the profile. Upon leaving the site, *JOIDES Resolution* streamed the seismic gear and started recording with a single water gun as the source about 2 nmi west of the site, passing the beacon again while underway to Site 700. The two records obtained over the same ground under global-positioning system navigation show considerable difference in the relative definition of some of the main seismic marker events (Fig. 31). This difference in spectral content results primarily from inadequate control on streamer depth and source depth under unfavorable weather conditions.

Lithostratigraphic Unit I is defined in the physical-property data by a basal inversion expressed most dramatically in the grain density and to a lesser degree in wet-bulk density and *P*-wave velocity variations (Fig. 31). This gives rise to a distinct reflection with a phase reversal. A hiatus is probably present because the basal part of Unit I downlaps on this reflection event. However, planktonic foraminifers from either side of the boundary fall within the same faunal zone, and the presence of a hiatus at the site location cannot be resolved. Grain densities vary considerably within the essentially carbonate-free siliceous ooze and siliceous clayey ooze. The clay content varies between 10% and 60% with two clay-free intervals at 45 mbsf and at the base of Unit I (85 mbsf). Impedance contrasts generated by variations in the clay content are probably responsible for the acoustic stratification of this unit, similar to that observed at DSDP Site 513 (Bayer and Ott, 1983). A major middle lower Miocene to upper middle Miocene hiatus is present at 67–69 mbsf, but is not resolvable in the seismic data.

Low *P*-wave velocities, wet-bulk densities, and grain densities characterize the siliceous nannofossil ooze in the upper part of Unit II, whereas the nannofossil ooze in the lower part is associated with significantly higher values. Subunit IIB is relatively carbonate rich and clay free. This gives rise to a reflection corresponding to the transition between Subunits IIA and IIB (Fig. 31). Downhole variation in *P*-wave velocity that is related to large variations in grain density in Subunit IIB is probably responsible for impedance contrasts forming the observed acoustic layering of this subunit. Constructive interference resulting from impedance contrasts generated by large variations in carbonate content must be responsible for the large amplitudes corresponding to the lower part of Subunit IIB.

No physical-property measurements were made of the 2-m-thick gravel layer that constitutes Unit III. Detection of the gravel layer requires that its thickness be comparable to the tuning thickness (3–6 m) for the frequencies considered here (60–150 Hz).

The transition from nannofossil ooze (Unit IV) to nannofossil chalk (Unit V) corresponds to the largest downhole increase in *P*-wave velocity and wet-bulk density at Site 699. This is associated with a reflection, which is not of the magnitude expected

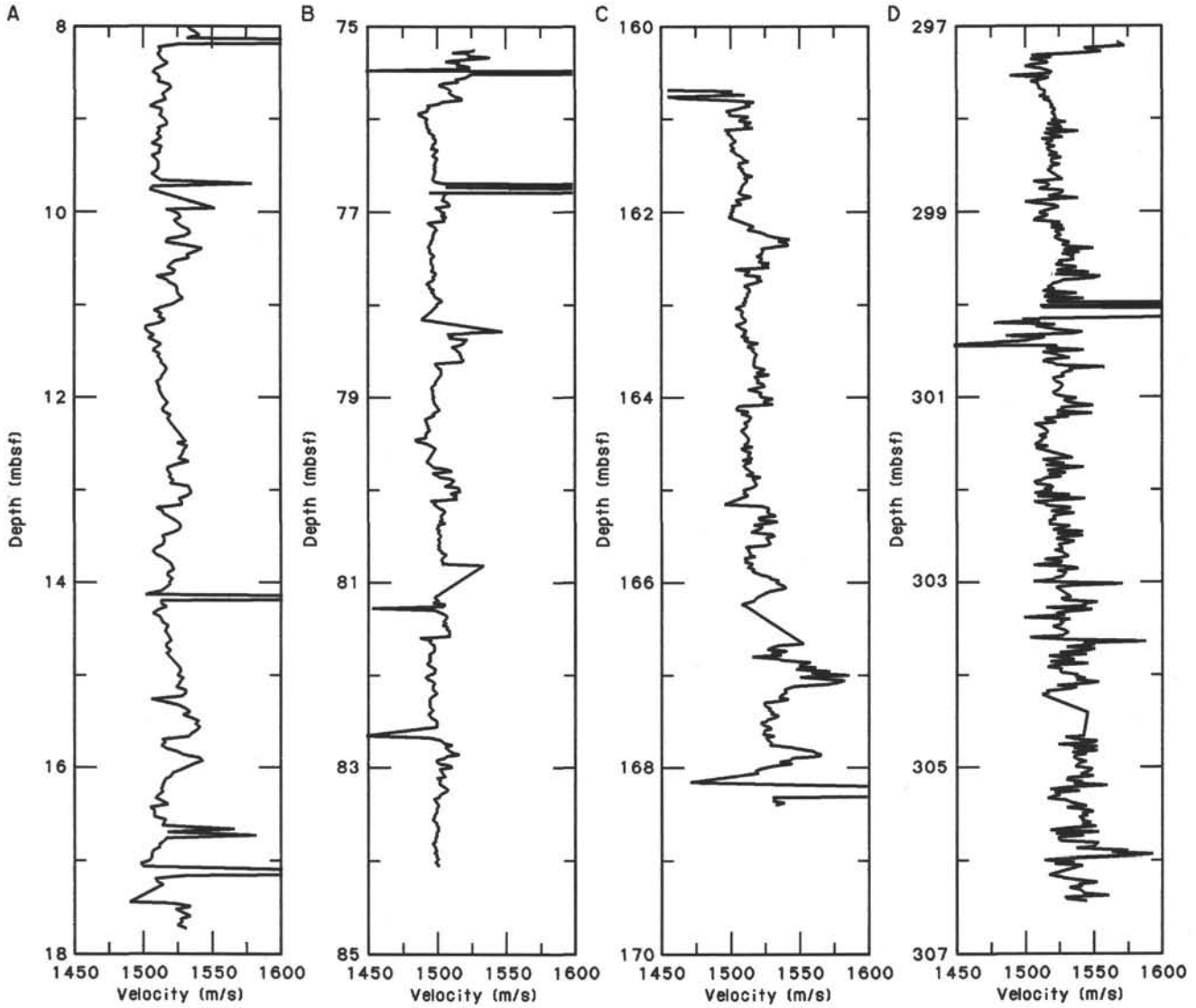

Figure 29. Plots of *P*-wave logger data vs. depth for a comparison of the paleoclimatic cyclicity as recorded in the velocity variations for different periods. **A.** Core 114-699A-2H (Quaternary). **B.** Core 14-699A-9H (lower Miocene). **C.** Core 114-699A-18H (upper Oligocene). **D.** Core 114-699A-33X (upper Eocene).

from the measurements. An essentially reflection-free ooze/chalk transition has also been observed in other instances (Packham and van der Lingen, 1973). However, a reflection seems to be related to the transition to a micritic texture in the chalk (Subunit VB). Incomplete *P*-wave velocity measurements in the upper part of Subunit VB make it difficult to identify the possible origin of at least two distinct reflectors in the upper part of this subunit. The transition to zeolite-bearing claystone at 496.6 mbsf does not have any significant acoustic expression.

A number of vertical faults with offsets of 10 m or less displace Oligocene strata. Their extension at depth cannot be confirmed with the available data. These minor faults are probably related to differential compaction.

SUMMARY AND CONCLUSIONS

Summary

Site 699 (Fig. 32) is in the western region of the East Georgia Basin (51°32.531′S, 30°40.603′W) on the northeastern slope of Northeast Georgia Rise in a water depth of 3705 m. The site is 150 km east of Site 698 along the same *Islas Orcadas* single-channel seismic-reflection line (Fig. 2). This site was selected to obtain a high-quality (APC, XCB, and NCB2 systems), continuously cored sequence of Late Cretaceous to Neogene age that records the role of the Georgia Basin as an avenue for deep-water communication between the Weddell Sea and the South Atlantic prior to the Eocene opening of the Islas Orcadas Rise–Meteor Rise gateway. Site 699 overlies crust that predates the opening of this gateway. Comparison of the sedimentary record of Site 699 with that of Site 701, which lies on crust within the early gateway between the Islas Orcadas Rise and the Meteor Rise, was intended to provide a means of interpreting the influence of gateway opening on the paleoenvironment in the subantarctic and other regions north and south of the gateway (Fig. 32). Carbonate-bearing sequences of Late Cretaceous and Paleogene age from Site 699 and other Leg 114 sites document the evolution of surface and vertical water-mass temperature gradients.

Single-channel seismic-reflection data show an 0.8-s-thick (TWT) section consisting of three acoustic units. An upper 400-m-thick unit with acoustic stratification overlies a more transparent, but weakly bedded, 300-m-thick section. An ap-

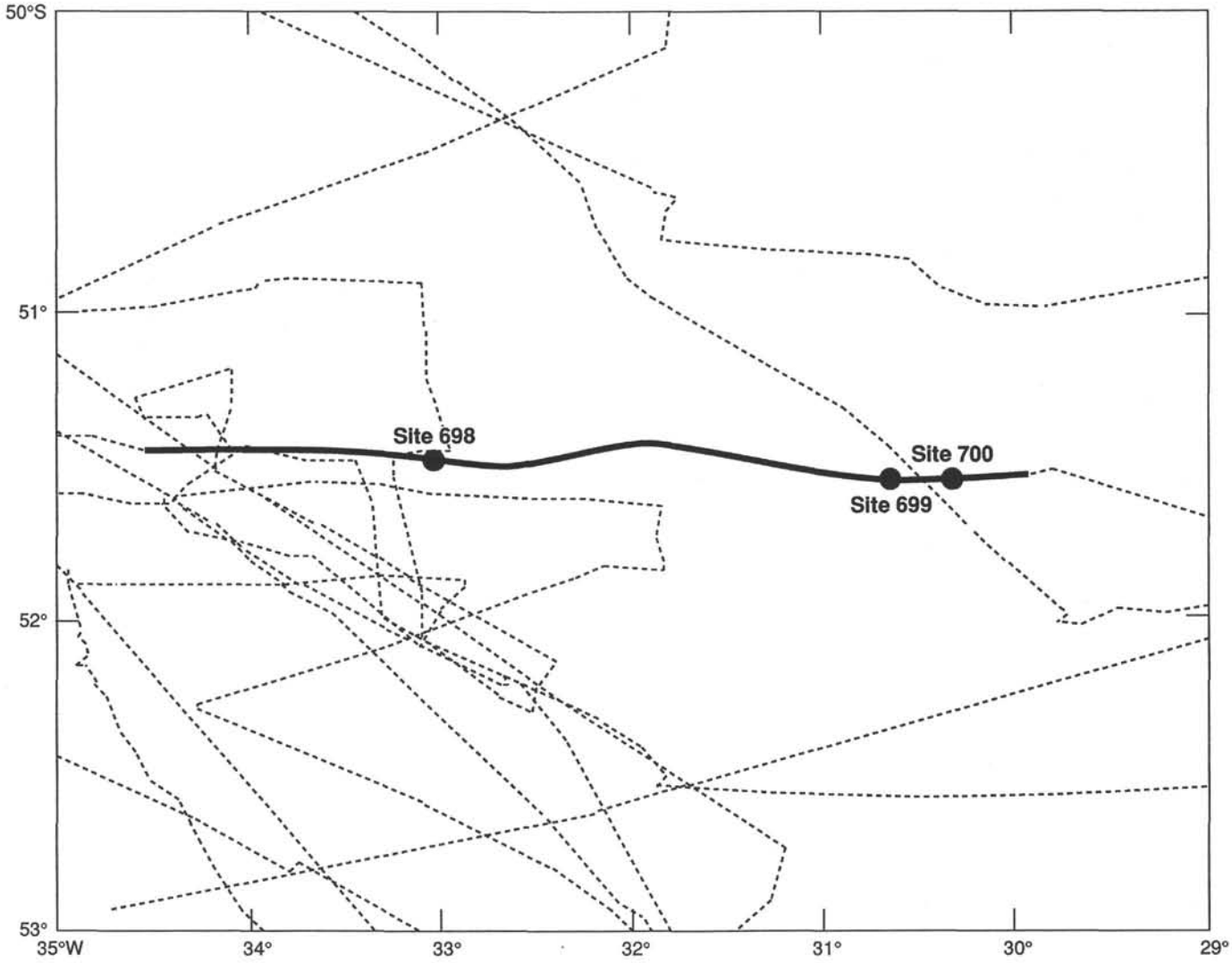

Figure 30. Location of Sites 698, 699, and 670 and single-channel seismic-reflection lines. *JOIDES Resolution* data shown by bold line.

proximately 80-m-thick basal unit defined by a few distinct reflections occurs above basement. The basement/sediment contact is not clearly expressed acoustically in the available data.

Site 699 consists of a single hole of 22 cores obtained with the APC system to a depth of 205.1 mbsf and 34 cores obtained with the XCB system to a depth of 518.1 mbsf. The sediment recovery rate varied, averaging 81% above 224.1 mbsf, but it was significantly reduced to 54% below this depth owing to the presence of gravel. The overall recovery for Hole 699A was 68.6%. The quality of the cores is generally excellent, except for the first sections of some cores, which were disturbed by gravel. The hole was abandoned after the core barrel became jammed with volcanic-rich quartz sand.

The sedimentary sequence at Site 699 is entirely pelagic and mostly biogenic, with a high clay content only in the basal 21 m. The section ranges in age from late Paleocene to Quaternary.

Hole 699A contains a remarkably complete Paleogene pelagic sedimentary sequence (~426 m thick), representing a 37-m.y. period above basal sediments assigned to foraminifer Zone P4 (~58.7–61.0 Ma) (Fig. 32). In contrast, only ~90 m of Neogene biosiliceous sediments punctuated by numerous hiatuses were cored. Only one significant hiatus was noted in the Paleogene (upper middle to lower upper Eocene), although there is some evidence that a brief hiatus formed within the lowermost Eocene (NP10). A major hiatus of regional significance occurs between the lower Miocene and the uppermost middle Miocene (~9 m.y. duration; at ~68.36 mbsf). Other Neogene hiatuses bracket the uppermost Miocene to lowermost Pliocene (~4.3–8.3 Ma; between 62.15 and 54.33 mbsf) and the lower/upper Miocene contact (~3.0–3.9 Ma; between 39.03 and 40.37 mbsf). An additional minor hiatus may occur within the upper Pliocene (~2.5–2.8 Ma; between 32.30 and 31.00 mbsf).

Sedimentation rates were ~3 m/m.y. for the late Paleocene and most of the early Eocene (<61.0 to 53.7 Ma), but they averaged 14 m/m.y. during the late early Eocene and middle Eocene, from ~53.7 to ~45.0 Ma. After the period of nondeposition or erosion that formed the upper middle to lower upper Eocene hiatus, sedimentation rates were ~25 m/m.y. during the late Eocene to earliest Oligocene (~39–34.6 Ma). Throughout the remainder of the Oligocene to earliest Miocene (~34.6 to 20 or 21 Ma), sedimentation rates were ~12 m/m.y. The mean sedimentation rate for the late Eocene to earliest Miocene was ~15 m/m.y. Neogene sedimentation rates are more difficult to evaluate because the Neogene record (~68 m thickness) is more fragmentary and attenuated by erosion and periods of nondeposition. Sedimentation appears to have been most continuous during the last 2.5 m.y., with an average sedimentation rate of ~12 m/m.y.

Calcareous nannofossils provide a high degree of biostratigraphic resolution for most of the Paleogene, whereas diatoms provide excellent stratigraphic control for the upper Paleogene and Neogene (Fig. 13). A good quality paleomagnetic record was obtained of the upper Oligocene, Pliocene, and Quaternary (see Fig. 26). The paleomagnetic record of the 90-m-thick upper Oligocene will provide the first opportunity to calibrate biosiliceous microfossil and calcareous nannofossil stratigraphy to the GPTS of this interval. The continuity of the Paleogene section and its relatively high sedimentation rates (Fig. 14) make this an important stratigraphic reference section for the subantarctic region. Correlations of sequences of similar age from antarctic Leg 113 will provide a biostratigraphic link between the Southern Ocean and lower latitude regions.

The section is characterized by the dominance of biosiliceous sediments in the upper section (0–85.7 mbsf, lower Miocene–Quaternary), below which there is a transition zone of mixed biosiliceous ooze and nannofossil ooze (85.7–233.6 mbsf, lower Oligocene–lower Miocene). Below this transition zone, there is a progressive decrease in the biosiliceous component to a depth of 335.4 mbsf (upper Eocene), where a thick lower sequence of nannofossil chalk occurs (335.4–487.1 mbsf, lower to middle/upper Eocene). Clay content is higher in the lowermost Eocene and upper Paleocene (488–513 mbsf), where zeolitic claystones were encountered.

The sedimentary sequence becomes more indurated with depth. The transition of ooze to chalk occurs in the upper Eocene (~335 mbsf) and is clearly apparent in the physical-property data (Fig. 27). Below ~400 mbsf nannofossil chalks are increasingly micritic (Fig. 5).

The sequence at Site 699 was divided into six lithostratigraphic units based upon compositional differences, in particular, changes in carbonate content and diagenetic maturity (Figs. 4 and 5). Lithostratigraphic Unit I extends from the seafloor to 85.7 mbsf and is early Miocene to Quaternary in age. The unit consists of siliceous and siliceous clayey sediments, predominantly diatom clay, clayey diatom ooze, and diatom ooze. Ice-rafted detritus and dropstones are common throughout the upper Miocene to Quaternary, significantly increasing in and above the Gauss Chronozone. Marking the lower to upper middle Miocene hiatus is a zone of manganese nodules (Cores 114-699A-8H and 114-699A-9H) found above and below the hiatus (Fig. 7).

Lithostratigraphic Unit II boundaries are defined by the last occurrence of carbonate at 85.7 mbsf and the top of an underlying gravel bed at 233.6 mbsf. The upper portion of the unit (Subunit IIA) consists of a upper Oligocene–lowermost Miocene mixture of siliceous nannofossil ooze and nannofossil siliceous ooze with varying clay content (85.7–142 mbsf). The dominant lithologies of Subunit IIB (141.6–233.6 mbsf) are similar to those of Subunit IIA; however, this upper Oligocene section differs by its high frequency of lithofacies alternations, decreasing clay content, and higher carbonate content.

Lithostratigraphic Unit III is a 2.06-m-thick gravel bed found in the lower Oligocene between 233.6 and 235.6 mbsf. This gravel unit appears normally graded and poorly sorted. The subrounded-to-angular rock types comprising Unit III include: quartz, schist, basalt, andesite, quartz arenite, granite, oligomict and polymict conglomerates, quartz diorite, and manganese nodules. Questions regarding the origin and *in-situ* nature of this unit are presented in the "Lithostratigraphy" section.

Lithostratigraphic Unit IV extends from 243.1 to 335.6 mbsf and consists primarily of siliceous nannofossil ooze and nannofossil ooze of late Eocene to early Oligocene age. Biosiliceous sediment decreases significantly in the lower portion of the unit and disappears altogether at the base (Fig. 5).

Lithostratigraphic Unit V extends from 335.44 to 487.91 mbsf and consists of nannofossil chalk of early to late Eocene age. The upper boundary of the unit is defined by a transition from nannofossil ooze to nannofossil chalk. The lower to middle Eocene of Subunit VB (487.9 to 375.2 mbsf) is distinguished from Subunit VA (375.2 to 335.4 mbsf) on the basis of a higher abundance of micrite (Fig. 5) and greater diagenesis in the basal subunit.

Lithostratigraphic Unit VI is the deepest lithologic unit recovered, extending from 487.9 to 516.3 mbsf. This lowermost Eocene to upper Paleocene unit consists of clay-bearing micritic nannofossil chalk, nannofossil micritic chalk, and zeolite-bearing claystone. The basal core (114-699A-56X) contains granitic gravel and a quartz sand rich in volcanic tephra, which was responsible for jamming the core barrel and forcing termination of the hole (Figs. 8 and 9).

Sediments of Hole 699A exhibit a progressive increase in the abundance, diversity, and preservation of calcareous microfossils with increasing age in the Paleogene. Changes in the dominance of microfossils in the section are as follows: upper Paleocene to middle Eocene—calcareous nannofossils and foraminifers; upper Eocene to lowermost Miocene—calcareous nannofossils, diatoms, and radiolarians; and lowermost Miocene to Quaternary—diatoms and radiolarians.

Calcareous nannofossils are abundant throughout the upper Paleocene to lowermost Miocene sequence. They exhibit relatively low diversity in the upper Eocene to lowermost Miocene but are diverse in the upper Paleocene through middle Eocene. Planktonic foraminifers are absent or sparse in the upper lower Oligocene–Quaternary, sparse but more consistently present in the upper Eocene and lowermost Oligocene, and abundant in the upper Paleocene–middle Eocene. Paleogene planktonic foraminifers are generally well preserved and reveal progressive decreases in diversity between the lower and middle Eocene. Benthic foraminifers are sparse or absent from the uppermost Oligocene to the Quaternary and common to abundant from the upper Paleocene through middle upper Oligocene. Diversity is limited above the middle middle Eocene but high below this level. Planktonic and benthic foraminifers are largely recrystallized in the upper Paleocene to middle Eocene. All siliceous microfossil groups (diatoms, radiolarians, silicoflagellates, and ebridians) are almost entirely limited in their occurrence to the upper Eocene to Quaternary above 335 mbsf. Their general absence below this level is interpreted to be a consequence of the dissolution of biogenic silica and its reprecipitation as authigenic clinoptilolite (see "Geochemistry" section; Fig. 18). Siliceous microfossil preservation is good above the upper Eocene, and diversity is high but somewhat decreased within the upper Oligocene to lowermost Miocene.

Conclusions

Seismic and Tectonic Interpretation

Site 699 lies on the northeastern slope of the Northeast Georgia Rise on crust that structurally must be considered to be part of the rise itself (Figs. 1 and 2). Basement recovered at Site 698 is Late Cretaceous (Campanian) in age, weakly differentiated, iron-rich oceanic basalt that had been subjected to subaerial weathering. In a plate tectonic framework, the rise lies between oceanic crust older than Campanian (Chron 34) to the east and younger than Aptian to the west (LaBrecque and Hayes, 1979). The rise is considered to have formed as a result of intraplate deformation in response to rotation of the Malvinas plate against the Falkland Plateau during the Campanian-Eocene. However, the depositional environment during this time interval at Site 698 and during the Paleogene at Site 699 does not reflect any tectonic activity. Any incipient subduction to form a fossil island arc therefore must be of pre-Campanian age. The Upper Cretaceous to Paleogene strata on the western ridge of the North-

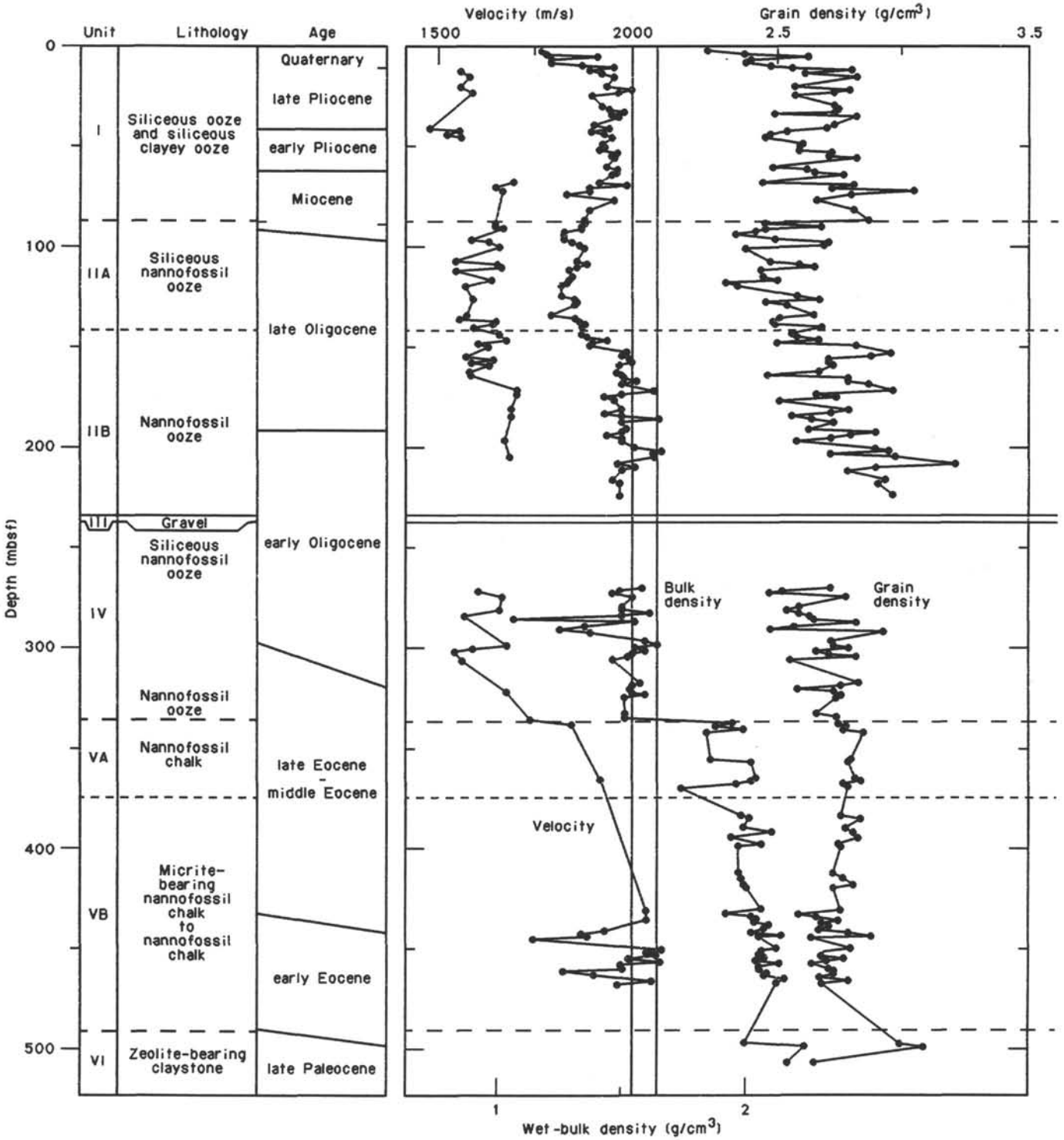

Figure 31. Summary of physical-properties, lithology, and age data from Site 699 correlated with single-channel seismic-reflection profiles obtained by *JOIDES Resolution* over the site.

east Georgia Rise were dissected by major faults that have been related tentatively to late Miocene interaction with the advancing South Georgia block (Barker et al., 1984). At Site 699 lower Oligocene and older strata appear to be conformable with basement, but younger units onlap a westward slope. The apparent change in surface inclination may be a result of block faulting with slight rotation or a change in the depositional environment. A number of vertical faults with offsets of 10 m or less displace Oligocene strata in the vicinity of Site 699. Their extension at depth cannot be confirmed with the available data. These minor faults are probably related to differential compaction.

The provenance of granitic and quartz diorite cobbles in the gravel deposit is intriguing but will remain uncertain because of drilling conditions.

Paleoenvironmental History

The sedimentologic, micropaleontologic, and erosional history of Site 699 provides the most detailed record obtained to

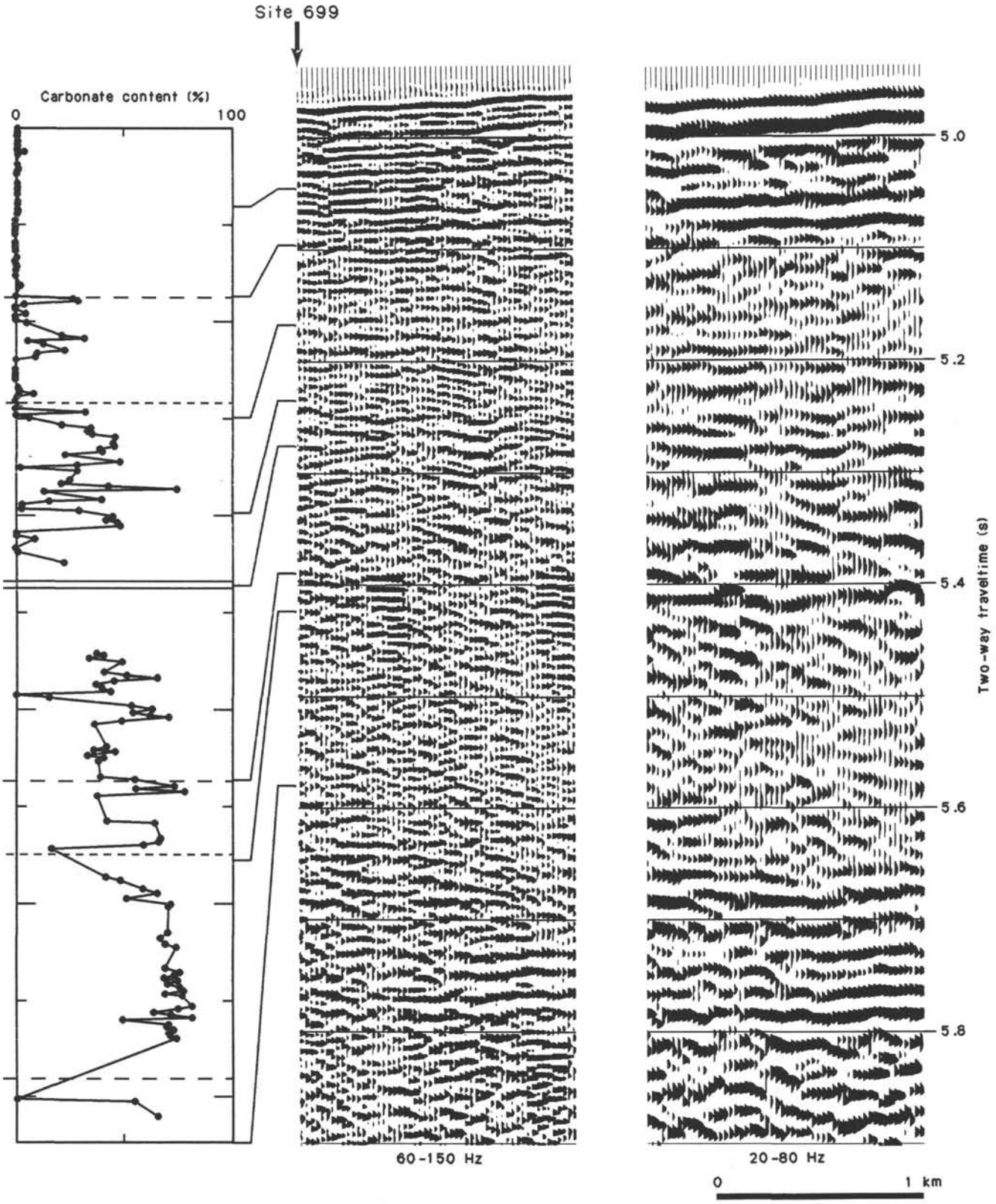

Figure 31 (continued).

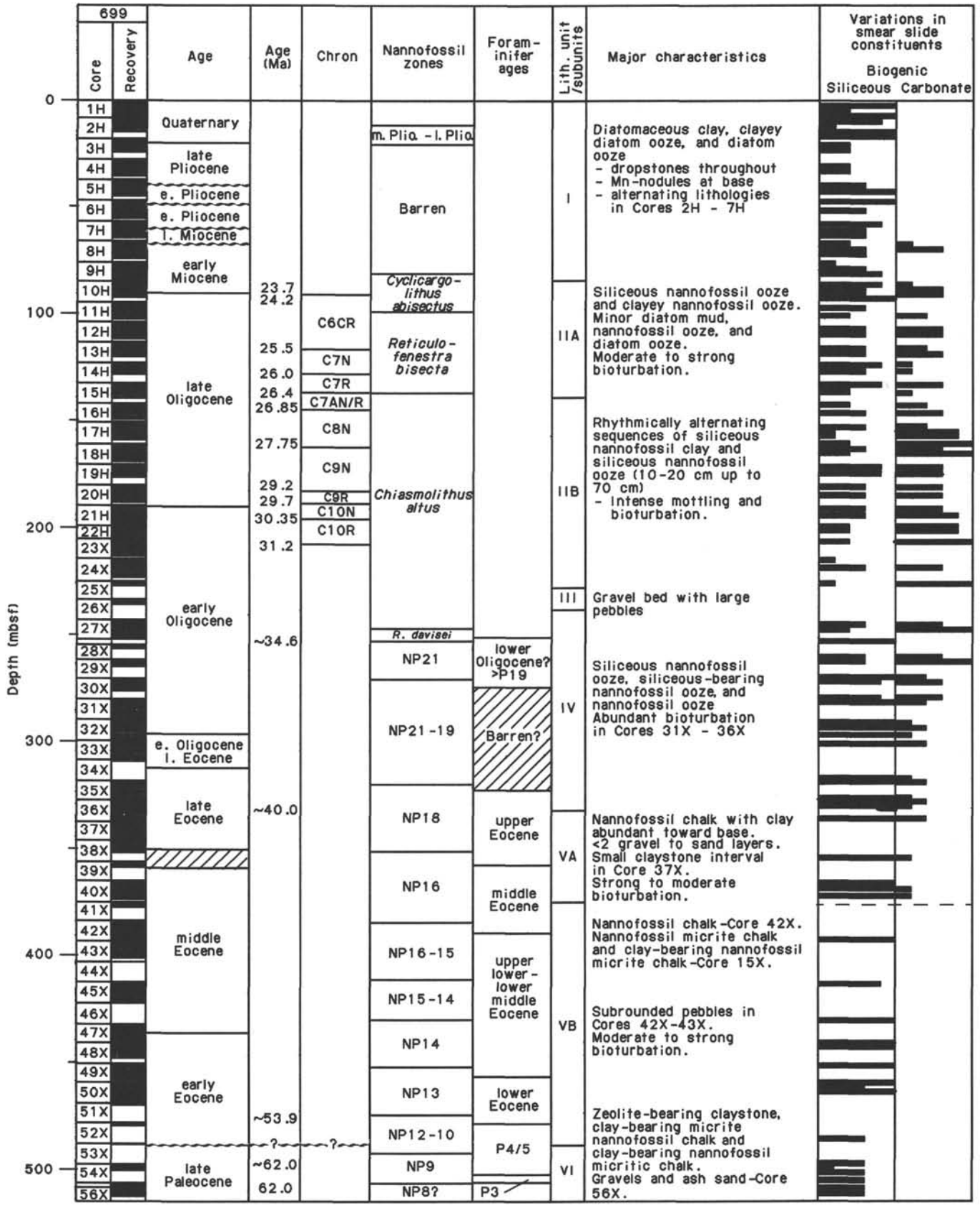

Figure 32. Summary of shipboard results from Hole 699A.

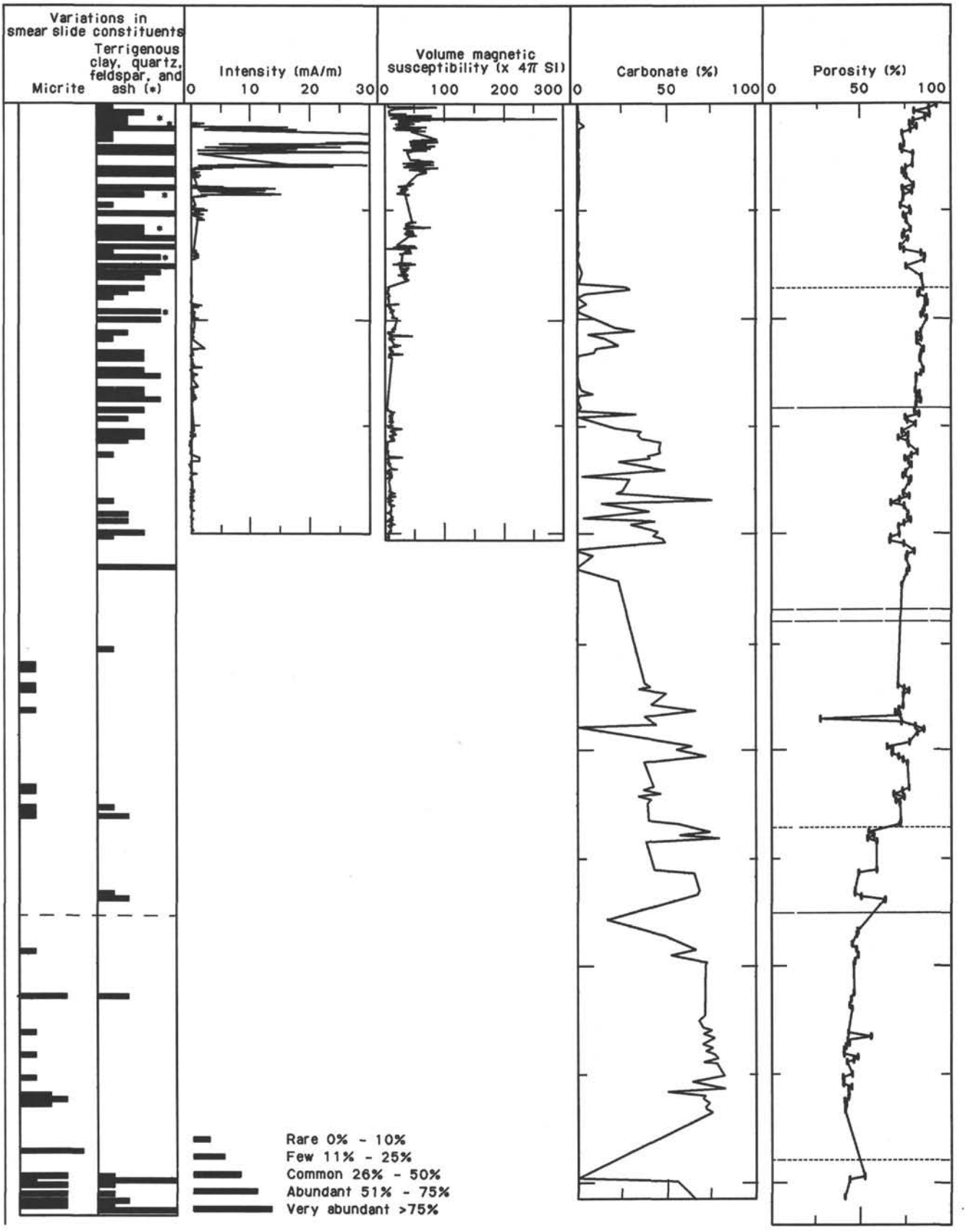

Figure 32 (continued).

date of large-scale Paleogene–early Neogene paleoenvironmental changes in the Southern Ocean. Although the results and conclusions reported here are only preliminary, they reveal a wealth of paleoenvironmental information.

Paleogene Environment

The basal sediment of Hole 699 (Unit VI) is late Paleocene in age and is assigned to foraminifer Zone P4 (~59–61 Ma). A high clay content occurs in parts of the upper Paleocene, exemplified by the occurrence of zeolitic claystone, clay-bearing micritic nannofossil chalk, and clay-bearing nannofossil chalk. Upper Paleocene sediments of Hole 699 have a greater clay content than the nannofossil chalks of Hole 698. The distribution of Upper Cretaceous to lower Paleocene clay-rich sediments in southern Argentina, the Falkland Plateau, and Georgia Basin was discussed in the "Summary and Conclusions" section of the "Site 698" chapter. It was concluded that the source of the clay-rich sediments of this age was the southern Andean Cordillera and that they were dispersed eastward as a thick nepheloid suspension in deep waters. If correct, the upper depth of clay transport by late Paleocene water masses in the Georgia Basin must have been intermediate between the paleodepths of Sites 698 and 699. Paleodepth estimates of these sites based upon benthic foraminifer assemblages suggest that clay transport was limited to depths greater than 1000 to 2000 mbsl.

Siliceous microfossils are absent from the upper Paleocene of Site 699; however, they are abundant, diverse, and generally well preserved in age-equivalent sediments of Site 698. This difference does not reflect productivity differences between these closely spaced sites but can be attributed to differences in post-depositional diagenesis that may have been influenced by detrital clay content. The absence of siliceous microfossils from upper Paleocene sediments at Site 699 would appear to be the consequence of the dissolution of biogenic opal, which was reprecipitated into authigenic silicates, particularly clinoptilolite (see "Geochemistry" section).

The warmest sea-surface temperatures occurred during the late Paleocene through early Eocene (Fig. 15). Abundant and relatively diverse assemblages of calcareous microfossils include warm-water planktonic foraminifers (species of the genera *Acarinina* and *Morozovella*) and warm-water calcareous nannofossils (*Discoaster* spp., *Sphenolithus* spp., and *Zygrhablithus bijugatus*). This period was dominated by calcareous microfossil productivity with carbonate percentages generally ranging from 60% to 80%. During this time the position of the lysocline appears to have remained deeper than the ~2000–3000 m paleodepth of Site 699.

During the early middle to middle middle Eocene, sea-surface temperatures began to decline, never again to attain temperatures as warm as during the early Eocene. A major decrease in the number of low-latitude taxa of calcareous nannofossils and foraminifers began in the earliest middle Eocene (NP14, ~50–51 Ma; Fig. 15). Evidence for this cooling includes the disappearance of sphenoliths and a reduction in the abundance of discoasters during NP14. Progressive cooling during the middle middle Eocene to early late Eocene is represented by a further reduction in the abundance and diversity of planktonic foraminifers (particularly the acarininid group) and only rare occurrences of discoasters, which disappeared completely during the early late Eocene.

Foraminifer and calcareous nannofossil assemblages took on definite high-latitude characteristics by 38 Ma (prior to the end of NP18). Late Eocene foraminifer assemblages exhibit low species diversity and are dominated by *Globigerinatheka index*. Calcareous nannofossils became dominated by typical high-latitude floras that include *Reticulofenestra* spp., *Chiasmolithus* spp., and *Isthmolithus recurvus*. These characteristics and the absence of low-latitude nannofossils and foraminifers may be interpreted unambiguously to represent a significant late Eocene cooling of surface waters.

Planktonic foraminifers are almost entirely absent from Oligocene and younger sediments; however, calcareous nannofossils are abundant through the lowermost Miocene. The decrease of foraminifer abundance in the upper middle Eocene to upper Eocene coincides with a decrease in benthic foraminifer diversity, suggesting that the site remained below the foraminifer lysocline for the remainder of the Paleogene. By the early Eocene, the site subsided to between 2500 and 3000 mbsf, as inferred from the benthic foraminifer assemblages. The increased dissolution of post-upper middle Eocene foraminifers may be the consequence of subsidence of the site and/or a shallowing of the foraminifer lysocline. As compared to other Oligocene DSDP sites in the vicinity (Site 511 on the Maurice Ewing Bank and Site 513 in the southeast Argentine Basin), Site 699 has a deeper benthic foraminifer assemblage. It is not surprising, therefore, that planktonic foraminifers are largely absent from Site 699, whereas they are present throughout most of the Oligocene in the shallower sites. Once the paleodepths of these regional sites are evaluated further, the paleodepth of the Oligocene foraminifer lysocline in the subantarctic can be well constrained.

The earliest presence of diatoms in upper Eocene and other siliceous microfossil groups in the uppermost Eocene–lowermost Oligocene coincides closely with the last consistent appearance of planktonic foraminifers. The abrupt appearance of siliceous microfossils is related to a diagenetic transition and has no known paleoenvironmental significance. Upper Eocene to lowermost Oligocene diatom assemblages contain a relatively high percentage (~10%) of low-latitude species, which completely disappear by the upper lower Oligocene (Fig. 15).

The abundance of siliceous microfossil groups decreased during the late early to early late Oligocene. At this time the diatom flora was dominated by cosmopolitan and high-latitude species. Frequent alternations between siliceous nannofossil ooze and siliceous nannofossil clay (Subunit IIB) were probably caused by high-frequency variations in the deposition of clay and carbonate. These alternating lithologies may represent variations in the rates of deposition of nepheloid-transported clay and fluctuations in the productivity of calcareous nannofossils.

Major lithologic and microfossil changes that occurred during the middle late Oligocene to earliest Miocene (Subunit IIA) are interpreted to have been caused by the earliest northward migration of cold antarctic surface waters to close to their present-day position. During this period, carbonate (nannofossil) deposition was only intermittent, ending ~35 m.y. of continuous carbonate sedimentation. The last two periods of carbonate deposition occurred during the late Oligocene (~26–25 Ma) and a major carbonate occurrence in the earliest Miocene (23.7-19.9 Ma). A few discoasters were found in the uppermost Oligocene (~24.5 to 25.5 Ma), representing the only Oligocene occurrence of this low- to midlatitude group of nannofossils. The relatively minor occurrence of calcareous nannofossils in the lowermost Miocene is more indicative of cooler surface waters because of their low diversity and the dominance of high-latitude species.

Neogene Environment

The decrease and disappearance of carbonate during the latest Oligocene-earliest Miocene is interpreted to reflect the northward advance of the ACZ (polar front) and the high-latitude biosiliceous province to near its present position. By the earliest Miocene the polar front apparently migrated over the site, bringing with it the biosiliceous productivity zone of the cold antarctic surface waters and causing an abrupt halt to calcareous productivity, which presently is confined to the warmer surface wa-

ters north of this major oceanographic boundary. The timing of this event was age equivalent at Site 513 (Ciesielski and Weaver, 1983), where the last occurrence of carbonate is also in the lowermost Miocene. A precise age for the early Neogene transition to predominantly siliceous sedimentation cannot be made because of the lack of paleomagnetic control in these sections or previous paleomagnetic calibration of lower Miocene biostratigraphic zonal schemes.

A major unconformity occurs at ~68.36 mbsf, only ~10 m above the last occurrence of carbonate, and is bracketed by sediments of early to late middle Miocene age. Unit I sediments above the unconformity are primarily diatom ooze, diatom clay, and clayey diatom ooze. The overall characteristics of this unit are indicative of significant and frequent variations in the intensity of CPDW through the late middle Miocene to Quaternary. No fewer than three hiatuses occur within the 85.7 m of Neogene sediments of Unit I. Some of these hiatuses appear to have been caused by erosion, rather than nondeposition, removing up to 200 m of sediment (see "Physical Properties" section). In contrast, the regional lower to upper middle Miocene hiatus appears to have been caused primarily by nondeposition on the basis of physical-properties characteristics and the presence of manganese nodules bracketing the hiatus. During periods of reduced CPDW circulation, Neogene sedimentation rates were high for brief intervals. The Neogene was thus a period of high biosiliceous productivity, the record of which was greatly attenuated through periodic erosion by CPDW. Large fluctuations in the clay content (10%–70%) may be related to the settling potential of nepheloid-transported clay under variable current velocity regimes.

The first occurrence of ice-rafted detritus is similar to that recorded from other subantarctic sites in the South Atlantic sector of the Southern Ocean (Bornhold, 1983; Ciesielski and Weaver, 1983). The initial deposition of dropstones occurred during the late Miocene. Dropstones and ice-rafted detritus appear in greater concentration within Pliocene-Quaternary sediments. The increase and subsequent variations in the abundance of ice-rafted detritus can be readily seen in the magnetic susceptibility values of Unit I (see "Paleomagnetics" section). The lack of residual ice-rafted detritus at the lower to upper middle Miocene hiatus suggests the absence of ice rafting during the intervening period.

Paleocirculation

An objective at Sites 699 and 700 was to evaluate what role the East Georgia Basin served as a deep-water passageway between the antarctic and South Atlantic prior to the formation of the Islas Orcadas Rise–Meteor Rise gateway (Fig. 33). The sedimentary record of Hole 699A is relatively complete from the lower Paleocene through lowermost Miocene, with the exception of an apparent upper middle to upper Eocene hiatus. The nondepositional or erosional episode that formed this hiatus postdates the opening of the Islas Orcadas Rise–Meteor Rise gateway (see "Site 701" chapter, this volume).

Lower Paleogene sedimentary sequences of the East Georgia Basin at Sites 699 and 700 reveal little evidence for strong benthic current activity prior to the formation of the Islas Orcadas–Meteor Rise gateway. Either this part of the Georgia Basin was not a conduit for passage of antarctic deep waters to the South Atlantic or thermohaline convection in this region was too weak to cause significant erosion.

In contrast to the earlier Paleogene, the East Georgia Basin (Sites 699 and 700) and Islas Orcadas Rise–Meteor Rise gateway (Site 701) experienced more dynamic benthic conditions in the late middle Eocene to late Eocene. This is expressed by changes in the preservation of calcareous microfossils, the hiatus in Hole 699A, lower sedimentation in Hole 700B, and a variety of evidence in Hole 701C. More vigorous benthic circulation in both deep-water passageways during the late middle to late Eocene is indicative of a regional change in the benthic environment that postdates the initial opening of the Islas Orcadas Rise–Meteor Rise gateway.

Low- to midlatitude faunas and floras found in the upper Paleocene to lower middle Eocene may be attributed in part to a more southerly position of the southern limb of the South Atlantic subtropical gyre. Austral affinities of planktonic foraminifers suggest that waters of shallow to intermediate depth were able to penetrate into the South Atlantic from the Pacific via an antarctic seaway, which existed in the West Antarctic region prior to development of the West Antarctic ice sheet. These waters were also relatively warm because of their short residence time in high latitudes prior to the faster spreading between Antarctica and Australia. The early middle Eocene cooling, inferred from the microfossil assemblages, coincides with the anomaly 18 (middle Eocene) increase in spreading rates between Australia and Antarctica. This event may have resulted in the establishment of a "shallow" ACC that flowed into the Atlantic through the West Antarctic Seaway. The advent of unrestricted but shallow circum-antarctic circulation would have resulted in cooler surface waters. More vigorous and cooler surface waters of this pre-ACC began displacing the subtropical South Atlantic gyre to the north, resulting in the gradual establishment of high-latitude floras and faunas.

The earliest Miocene northward advance of the polar front and the biosiliceous province appears to have been intimately related to the early phase of the opening of the Drake Passage and the advent of a less-restricted ACC. Much more vigorous circulation of deep and bottom waters quickly followed the opening of a deep-water passage between Antarctica and South America, resulting in the formation of regional hiatuses formed by antarctic CPDW and AABW. Multiple disconformities and the thin (85-m) upper middle Miocene–Quaternary section are a testimony to the vigor of Neogene circum-antarctic circulation.

The possible influence of Neogene tectonic events in the Drake Passage region (see "Background and Objectives" section, this chapter) upon deep-water circulation into the Atlantic sector is difficult to evaluate from the Neogene record of this site. Multiple erosional and/or nondepositional events have removed too much of the Neogene sedimentary record to evaluate the relative timing of depositional and erosional episodes to these tectonic events.

REFERENCES

Barker, P., Barber, P. L., and King, E. C., 1984. An early Miocene ridge crest-trench collision on the South Scotia Ridge near 36°W. *Tectonophysics*, 102:315–332.

Barker, P. E., and Burrell, J., 1977. The opening of the Drake Passage. *Mar. Geol.*, 25:15–34.

———, 1982. The influence upon Southern Ocean circulation, sedimentation, and climate of the opening of the Drake Passage. *Antarct. Geosci. Symp. Antarct. Geol. Geophys., 3rd*, 377–385.

Barker, P., and Hill, I. A., 1981. Back-arc extension in the Scotia Sea. *Philos. Trans. R. S. London, A*, 300:249–262.

Barron, J. A. 1985. Miocene to Holocene planktic diatoms. *In* Bolli, H. M., Saunders, J. B., and Perch-Nielsen, K. (Eds.), *Plankton Stratigraphy*: Cambridge (Cambridge Univ. Press), 763–809.

Barron, J., Nigrini, C. A., Pujos, A., Saito, T., Thayer, F., Thomas, E., and Weinrich, N., 1985. Synthesis of biostratigraphy, central Equatorial Pacific, Deep Sea Drilling Project Leg 85: refinement of Oligocene to Quaternary biochronology. *In* Mayer, L., Thayer, F., Thomas, E., et al., *Init. Repts. DSDP*, 85: Washington (U.S. Govt. Printing Office), 905–934.

Basov, I. A., and Krasheninnikov, V. A., 1983. Southwest Atlantic Mesozoic and Cenozoic foraminifers. *In* Ludwig, W. J., Krasheninnikov, V. A., et al., *Init. Repts. DSDP*, 71: Washington (U.S. Govt. Printing Office), 739–787.

Bayer, U., and Ott, R., 1983. Correlation of acoustic stratigraphy with cored lithology by means of physical property data for Deep Sea Drilling Project Sites 511, 513, and 514, Leg 71. *In* Ludwig, W. J., Krasheninnikiv, V. A., et al., *Init. Repts. DSDP*, 71: Washington (U.S. Govt. Printing Office), 1133–1137.

Berggren, W. A., Kent, K. V., and Flynn, J. J., 1985a. Paleogene geochronology and chronostratigraphy. *In* Snelling, N. J. (Ed.), *The Chronology of the Geological Record*: Geol. Soc. London Mem., 10:141–195.

Berggren, W. A., Kent, K. V., and Van Couvering, J. A., 1985b. Neogene geochronology and chronostratigraphy. *In* Snelling, N. J. (Ed.), *The Chronology of the Geological Record*: Geol. Soc. London Mem., 10:211–260.

Blow, W. H., 1969. Late middle Eocene to Recent planktonic foraminiferal biostratigraphy. *In* Brönniman, P., and Renz, H. H. (Eds.), *First Int. Conf. Plankt. Microfossils*, Leiden (E. J. Brill), 1:99–422.

_____, 1979. *The Cainozoic Globigerinida*: Leiden (E. J. Brill).

Bornhold, B. D., 1983. Ice-rafted debris in sediments from Leg 71, southwest Atlantic Ocean. *In* Ludwig, W. J., Krasheninnikov, V. A., et al., *Init. Repts. DSDP*, 71: Washington (U.S. Govt. Printing Office), 307–316.

Bromley, R. G., and Ekdale, A. A., 1984. *Chrondites*: a trace fossil indicator of anoxia in sediments. *Science*, 224:872–874.

Callahan, J. E., 1972. The structure and circulation of deep water in the Antarctic. *Deep Sea Res., Part A*, 19:563–575.

Carmack, E. C., and Foster, T. D., 1975. On the flow of water out of the Weddell Sea. *Deep Sea Res., Part A*, 20:927–932.

Chen, P. H., 1975. Antartic Radiolaria. *In* Hayes, D. E., and Frakes, L. A., et al., *Init. Repts. DSDP*, 28: Washington (U.S. Govt. Printing Office), 437–513.

Ciesielski, P. F., 1983. The Neogene and Quaternary diatom biostratigraphy of subantarctic sediments, Deep Sea Drilling Project Leg 71. *In* Ludwig, W. J., Krasheninnikov, V. A., et al., *Init. Repts. DSDP*, 71: Washington (U.S. Govt. Printing Office), 635–666.

_____, 1986. Middle Miocene to Quarternary diatom biostratigraphy of Deep Sea Drilling Project Site 594, Chatham Rise, Southwest Pacific. *In* Kenneth, J. P., von der Borch, C. C., et al., *Init. Repts. DSDP*, 90: Washington (U.S. Govt. Printing Office), 863–885.

Ciesielski, P. F., and Weaver, F. M., 1983. Neogene and Quarternary paleoenvironmental history of Deep Sea Drilling Project Leg 71 sediments, southwest Atlantic Ocean. *In* Ludwig, W. J., Krasheninnikov, V. A., et al., *Init. Repts. DSDP*, 71: Washington (U.S. Govt. Printing Office), 461–477.

Eager, R.M.C., Baines, J. G., Collinson, J. D., Hardy, P. G., Okolo, S. A., and Pollard, J. E., 1985. Trace fossil assemblages and their occurrence in Silesian (Mid Carboniferous) deltaic sediments of the central Pennine basin, England. *Spec. Publ. Soc. Econ. Paleontol. Mineral.*, 35:99–149.

Fenner, J., 1984. Eocene-Oligocene planktic diatom stratigraphy in the low latitudes and high southern latitudes. *Micropaleontology*, 30: 319–342.

Froelich, P. N., Kim, K. K., Jahnke, R. J., Burnett, W. R., and Deakin, M., 1983. Pore water fluoride in Peru continental margin sediments: uptake from seawater. *Geochim. Cosmochim. Acta*, 47:1605–1612.

Gieskes, J. M., 1983. The chemistry of interstitial waters of deep-sea sediments: interpretation of Deep-Sea Drilling data. *In* Riley, J. P., and Chester, R. (Eds.), *Chemical Oceanography* (Vol. 8): London (Academic Press), 222–269.

Gieskes, J. M., and Lawrence, J. R., 1981. Alteration of volcanic matter in deep-sea sediments: evidence from the chemical composition of interstitial waters from deep-sea drilling cores. *Geochim. Cosmochim. Acta*, 45:1687–1703.

Gombos, A. M., Jr., 1983. Middle Eocene diatoms from the South Atlantic. *In* Ludwig, W. J., Krasheninnikov, V. A., et al., *Init. Repts. DSDP*, 71: Washington (U.S. Govt. Printing Office), 565–582.

Gombos, A. M., Jr., and Ciesielski, P. F., 1983. Late Eocene to early Miocene diatoms from the southwest Atlantic. *In* Ludwig, W. J., Krasheninnikov, V. A., et al., *Init. Repts. DSDP*, 71: Washington (U.S. Govt. Printing Office), 583–634.

Hays, J. D., and Shackleton, N. J., 1976. Globally synchronous extinction of the radiolarian *Stylatractus universus*. *Geology*, 4:649–652.

Hill, I. A., and Barker, P., 1980. Evidence for back-arc extension in the central Scotia Sea. *Geophys. J. R. Astron. Soc.*, 63:427–440.

Jenkins, D. G., 1985. Southern mid-latitude Paleocene to Holocene planktic foraminifera. *In* Bolli, H. M., Saunders, J. B., and Perch-Nielsen, K. (Eds.), *Plankton Stratigraphy*: Cambridge (Cambridge Univ. Press), 263–282.

Kennett, J. P. 1982. *Marine Geology*: Englewood Cliffs, NJ (Prentice Hall).

Kennett, J. P., Houtz, R. E., et al., 1975. *Init. Repts. DSDP*, 29: Washington (U.S. Govt. Printing Office).

Kennett, J. P., and Watkins, N. D., 1975. Deep sea erosion and manganese nodule develoment in the southwest Indian Ocean. *Science*, 188: 1011–1013.

LaBrecque, J. L., and Hayes, D. E., 1979. Seafloor spreading history of the Agulhas Basin. *Earth Planet. Sci. Lett.*, 45:411–428.

Ledbetter, M. T., 1986. Bottom-current pathways in the Argentine Basin revealed by mean silt particle size. *Nature*, 321:423–425.

Ling, H. Y., 1973. Silicoflagellates and ebridians from Leg 19. *In* Creager, J. S., Scholl, D. W., et al., *Init. Repts. DSDP*, 19: Washington (U.S. Govt. Printing Office), 751–775.

Ludwig, W. J., Krasheninnikov, V., and Basov, I. A., 1980. Tertiary and Cretaceous paleoenvironments in the southwest Atlantic Ocean: preliminary results of Deep Sea Drilling Project Leg 71. *Geol. Soc. Am. Bull.*, 91:655–664.

Martini, E., 1971. Standard Tertiary and Quaternary calcareous nannoplankton zonation. *In* Farinacci, A. (Ed.), *Proc. Planktonic Conf. II Rome 1970*: Rome (Technoscienze), 2:739–785.

Martini, E., and Müller, C., 1986. Current Tertiary and Quaternary calcareous nannoplankton stratigraphy and correlations. *Newsl. Stratigr.*, 16:99–112.

McCollum, D. W., 1975. Diatom stratigraphy of the Southern Ocean. *In* Hayes, D. E., Frakes, L. A., et al., *Init. Repts. DSDP*, 28: Washington (U.S. Govt. Printing Office), 515–572.

McDuff, R. E., 1981. Major cation gradients in DSDP interstitial waters: the role of diffusive exchange between seawater and upper oceanic crust. *Geochim. Cosmochim. Acta*, 45:1703–1713.

_____, 1985. The chemistry of interstitial waters, Deep Sea Drilling Project, Leg 86. *In* Heath, G. R., Burckle, L. H., et al., *Init. Repts. DSDP*, 86: Washington (U.S. Govt. Printing Office), 675–687.

McGowran, B., 1986. Cainozoic oceanic and climatic events: the Indo-Pacific foraminiferal biostratigraphy record. *Palaeogeogr., Palaeoclimatol., Palaeoecol.*, 55:247–265.

Morkhoven, F.P.C.M. van, Berggren, W. A., and Edwards, A. S., 1986. Cenozoic cosmopolitan deep-water benthic foraminifera. *Mem. Cent. Rech. Explor. Prod. Elf Aquitaine*, 11.

Packham, G. H., and van der Lingen, G. J., 1973. Progressive carbonate diagenesis at Deep Sea Drilling Sites 206, 207, 208, and 210 in the southwest Pacific and its relationship to sediment physical properties and seismic reflectors. *In* Burns, R. E., Andrews, J. E., et al., *Init. Repts. DSDP*, 21: Washington (U.S. Govt. Printing Office), 495–521.

Perch-Nielsen, K., 1975. Late Cretaceous to Pleistocene archaeomonads, ebridians, endoskeletal dinoflagellates, and other siliceous microfossils from the subantarctic Southwest Pacific, DSDP, Leg 29. *In* Kennett, J. P. Houtz, R. E., et al., *Init. Repts. DSDP*, 29: Washington (U.S Govt. Printing Office), 873–907.

_____, 1985. Cenozoic calcareous nannofossils. *In* Bolli, H. M., Saunders, J. B., and Perch-Nielsen, K. (Eds.), *Plankton Stratigraphy*: Cambridge (Cambridge Univ. Press), 427–554.

Reid, J. R., Nowlin, W. D., Jr., and Patzert, W. C., 1977. On the characteristics and circulation of the southwestern Atlantic Ocean. *J. Phys. Oceanogr.*, 7:62–91.

Seilacher, A., 1967. Bathymetry of trace fossils. *Mar. Geol.*, 5:413–428.

_____, 1975. Use of trace fossil assemblages for recognizing depositional environments. *In* Basan, P. (Ed.), *Trace Fossil Concepts*: SEPM Short Course, 5:167–181.

Shaw, C. A., and Ciesielski, P. F., 1983. Silicoflagellate biostratigraphy of middle Eocene to Holocene subantartic sediments recovered by Deep Sea Drilling Project Leg 71. *In* Ludwig, W. J., Krasheninnikov, V. A., et al., *Init. Repts. DSDP*, 71: Washington (U.S. Govt. Printing Office), 687–737.

Tjalsma, R. C., 1977. Cenozoic foraminifera from the South Atlantic, DSDP Leg 36. *In* Barker, P., Danziel, I.W.D., et al., *Init. Repts. DSDP*, 36: Washington (U.S. Govt. Printing Office), 493–517.

Tjalsma, R. C., and Lohmann, G. P., 1983. Paleocene-Eocene bathyal and abyssal benthic foraminifera from the Atlantic Ocean. *Micropaleontol. Spec. Publ.*, 4.

Weaver, F. M., 1983. Cenozoic radiolarians from the southwest Atlantic, Falkland Plateau region, Deep Sea Drilling Project Leg 71. *In*

Ludwig, W. J., Krasheninnikov, V. A., et al., *Init. Repts. DSDP*, 71: Washington (U.S. Govt. Printing Office), 667–686.

Weaver, F. M., and Gombos, A. M., Jr., 1981. Southern high-latitude diatom biostratigraphy. *In* Warme, J. E., Douglas, R. G., and Winterer, E. L. (Eds.), *The Deep Sea Drilling Project: A Decade of Progress*: Spec. Publ. Soc. Econ. Paleontol. Mineral., 32:445–470.

Wise, S. W., 1983. Mesozoic and Cenozoic calcareous nannofossils recovered by Deep Sea Drilling Project Leg 71 in the Falkland Plateau Region, southwest Atlantic Ocean. *In* Ludwig, W. J., Krasheninnikov, V. A., et al., *Init. Repts. DSDP*, 71: Washington (U.S. Govt. Printing Office), 481–550.

Ms 114A-106

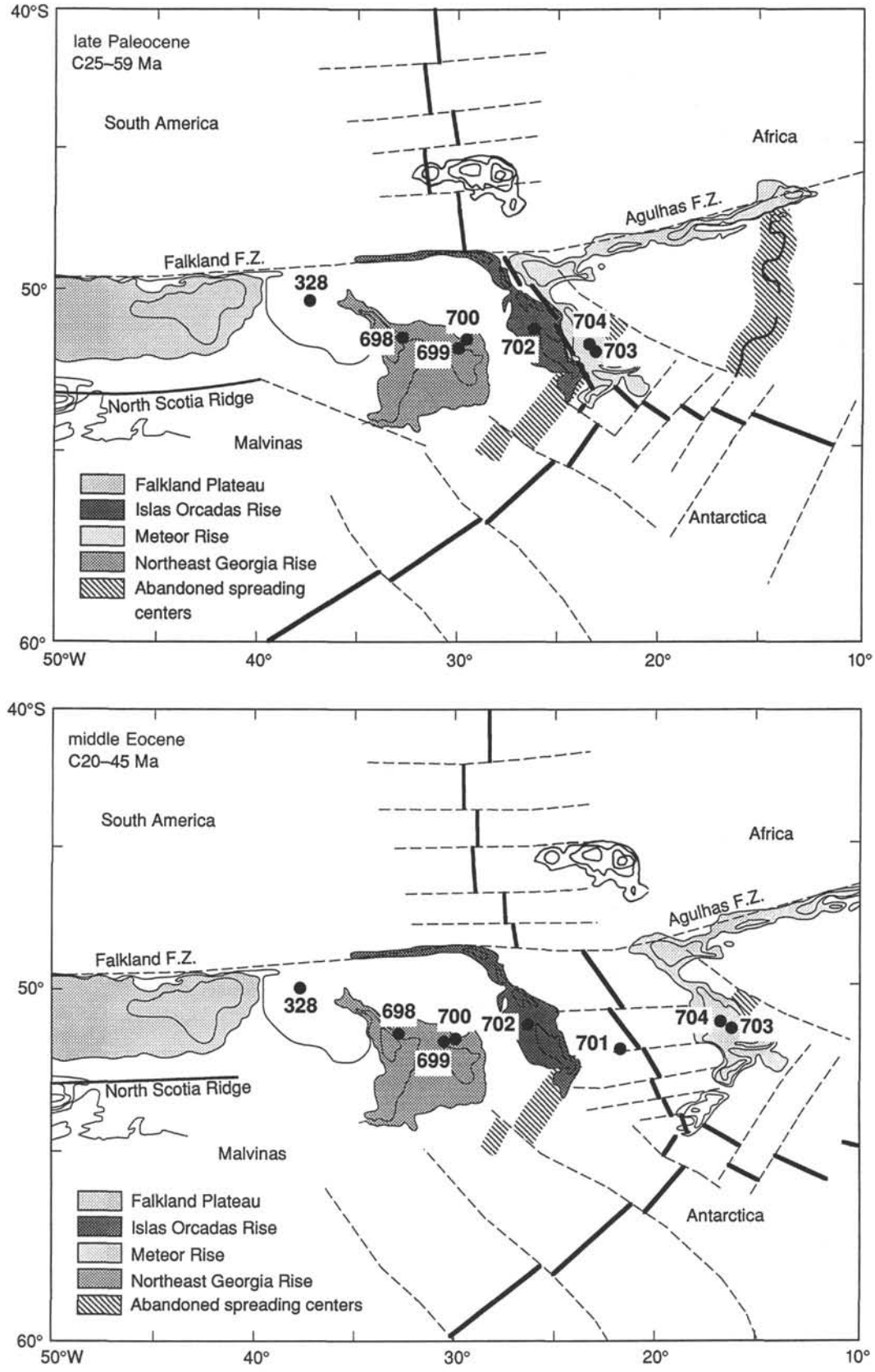

Figure 33. Reconstruction of the Leg 114 drilling region for the late Paleocene and the middle Eocene.

SITE 699 HOLE A CORE 1H CORED INTERVAL 3705.5-3714.1 mbsl; 0.00-8.6 mbsf

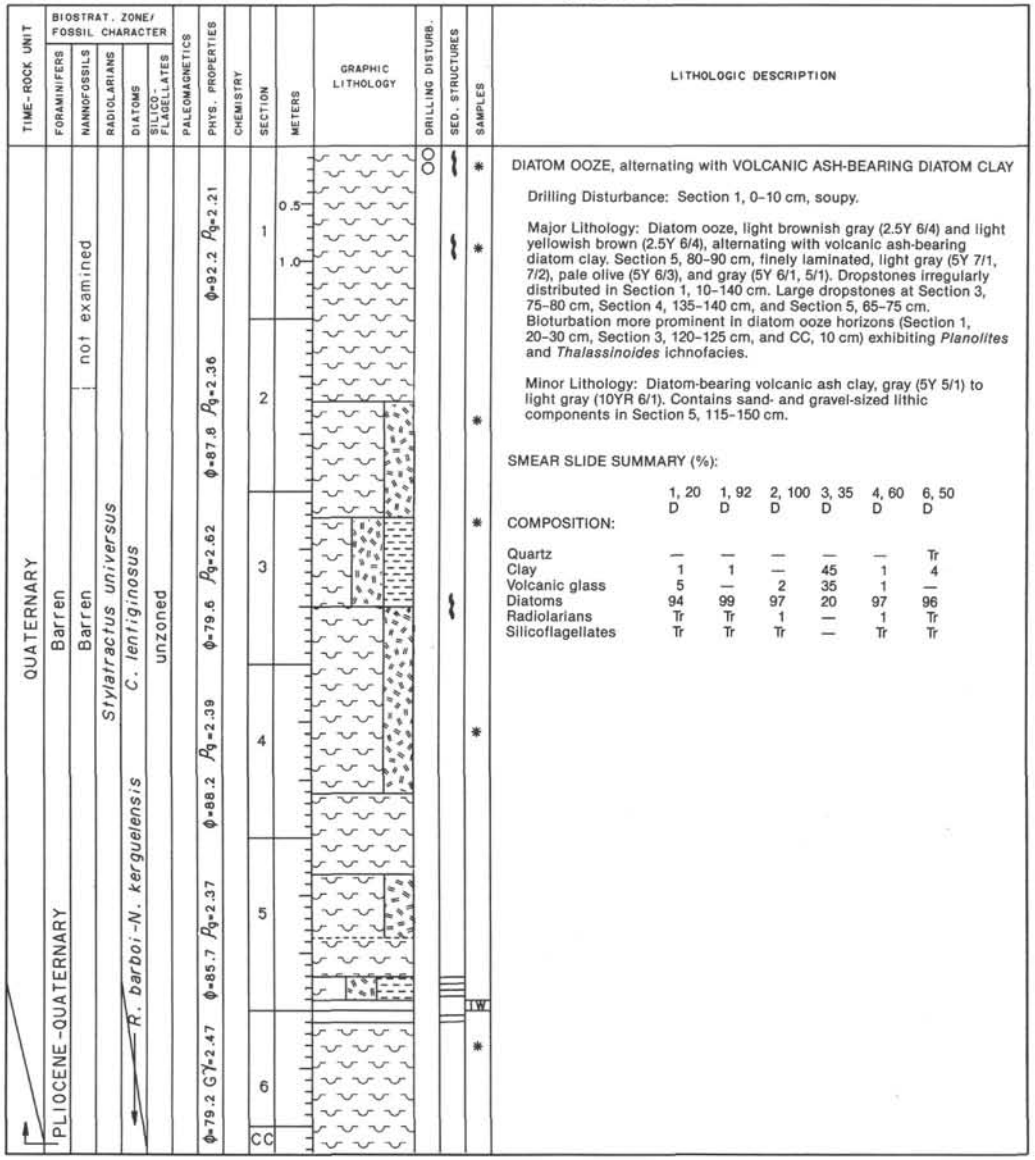

LITHOLOGIC DESCRIPTION

DIATOM OOZE, alternating with VOLCANIC ASH-BEARING DIATOM CLAY

Drilling Disturbance: Section 1, 0–10 cm, soupy.

Major Lithology: Diatom ooze, light brownish gray (2.5Y 6/4) and light yellowish brown (2.5Y 6/4), alternating with volcanic ash-bearing diatom clay. Section 5, 80–90 cm, finely laminated, light gray (5Y 7/1, 7/2), pale olive (5Y 6/3), and gray (5Y 6/1, 5/1). Dropstones irregularly distributed in Section 1, 10–140 cm. Large dropstones at Section 3, 75–80 cm, Section 4, 135–140 cm, and Section 5, 65–75 cm. Bioturbation more prominent in diatom ooze horizons (Section 1, 20–30 cm, Section 3, 120–125 cm, and CC, 10 cm) exhibiting *Planolites* and *Thalassinoides* ichnofacies.

Minor Lithology: Diatom-bearing volcanic ash clay, gray (5Y 5/1) to light gray (10YR 6/1). Contains sand- and gravel-sized lithic components in Section 5, 115–150 cm.

SMEAR SLIDE SUMMARY (%):

	1, 20 D	1, 92 D	2, 100 D	3, 35 D	4, 60 D	6, 50 D
COMPOSITION:						
Quartz	—	—	—	—	—	Tr
Clay	1	1	—	45	1	4
Volcanic glass	5	—	2	35	1	—
Diatoms	94	99	97	20	97	96
Radiolarians	Tr	Tr	1	—	1	Tr
Silicoflagellates	Tr	Tr	Tr	—	Tr	Tr

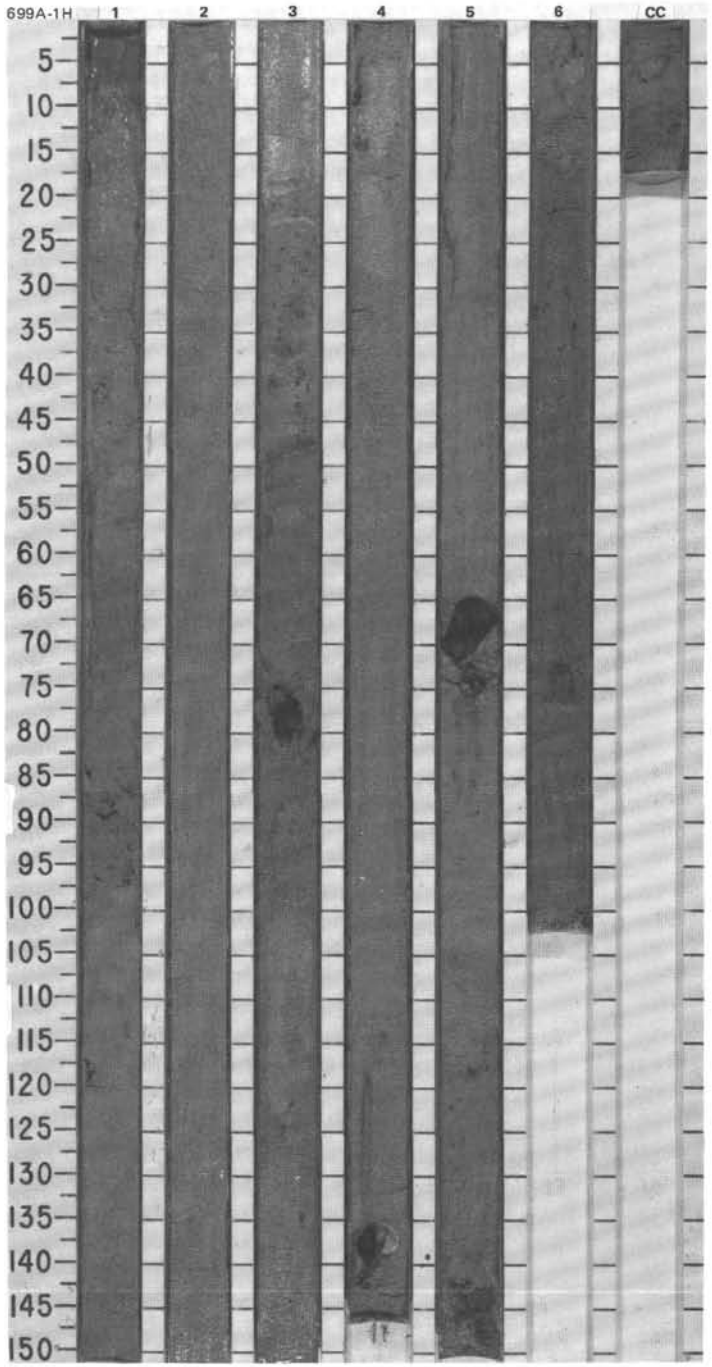

SITE 699 HOLE A CORE 2H CORED INTERVAL 3714.1-3723.6 mbsl; 8.6-18.1 mbsf

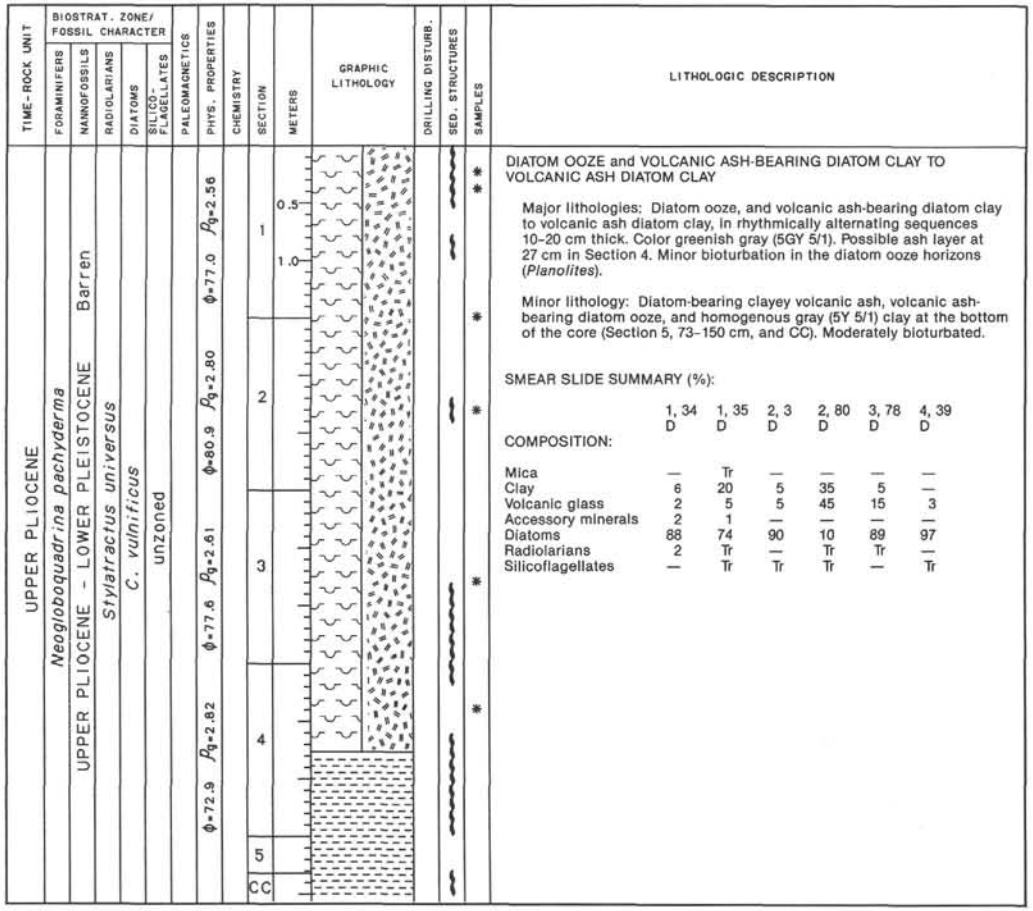

LITHOLOGIC DESCRIPTION

DIATOM OOZE and VOLCANIC ASH-BEARING DIATOM CLAY TO VOLCANIC ASH DIATOM CLAY

Major lithologies: Diatom ooze, and volcanic ash-bearing diatom clay to volcanic ash diatom clay, in rhythmically alternating sequences 10-20 cm thick. Color greenish gray (5GY 5/1). Possible ash layer at 27 cm in Section 4. Minor bioturbation in the diatom ooze horizons (*Planolites*).

Minor lithology: Diatom-bearing clayey volcanic ash, volcanic ash-bearing diatom ooze, and homogenous gray (5Y 5/1) clay at the bottom of the core (Section 5, 73-150 cm, and CC). Moderately bioturbated.

SMEAR SLIDE SUMMARY (%):

	1, 34 D	1, 35 D	2, 3 D	2, 80 D	3, 78 D	4, 39 D
COMPOSITION:						
Mica	—	Tr	—	—	—	—
Clay	6	20	5	35	5	—
Volcanic glass	2	5	5	45	15	3
Accessory minerals	2	1	—	—	—	—
Diatoms	88	74	90	10	89	97
Radiolarians	2	Tr	—	Tr	Tr	—
Silicoflagellates	—	Tr	Tr	Tr	—	Tr

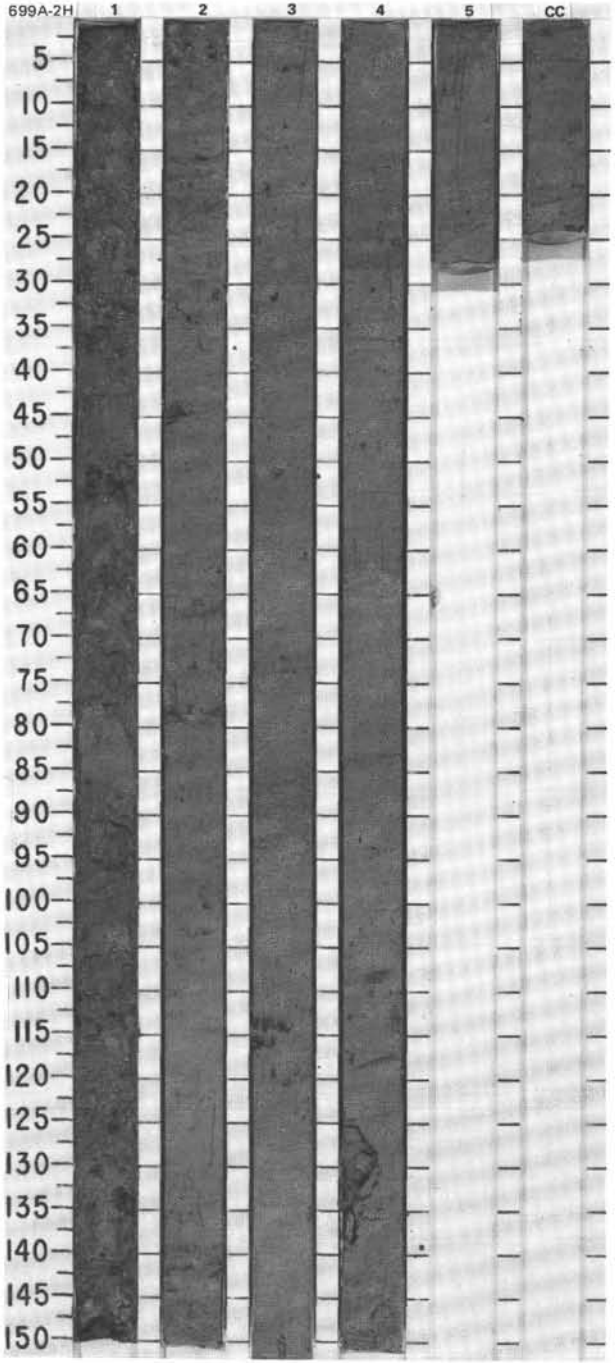

SITE 699 HOLE A CORE 3H CORED INTERVAL 3723.6-3733.1 mbsl; 18.1-27.6 mbsf

TIME-ROCK UNIT	BIOSTRAT. ZONE/ FOSSIL CHARACTER: FORAMINIFERS	NANNOFOSSILS	RADIOLARIANS	DIATOMS	SILICO-FLAGELLATES	PALEOMAGNETICS	PHYS. PROPERTIES	CHEMISTRY	SECTION	METERS	GRAPHIC LITHOLOGY	DRILLING DISTURB.	SED. STRUCTURES	SAMPLES
UPPER PLIOCENE	Barren	Barren	*Saturnalis circularis*	*C. vulnificus*	unzoned	ϕ=79.0 ρ_g=2.57 ϕ=72.9 ρ_g=2.73 ϕ=72.0 ρ_g=2.79 ϕ=74.0 ρ_g=2.57			1, 2, 3, 4, CC	0.5, 1.0	VOID			IW

LITHOLOGIC DESCRIPTION

VOLCANIC ASH-BEARING DIATOM OOZE to VOLCANIC ASH DIATOM OOZE

Major lithology: Olive gray (5Y 5/1, 5/2) volcanic ash-bearing diatom ooze to volcanic ash diatom ooze. Ice-rafted debris in Section 1, 21, 66-69, and 94 cm; Section 2, 21, 106, and 112 cm; Section 3, 30 cm; Section 4, 45, 53, 61-65, 68, 71, and 108-110 cm; and CC, 5 and 15 cm.

Minor lithology: Diatom ooze occurring in patches and horizons in Section 1, 22-53 and 66-69 cm; Section 3, 21-31 cm; and Section 4, 18-21 and 45-55 cm. Color gray (5Y 6/1). Diatom-bearing volcanic ash, olive (5Y 5/5).

SMEAR SLIDE SUMMARY (%):

	2, 20 D	4, 20 D
COMPOSITION:		
Clay	33	20
Volcanic glass	45	58
Diatoms	20	20
Radiolarians	2	2
Silicoflagellates	Tr	Tr

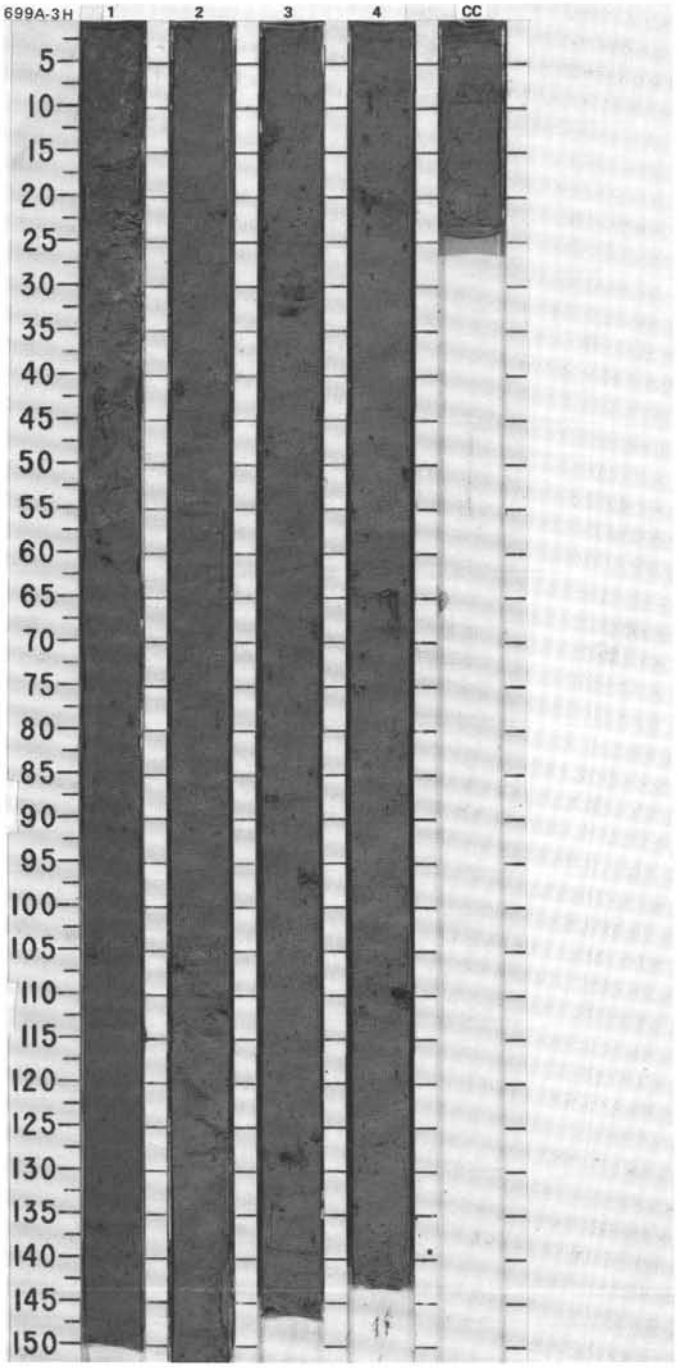

SITE 699 HOLE A CORE 4H CORED INTERVAL 3733.1-3742.6 mbsl; 27.6-37.1 mbsf

TIME-ROCK UNIT	BIOSTRAT. ZONE/ FOSSIL CHARACTER: FORAMINIFERS	NANNOFOSSILS	RADIOLARIANS	DIATOMS	SILICO-FLAGELLATES	PALEOMAGNETICS	PHYS. PROPERTIES	CHEMISTRY	SECTION	METERS	GRAPHIC LITHOLOGY	DRILLING DISTURB.	SED. STRUCTURES	SAMPLES
UPPER PLIOCENE	Barren	Barren	*Helotholus vema*	*N. interfrigidaria-C. vulnificus*	unzoned	ϕ=75.1 ρ_g=2.82 ϕ=74.1 ρ_g=2.43 ϕ=72.9 ρ_g=2.73 ϕ=74.9 ρ_g=2.75 ϕ=78.7 ρ_g=2.73			1, 2, 3, 4, 5, 6, CC	0.5, 1.0	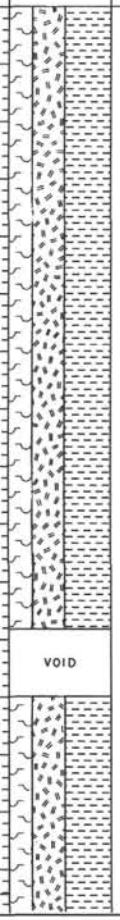			* *

LITHOLOGIC DESCRIPTION

DIATOM-BEARING VOLCANIC ASH CLAY

Drilling disturbance: Soupy sediment in Section 1, 0-100 cm, highly mixed sediments in Section 1, 100-150 cm, and Section 2, 0-25 cm.

Major lithology: Diatom-bearing volcanic ash clay, greenish gray (5GY 5/1). Small lithic fragments (ice-rafted debris) disseminated sporadically throughout core. Large dropstones in Section 1, 102-105 cm; Section 2, 33-35 and 84-86 cm; Section 4, 18-26 and 67-69 cm; and Section 5, 67-69 cm.

SMEAR SLIDE SUMMARY (%):

	1, 50 D	3, 100 D
COMPOSITION:		
Clay	48	50
Volcanic glass	42	40
Accessory minerals	—	Tr
Diatoms	10	10
Radiolarians	Tr	—

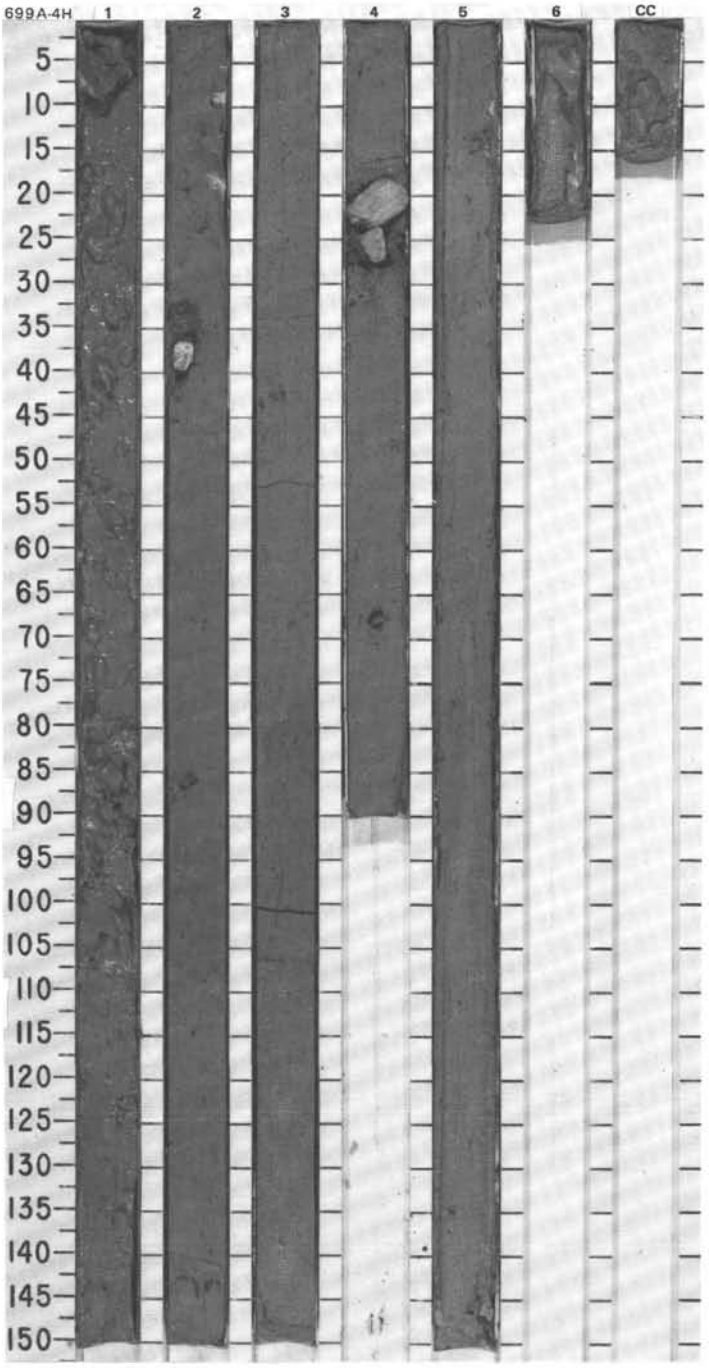

SITE 699 HOLE A CORE 5H CORED INTERVAL 3742.6-3752.1 mbsl; 37.1-46.6 mbsf

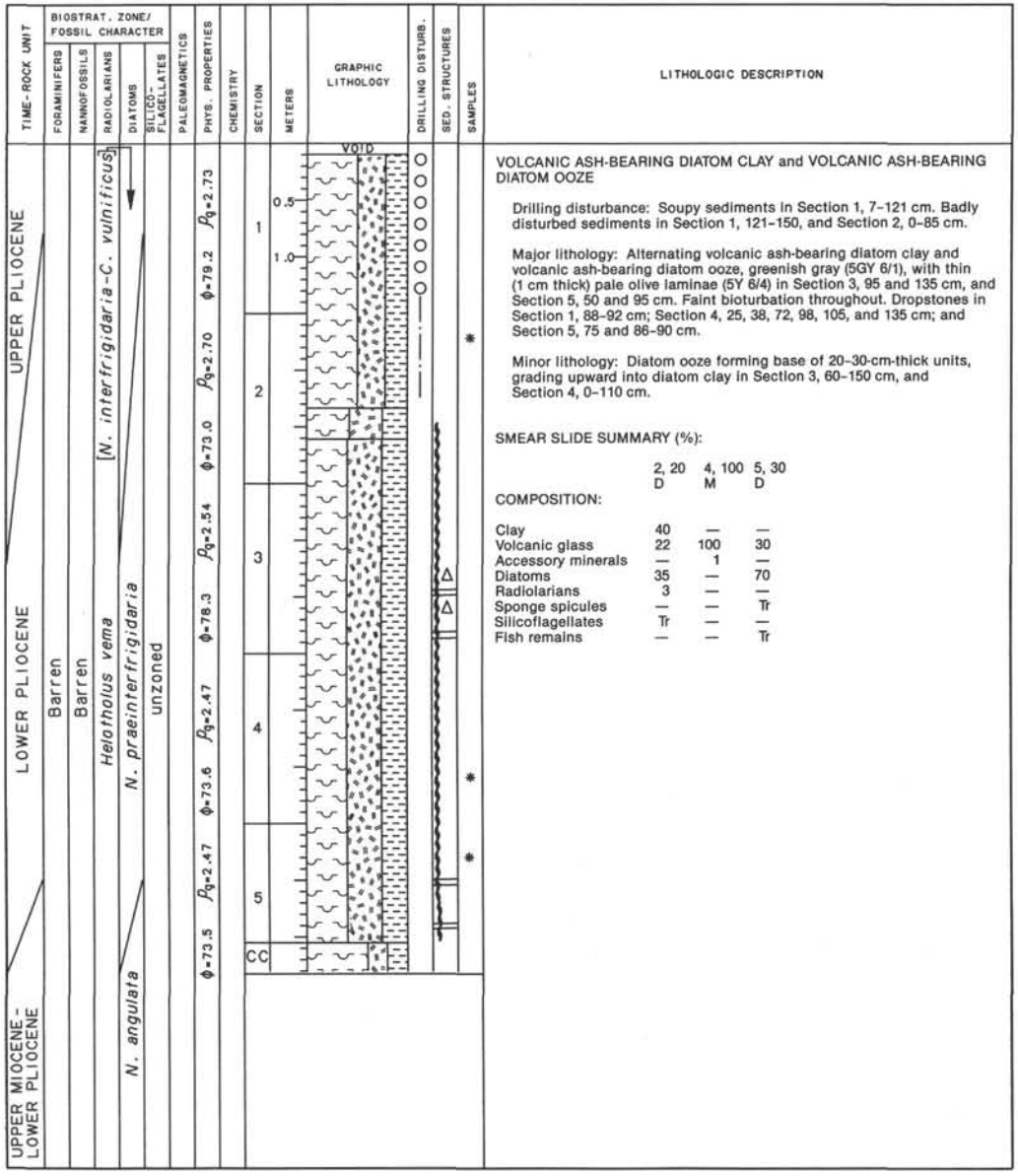

LITHOLOGIC DESCRIPTION

VOLCANIC ASH-BEARING DIATOM CLAY and VOLCANIC ASH-BEARING DIATOM OOZE

Drilling disturbance: Soupy sediments in Section 1, 7–121 cm. Badly disturbed sediments in Section 1, 121–150, and Section 2, 0–85 cm.

Major lithology: Alternating volcanic ash-bearing diatom clay and volcanic ash-bearing diatom ooze, greenish gray (5GY 6/1), with thin (1 cm thick) pale olive laminae (5Y 6/4) in Section 3, 95 and 135 cm, and Section 5, 50 and 95 cm. Faint bioturbation throughout. Dropstones in Section 1, 88–92 cm; Section 4, 25, 38, 72, 98, 105, and 135 cm; and Section 5, 75 and 86–90 cm.

Minor lithology: Diatom ooze forming base of 20–30-cm-thick units, grading upward into diatom clay in Section 3, 60–150 cm, and Section 4, 0–110 cm.

SMEAR SLIDE SUMMARY (%):

	2, 20 D	4, 100 M	5, 30 D
COMPOSITION:			
Clay	40	—	—
Volcanic glass	22	100	30
Accessory minerals	—	1	—
Diatoms	35	—	70
Radiolarians	3	—	—
Sponge spicules	—	—	Tr
Silicoflagellates	Tr	—	—
Fish remains	—	—	Tr

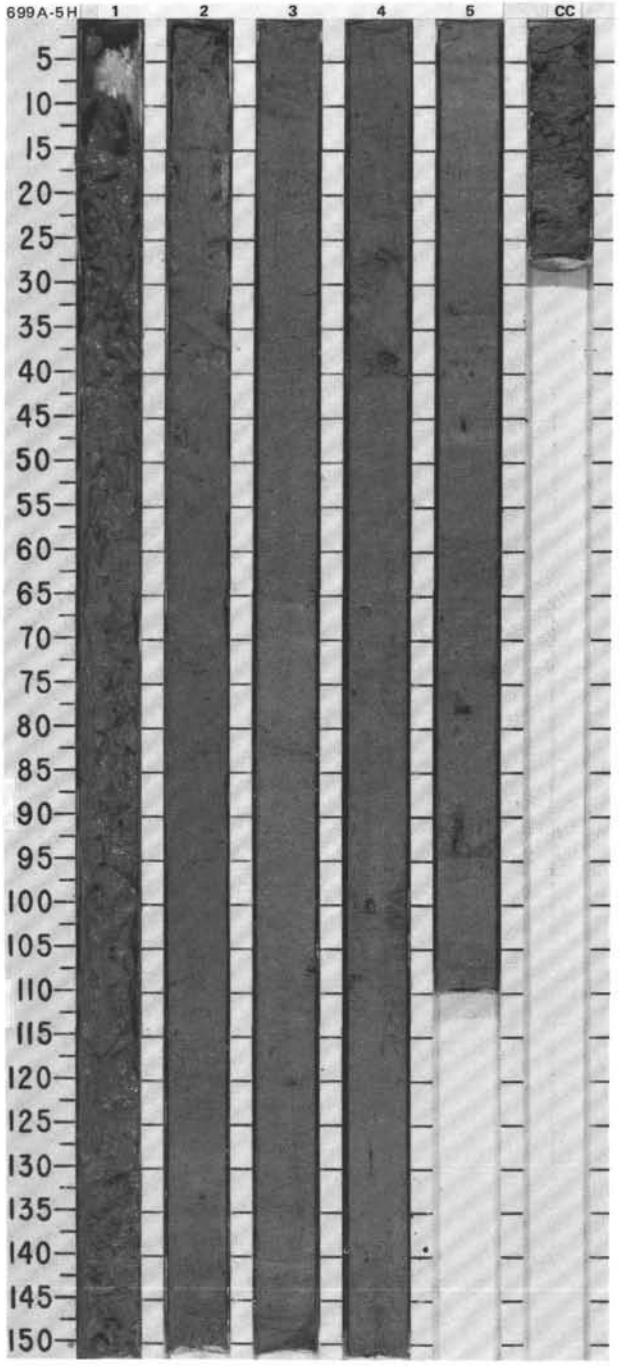

SITE 699 HOLE A CORE 6H CORED INTERVAL 3752.1-3761.6 mbsl; 46.6-56.1 mbsf

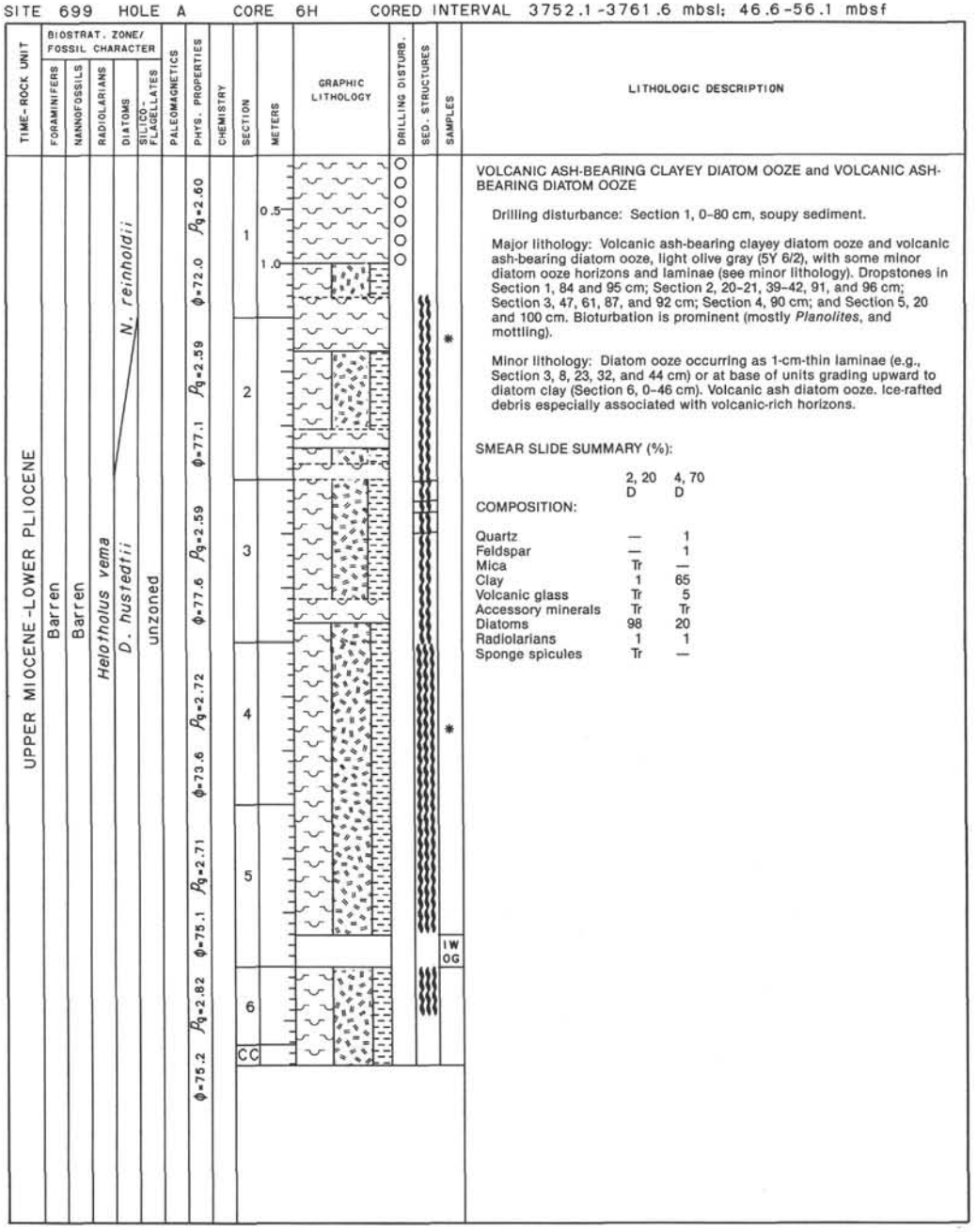

LITHOLOGIC DESCRIPTION

VOLCANIC ASH-BEARING CLAYEY DIATOM OOZE and VOLCANIC ASH-BEARING DIATOM OOZE

Drilling disturbance: Section 1, 0-80 cm, soupy sediment.

Major lithology: Volcanic ash-bearing clayey diatom ooze and volcanic ash-bearing diatom ooze, light olive gray (5Y 6/2), with some minor diatom ooze horizons and laminae (see minor lithology). Dropstones in Section 1, 84 and 95 cm; Section 2, 20-21, 39-42, 91, and 96 cm; Section 3, 47, 61, 87, and 92 cm; Section 4, 90 cm; and Section 5, 20 and 100 cm. Bioturbation is prominent (mostly *Planolites*, and mottling).

Minor lithology: Diatom ooze occurring as 1-cm-thin laminae (e.g., Section 3, 8, 23, 32, and 44 cm) or at base of units grading upward to diatom clay (Section 6, 0-46 cm). Volcanic ash diatom ooze. Ice-rafted debris especially associated with volcanic-rich horizons.

SMEAR SLIDE SUMMARY (%):

	2, 20 D	4, 70 D
COMPOSITION:		
Quartz	—	1
Feldspar	—	1
Mica	Tr	—
Clay	1	65
Volcanic glass	Tr	5
Accessory minerals	Tr	Tr
Diatoms	98	20
Radiolarians	1	1
Sponge spicules	Tr	—

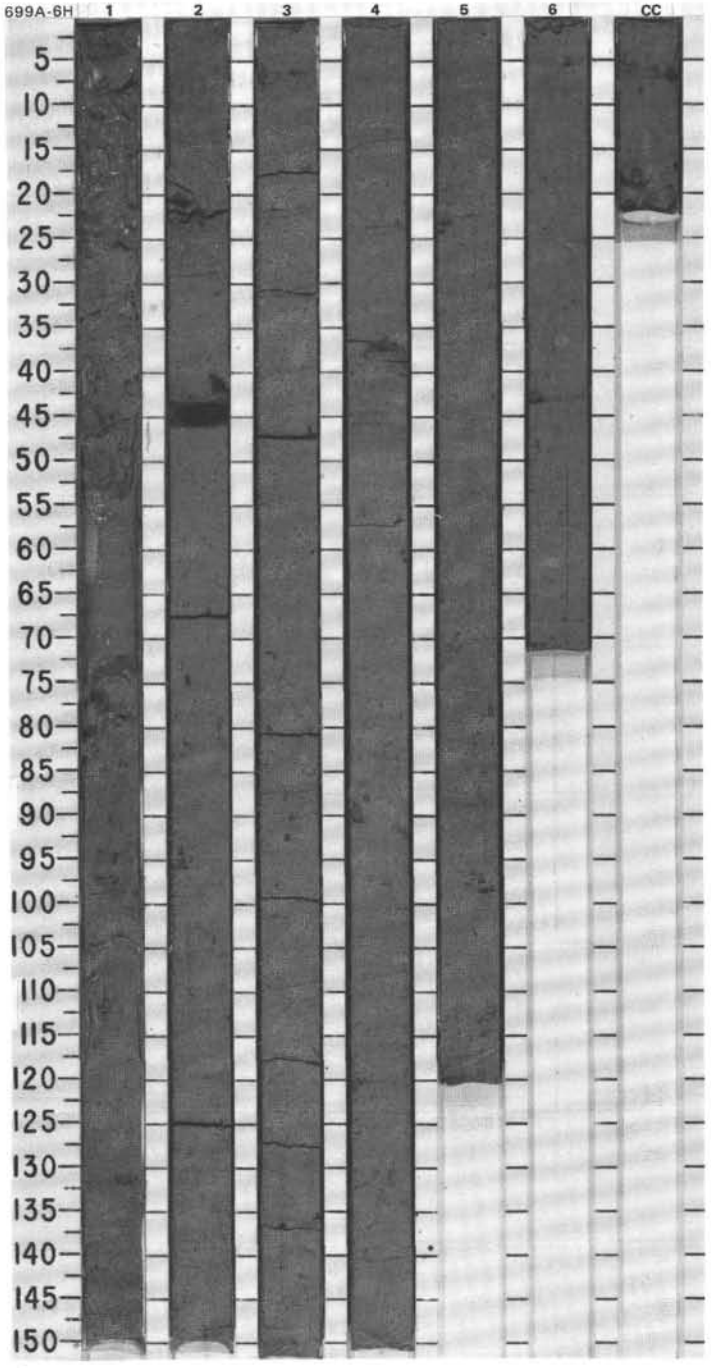

SITE 699 HOLE A CORE 7H CORED INTERVAL 3761.6-3771.1 mbsl; 56.1-65.6 mbsf

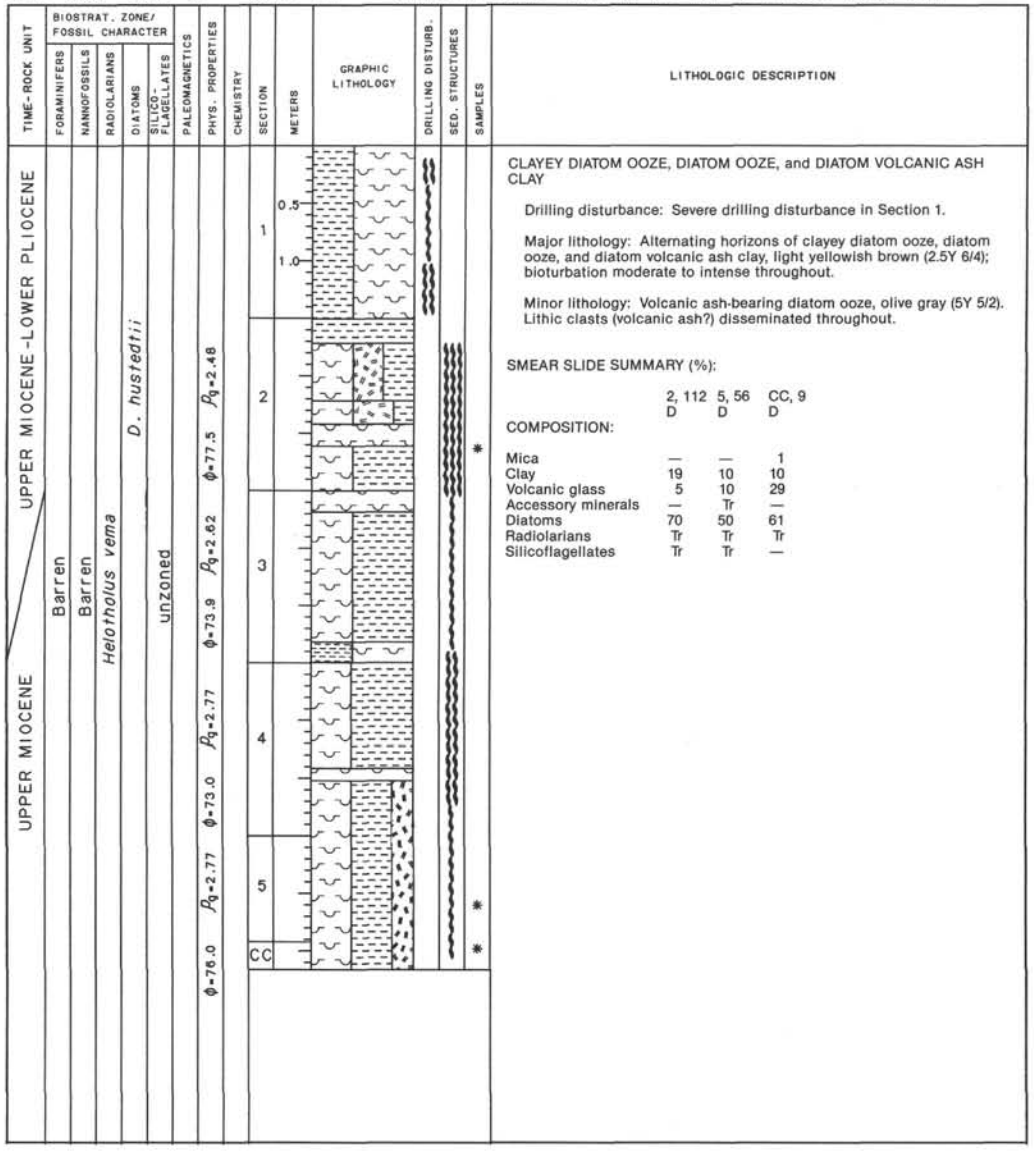

LITHOLOGIC DESCRIPTION

CLAYEY DIATOM OOZE, DIATOM OOZE, and DIATOM VOLCANIC ASH CLAY

Drilling disturbance: Severe drilling disturbance in Section 1.

Major lithology: Alternating horizons of clayey diatom ooze, diatom ooze, and diatom volcanic ash clay, light yellowish brown (2.5Y 6/4); bioturbation moderate to intense throughout.

Minor lithology: Volcanic ash-bearing diatom ooze, olive gray (5Y 5/2). Lithic clasts (volcanic ash?) disseminated throughout.

SMEAR SLIDE SUMMARY (%):

	2, 112 D	5, 56 D	CC, 9 D
COMPOSITION:			
Mica	—	—	1
Clay	19	10	10
Volcanic glass	5	10	29
Accessory minerals	—	Tr	—
Diatoms	70	50	61
Radiolarians	Tr	Tr	Tr
Silicoflagellates	Tr	Tr	—

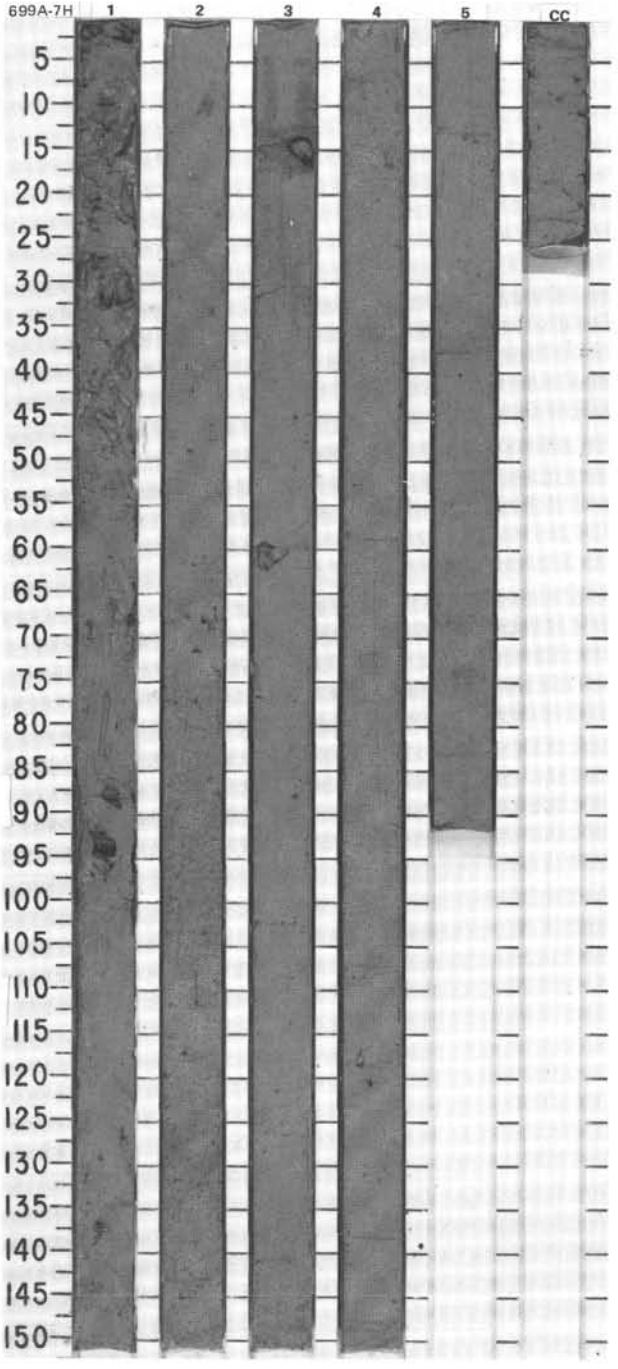

SITE 699 HOLE A CORE 8H CORED INTERVAL 3771.1-3780.6 mbsl; 65.6-75.1 mbsf

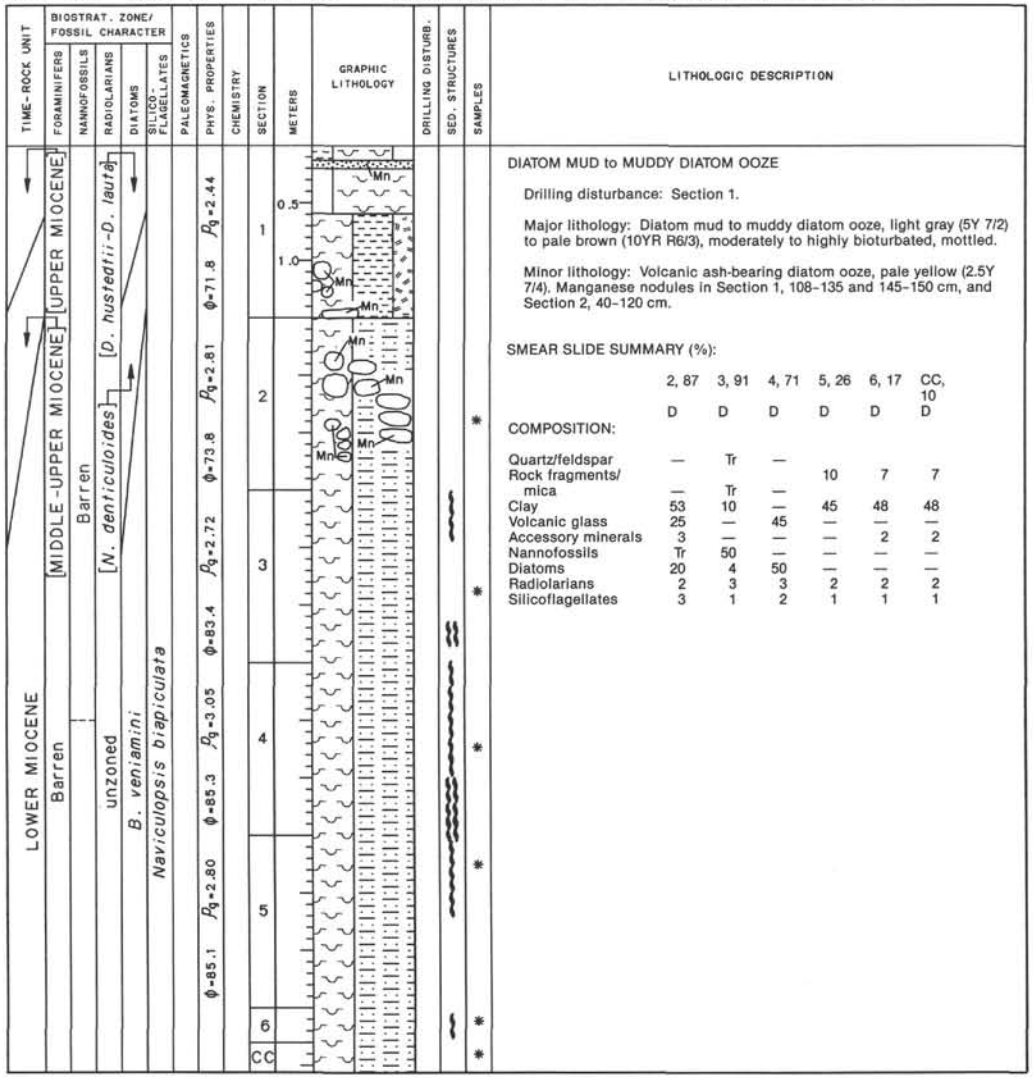

LITHOLOGIC DESCRIPTION

DIATOM MUD to MUDDY DIATOM OOZE

Drilling disturbance: Section 1.

Major lithology: Diatom mud to muddy diatom ooze, light gray (5Y 7/2) to pale brown (10YR R6/3), moderately to highly bioturbated, mottled.

Minor lithology: Volcanic ash-bearing diatom ooze, pale yellow (2.5Y 7/4). Manganese nodules in Section 1, 108-135 and 145-150 cm, and Section 2, 40-120 cm.

SMEAR SLIDE SUMMARY (%):

	2, 87	3, 91	4, 71	5, 26	6, 17	CC, 10
	D	D	D	D	D	D
COMPOSITION:						
Quartz/feldspar	—	Tr	—			
Rock fragments/ mica	—	Tr	—	10	7	7
Clay	53	10	—	45	48	48
Volcanic glass	25	—	45	—	—	—
Accessory minerals	3	—	—	—	2	2
Nannofossils	Tr	50	—	—	—	—
Diatoms	20	4	50	—	—	—
Radiolarians	2	3	3	2	2	2
Silicoflagellates	3	1	2	1	1	1

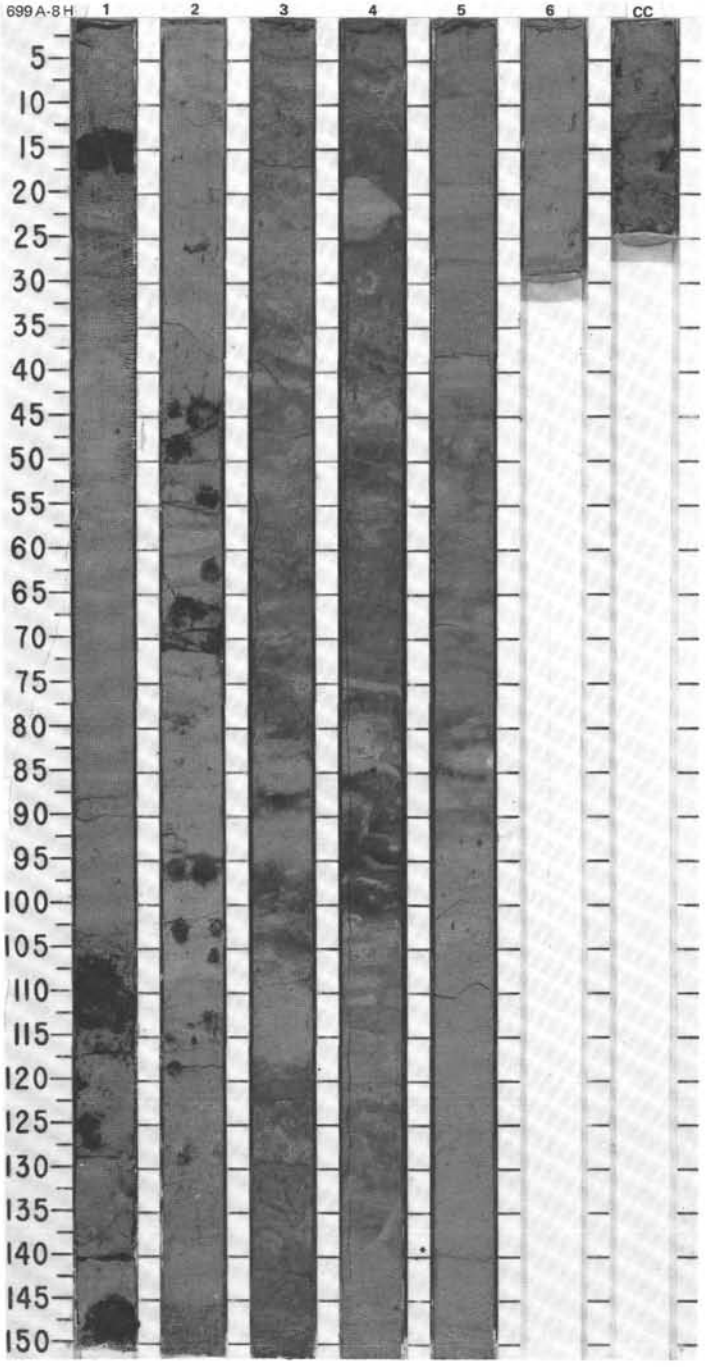

SITE 699 HOLE A CORE 9H CORED INTERVAL 3780.6-3790.1 mbsl; 75.1-84.6 mbsf

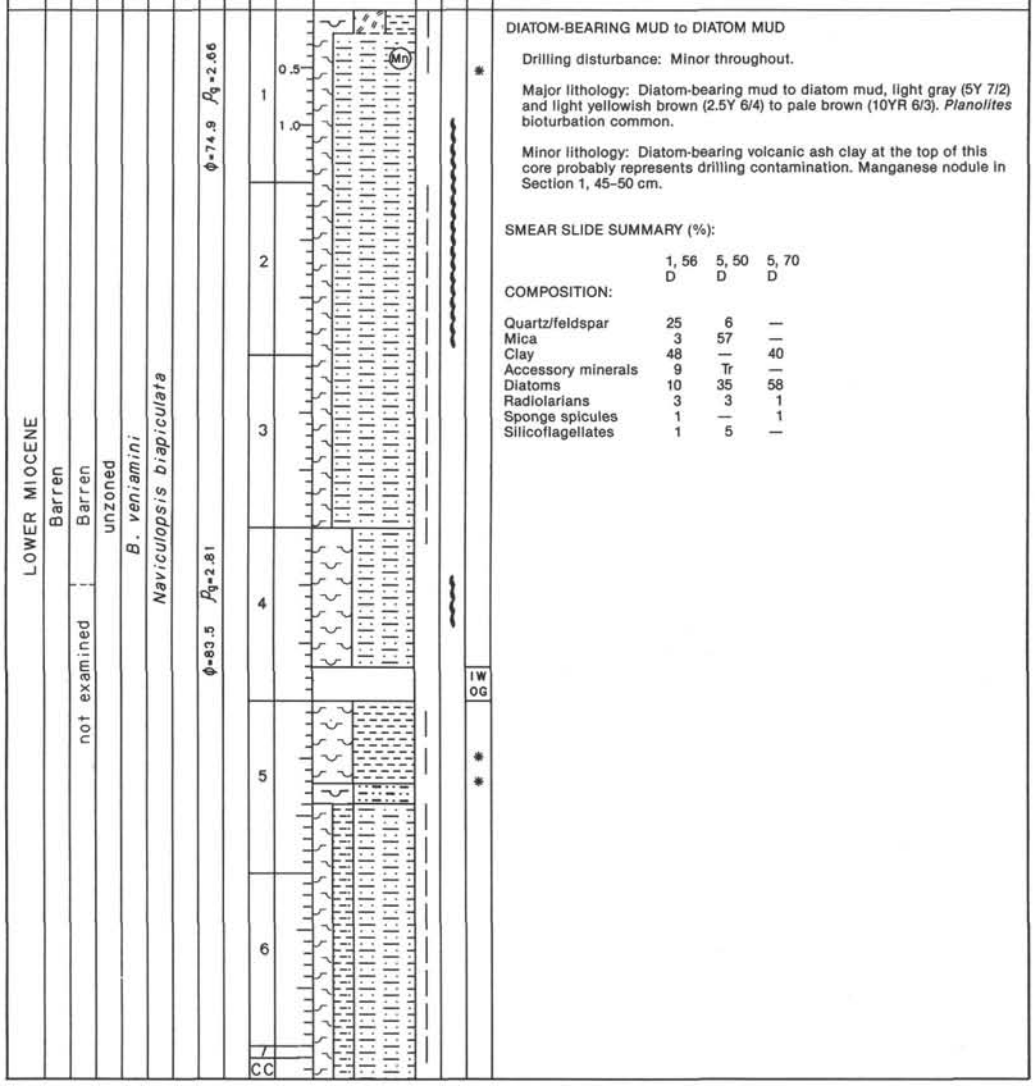

LITHOLOGIC DESCRIPTION

DIATOM-BEARING MUD to DIATOM MUD

Drilling disturbance: Minor throughout.

Major lithology: Diatom-bearing mud to diatom mud, light gray (5Y 7/2) and light yellowish brown (2.5Y 6/4) to pale brown (10YR 6/3). *Planolites* bioturbation common.

Minor lithology: Diatom-bearing volcanic ash clay at the top of this core probably represents drilling contamination. Manganese nodule in Section 1, 45-50 cm.

SMEAR SLIDE SUMMARY (%):

	1, 56 D	5, 50 D	5, 70 D
COMPOSITION:			
Quartz/feldspar	25	6	—
Mica	3	57	—
Clay	48	—	40
Accessory minerals	9	Tr	—
Diatoms	10	35	58
Radiolarians	3	3	1
Sponge spicules	1	—	1
Silicoflagellates	1	5	—

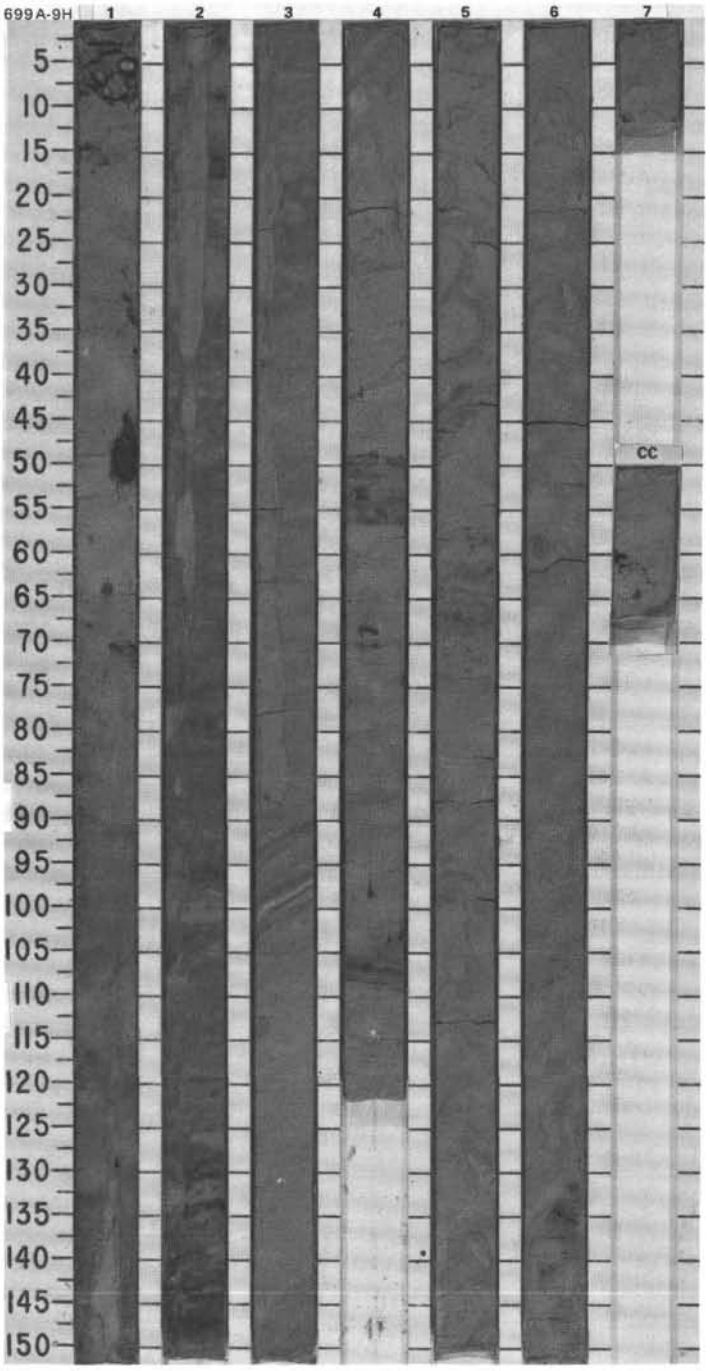

SITE 699 HOLE A CORE 10H CORED INTERVAL 3790.1-3799.6 mbsl; 84.6-94.1 mbsf

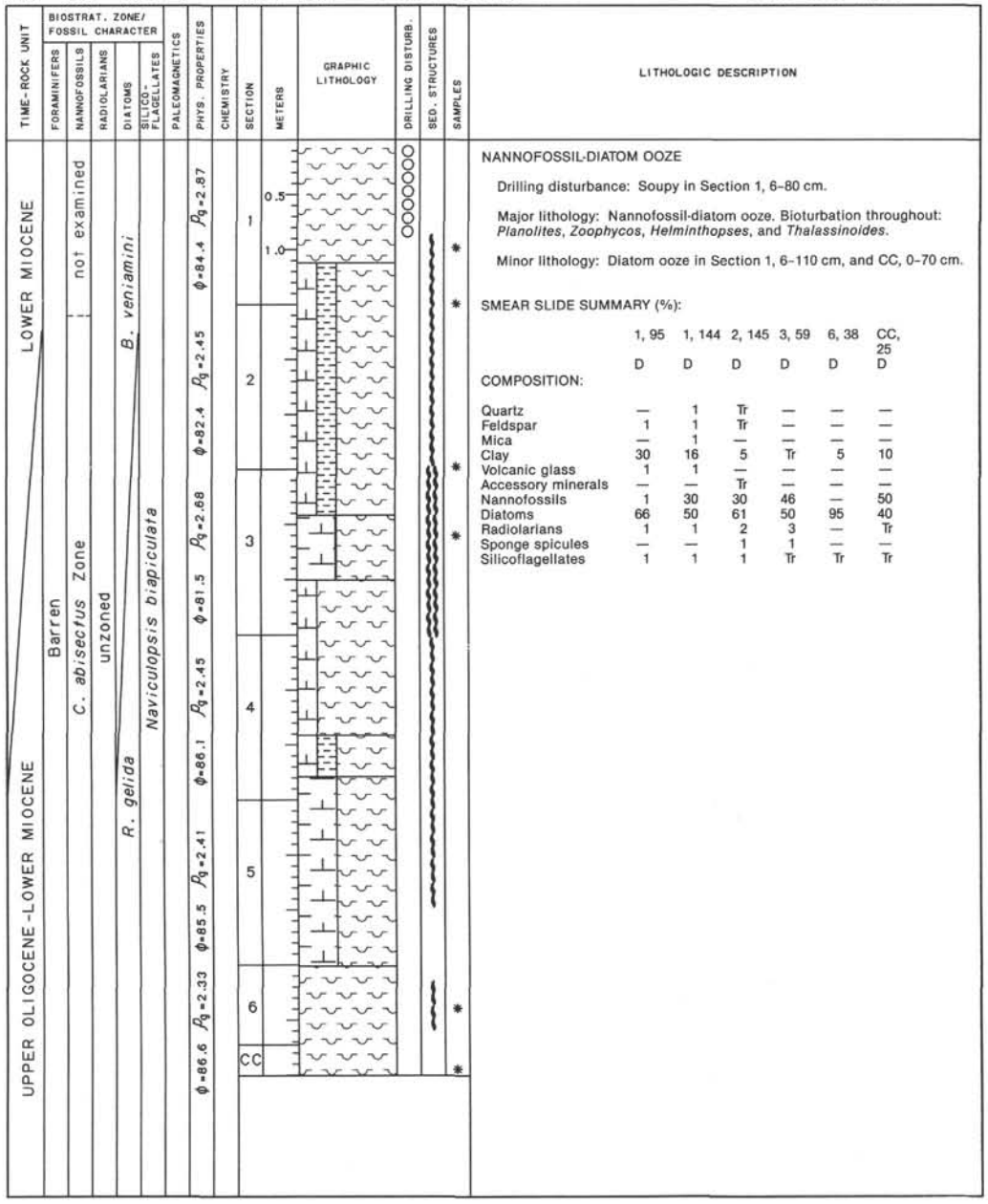

NANNOFOSSIL-DIATOM OOZE

Drilling disturbance: Soupy in Section 1, 6-80 cm.

Major lithology: Nannofossil-diatom ooze. Bioturbation throughout: *Planolites*, *Zoophycos*, *Helminthopses*, and *Thalassinoides*.

Minor lithology: Diatom ooze in Section 1, 6-110 cm, and CC, 0-70 cm.

SMEAR SLIDE SUMMARY (%):

	1, 95	1, 144	2, 145	3, 59	6, 38	CC, 25
	D	D	D	D	D	D
COMPOSITION:						
Quartz	—	1	Tr	—	—	—
Feldspar	1	1	Tr	—	—	—
Mica	—	1	—	—	—	—
Clay	30	16	5	Tr	5	10
Volcanic glass	1	1	—	—	—	—
Accessory minerals	—	—	Tr	—	—	—
Nannofossils	1	30	30	46	—	50
Diatoms	66	50	61	50	95	40
Radiolarians	1	1	2	3	—	Tr
Sponge spicules	—	—	1	1	—	—
Silicoflagellates	1	1	1	Tr	Tr	Tr

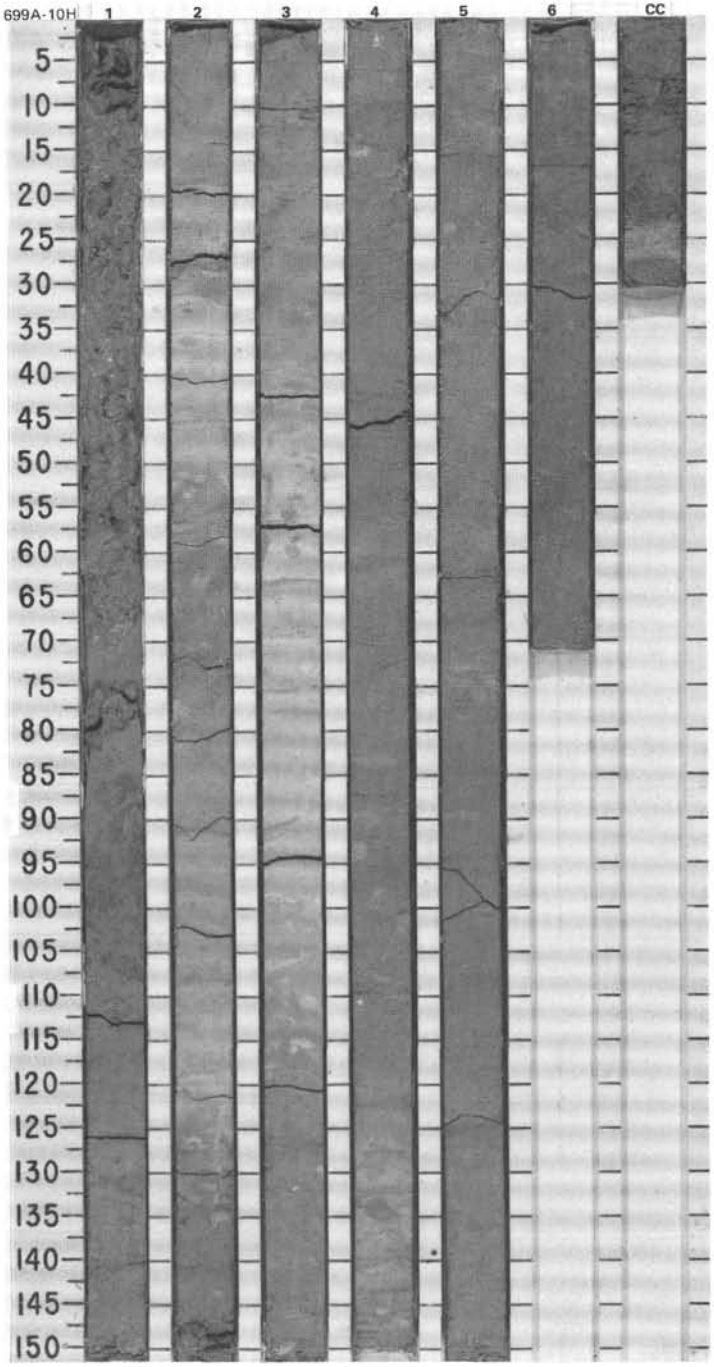

SITE 699 HOLE A CORE 11H CORED INTERVAL 3799.6-3809.1 mbsl; 94.1-103.6 mbsf

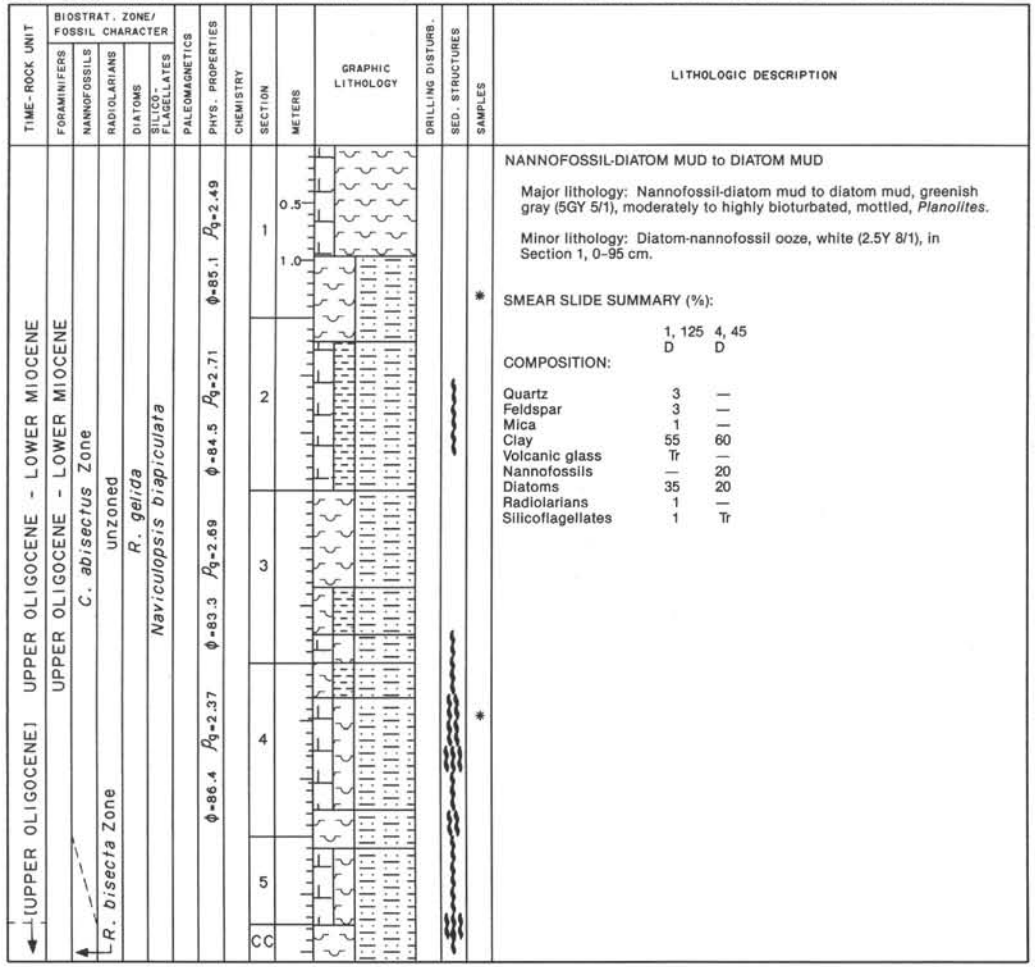

LITHOLOGIC DESCRIPTION

NANNOFOSSIL-DIATOM MUD to DIATOM MUD

Major lithology: Nannofossil-diatom mud to diatom mud, greenish gray (5GY 5/1), moderately to highly bioturbated, mottled, *Planolites*.

Minor lithology: Diatom-nannofossil ooze, white (2.5Y 8/1), in Section 1, 0-95 cm.

SMEAR SLIDE SUMMARY (%):

	1, 125 D	4, 45 D
COMPOSITION:		
Quartz	3	—
Feldspar	3	—
Mica	1	—
Clay	55	60
Volcanic glass	Tr	—
Nannofossils	—	20
Diatoms	35	20
Radiolarians	1	—
Silicoflagellates	1	Tr

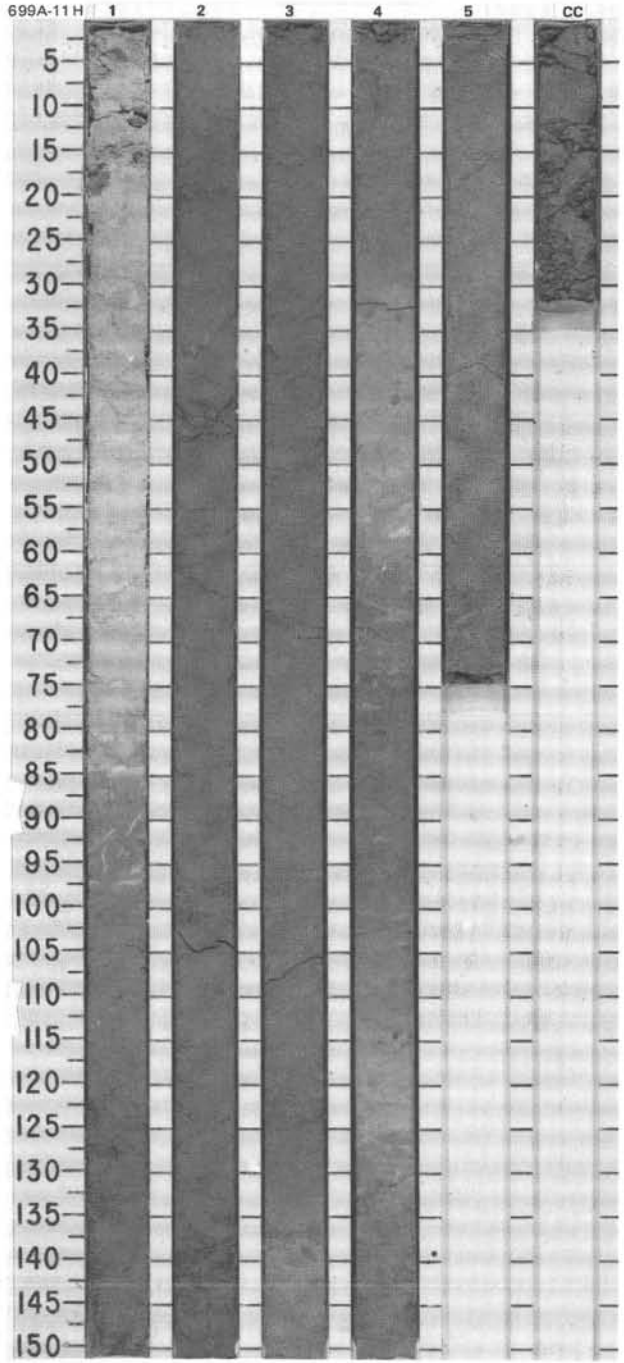

SITE 699 HOLE A CORE 12H CORED INTERVAL 3809.1-3819.1 mbsl; 103.6-113.1 mbsf

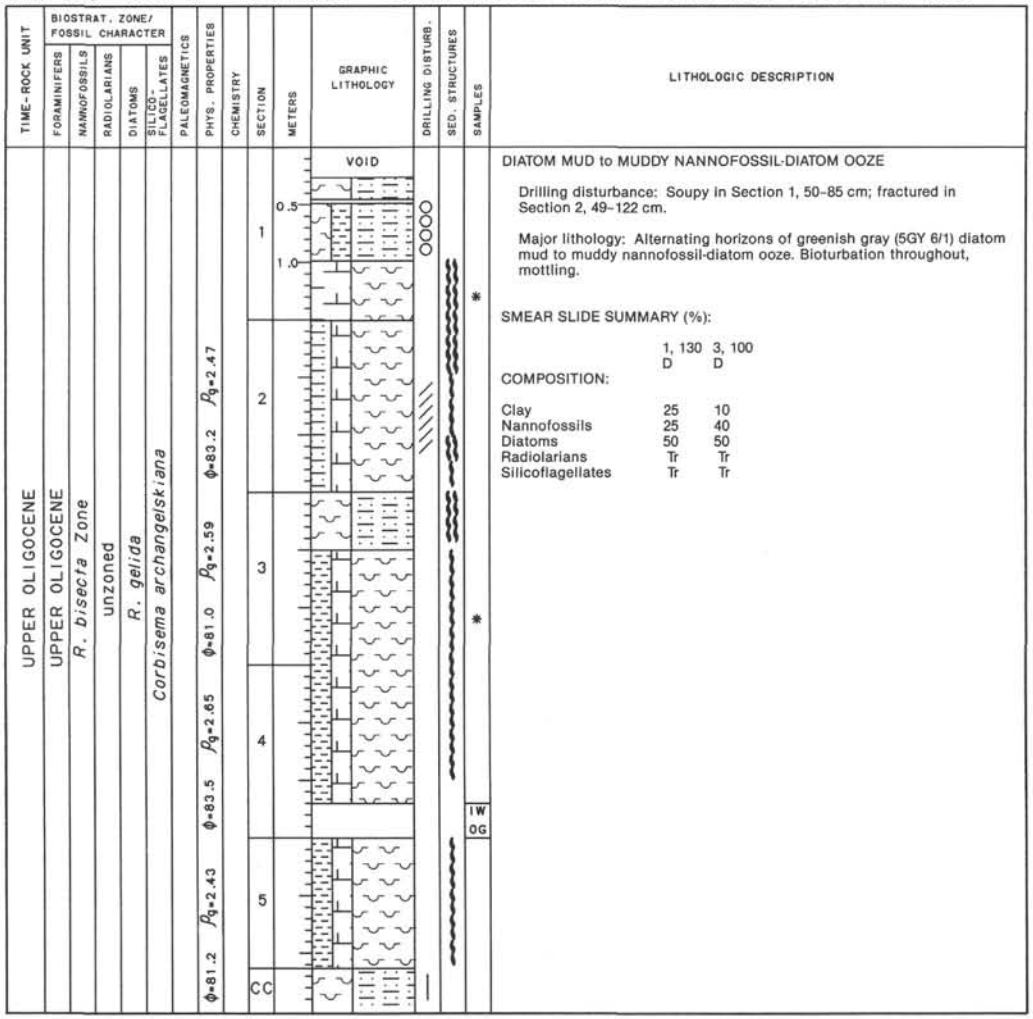

LITHOLOGIC DESCRIPTION

DIATOM MUD to MUDDY NANNOFOSSIL-DIATOM OOZE

Drilling disturbance: Soupy in Section 1, 50-85 cm; fractured in Section 2, 49-122 cm.

Major lithology: Alternating horizons of greenish gray (5GY 6/1) diatom mud to muddy nannofossil-diatom ooze. Bioturbation throughout, mottling.

SMEAR SLIDE SUMMARY (%):

	1, 130 D	3, 100 D
COMPOSITION:		
Clay	25	10
Nannofossils	25	40
Diatoms	50	50
Radiolarians	Tr	Tr
Silicoflagellates	Tr	Tr

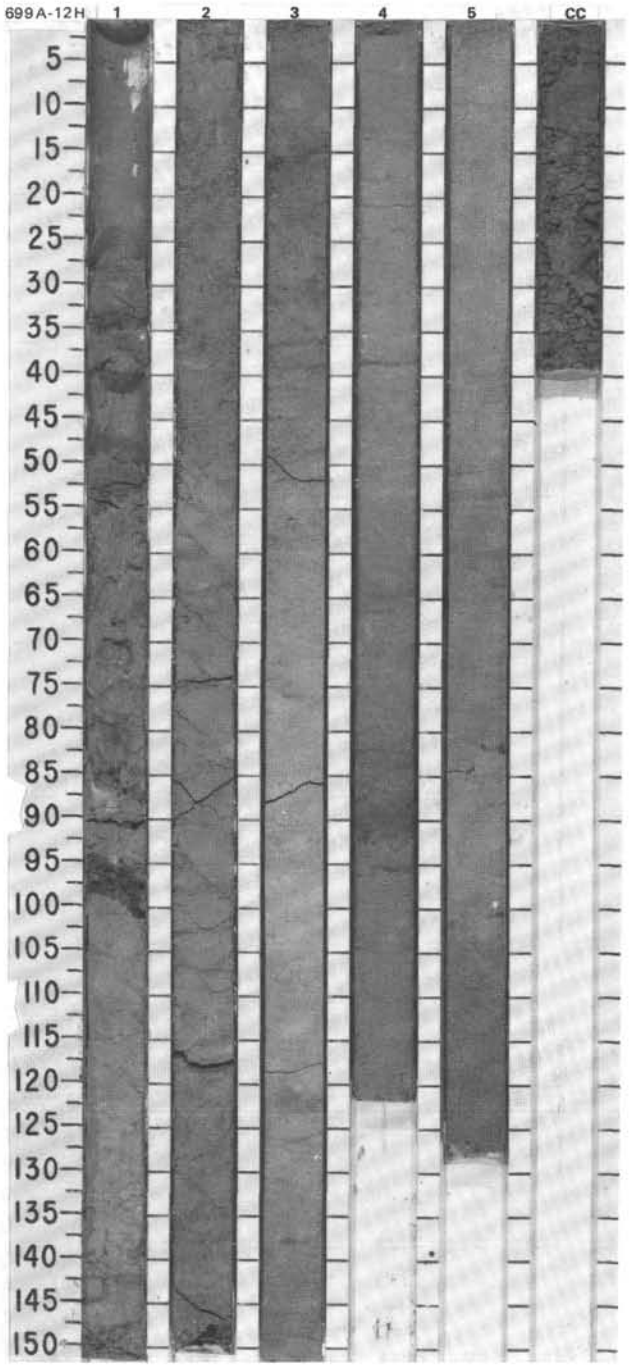

SITE 699 HOLE A CORE 13H CORED INTERVAL 3819.1-3828.1 mbsl; 113.1-122.6 mbsf

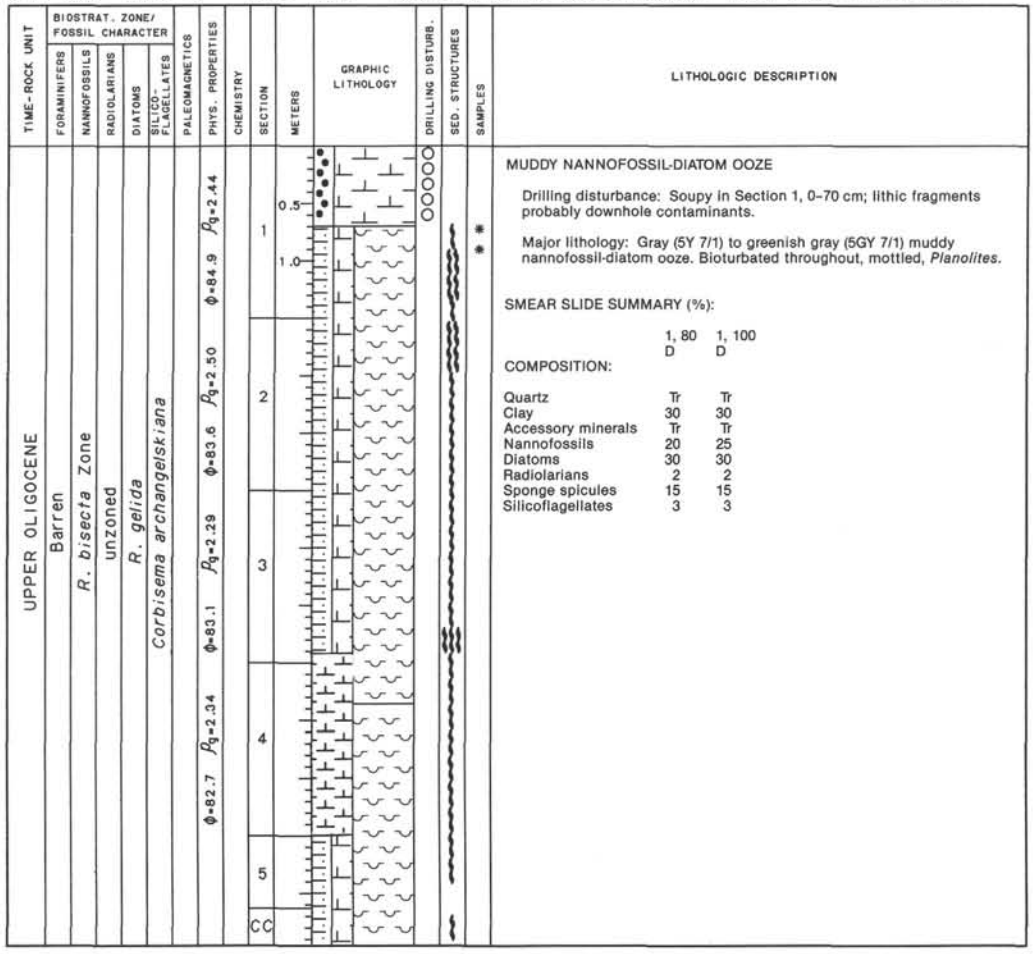

LITHOLOGIC DESCRIPTION

MUDDY NANNOFOSSIL-DIATOM OOZE

Drilling disturbance: Soupy in Section 1, 0-70 cm; lithic fragments probably downhole contaminants.

Major lithology: Gray (5Y 7/1) to greenish gray (5GY 7/1) muddy nannofossil-diatom ooze. Bioturbated throughout, mottled, *Planolites*.

SMEAR SLIDE SUMMARY (%):

	1, 80 D	1, 100 D
COMPOSITION:		
Quartz	Tr	Tr
Clay	30	30
Accessory minerals	Tr	Tr
Nannofossils	20	25
Diatoms	30	30
Radiolarians	2	2
Sponge spicules	15	15
Silicoflagellates	3	3

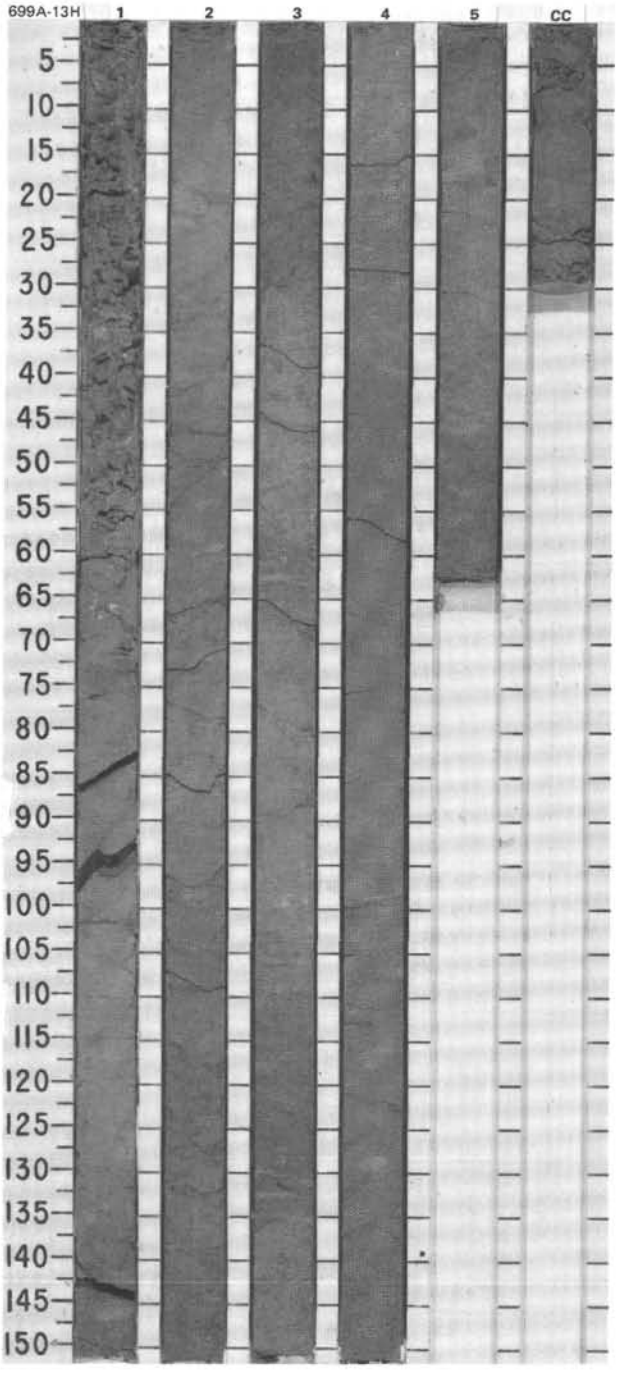

SITE 699 HOLE A CORE 14H CORED INTERVAL 3828.1-3837.6 mbsl; 122.6-132.1 mbsf

TIME-ROCK UNIT	BIOSTRAT. ZONE/ FOSSIL CHARACTER: FORAMINIFERS	NANNOFOSSILS	RADIOLARIANS	DIATOMS	SILICO-FLAGELLATES	PALEOMAGNETICS	PHYS. PROPERTIES	CHEMISTRY	SECTION	METERS	GRAPHIC LITHOLOGY	DRILLING DISTURB.	SED. STRUCTURES	SAMPLES
UPPER OLIGOCENE	Barren	*R. bisecta* Zone	unzoned	*R. gelida*	*Corbisema archangelskiana*	ρ_q=2.54 ϕ=80.7	ϕ=80.7 ρ_q=2.45 ϕ=83.4 ρ_q=2.67 ϕ=84.7 ρ_q=2.58		1 2 3 4 CC	0.5 1.0				* *

LITHOLOGIC DESCRIPTION

MUDDY DIATOM OOZE, MUDDY NANNOFOSSIL OOZE, and DIATOM CLAYEY MUD

Drilling disturbance: Fracturing in Section 3.

Major lithology: Alternating horizons of light brownish gray (2.5Y 6/2) muddy diatom ooze, muddy nannofossil ooze, and diatom clayey mud, bioturbated, mottled, *Zoophycos* burrows.

SMEAR SLIDE SUMMARY (%):

	2, 40 D	4, 50 D
COMPOSITION:		
Clay	40	55
Nannofossils	1	Tr
Diatoms	59	45
Sponge spicules	Tr	Tr
Silicoflagellates	Tr	Tr

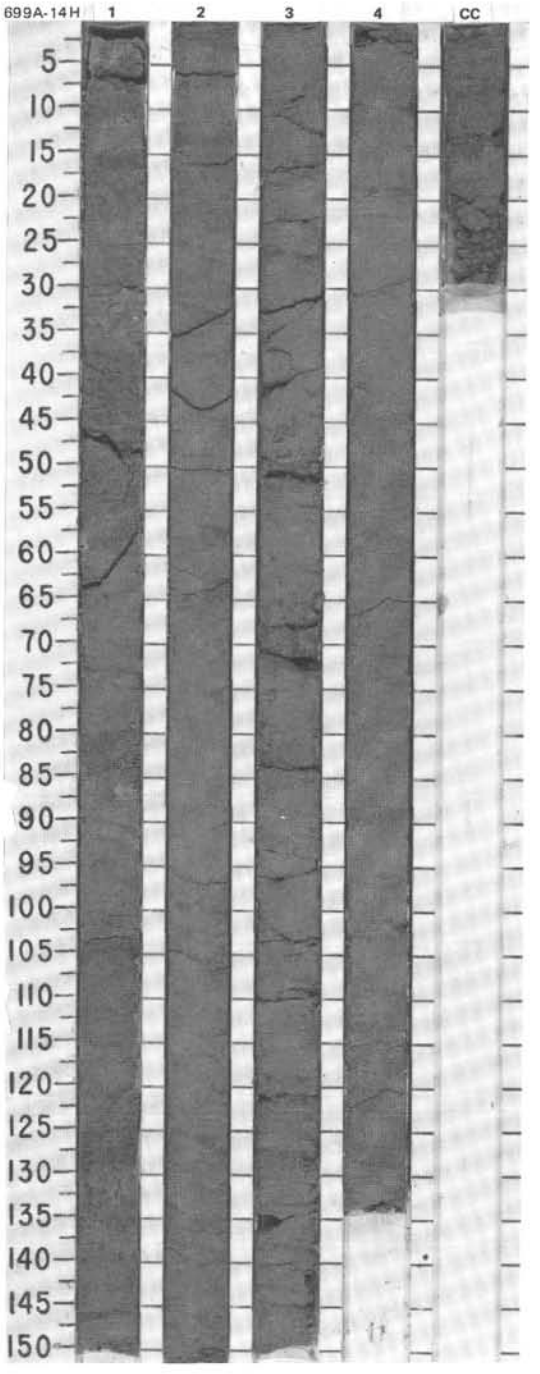

SITE 699 HOLE A CORE 15H CORED INTERVAL 3837.6-3847.1 mbsl; 132.1-141.6 mbsf

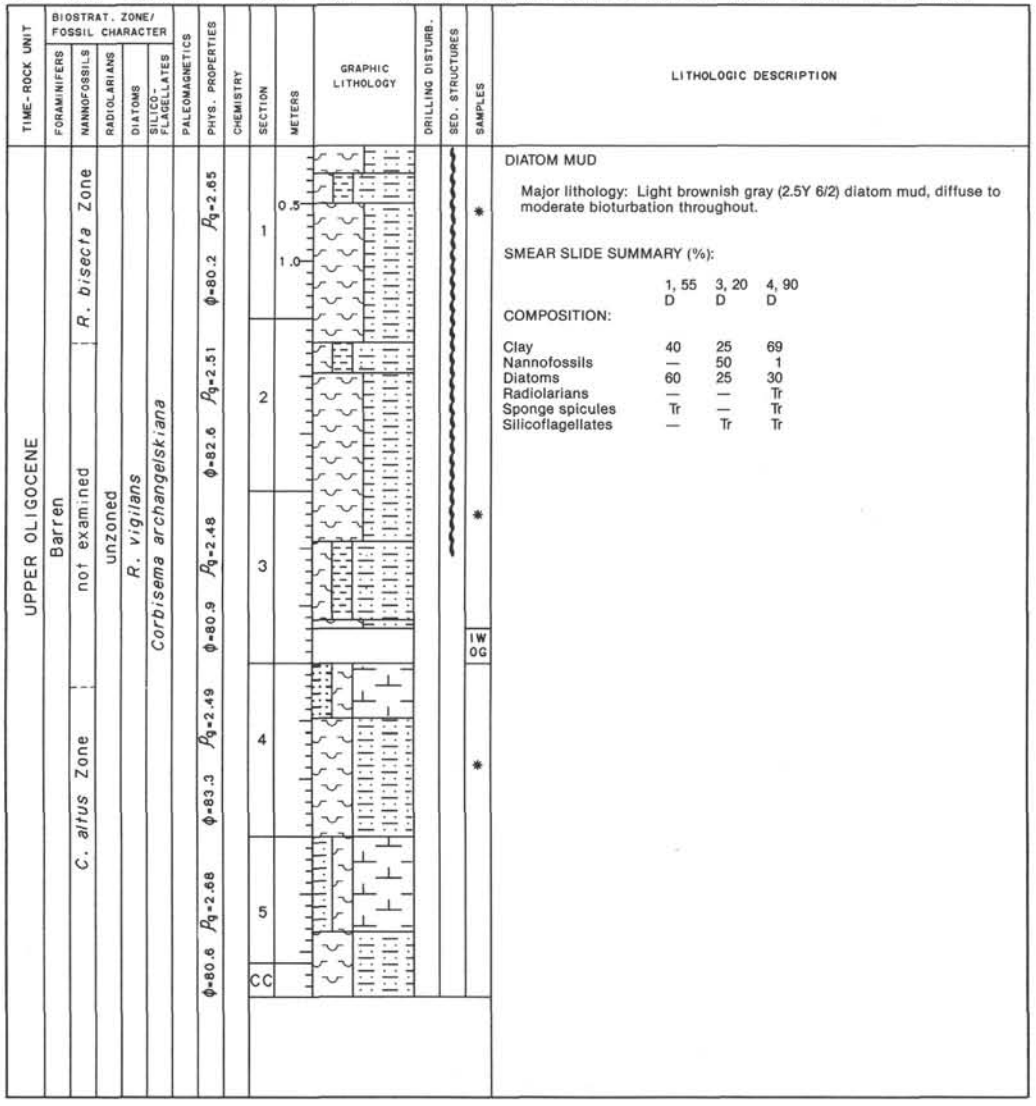

LITHOLOGIC DESCRIPTION

DIATOM MUD

Major lithology: Light brownish gray (2.5Y 6/2) diatom mud, diffuse to moderate bioturbation throughout.

SMEAR SLIDE SUMMARY (%):

	1, 55 D	3, 20 D	4, 90 D
COMPOSITION:			
Clay	40	25	69
Nannofossils	—	50	1
Diatoms	60	25	30
Radiolarians	—	—	Tr
Sponge spicules	Tr	—	Tr
Silicoflagellates	—	Tr	Tr

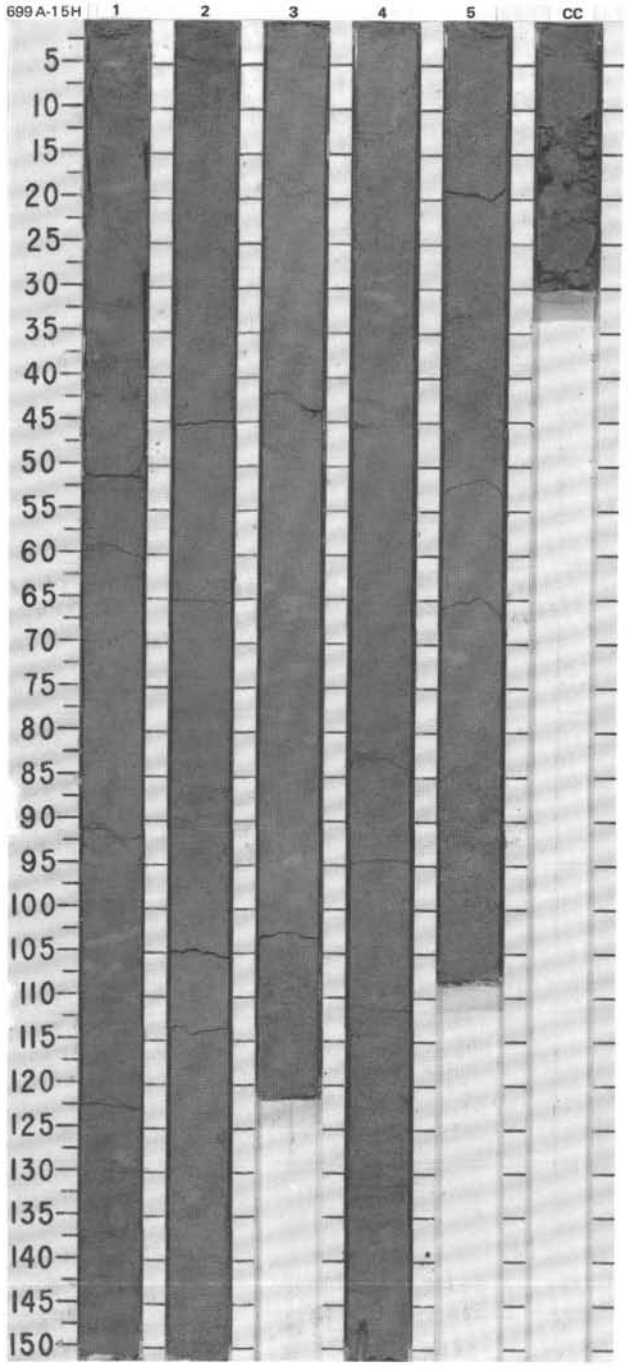

SITE 699 HOLE A CORE 16H CORED INTERVAL 3847.1-3856.6 mbsl; 141.6-151.1 mbsf

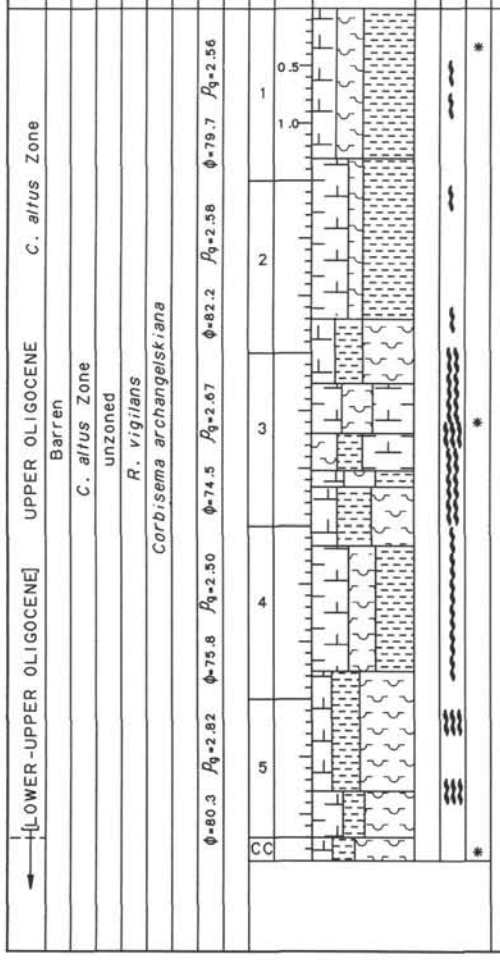

LITHOLOGIC DESCRIPTION

NANNOFOSSIL-SILICEOUS CLAY, alternating with NANNOFOSSIL-BEARING CLAYEY SILICEOUS OOZE

Major lithology: Nannofossil-siliceous clay, gray (5Y 5/1, 6/1), alternating with nannofossil-bearing clayey siliceous ooze, light gray (5Y 7/1). Lithic fragments in Section 1, 10-14 cm. Bioturbation moderate in Sections 3, 4, and 5; *Planolites* and extensive *Zoophycos* in Section 5, 7-25 and 71-87 cm.

SMEAR SLIDE SUMMARY (%):

	1, 30	3, 60	CC, 12
	D	D	D
COMPOSITION:			
Clay	50	50	25
Nannofossils	20	20	25
Diatoms	30	30	50
Radiolarians	—	Tr	—
Sponge spicules	Tr	Tr	Tr
Silicoflagellates	Tr	Tr	—

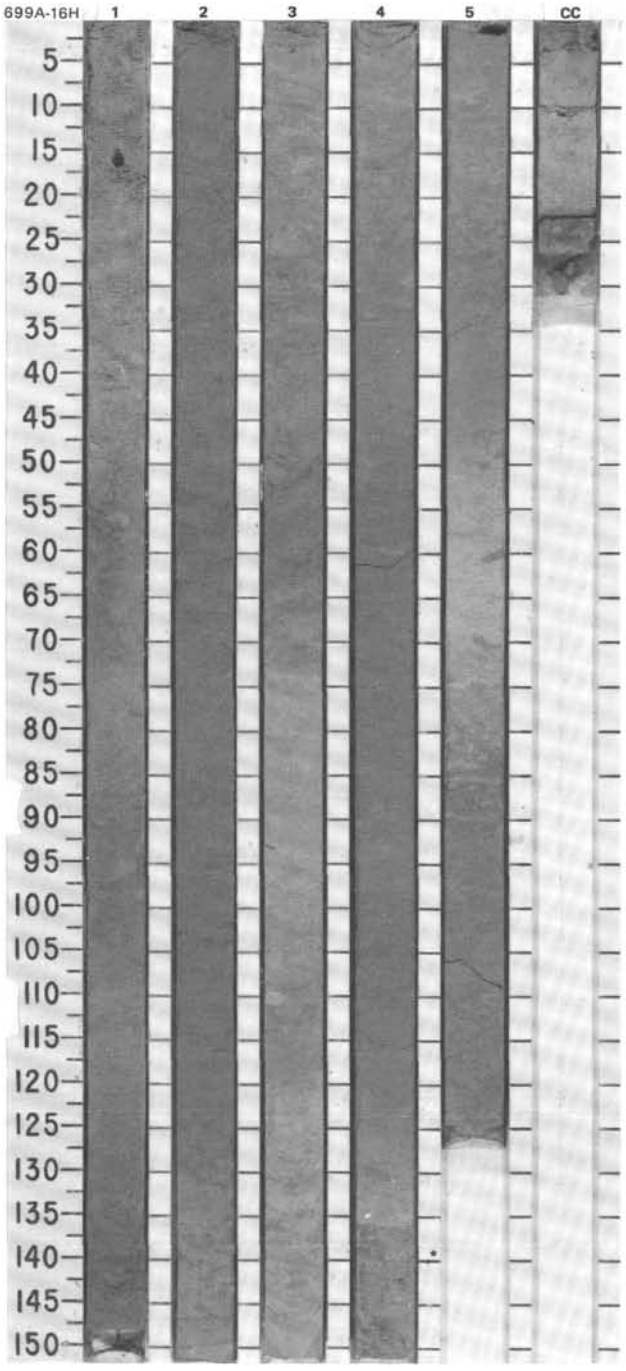

SITE 699 HOLE A CORE 17H CORED INTERVAL 3856.6-3866.1 mbsl; 151.1-160.6 mbsf

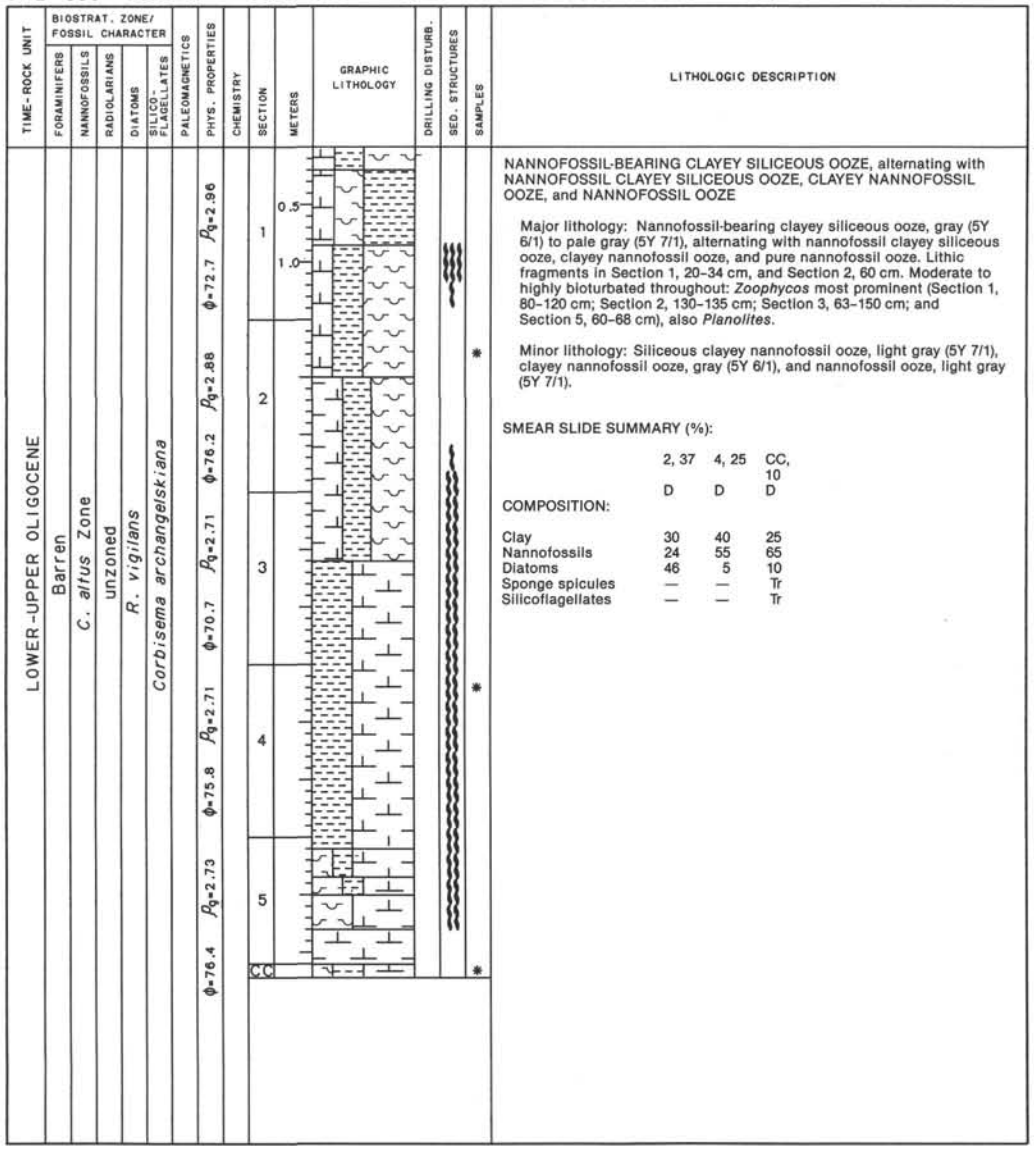

LITHOLOGIC DESCRIPTION

NANNOFOSSIL-BEARING CLAYEY SILICEOUS OOZE, alternating with NANNOFOSSIL CLAYEY SILICEOUS OOZE, CLAYEY NANNOFOSSIL OOZE, and NANNOFOSSIL OOZE

Major lithology: Nannofossil-bearing clayey siliceous ooze, gray (5Y 6/1) to pale gray (5Y 7/1), alternating with nannofossil clayey siliceous ooze, clayey nannofossil ooze, and pure nannofossil ooze. Lithic fragments in Section 1, 20–34 cm, and Section 2, 60 cm. Moderate to highly bioturbated throughout: *Zoophycos* most prominent (Section 1, 80–120 cm; Section 2, 130–135 cm; Section 3, 63–150 cm; and Section 5, 60–68 cm), also *Planolites*.

Minor lithology: Siliceous clayey nannofossil ooze, light gray (5Y 7/1), clayey nannofossil ooze, gray (5Y 6/1), and nannofossil ooze, light gray (5Y 7/1).

SMEAR SLIDE SUMMARY (%):

	2, 37	4, 25	CC, 10
	D	D	D
COMPOSITION:			
Clay	30	40	25
Nannofossils	24	55	65
Diatoms	46	5	10
Sponge spicules	—	—	Tr
Silicoflagellates	—	—	Tr

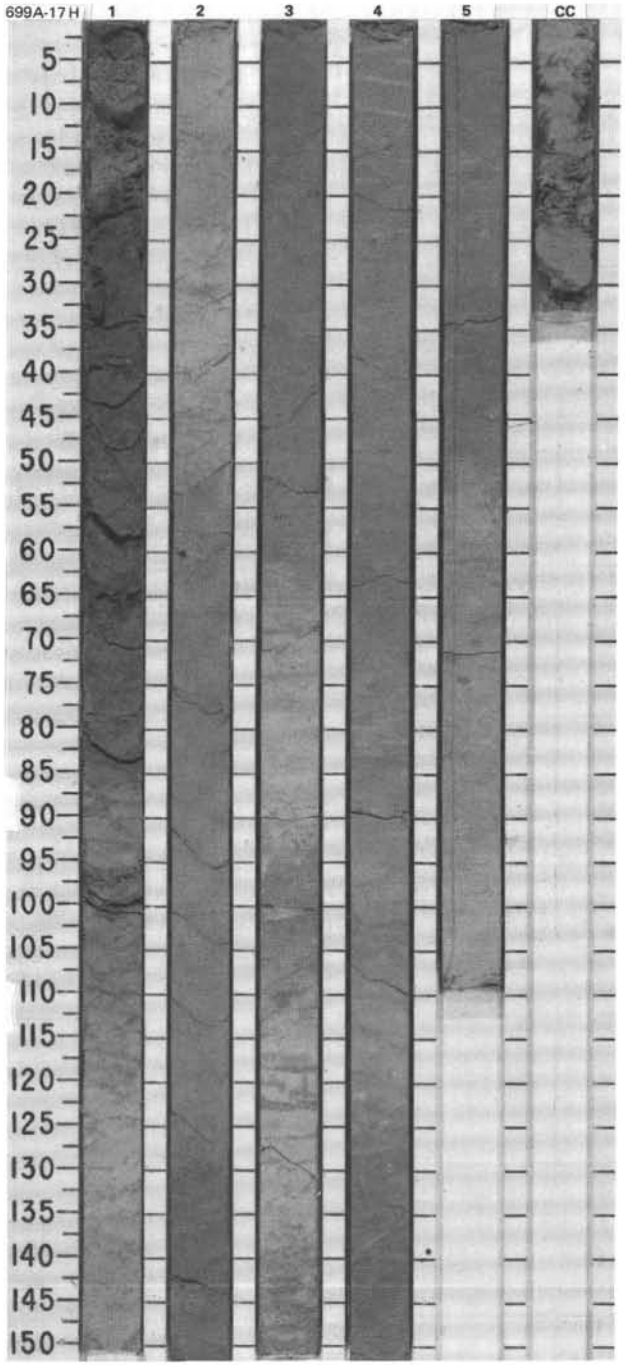

SITE 699 HOLE A CORE 18H CORED INTERVAL 3866.1-3875.6 mbsl; 160.6-170.1 mbsf

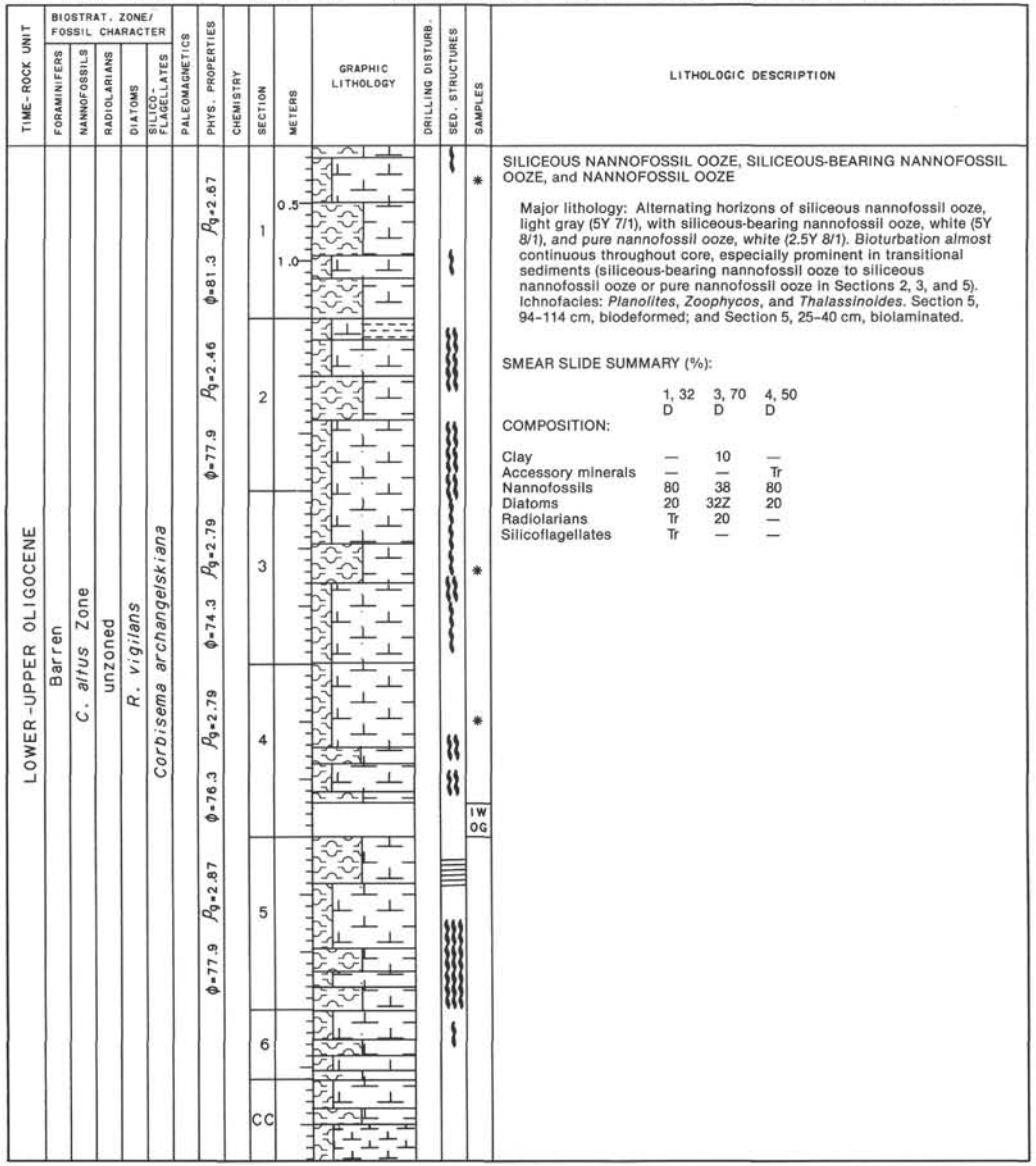

SILICEOUS NANNOFOSSIL OOZE, SILICEOUS-BEARING NANNOFOSSIL OOZE, and NANNOFOSSIL OOZE

Major lithology: Alternating horizons of siliceous nannofossil ooze, light gray (5Y 7/1), with siliceous-bearing nannofossil ooze, white (5Y 8/1), and pure nannofossil ooze, white (2.5Y 8/1). Bioturbation almost continuous throughout core, especially prominent in transitional sediments (siliceous-bearing nannofossil ooze to siliceous nannofossil ooze or pure nannofossil ooze in Sections 2, 3, and 5). Ichnofacies: *Planolites*, *Zoophycos*, and *Thalassinoides*. Section 5, 94-114 cm, biodeformed; and Section 5, 25-40 cm, biolaminated.

SMEAR SLIDE SUMMARY (%):

	1, 32 D	3, 70 D	4, 50 D
COMPOSITION:			
Clay	—	10	—
Accessory minerals	—	—	Tr
Nannofossils	80	38	80
Diatoms	20	32Z	20
Radiolarians	Tr	20	—
Silicoflagellates	Tr	—	—

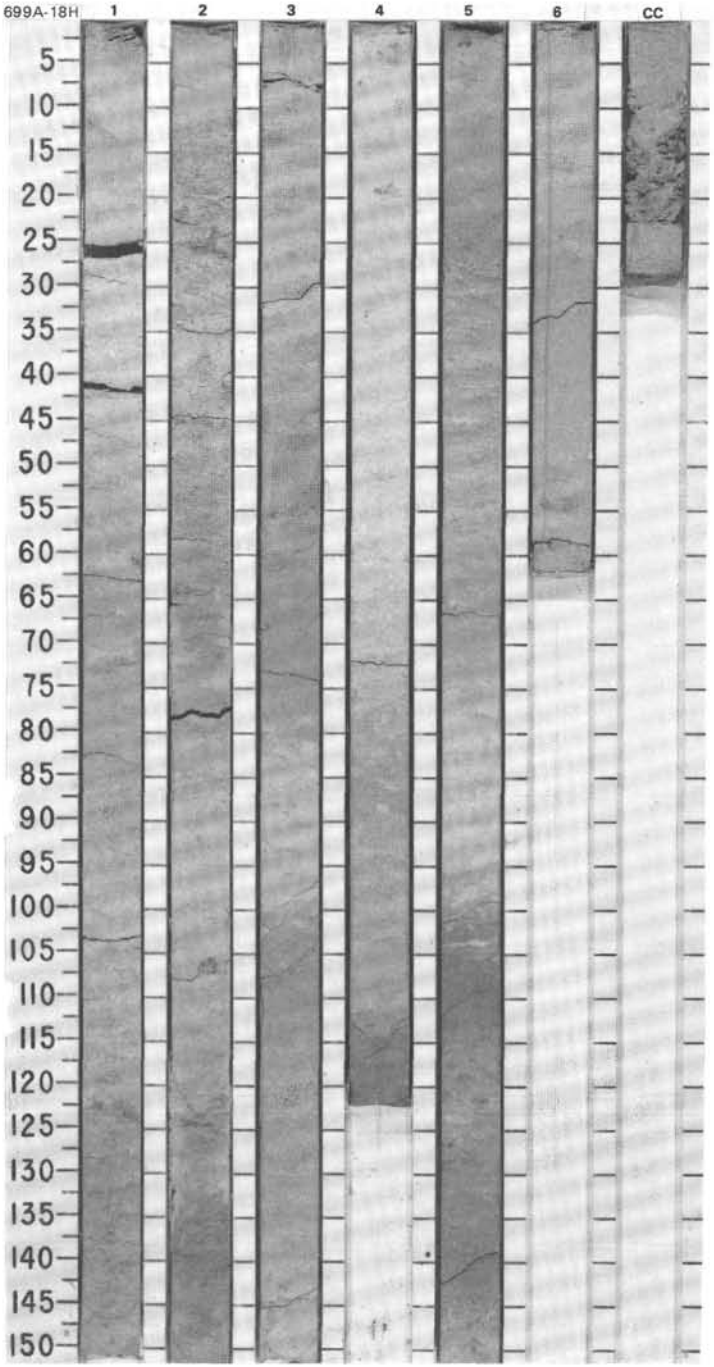

SITE 699 HOLE A CORE 19H CORED INTERVAL 3875.6-3885.1 mbsl; 170.1-179.6 mbsf

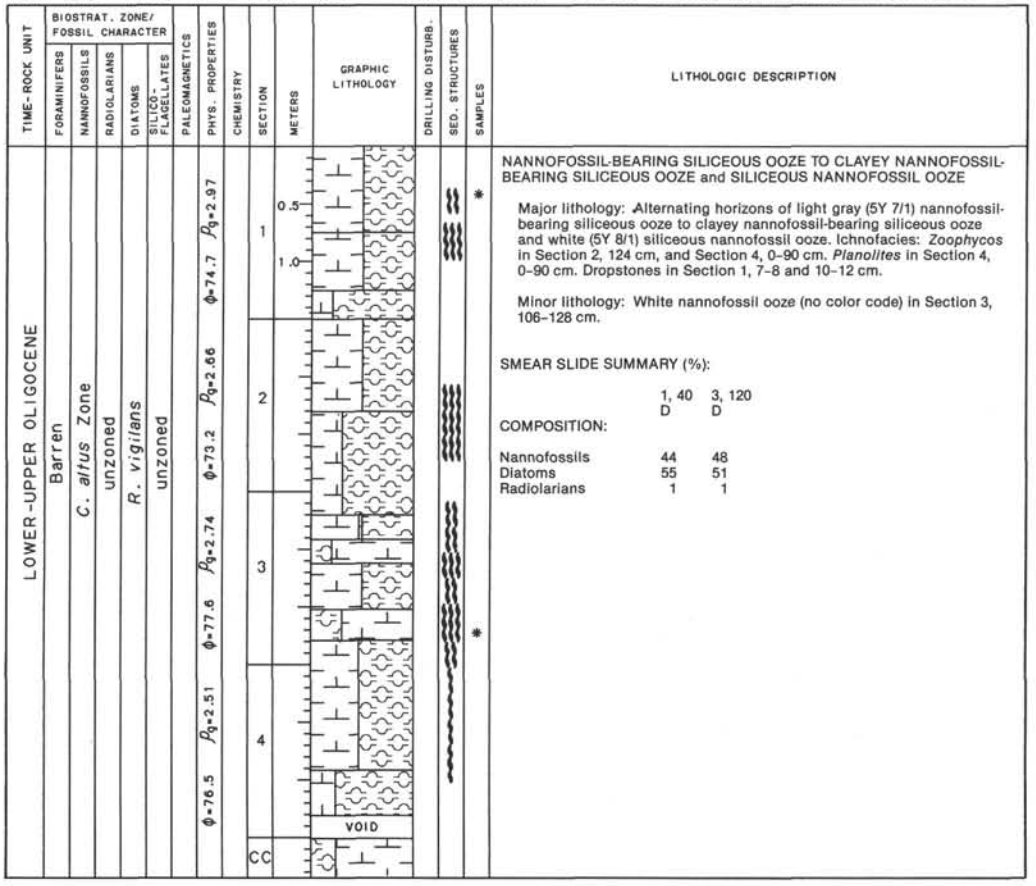

NANNOFOSSIL-BEARING SILICEOUS OOZE TO CLAYEY NANNOFOSSIL-BEARING SILICEOUS OOZE and SILICEOUS NANNOFOSSIL OOZE

Major lithology: Alternating horizons of light gray (5Y 7/1) nannofossil-bearing siliceous ooze to clayey nannofossil-bearing siliceous ooze and white (5Y 8/1) siliceous nannofossil ooze. Ichnofacies: *Zoophycos* in Section 2, 124 cm, and Section 4, 0-90 cm. *Planolites* in Section 4, 0-90 cm. Dropstones in Section 1, 7-8 and 10-12 cm.

Minor lithology: White nannofossil ooze (no color code) in Section 3, 106-128 cm.

SMEAR SLIDE SUMMARY (%):

COMPOSITION:	1, 40 D	3, 120 D
Nannofossils	44	48
Diatoms	55	51
Radiolarians	1	1

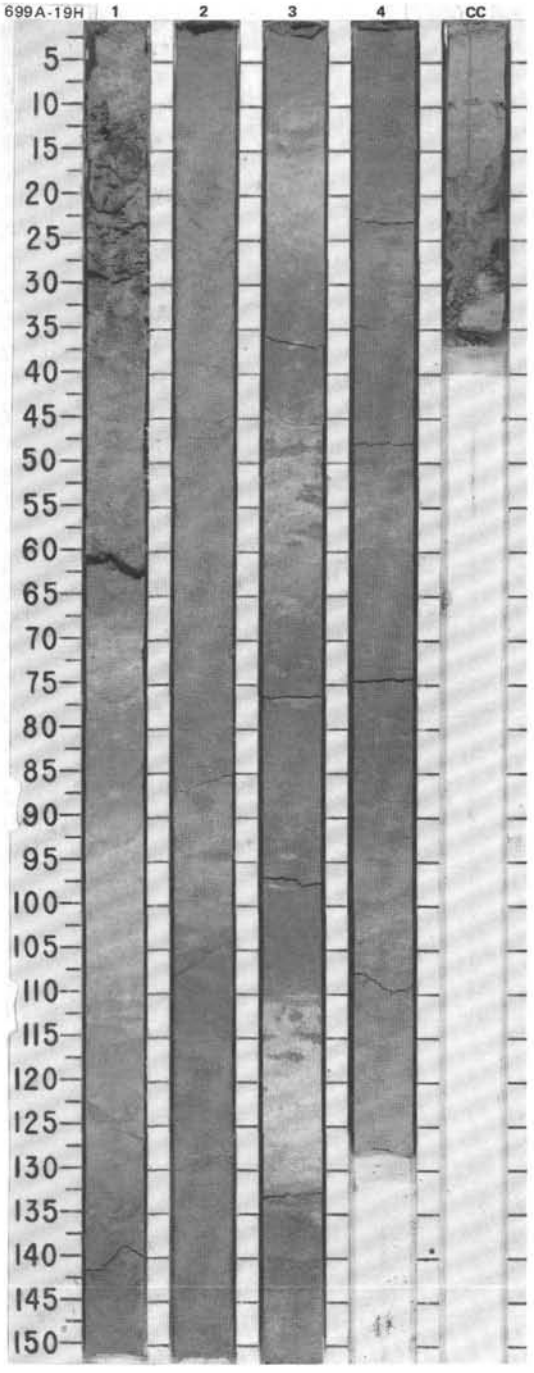

SITE 699 HOLE A CORE 20H CORED INTERVAL 3885.1-3894.6 mbsl; 179.6-189.1 mbsf

TIME-ROCK UNIT	BIOSTRAT. ZONE/ FOSSIL CHARACTER: FORAMINIFERS	NANNOFOSSILS	RADIOLARIANS	DIATOMS	SILICO-FLAGELLATES	PALEOMAGNETICS	PHYS. PROPERTIES	CHEMISTRY	SECTION	METERS	GRAPHIC LITHOLOGY	DRILLING DISTURB.	SED. STRUCTURES	SAMPLES	LITHOLOGIC DESCRIPTION
LOWER-UPPER OLIGOCENE	Barren	*C. altus* Zone	unzoned	*R. vigilans*	unzoned		ρ_g=2.79; ϕ=73.4; ρ_g=2.72; ϕ=76.7; ρ_g=2.56; ϕ=71.3; ρ_g=2.64; ϕ=66.5; ρ_g=2.73; ϕ=73.8		1, 2, 3, 4, 5, 6, CC	0.5, 1.0	VOID			*	SILICEOUS-BEARING NANNOFOSSIL OOZE to CLAYEY SILICEOUS-BEARING NANNOFOSSIL OOZE

Major lithology: Light gray (5Y 7/1) siliceous-bearing nannofossil ooze to gray (5Y 6/1) clayey siliceous-bearing nannofossil ooze. Ichnofacies; *Chondrites* in Section 3, 84–90 cm.

Minor lithology: White (5Y 8/1) to light gray (5Y 7/1) siliceous nannofossil ooze.

SMEAR SLIDE SUMMARY (%):

	3, 23 D	6, 10 D
COMPOSITION:		
Volcanic glass	10	10
Accessory minerals	—	Tr
Opaques	—	Tr
Nannofossils	45	42
Diatoms	45	48
Radiolarians	Tr	—
Sponge spicules	—	Tr
Silicoflagellates	Tr	—

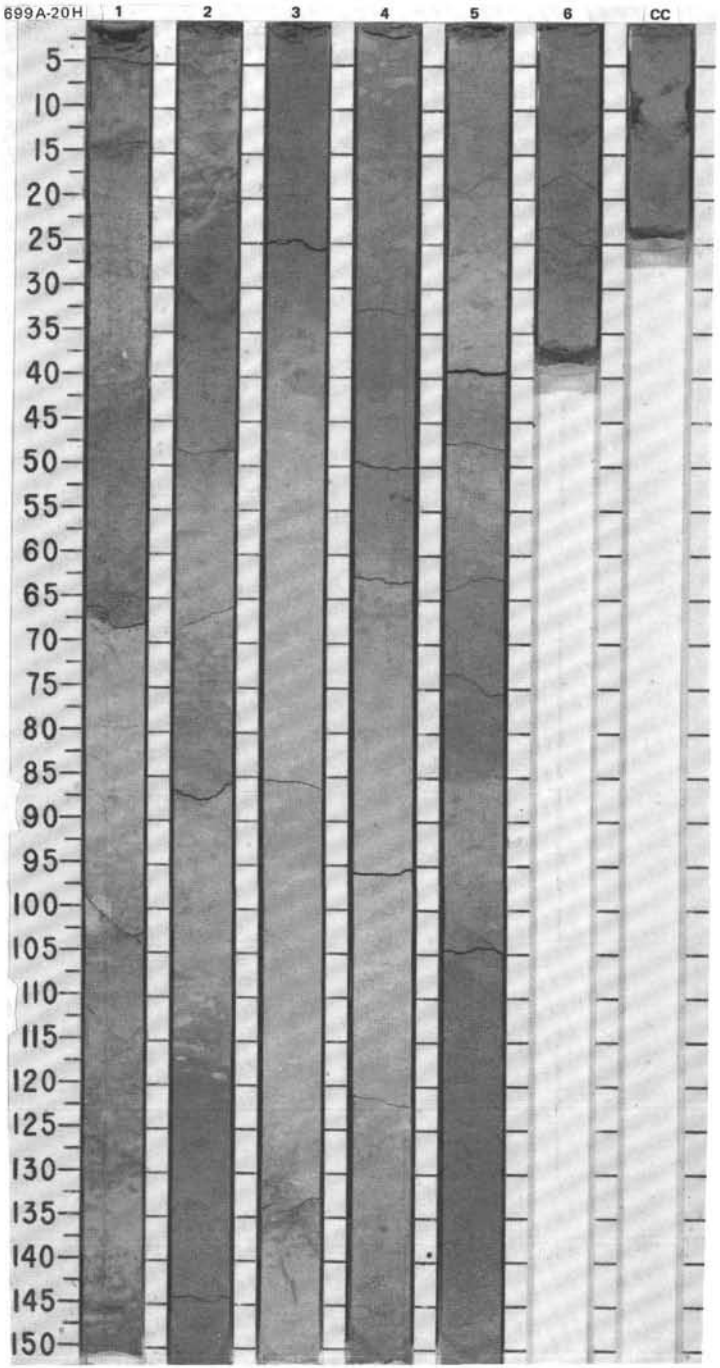

SITE 699 HOLE A CORE 21H CORED INTERVAL 3894.6-3904.1 mbsl; 189.1-198.6 mbsf

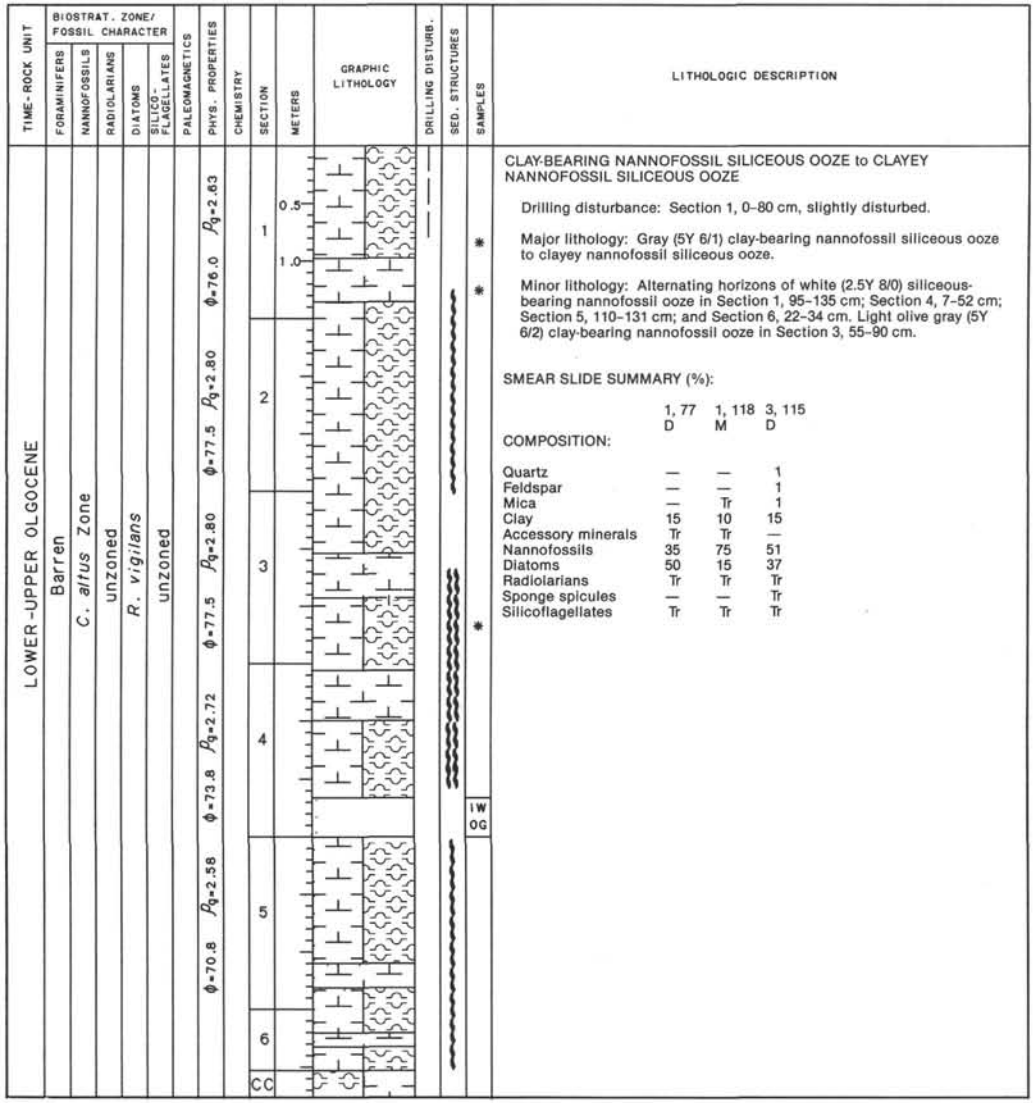

LITHOLOGIC DESCRIPTION

CLAY-BEARING NANNOFOSSIL SILICEOUS OOZE to CLAYEY NANNOFOSSIL SILICEOUS OOZE

Drilling disturbance: Section 1, 0–80 cm, slightly disturbed.

Major lithology: Gray (5Y 6/1) clay-bearing nannofossil siliceous ooze to clayey nannofossil siliceous ooze.

Minor lithology: Alternating horizons of white (2.5Y 8/0) siliceous-bearing nannofossil ooze in Section 1, 95–135 cm; Section 4, 7–52 cm; Section 5, 110–131 cm; and Section 6, 22–34 cm. Light olive gray (5Y 6/2) clay-bearing nannofossil ooze in Section 3, 55–90 cm.

SMEAR SLIDE SUMMARY (%):

	1, 77 D	1, 118 M	3, 115 D
COMPOSITION:			
Quartz	—	—	1
Feldspar	—	—	1
Mica	—	Tr	1
Clay	15	10	15
Accessory minerals	Tr	Tr	—
Nannofossils	35	75	51
Diatoms	50	15	37
Radiolarians	Tr	Tr	Tr
Sponge spicules	—	—	Tr
Silicoflagellates	Tr	Tr	Tr

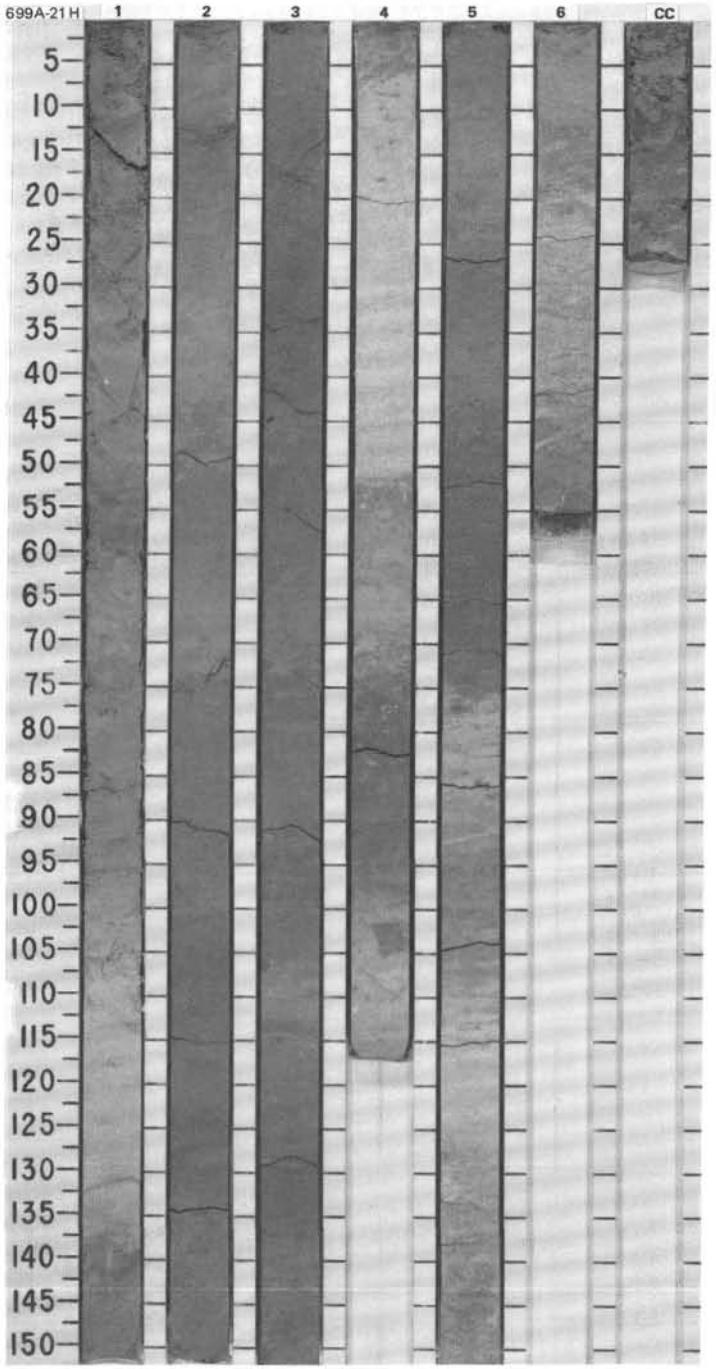

SITE 699 HOLE A CORE 22H CORED INTERVAL 3904.1-3910.6 mbsl; 198.6-205.1 mbsf

TIME-ROCK UNIT	BIOSTRAT. ZONE/ FOSSIL CHARACTER: FORAMINIFERS	NANNOFOSSILS	RADIOLARIANS	DIATOMS	SILICO-FLAGELLATES	PALEOMAGNETICS	PHYS. PROPERTIES	CHEMISTRY	SECTION	METERS	GRAPHIC LITHOLOGY	DRILLING DISTURB.	SED. STRUCTURES	SAMPLES
LOWER-UPPER OLIGOCENE	Barren	*C. altus* Zone	unzoned	*R. vigilans*	unzoned	ϕ=73.6	ρ_g=2.98 ϕ=65.8 ρ_g=2.72 ϕ=66.3 ρ_g=2.95 ϕ=71.1 ρ_g=2.90		1 2 3 4 5 CC	0.5 1.0				* *

LITHOLOGIC DESCRIPTION

CLAY-BEARING SILICEOUS-BEARING NANNOFOSSIL OOZE

Major lithology: Light gray (5Y 7/1) to light greenish gray (5GY 7/1) clay-bearing siliceous-bearing nannofossil ooze.

Minor lithology: Gray (5Y 6/1) clayey siliceous nannofossil ooze.

SMEAR SLIDE SUMMARY (%):

	2, 80 D	5, 7 D
COMPOSITION:		
Clay	25	5
Volcanic glass	—	Tr
Nannofossils	55	75
Diatoms	20	20
Radiolarians	Tr	—
Silicoflagellates	—	Tr

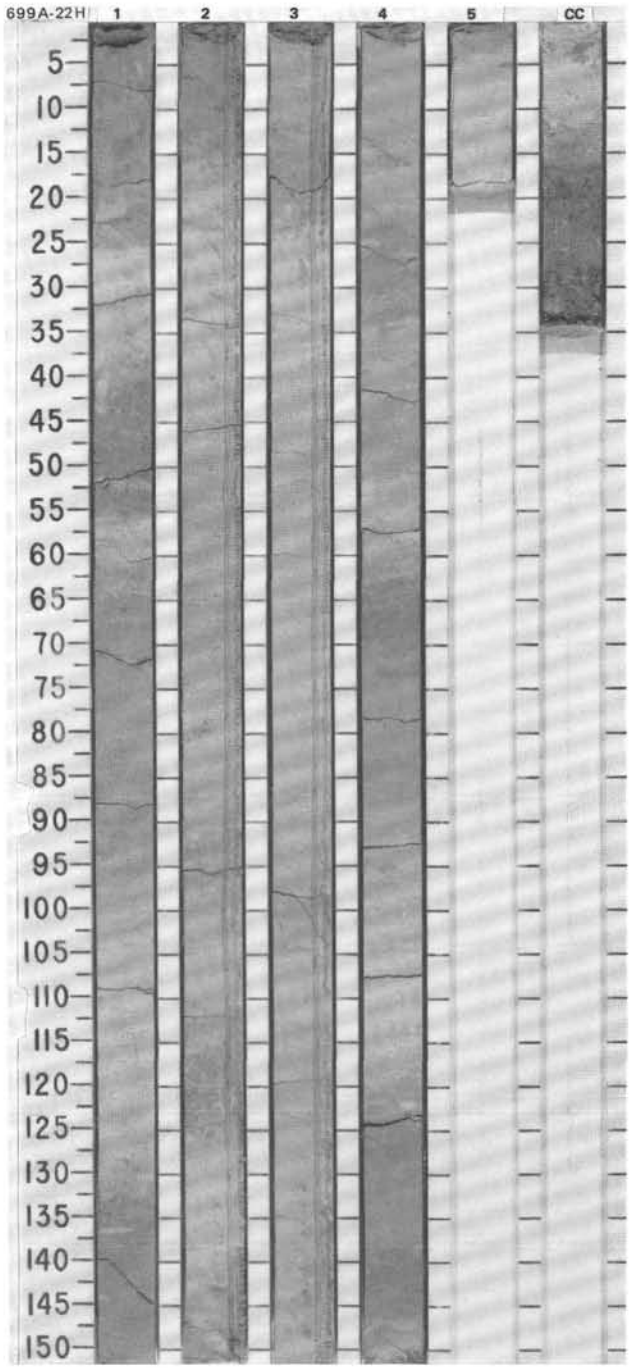

SITE 699 HOLE A CORE 23X CORED INTERVAL 3910.6-3920.1 mbsl; 205.1-214.6 mbsf

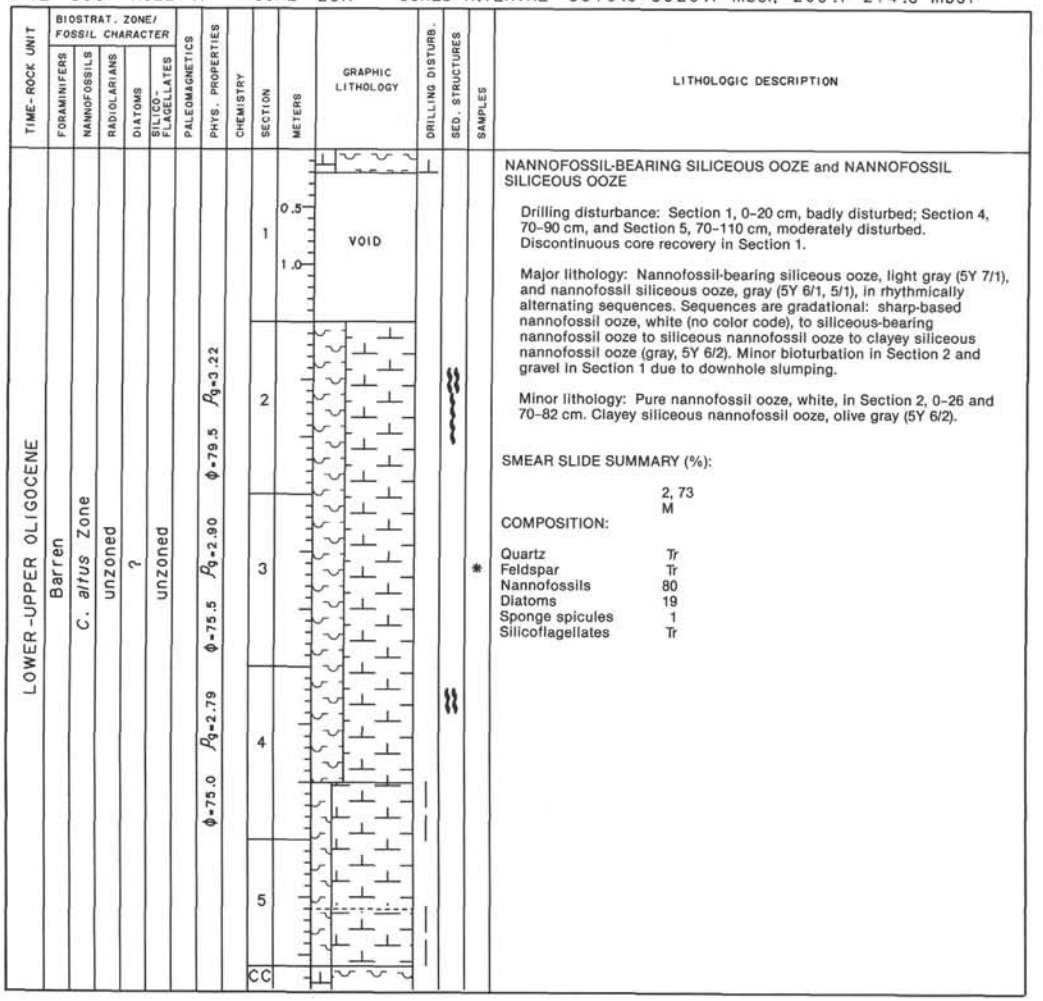

LITHOLOGIC DESCRIPTION

NANNOFOSSIL-BEARING SILICEOUS OOZE and NANNOFOSSIL SILICEOUS OOZE

Drilling disturbance: Section 1, 0-20 cm, badly disturbed; Section 4, 70-90 cm, and Section 5, 70-110 cm, moderately disturbed. Discontinuous core recovery in Section 1.

Major lithology: Nannofossil-bearing siliceous ooze, light gray (5Y 7/1), and nannofossil siliceous ooze, gray (5Y 6/1, 5/1), in rhythmically alternating sequences. Sequences are gradational: sharp-based nannofossil ooze, white (no color code), to siliceous-bearing nannofossil ooze to siliceous nannofossil ooze to clayey siliceous nannofossil ooze (gray, 5Y 6/2). Minor bioturbation in Section 2 and gravel in Section 1 due to downhole slumping.

Minor lithology: Pure nannofossil ooze, white, in Section 2, 0-26 and 70-82 cm. Clayey siliceous nannofossil ooze, olive gray (5Y 6/2).

SMEAR SLIDE SUMMARY (%):

	2, 73 M
COMPOSITION:	
Quartz	Tr
Feldspar	Tr
Nannofossils	80
Diatoms	19
Sponge spicules	1
Silicoflagellates	Tr

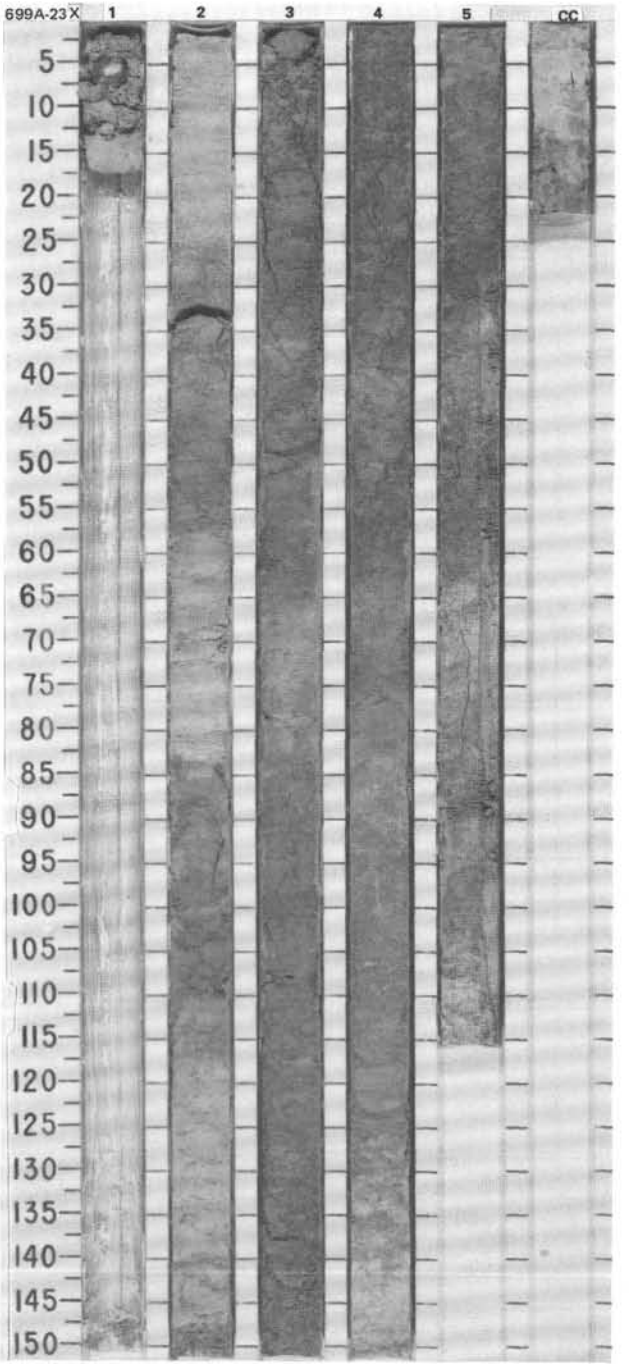

SITE 699 HOLE A CORE 24X CORED INTERVAL 3920.1-3929.6 mbsl; 214.6-224.1 mbsf

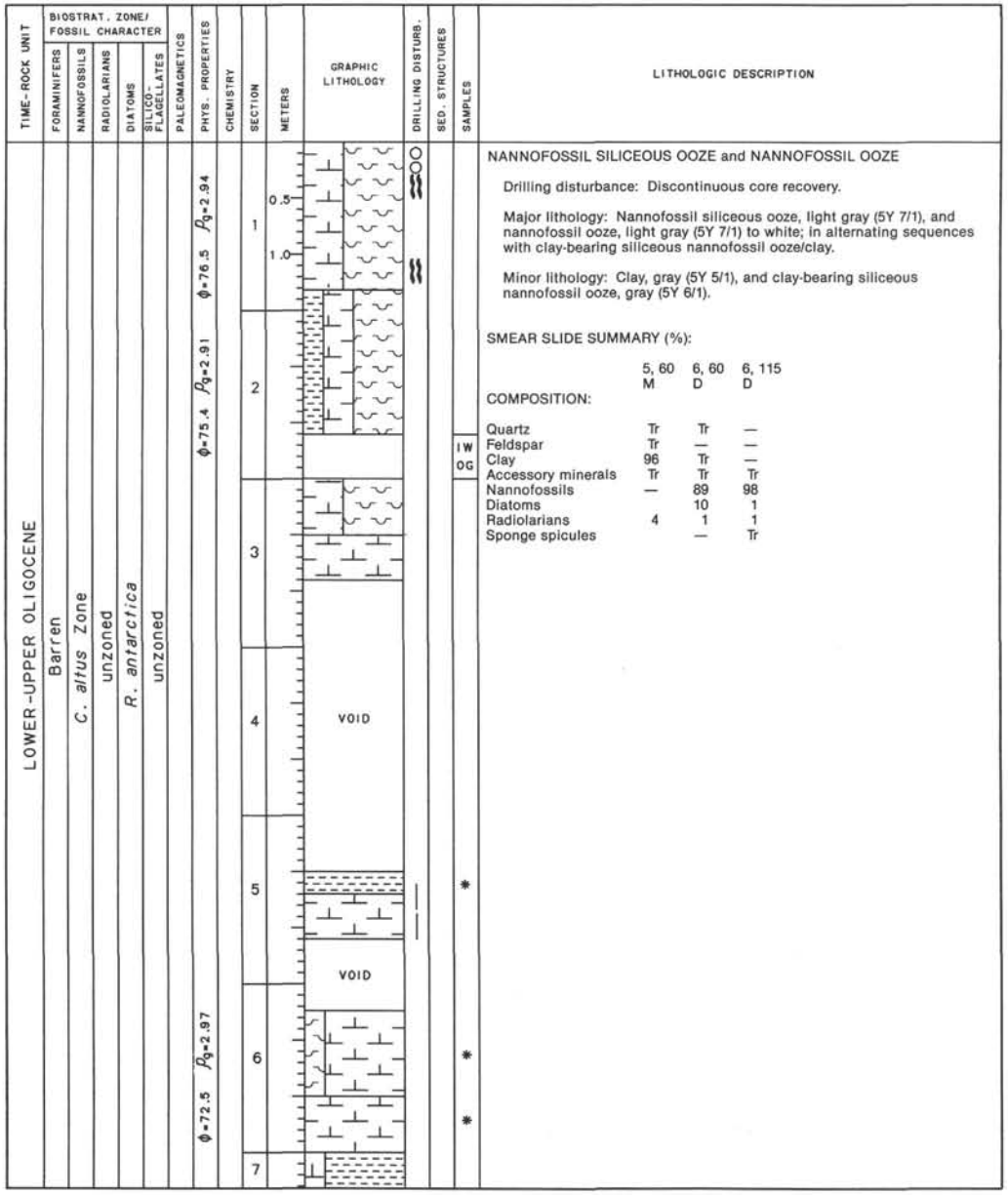

LITHOLOGIC DESCRIPTION

NANNOFOSSIL SILICEOUS OOZE and NANNOFOSSIL OOZE

Drilling disturbance: Discontinuous core recovery.

Major lithology: Nannofossil siliceous ooze, light gray (5Y 7/1), and nannofossil ooze, light gray (5Y 7/1) to white; in alternating sequences with clay-bearing siliceous nannofossil ooze/clay.

Minor lithology: Clay, gray (5Y 5/1), and clay-bearing siliceous nannofossil ooze, gray (5Y 6/1).

SMEAR SLIDE SUMMARY (%):

COMPOSITION:	5, 60 M	6, 60 D	6, 115 D
Quartz	Tr	Tr	—
Feldspar	Tr	—	—
Clay	96	Tr	—
Accessory minerals	Tr	Tr	Tr
Nannofossils	—	89	98
Diatoms		10	1
Radiolarians	4	1	1
Sponge spicules		—	Tr

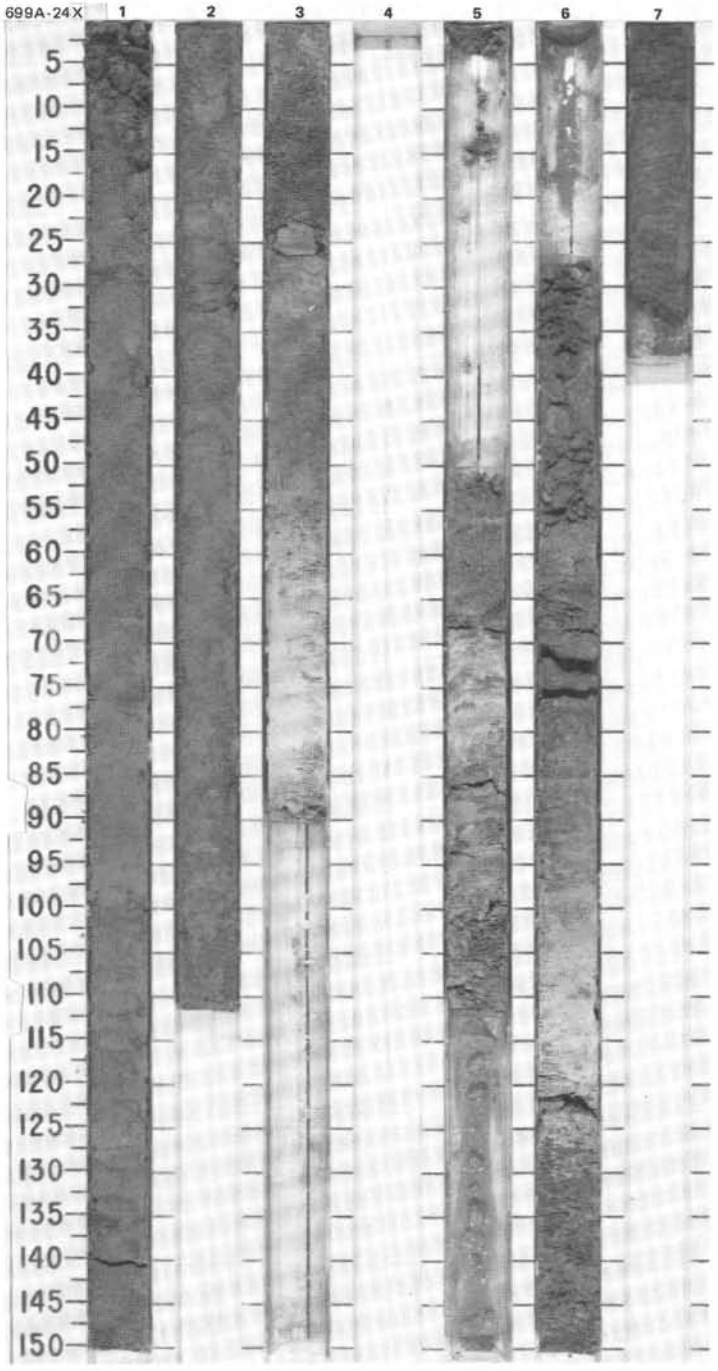

SITE 699 HOLE A CORE 25X CORED INTERVAL 3929.6-3939.1 mbsl; 224.1-233.6 mbsf

TIME-ROCK UNIT	BIOSTRAT. ZONE/ FOSSIL CHARACTER: FORAMINIFERS	NANNOFOSSILS	RADIOLARIANS	DIATOMS	SILICO-FLAGELLATES	PALEOMAGNETICS	PHYS. PROPERTIES	CHEMISTRY	SECTION	METERS	GRAPHIC LITHOLOGY	DRILLING DISTURB.	SED. STRUCTURES	SAMPLES	LITHOLOGIC DESCRIPTION
LOWER-UPPER OLIGOCENE	Barren	*C. altus* Zone	unzoned	*R. antarctica*	unzoned				1, 2, CC	0.5, 1.0					

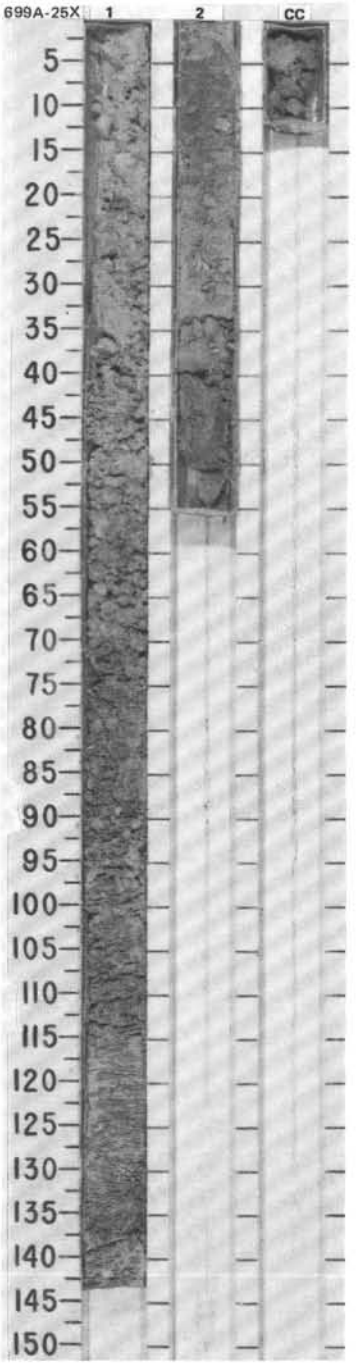

NANNOFOSSIL OOZE

Drilling disturbance: Sections 1 and 2, badly to moderately disturbed.

Major lithology: Nannofossil ooze, light gray (5Y N7/1).

SMEAR SLIDE SUMMARY (%):

	1, 20 D
COMPOSITION:	
Clay	Tr
Accessory minerals	Tr
Nannofossils	98
Diatoms	1
Radiolarians	1

SITE 699 HOLE A CORE 26X CORED INTERVAL 3939.1-3948.6 mbsl; 233.6-243.1 mbsf

TIME-ROCK UNIT	BIOSTRAT. ZONE/ FOSSIL CHARACTER: FORAMINIFERS	NANNOFOSSILS	RADIOLARIANS	DIATOMS	SILICO-FLAGELLATES	PALEOMAGNETICS	PHYS. PROPERTIES	CHEMISTRY	SECTION	METERS	GRAPHIC LITHOLOGY	DRILLING DISTURB.	SED. STRUCTURES	SAMPLES	LITHOLOGIC DESCRIPTION
									1	0.5 1.0					GRAVEL and PEBBLES Major lithology: Graded gravel bed with large pebbles (>5 cm) in Section 3, grading upward to 1-cm-diameter gravel toward the top of the section. Pebbles and gravel are subangular, subrounded, or rounded and consist of manganese nodules, quartz (smoky, rose, and milky white), schists and other metamorphic fragments, basalt, andesite, quartz arenite, granite, oligmict and polymict conglomerates, quartz diorite, and clasts of indurated sediment.
									2		VOID				
									CC						

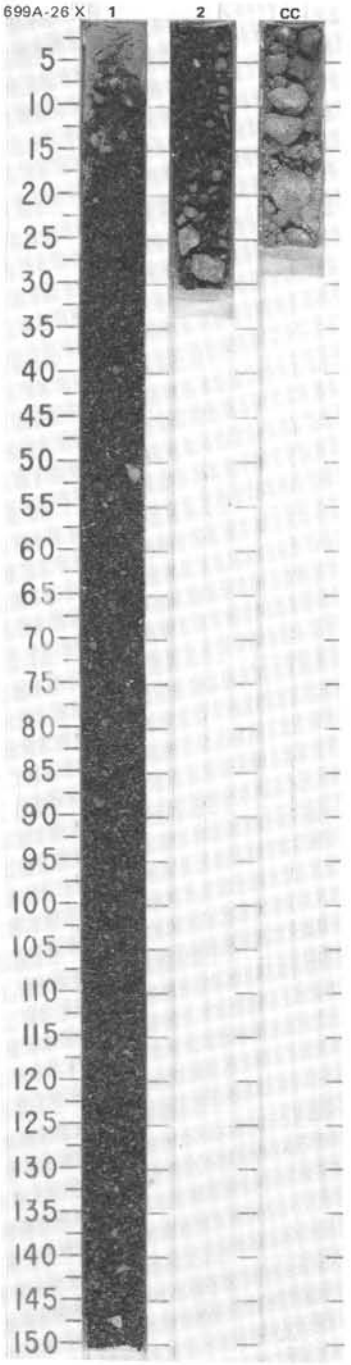

SITE 699 HOLE A CORE 27X CORED INTERVAL 3948.6-3958.1 mbsl; 243.1-252.6 mbsf

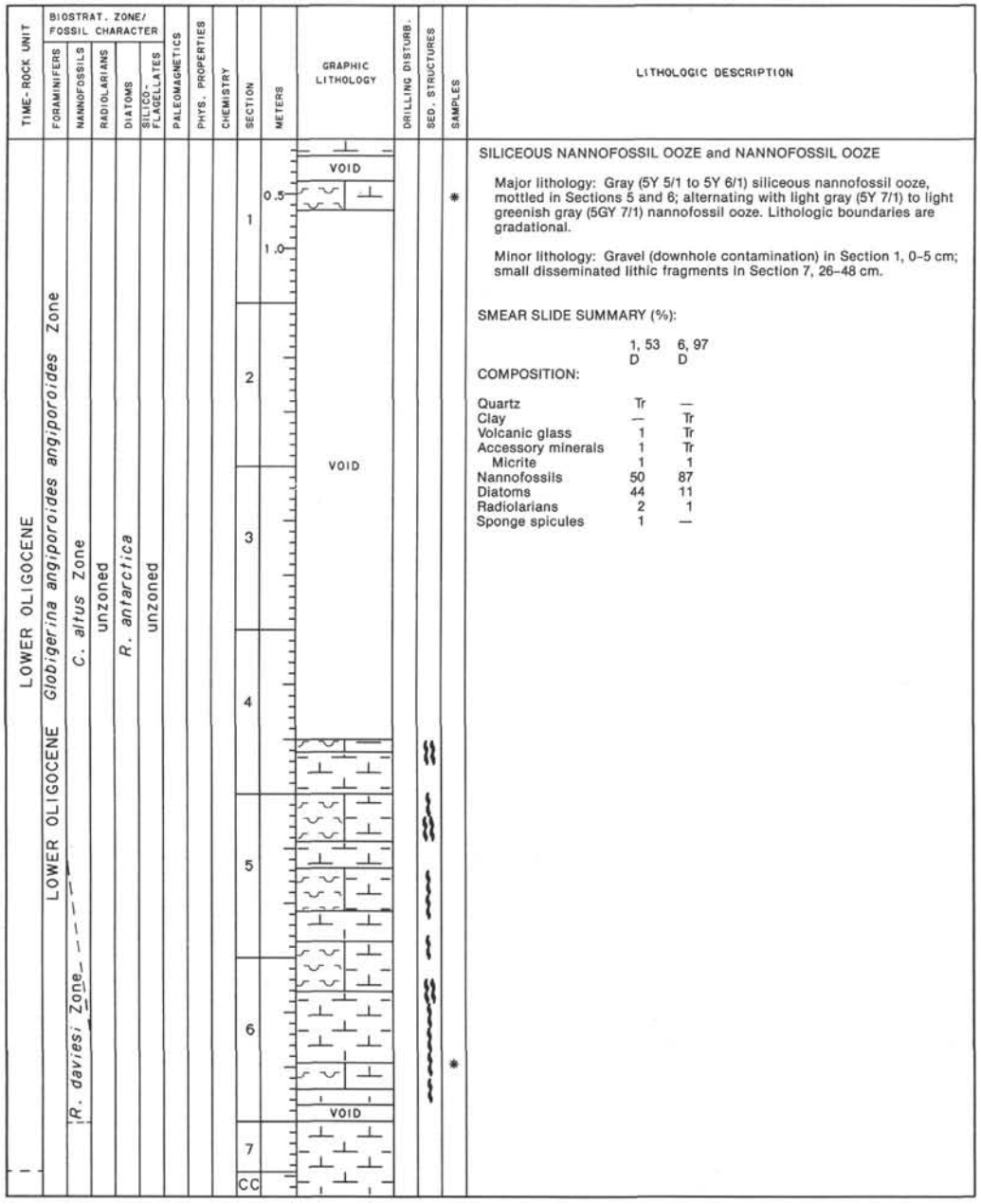

LITHOLOGIC DESCRIPTION

SILICEOUS NANNOFOSSIL OOZE and NANNOFOSSIL OOZE

Major lithology: Gray (5Y 5/1 to 5Y 6/1) siliceous nannofossil ooze, mottled in Sections 5 and 6; alternating with light gray (5Y 7/1) to light greenish gray (5GY 7/1) nannofossil ooze. Lithologic boundaries are gradational.

Minor lithology: Gravel (downhole contamination) in Section 1, 0-5 cm; small disseminated lithic fragments in Section 7, 26-48 cm.

SMEAR SLIDE SUMMARY (%):

	1, 53 D	6, 97 D
COMPOSITION:		
Quartz	Tr	—
Clay	—	Tr
Volcanic glass	1	Tr
Accessory minerals	1	Tr
Micrite	1	1
Nannofossils	50	87
Diatoms	44	11
Radiolarians	2	1
Sponge spicules	1	—

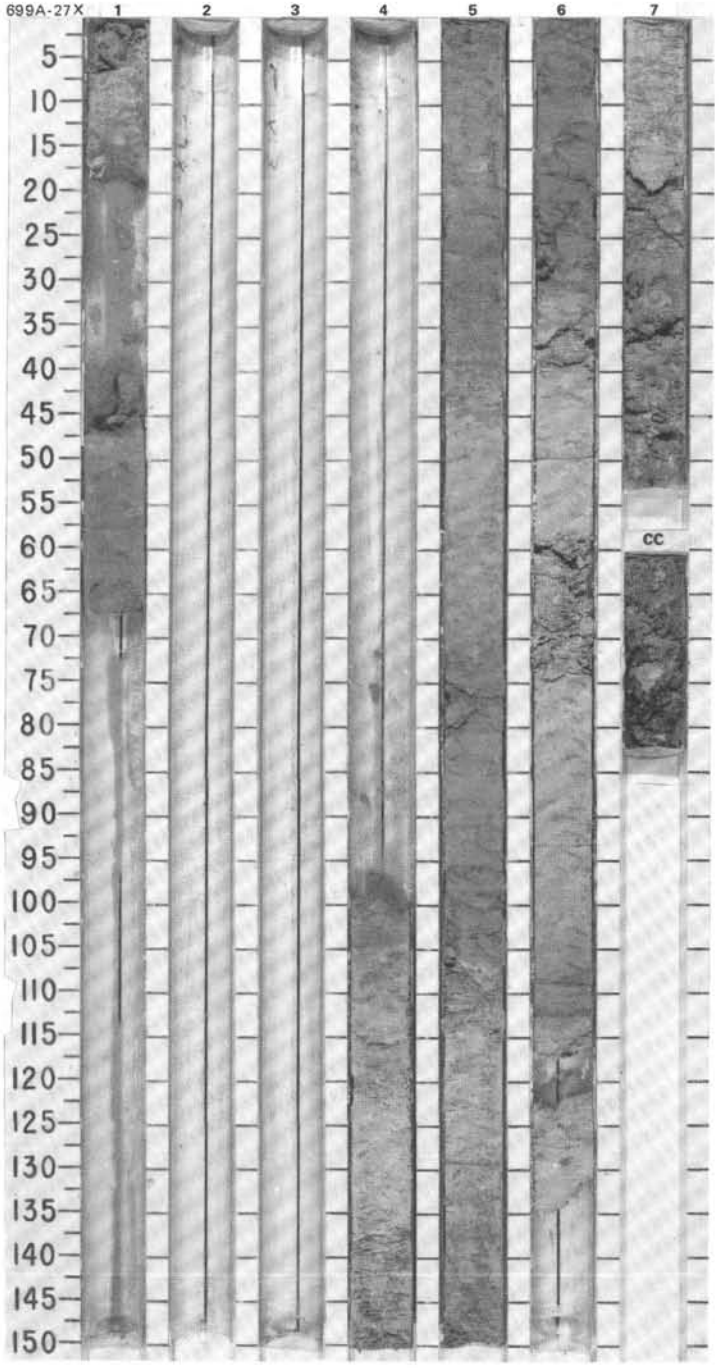

SITE 699 HOLE A CORE 28X CORED INTERVAL 3958.1-3964.6 mbsl; 252.6-259.1 mbsf

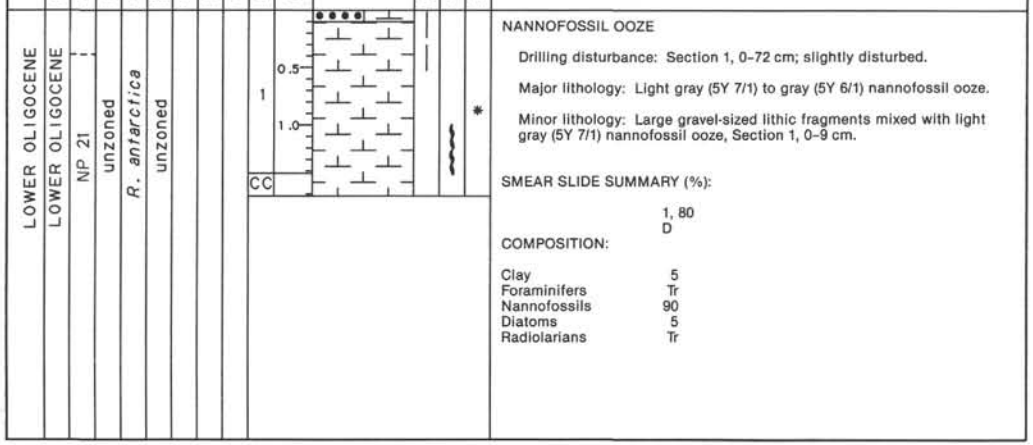

NANNOFOSSIL OOZE

Drilling disturbance: Section 1, 0-72 cm; slightly disturbed.

Major lithology: Light gray (5Y 7/1) to gray (5Y 6/1) nannofossil ooze.

Minor lithology: Large gravel-sized lithic fragments mixed with light gray (5Y 7/1) nannofossil ooze, Section 1, 0-9 cm.

SMEAR SLIDE SUMMARY (%):

	1, 80 D
COMPOSITION:	
Clay	5
Foraminifers	Tr
Nannofossils	90
Diatoms	5
Radiolarians	Tr

SITE 699 HOLE A CORE 29X CORED INTERVAL 3964.6-3974.1 mbsl; 259.1-268.6 mbsf

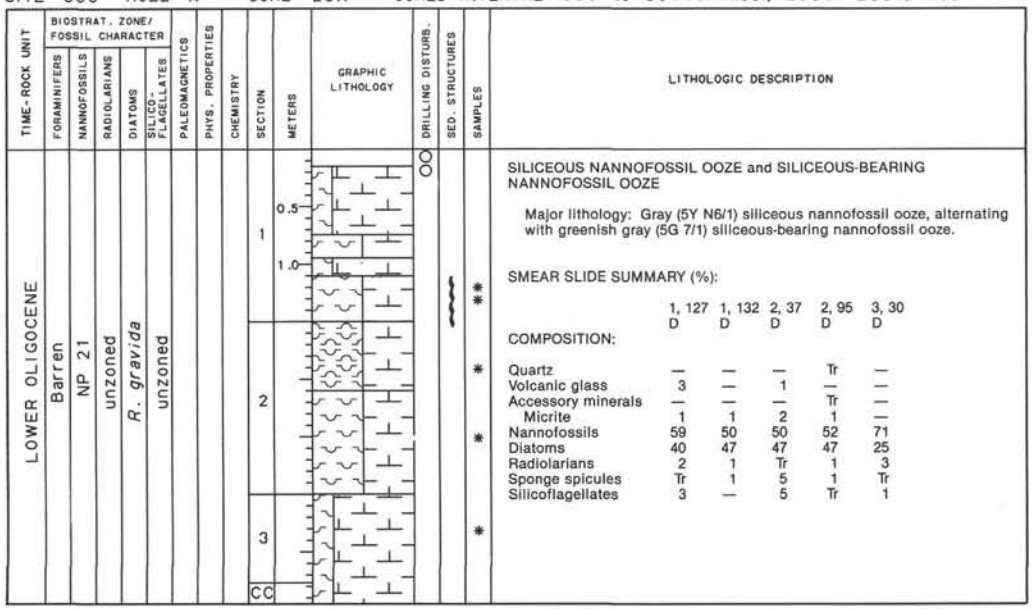

SILICEOUS NANNOFOSSIL OOZE and SILICEOUS-BEARING NANNOFOSSIL OOZE

Major lithology: Gray (5Y N6/1) siliceous nannofossil ooze, alternating with greenish gray (5G 7/1) siliceous-bearing nannofossil ooze.

SMEAR SLIDE SUMMARY (%):

	1, 127 D	1, 132 D	2, 37 D	2, 95 D	3, 30 D
COMPOSITION:					
Quartz	—	—	—	Tr	—
Volcanic glass	3	—	1	—	—
Accessory minerals	—	—	—	Tr	—
Micrite	1	1	2	1	—
Nannofossils	59	50	50	52	71
Diatoms	40	47	47	47	25
Radiolarians	2	1	Tr	1	3
Sponge spicules	Tr	1	5	1	Tr
Silicoflagellates	3	—	5	Tr	1

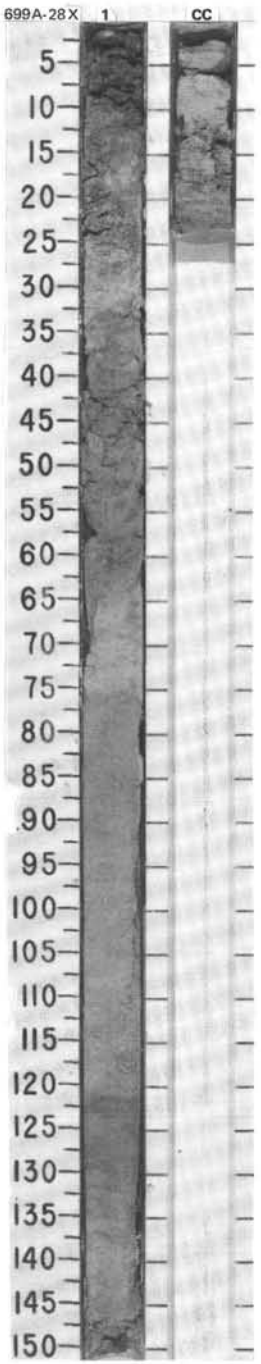

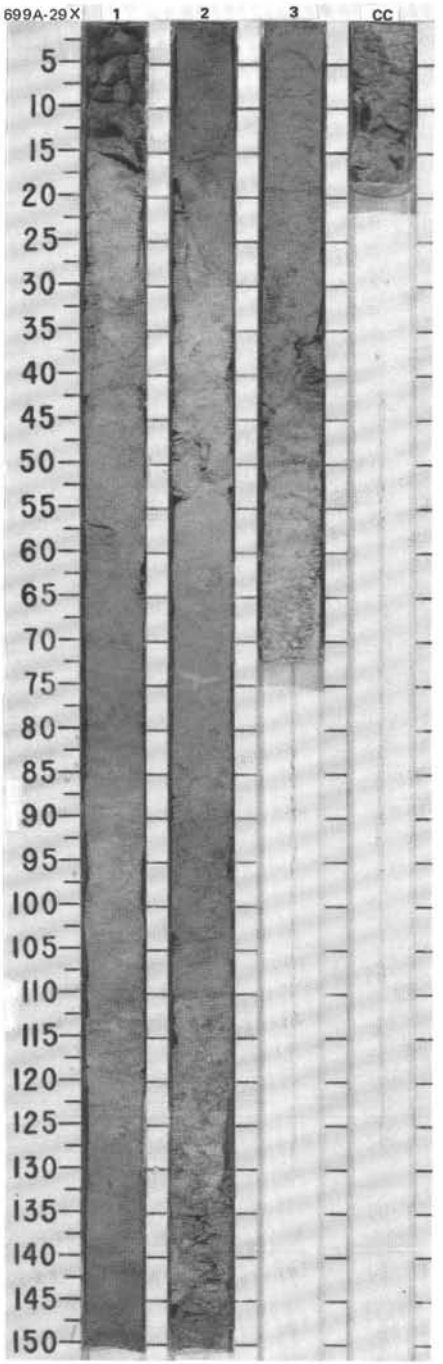

SITE 699 HOLE A CORE 30X CORED INTERVAL 3974.1-3983.6 mbsl; 268.6-278.1 mbsf

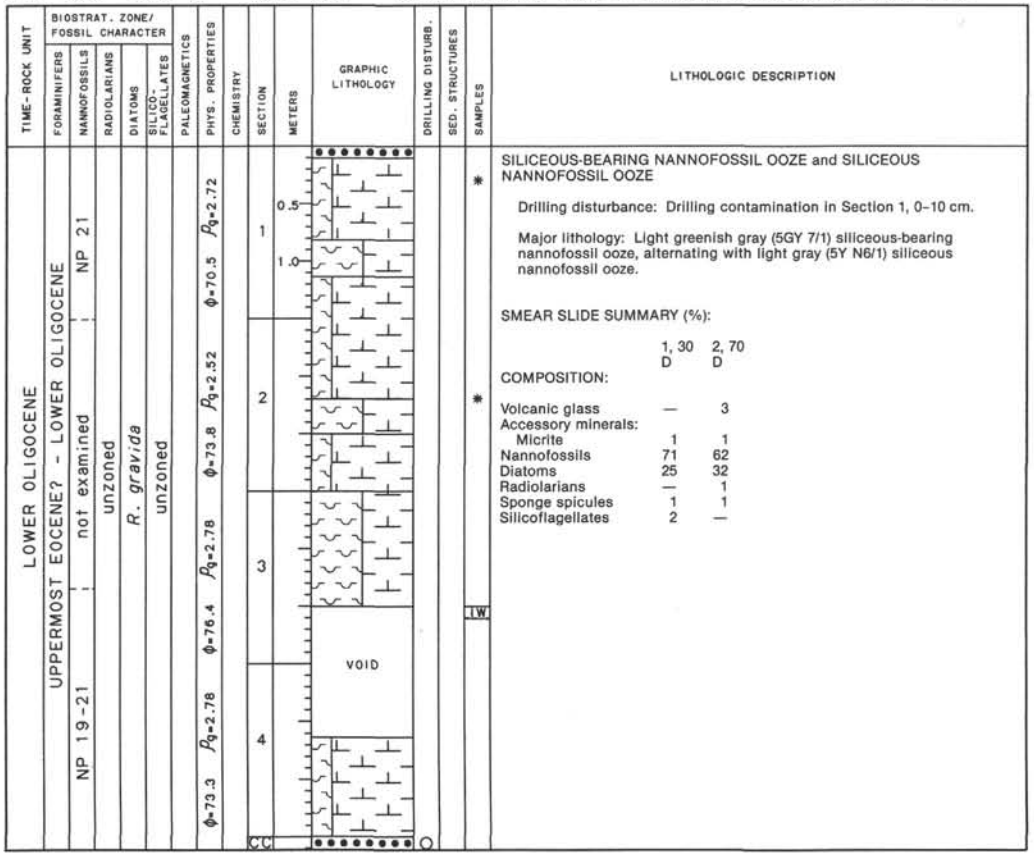

SILICEOUS-BEARING NANNOFOSSIL OOZE and SILICEOUS NANNOFOSSIL OOZE

Drilling disturbance: Drilling contamination in Section 1, 0-10 cm.

Major lithology: Light greenish gray (5GY 7/1) siliceous-bearing nannofossil ooze, alternating with light gray (5Y N6/1) siliceous nannofossil ooze.

SMEAR SLIDE SUMMARY (%):

	1, 30 D	2, 70 D
COMPOSITION:		
Volcanic glass	—	3
Accessory minerals:		
Micrite	1	1
Nannofossils	71	62
Diatoms	25	32
Radiolarians	—	1
Sponge spicules	1	1
Silicoflagellates	2	—

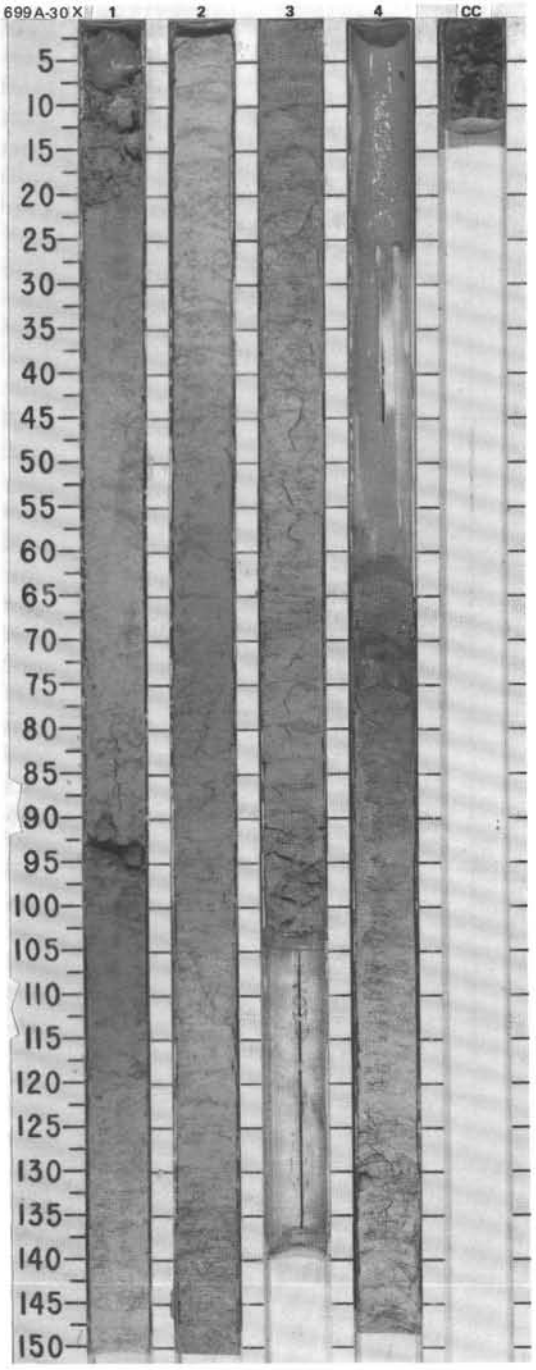

SITE 699 HOLE A CORE 31X CORED INTERVAL 3983.6-3993.1 mbsl; 278.1-287.6 mbsf

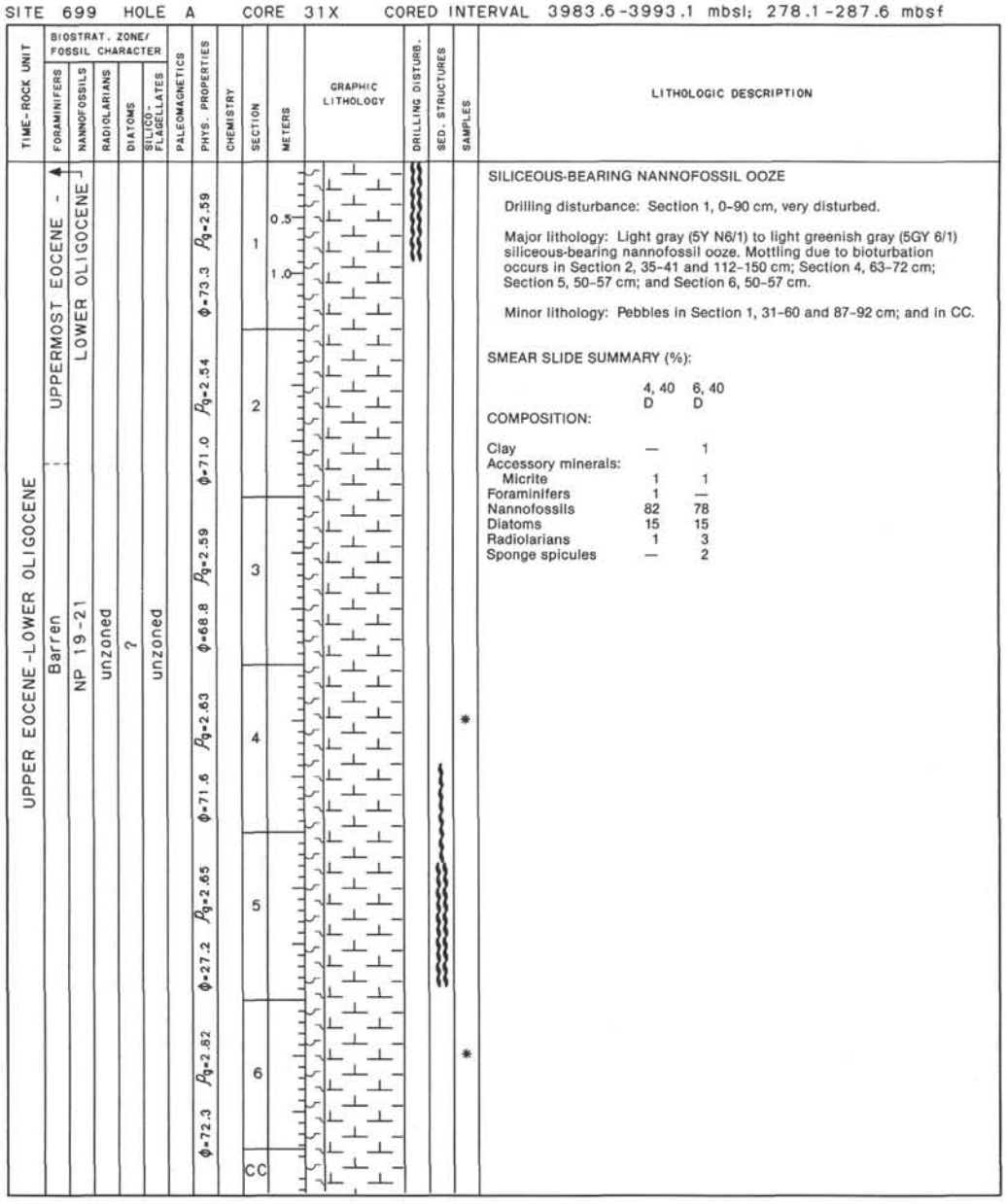

LITHOLOGIC DESCRIPTION

SILICEOUS-BEARING NANNOFOSSIL OOZE

Drilling disturbance: Section 1, 0-90 cm, very disturbed.

Major lithology: Light gray (5Y N6/1) to light greenish gray (5GY 6/1) siliceous-bearing nannofossil ooze. Mottling due to bioturbation occurs in Section 2, 35-41 and 112-150 cm; Section 4, 63-72 cm; Section 5, 50-57 cm; and Section 6, 50-57 cm.

Minor lithology: Pebbles in Section 1, 31-60 and 87-92 cm; and in CC.

SMEAR SLIDE SUMMARY (%):

	4, 40 D	6, 40 D
COMPOSITION:		
Clay	—	1
Accessory minerals:		
Micrite	1	1
Foraminifers	1	—
Nannofossils	82	78
Diatoms	15	15
Radiolarians	1	3
Sponge spicules	—	2

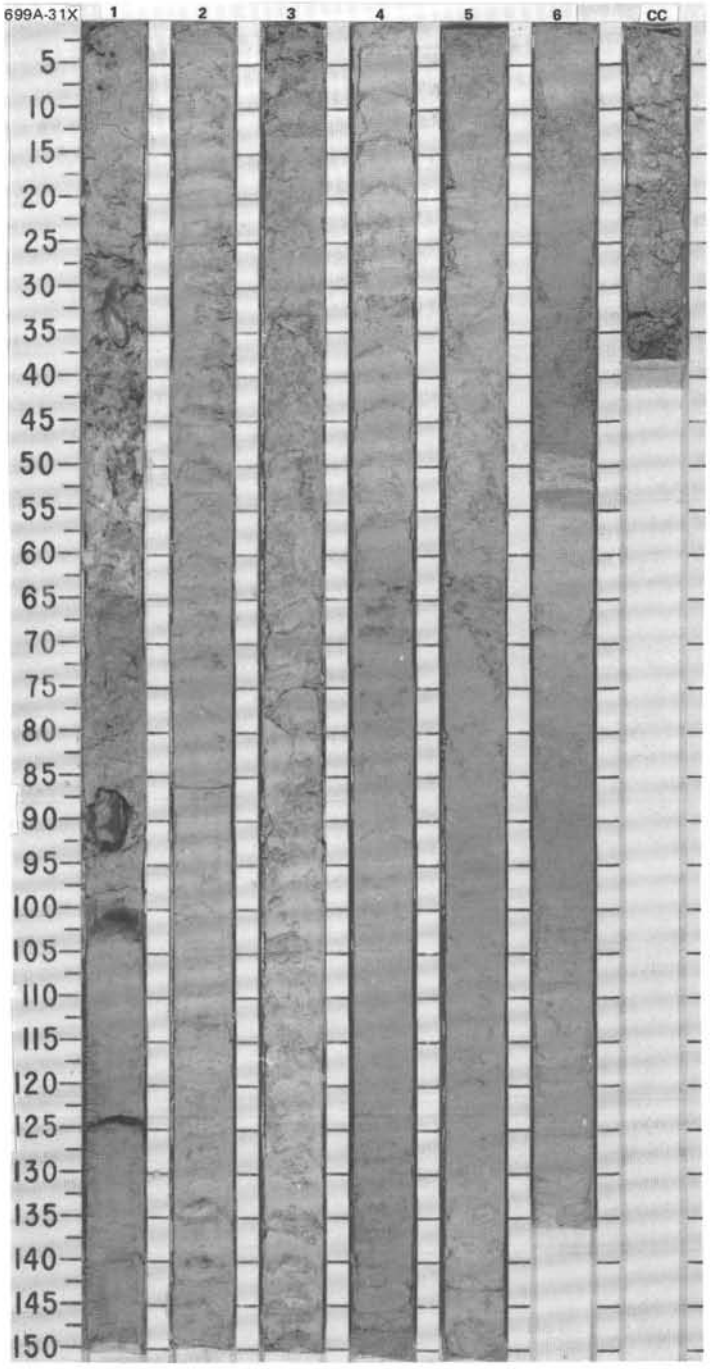

SITE 699 HOLE A CORE 32X CORED INTERVAL 3993.1-4002.6 mbsl; 287.6-297.1 mbsf

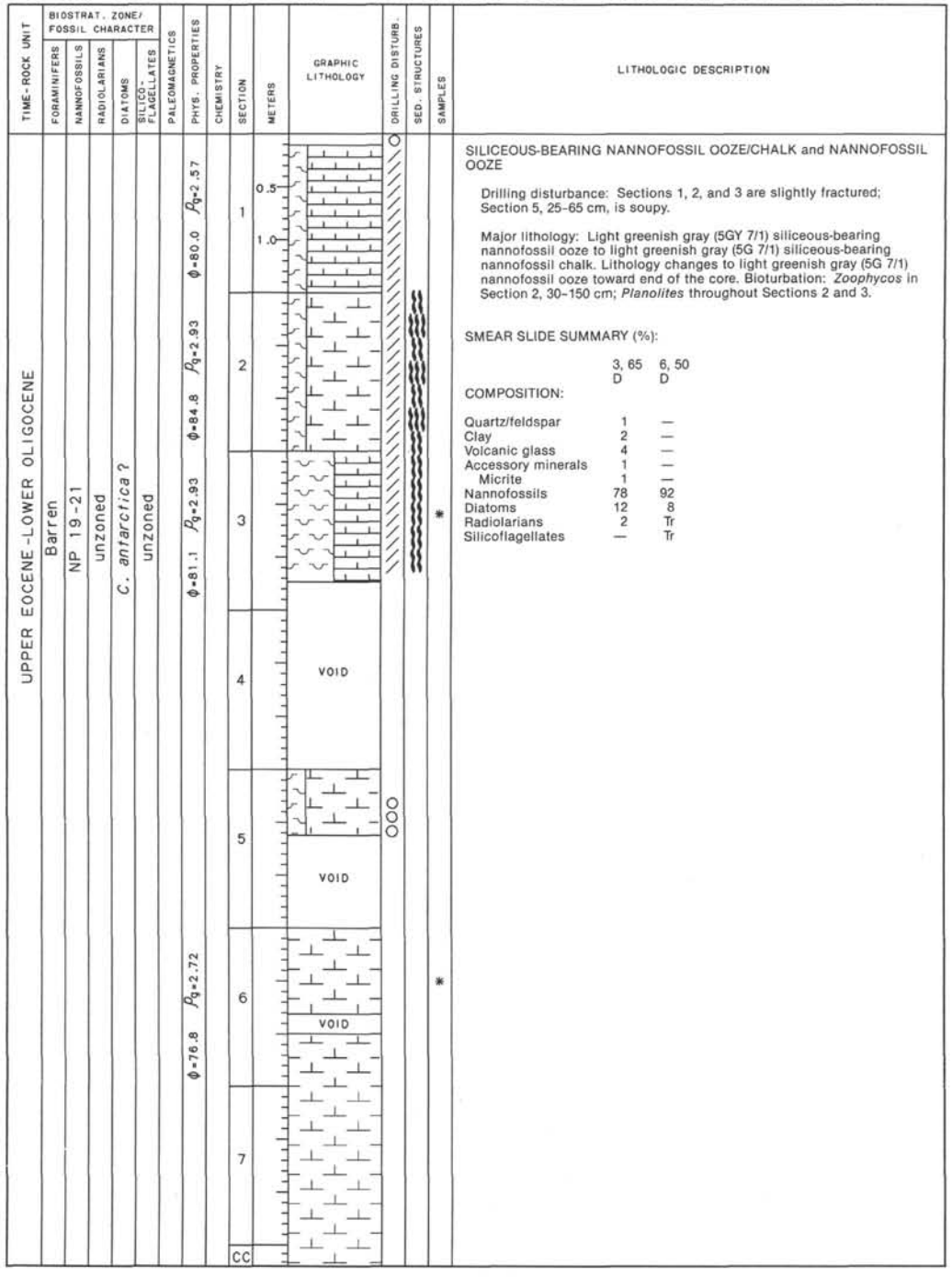

LITHOLOGIC DESCRIPTION

SILICEOUS-BEARING NANNOFOSSIL OOZE/CHALK and NANNOFOSSIL OOZE

Drilling disturbance: Sections 1, 2, and 3 are slightly fractured; Section 5, 25-65 cm, is soupy.

Major lithology: Light greenish gray (5GY 7/1) siliceous-bearing nannofossil ooze to light greenish gray (5G 7/1) siliceous-bearing nannofossil chalk. Lithology changes to light greenish gray (5G 7/1) nannofossil ooze toward end of the core. Bioturbation: *Zoophycos* in Section 2, 30-150 cm; *Planolites* throughout Sections 2 and 3.

SMEAR SLIDE SUMMARY (%):

	3, 65 D	6, 50 D
COMPOSITION:		
Quartz/feldspar	1	—
Clay	2	—
Volcanic glass	4	—
Accessory minerals	1	—
Micrite	1	—
Nannofossils	78	92
Diatoms	12	8
Radiolarians	2	Tr
Silicoflagellates	—	Tr

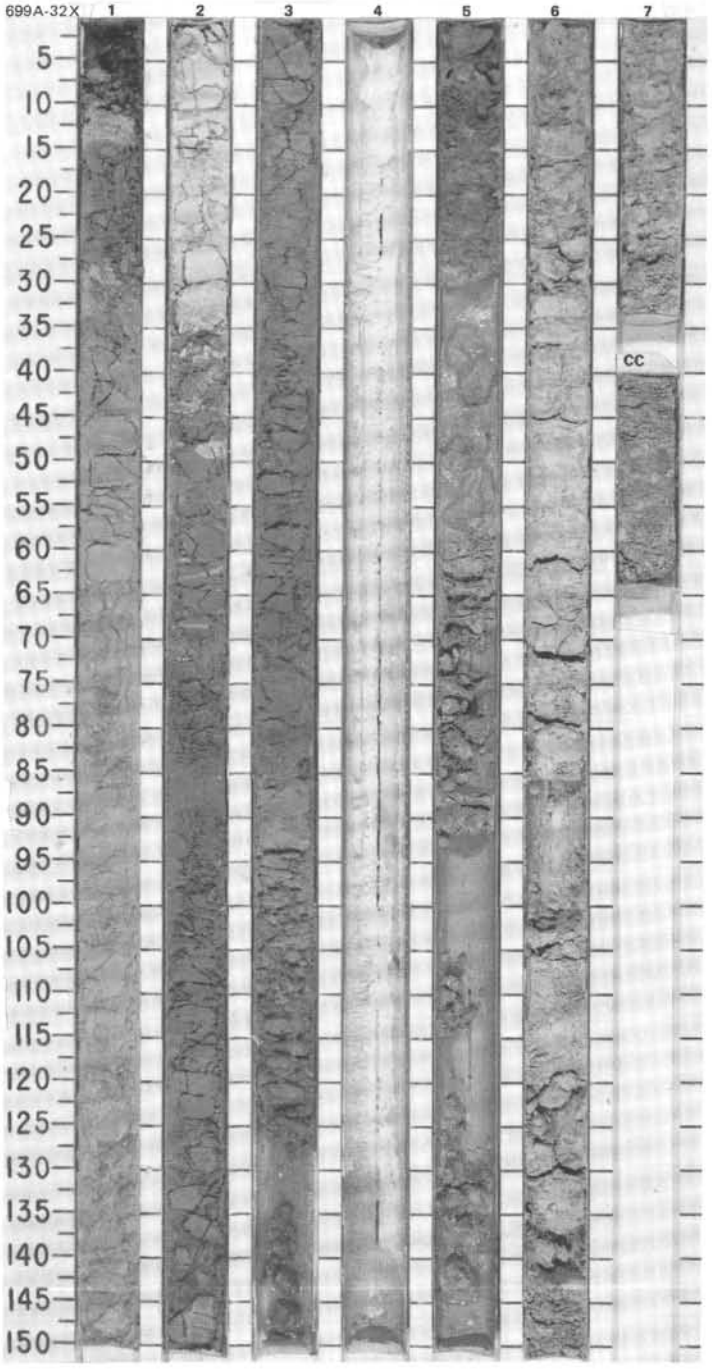

SITE 699 HOLE A CORE 33X CORED INTERVAL 4002.6-4012.1 mbsl; 297.1-306.6 mbsf

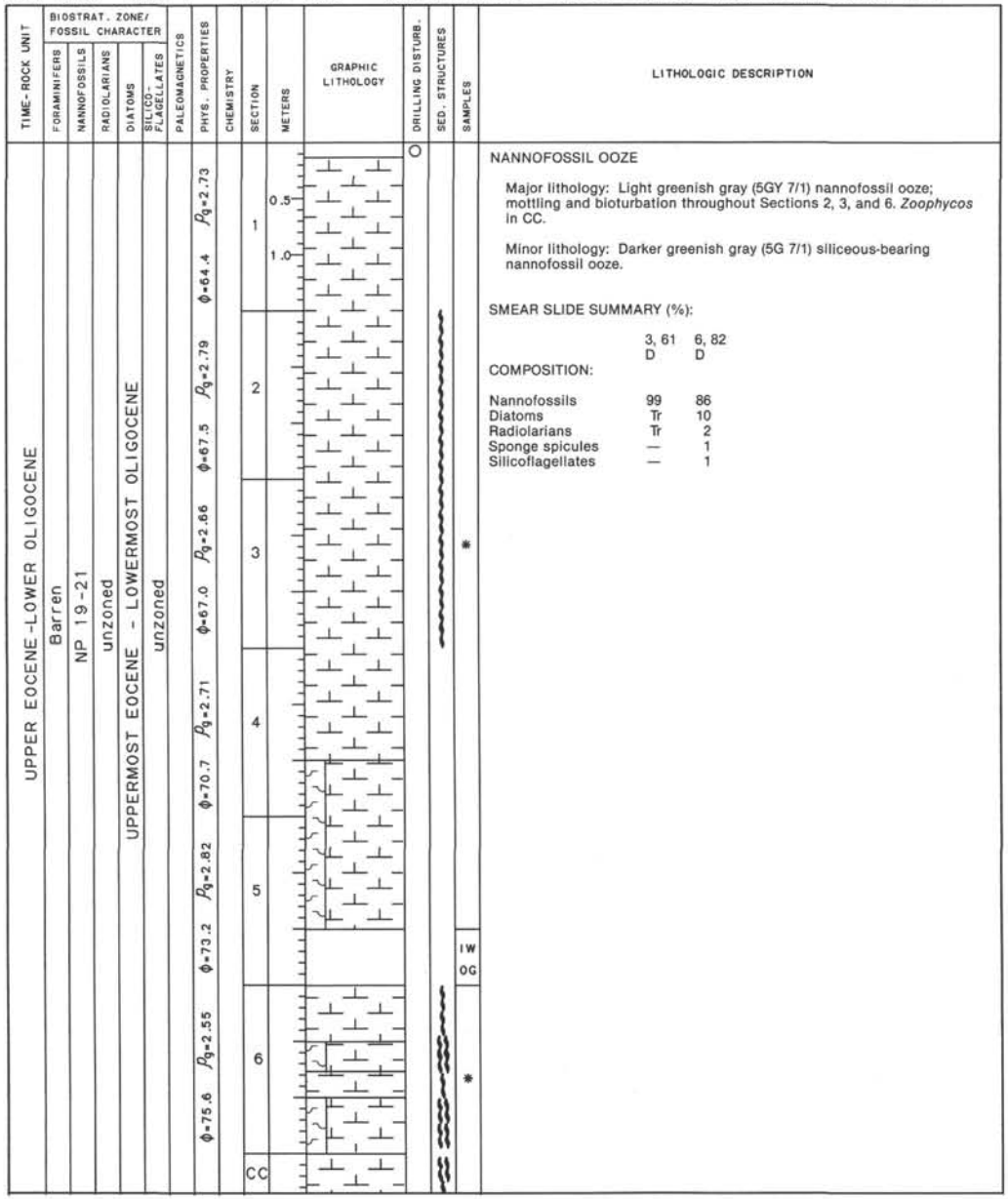

LITHOLOGIC DESCRIPTION

NANNOFOSSIL OOZE

Major lithology: Light greenish gray (5GY 7/1) nannofossil ooze; mottling and bioturbation throughout Sections 2, 3, and 6. *Zoophycos* in CC.

Minor lithology: Darker greenish gray (5G 7/1) siliceous-bearing nannofossil ooze.

SMEAR SLIDE SUMMARY (%):

	3, 61	6, 82
	D	D
COMPOSITION:		
Nannofossils	99	86
Diatoms	Tr	10
Radiolarians	Tr	2
Sponge spicules	—	1
Silicoflagellates	—	1

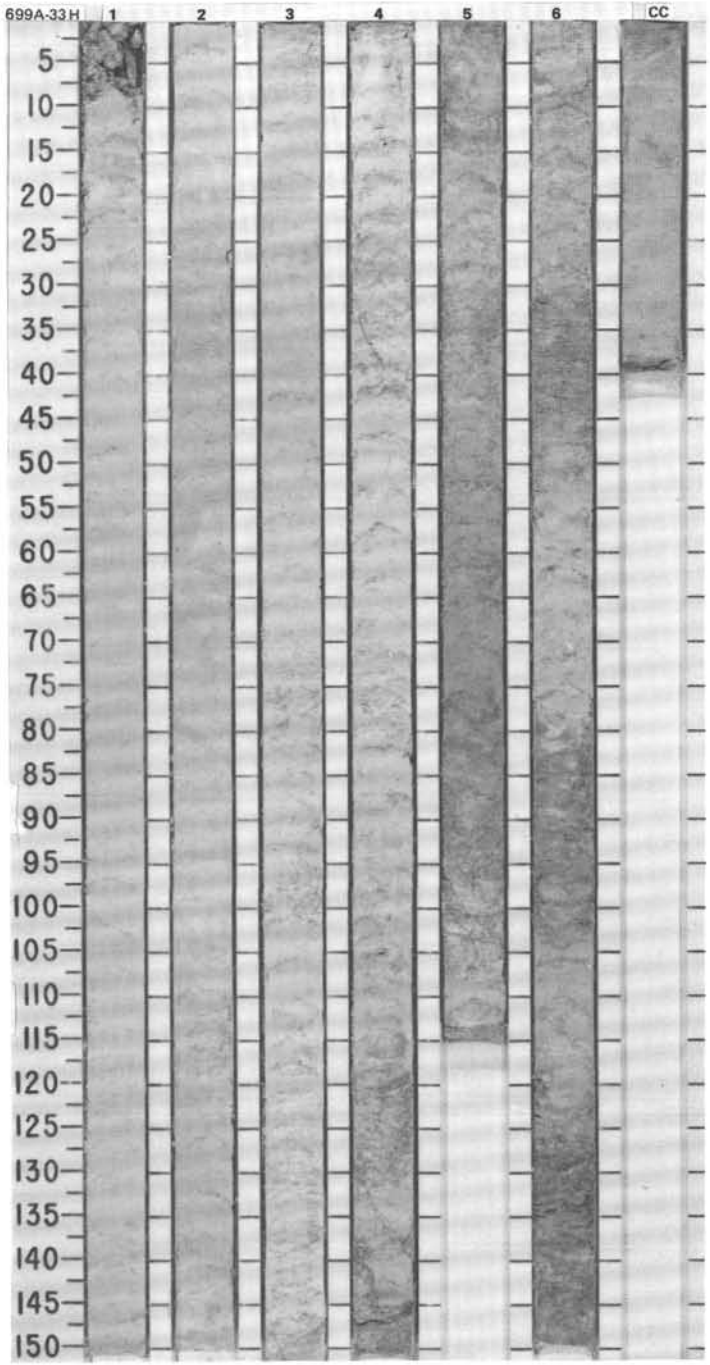

SITE 699 HOLE A CORE 34X CORED INTERVAL 4012.1-4021.6 mbsl; 306.6-316.1 mbsf

TIME-ROCK UNIT	BIOSTRAT. ZONE/ FOSSIL CHARACTER: FORAMINIFERS	NANNOFOSSILS	RADIOLARIANS	DIATOMS	SILICO-FLAGELLATES	PALEOMAGNETICS	PHYS. PROPERTIES	CHEMISTRY	SECTION	METERS	GRAPHIC LITHOLOGY	DRILLING DISTURB.	SED. STRUCTURES	SAMPLES	LITHOLOGIC DESCRIPTION
UPPER EOCENE-LOWER OLIGOCENE	Barren	NP 19-21	unzoned	UPPER EOCENE?	unzoned				CC						SILICEOUS NANNOFOSSIL OOZE Major lithology: Greenish gray (5G 6/1) gritty siliceous nannofossil ooze. Minor lithology: Gravel layer (downhole contamination) consisting of schist, mudstone, and fine-grained basalt pebbles.

SITE 699 HOLE A CORE 35X CORED INTERVAL 4021.6-4031.1 mbsl; 316.1-325.6 mbsf

TIME-ROCK UNIT	BIOSTRAT. ZONE/ FOSSIL CHARACTER: FORAMINIFERS	NANNOFOSSILS	RADIOLARIANS	DIATOMS	SILICO-FLAGELLATES	PALEOMAGNETICS	PHYS. PROPERTIES	CHEMISTRY	SECTION	METERS	GRAPHIC LITHOLOGY	DRILLING DISTURB.	SED. STRUCTURES	SAMPLES
UPPER EOCENE-LOWER OLIGOCENE	Barren	NP 19-21	Barren	Barren	Barren		ρ_g=2.83 ϕ=76.4 ρ_g=2.76 ϕ=72.8 ρ_g=2.58 ϕ=68.0 ρ_g=2.73 ϕ=73.8 ρ_g=2.76 ϕ=69.2 ρ_g=2.74 ϕ=71.4		1 2 3 4 5 6 7	0.5 1.0			* *

LITHOLOGIC DESCRIPTION

NANNOFOSSIL OOZE and SILICEOUS-BEARING NANNOFOSSIL OOZE

Major lithology: Light greenish gray (5GY 7/1) nannofossil ooze. Manganese staining in this lithology throughout the core. Regular alternation with greenish gray (5GY 6/1) siliceous-bearing nannofossil ooze toward the end of the core (gradational contacts). Bioturbation: *Chondrites* in Section 2, 101-130 cm; *Thalassinoides* in Section 3, 64-84 cm; *Planolites* in Section 4, 101-118 cm and Section 5, 39-55 cm; *Zoophycos* in Section 3, 126 cm, Section 5, 17 and 27-34 cm, and Section 6, 9, 21, and 28 cm.

SMEAR SLIDE SUMMARY (%):

	1, 50	6, 42
	D	D
COMPOSITION:		
Accessory minerals:		
Micrite	1	2
Foraminifers	—	Tr
Nannofossils	97	82
Diatoms	2	15
Radiolarians	Tr	1

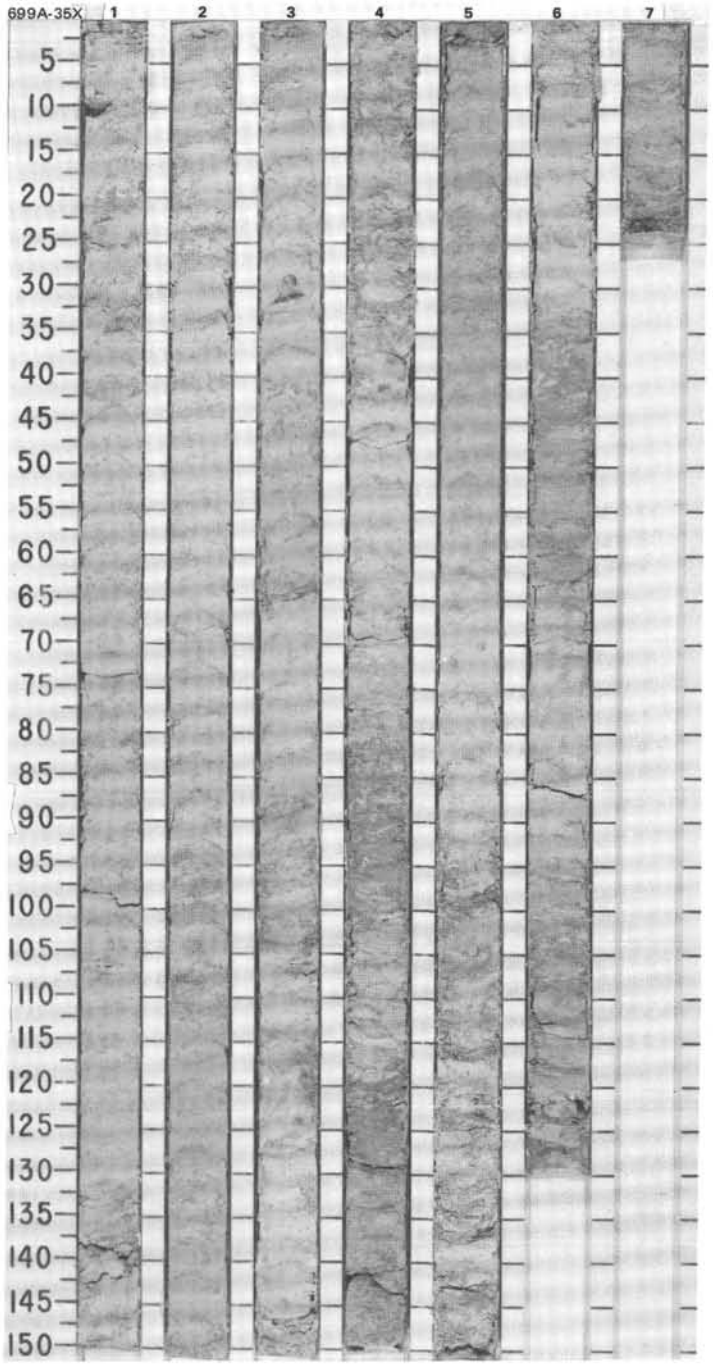

SITE 699 HOLE A CORE 36X CORED INTERVAL 4031.1-4040.6 mbsl; 325.6-335.1 mbsf

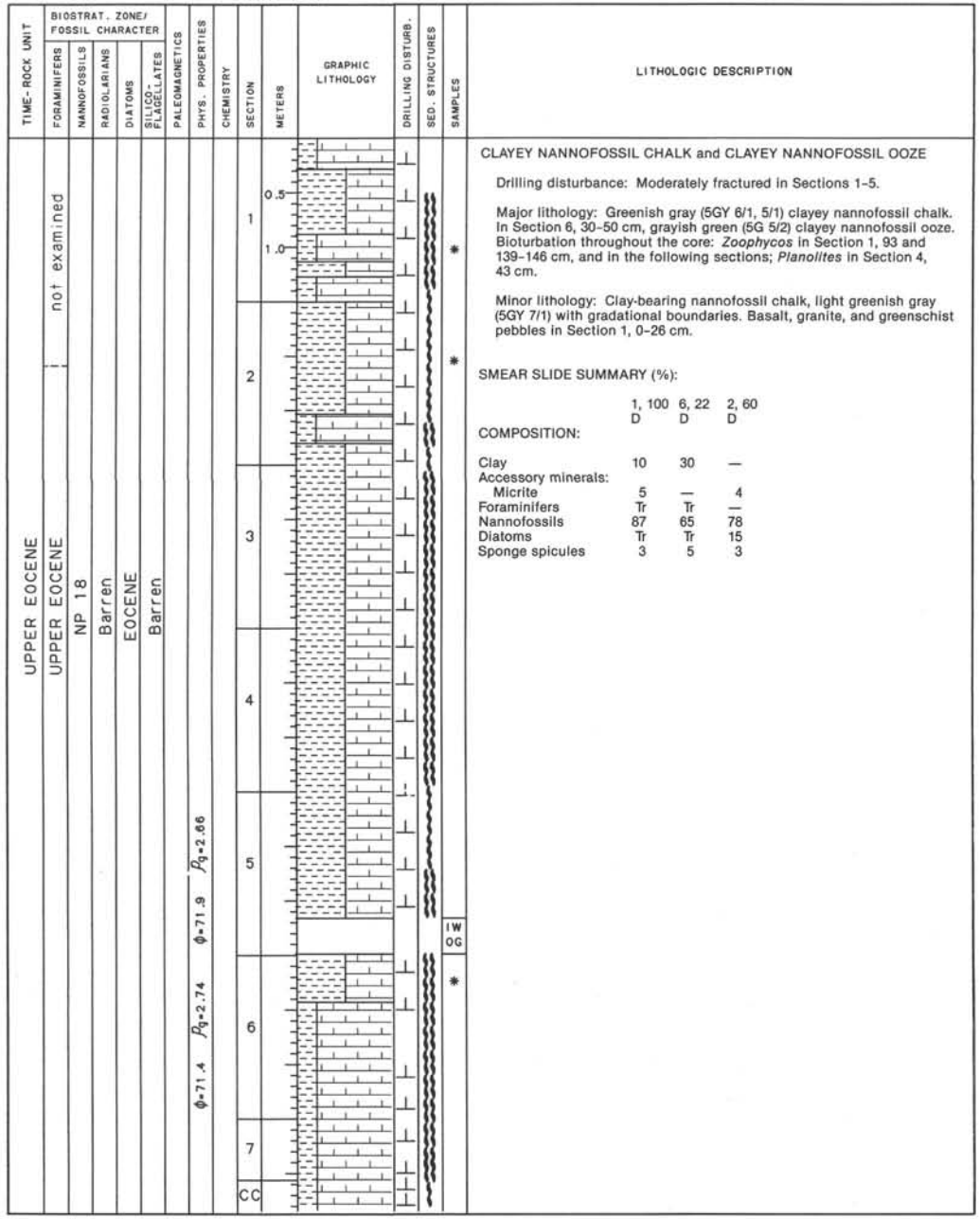

LITHOLOGIC DESCRIPTION

CLAYEY NANNOFOSSIL CHALK and CLAYEY NANNOFOSSIL OOZE

Drilling disturbance: Moderately fractured in Sections 1-5.

Major lithology: Greenish gray (5GY 6/1, 5/1) clayey nannofossil chalk. In Section 6, 30-50 cm, grayish green (5G 5/2) clayey nannofossil ooze. Bioturbation throughout the core: *Zoophycos* in Section 1, 93 and 139-146 cm, and in the following sections; *Planolites* in Section 4, 43 cm.

Minor lithology: Clay-bearing nannofossil chalk, light greenish gray (5GY 7/1) with gradational boundaries. Basalt, granite, and greenschist pebbles in Section 1, 0-26 cm.

SMEAR SLIDE SUMMARY (%):

	1, 100 D	6, 22 D	2, 60 D
COMPOSITION:			
Clay	10	30	—
Accessory minerals:			
Micrite	5	—	4
Foraminifers	Tr	Tr	—
Nannofossils	87	65	78
Diatoms	Tr	Tr	15
Sponge spicules	3	5	3

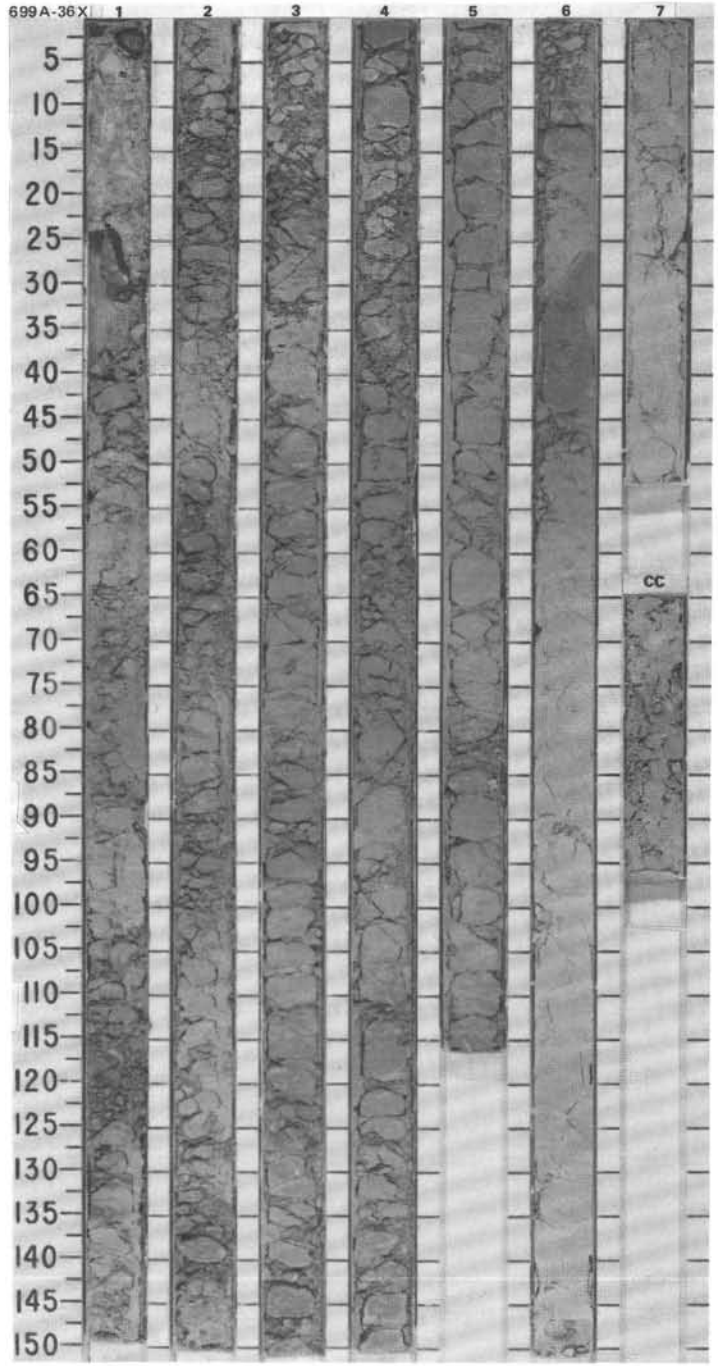

SITE 699 HOLE A CORE 37X CORED INTERVAL 4040.6-4050.1 mbsl; 335.1-344.6 mbsf

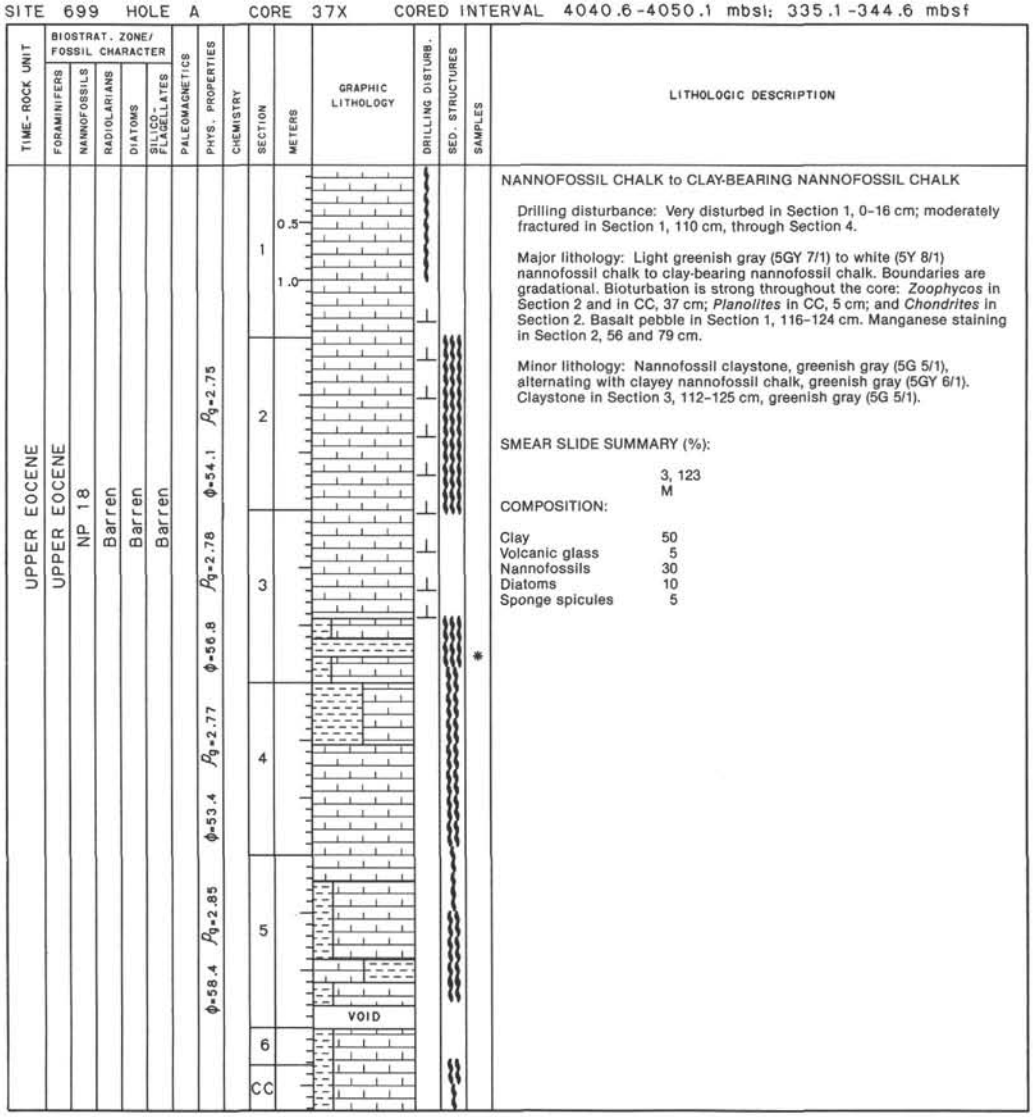

NANNOFOSSIL CHALK to CLAY-BEARING NANNOFOSSIL CHALK

Drilling disturbance: Very disturbed in Section 1, 0-16 cm; moderately fractured in Section 1, 110 cm, through Section 4.

Major lithology: Light greenish gray (5GY 7/1) to white (5Y 8/1) nannofossil chalk to clay-bearing nannofossil chalk. Boundaries are gradational. Bioturbation is strong throughout the core: *Zoophycos* in Section 2 and in CC, 37 cm; *Planolites* in CC, 5 cm; and *Chondrites* in Section 2. Basalt pebble in Section 1, 116-124 cm. Manganese staining in Section 2, 56 and 79 cm.

Minor lithology: Nannofossil claystone, greenish gray (5G 5/1), alternating with clayey nannofossil chalk, greenish gray (5GY 6/1). Claystone in Section 3, 112-125 cm, greenish gray (5G 5/1).

SMEAR SLIDE SUMMARY (%):

	3, 123 M
COMPOSITION:	
Clay	50
Volcanic glass	5
Nannofossils	30
Diatoms	10
Sponge spicules	5

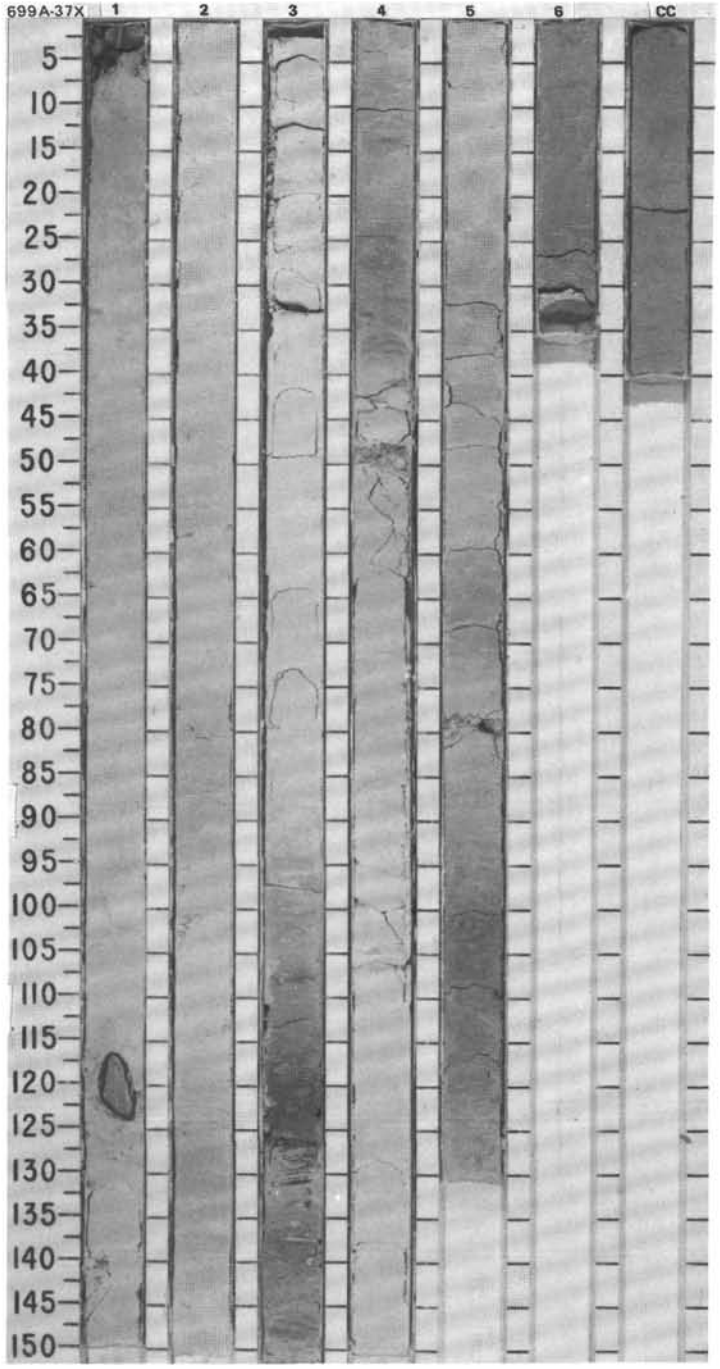

SITE 699 HOLE A CORE 38X CORED INTERVAL 4050.1-4059.6 mbsl; 344.6-354.1 mbsf

TIME-ROCK UNIT	BIOSTRAT. ZONE/ FOSSIL CHARACTER: FORAMINIFERS	NANNOFOSSILS	RADIOLARIANS	DIATOMS	SILICO-FLAGELLATES	PALEOMAGNETICS	PHYS. PROPERTIES	CHEMISTRY	SECTION	METERS	GRAPHIC LITHOLOGY	DRILLING DISTURB.	SED. STRUCTURES	SAMPLES	LITHOLOGIC DESCRIPTION
UPPER EOCENE	UPPER EOCENE	NP 18	Barren	Barren	Barren				1, 2, 3, 4	0.5, 1.0	VOID				NANNOFOSSIL CHALK Drilling disturbance: Sections 3 and 4 very disturbed. Major lithology: Nannofossil chalk, light greenish gray (5GY 7/1). Minor lithology: Downhole contamination with gravel (basalt, granites, quartzite, and greenschist) within a nannofossil ooze, light greenish gray (5GY 7/1).

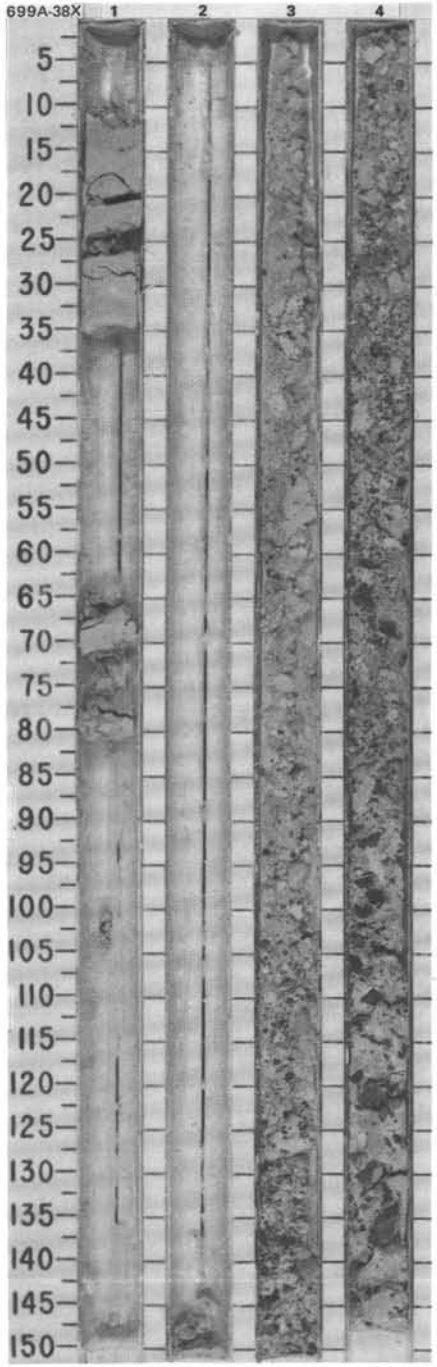

SITE 699 HOLE A CORE 39X CORED INTERVAL 4059.6-4069.1 mbsl; 354.1-363.6 mbsf

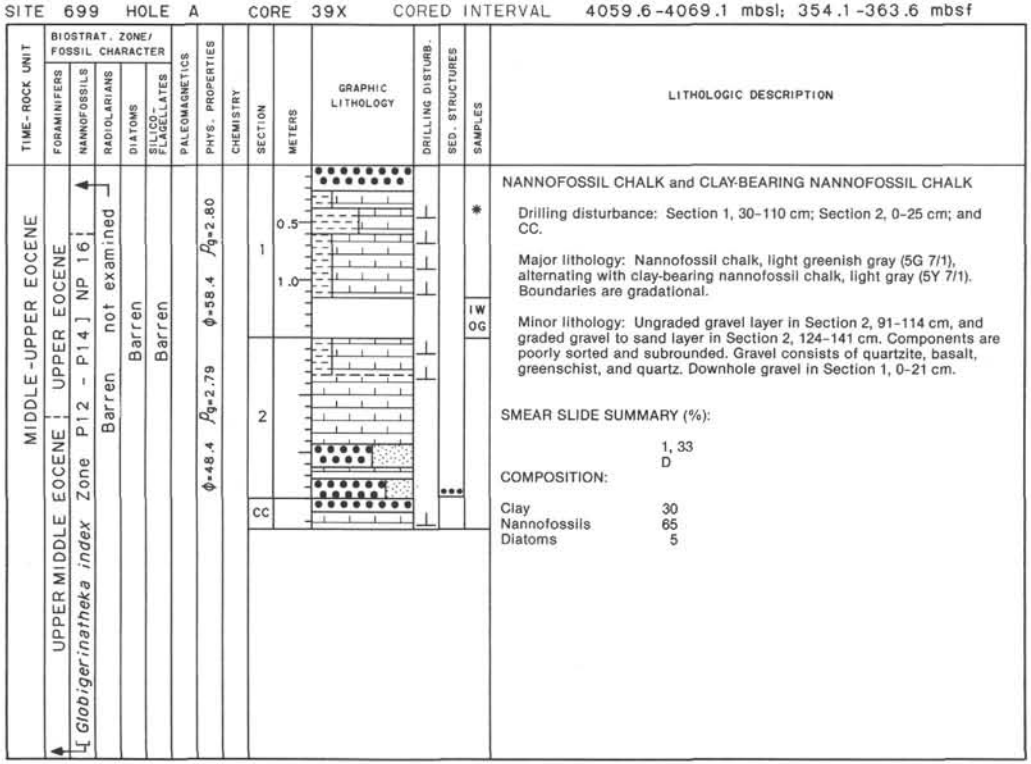

NANNOFOSSIL CHALK and CLAY-BEARING NANNOFOSSIL CHALK

Drilling disturbance: Section 1, 30-110 cm; Section 2, 0-25 cm; and CC.

Major lithology: Nannofossil chalk, light greenish gray (5G 7/1), alternating with clay-bearing nannofossil chalk, light gray (5Y 7/1). Boundaries are gradational.

Minor lithology: Ungraded gravel layer in Section 2, 91-114 cm, and graded gravel to sand layer in Section 2, 124-141 cm. Components are poorly sorted and subrounded. Gravel consists of quartzite, basalt, greenschist, and quartz. Downhole gravel in Section 1, 0-21 cm.

SMEAR SLIDE SUMMARY (%):

	1, 33
	D
COMPOSITION:	
Clay	30
Nannofossils	65
Diatoms	5

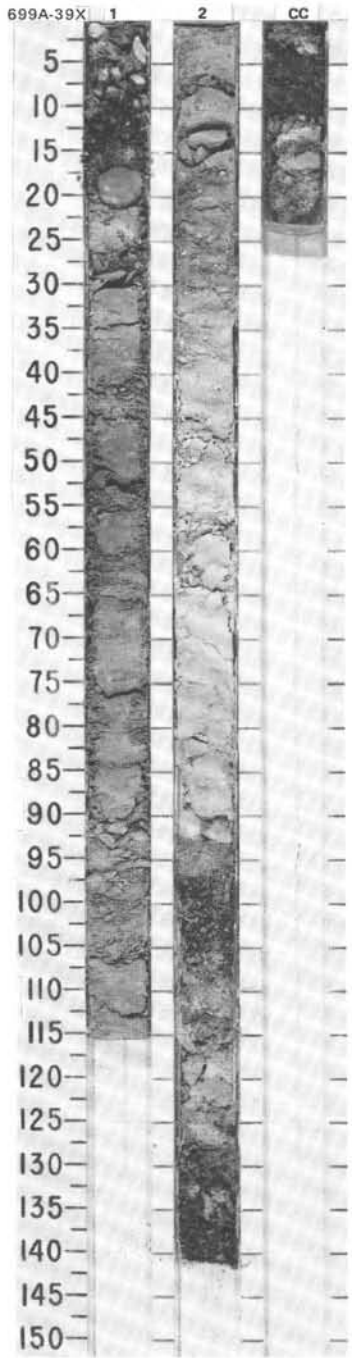

SITE 699 HOLE A CORE 40X CORED INTERVAL 4069.1-4078.6 mbsl; 363.6-373.1 mbsf

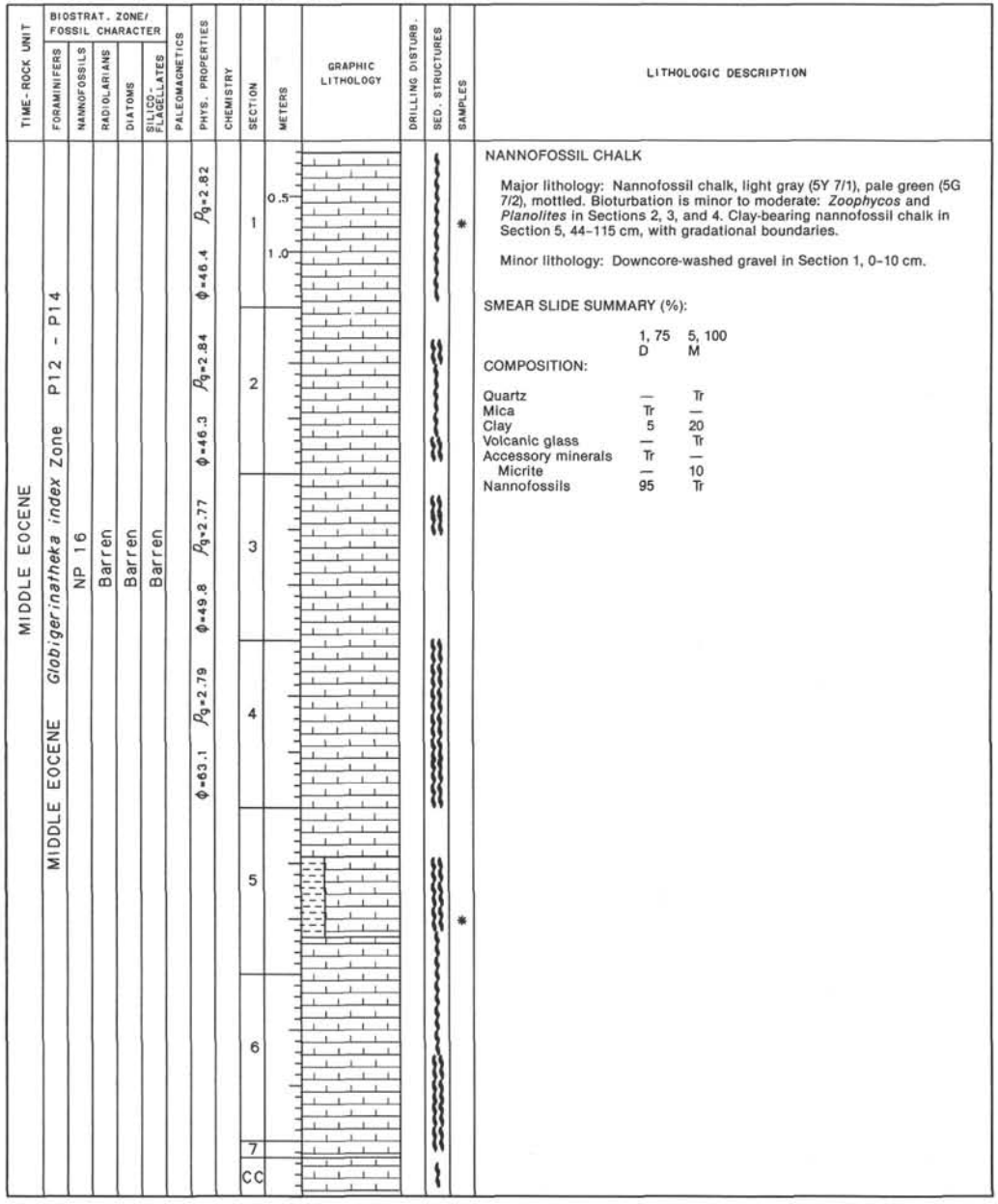

LITHOLOGIC DESCRIPTION

NANNOFOSSIL CHALK

Major lithology: Nannofossil chalk, light gray (5Y 7/1), pale green (5G 7/2), mottled. Bioturbation is minor to moderate: *Zoophycos* and *Planolites* in Sections 2, 3, and 4. Clay-bearing nannofossil chalk in Section 5, 44–115 cm, with gradational boundaries.

Minor lithology: Downcore-washed gravel in Section 1, 0–10 cm.

SMEAR SLIDE SUMMARY (%):

	1, 75 D	5, 100 M
COMPOSITION:		
Quartz	—	Tr
Mica	Tr	—
Clay	5	20
Volcanic glass	—	Tr
Accessory minerals	Tr	—
Micrite	—	10
Nannofossils	95	Tr

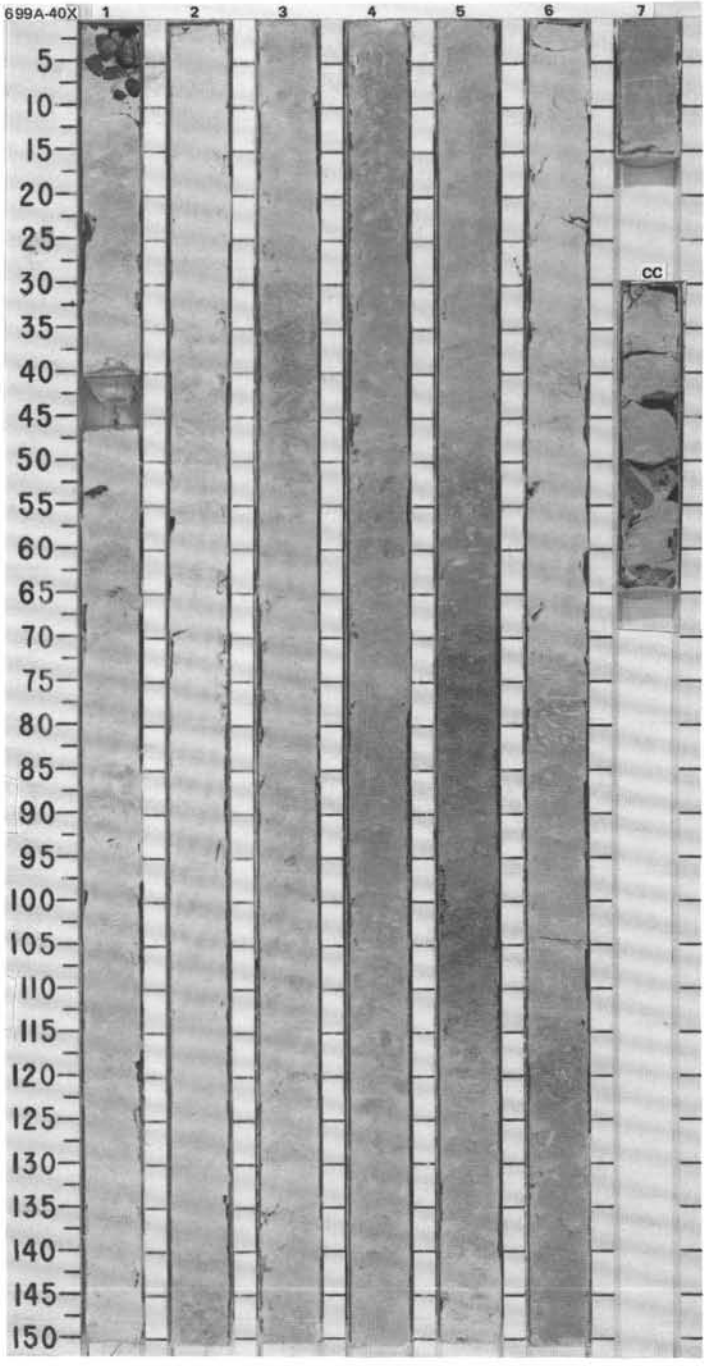

SITE 699 HOLE A CORE 41X CORED INTERVAL 4078.6-4088.1 mbsl; 373.1-382.6 mbsf

TIME-ROCK UNIT	BIOSTRAT. ZONE/ FOSSIL CHARACTER: FORAMINIFERS	NANNOFOSSILS	RADIOLARIANS	DIATOMS	SILICO-FLAGELLATES	PALEOMAGNETICS	PHYS. PROPERTIES	CHEMISTRY	SECTION	METERS	GRAPHIC LITHOLOGY	DRILLING DISTURB.	SED. STRUCTURES	SAMPLES	LITHOLOGIC DESCRIPTION
MIDDLE EOCENE	LOWER MIDDLE EOCENE?	NP 16	Barren	Barren	Barren				1, 2, CC	0.5, 1.0				*	

CLAY-BEARING NANNOFOSSIL CHALK and CLAYEY NANNOFOSSIL CHALK

Drilling disturbance: Section 1, 0-110 cm, moderately fractured.

Major lithology: Clay-bearing nannofossil chalk, light olive brown (2.5Y 5/4). Gradational boundary with clayey nannofossil chalk, olive gray (5Y 5/2), in Section 1, 113 cm.

Minor lithology: Washed-in pebbles in the disturbed Section 1, 0-20 and 75-111 cm (granite, gneiss, and basalt).

SMEAR SLIDE SUMMARY (%):

	1, 23 D
COMPOSITION:	
Clay	15
Nannofossils	83
Diatoms	2

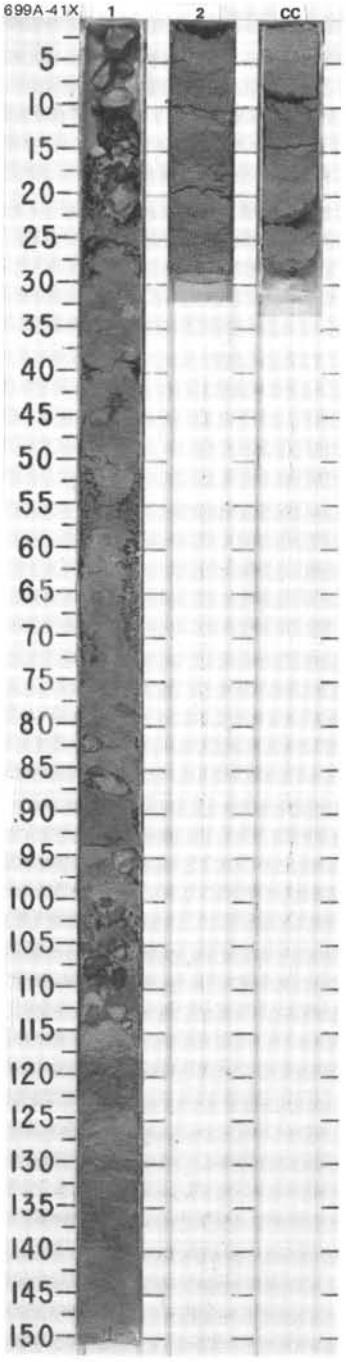

SITE 699 HOLE A CORE 42X CORED INTERVAL 4088.1-4097.6 mbsl; 382.6-392.1 mbsf

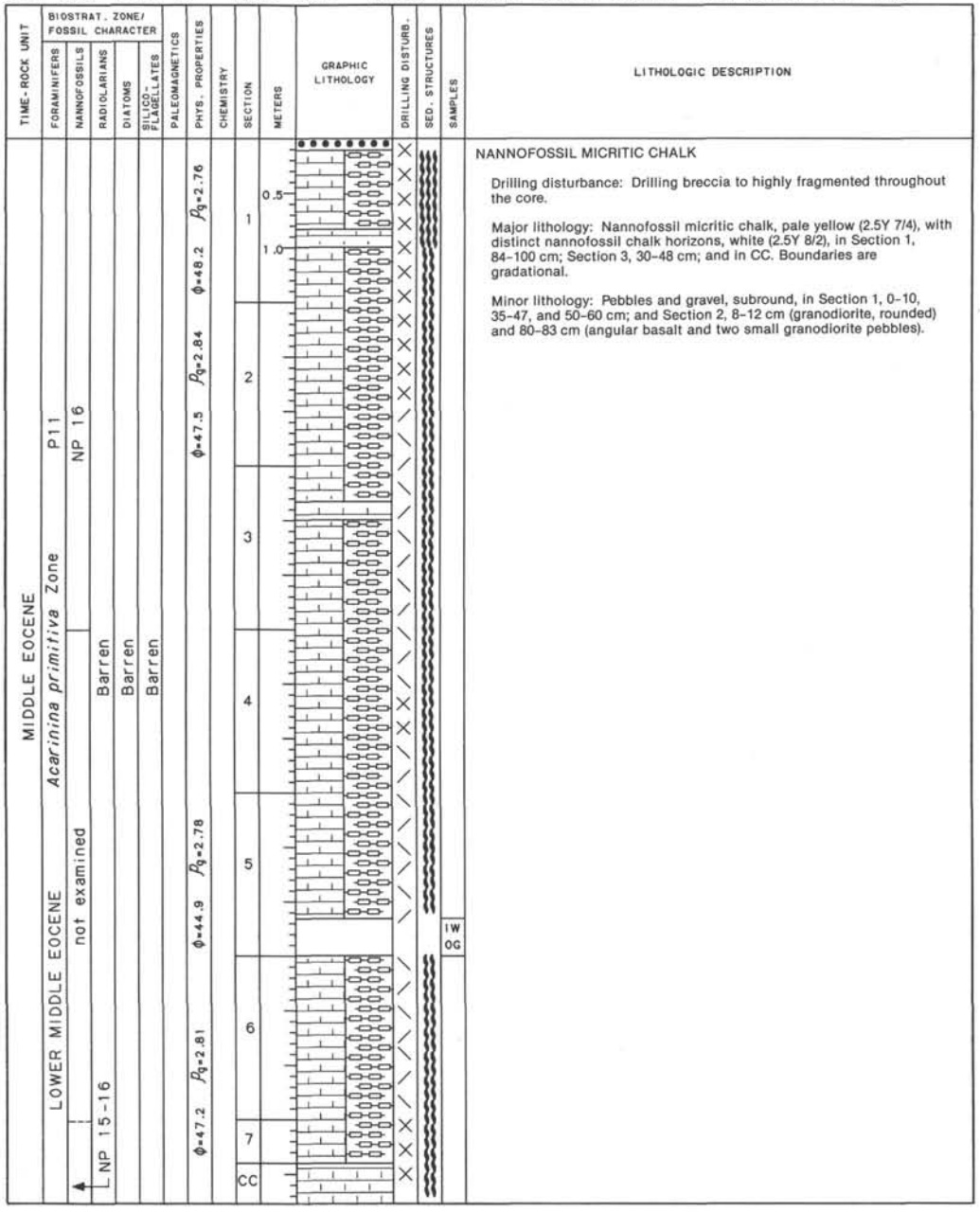

LITHOLOGIC DESCRIPTION

NANNOFOSSIL MICRITIC CHALK

Drilling disturbance: Drilling breccia to highly fragmented throughout the core.

Major lithology: Nannofossil micritic chalk, pale yellow (2.5Y 7/4), with distinct nannofossil chalk horizons, white (2.5Y 8/2), in Section 1, 84-100 cm; Section 3, 30-48 cm; and in CC. Boundaries are gradational.

Minor lithology: Pebbles and gravel, subround, in Section 1, 0-10, 35-47, and 50-60 cm; and Section 2, 8-12 cm (granodiorite, rounded) and 80-83 cm (angular basalt and two small granodiorite pebbles).

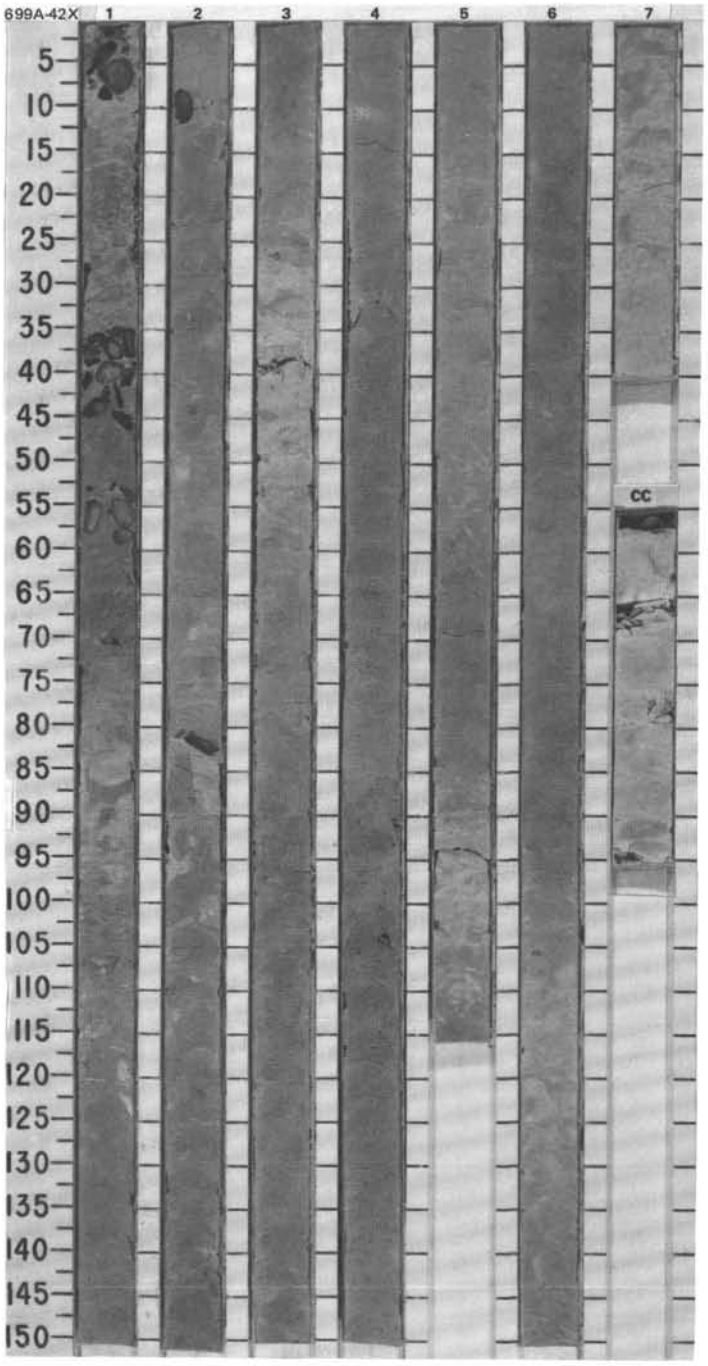

SITE 699 HOLE A CORE 43X CORED INTERVAL 4097.6-4107.1 mbsl; 392.1-401.6 mbsf

TIME-ROCK UNIT	BIOSTRAT. ZONE/ FOSSIL CHARACTER: FORAMINIFERS	NANNOFOSSILS	RADIOLARIANS	DIATOMS	SILICO-FLAGELLATES	PALEOMAGNETICS	PHYS. PROPERTIES	CHEMISTRY	SECTION	METERS	GRAPHIC LITHOLOGY	DRILLING DISTURB.	SED. STRUCTURES	SAMPLES
MIDDLE EOCENE	P11								1	0.5, 1.0		X		
	Acarinina primitiva Zone								2			X		
									3			X		
	LOWER MIDDLE EOCENE	NP15-16	Barren	Barren	Barren				4			⊥		*
									5			⊥		
									6			⊥	~	
									CC			⊥		

LITHOLOGIC DESCRIPTION

NANNOFOSSIL MICRITIC CHALK

Drilling disturbance: Drilling breccia to moderately fractured throughout the core.

Major lithology: Nannofossil micritic chalk, light gray (2.5Y 7/2) in Section 1, to light yellowish brown (2.5Y 6/4) in Section 2, to light brownish gray (2.5Y 6/2) and white (5Y 8/1) in the rest of the core.

Minor lithology: Pebbles in Section 1, 21 cm (subround greenschist), 36 cm (subround granodiorite), and 147 cm (subround greenschist); Section 2, 10 cm (amphibolite), 55 cm (basalt with hematite), and 146 cm (subround amphibolite); and Section 4, 60 cm (fine-grained quartzite).

SMEAR SLIDE SUMMARY (%):

	4, 111 D
COMPOSITION:	
Accessory minerals:	
Micrite	5
Nannofossils	95

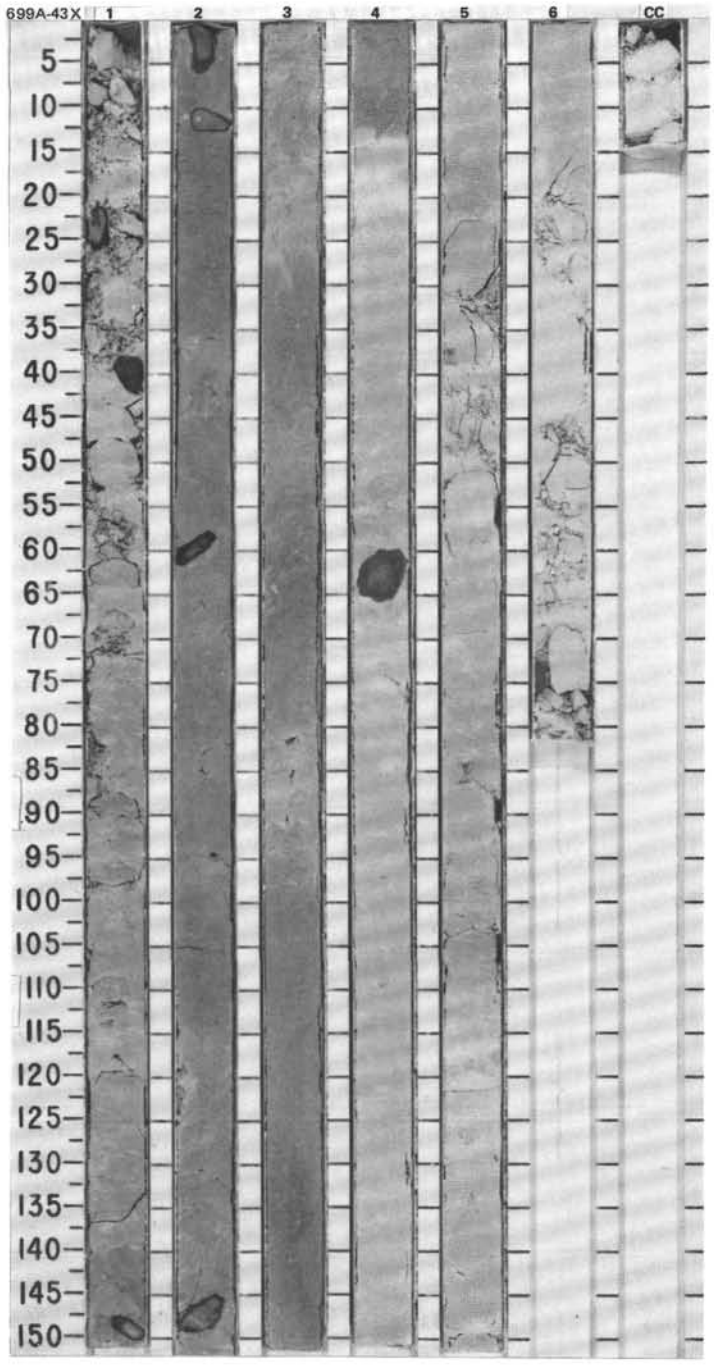

SITE 699 HOLE A CORE 44X CORED INTERVAL 4107.1-4116.6 mbsl; 401.6-411.1 mbsf

TIME-ROCK UNIT	BIOSTRAT. ZONE/ FOSSIL CHARACTER: FORAMINIFERS	NANNOFOSSILS	RADIOLARIANS	DIATOMS	SILICO-FLAGELLATES	PALEOMAGNETICS	PHYS. PROPERTIES	CHEMISTRY	SECTION	METERS	GRAPHIC LITHOLOGY	DRILLING DISTURB.	SED. STRUCTURES	SAMPLES	LITHOLOGIC DESCRIPTION
MIDDLE EOCENE	LOWER MIDDLE EOCENE *A. primitiva* Zone P11	NP 15-16	Barren	Barren	Barren				1, 2, 3	0.5, 1.0					PEBBLES Major lithology: No sediments. Three subangular fine-grained granodiorite pebbles.

SITE 699 HOLE A CORE 45X CORED INTERVAL 4116.6-4126.1 mbsl; 411.1-420.6 mbsf

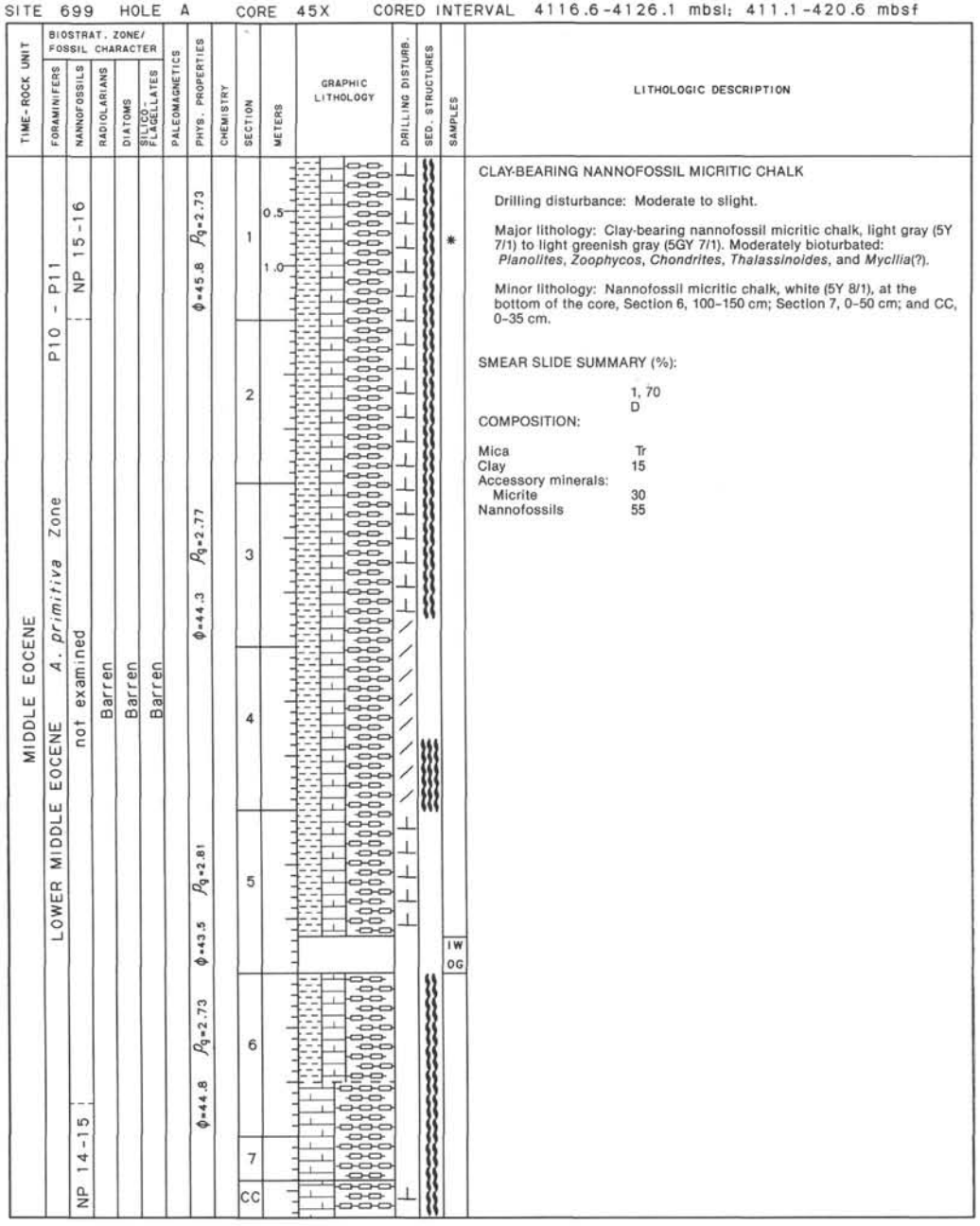

LITHOLOGIC DESCRIPTION

CLAY-BEARING NANNOFOSSIL MICRITIC CHALK

Drilling disturbance: Moderate to slight.

Major lithology: Clay-bearing nannofossil micritic chalk, light gray (5Y 7/1) to light greenish gray (5GY 7/1). Moderately bioturbated: *Planolites*, *Zoophycos*, *Chondrites*, *Thalassinoides*, and *Mycilia*(?).

Minor lithology: Nannofossil micritic chalk, white (5Y 8/1), at the bottom of the core, Section 6, 100-150 cm; Section 7, 0-50 cm; and CC, 0-35 cm.

SMEAR SLIDE SUMMARY (%):

	1, 70 D
COMPOSITION:	
Mica	Tr
Clay	15
Accessory minerals:	
Micrite	30
Nannofossils	55

699A-46X NO RECOVERY

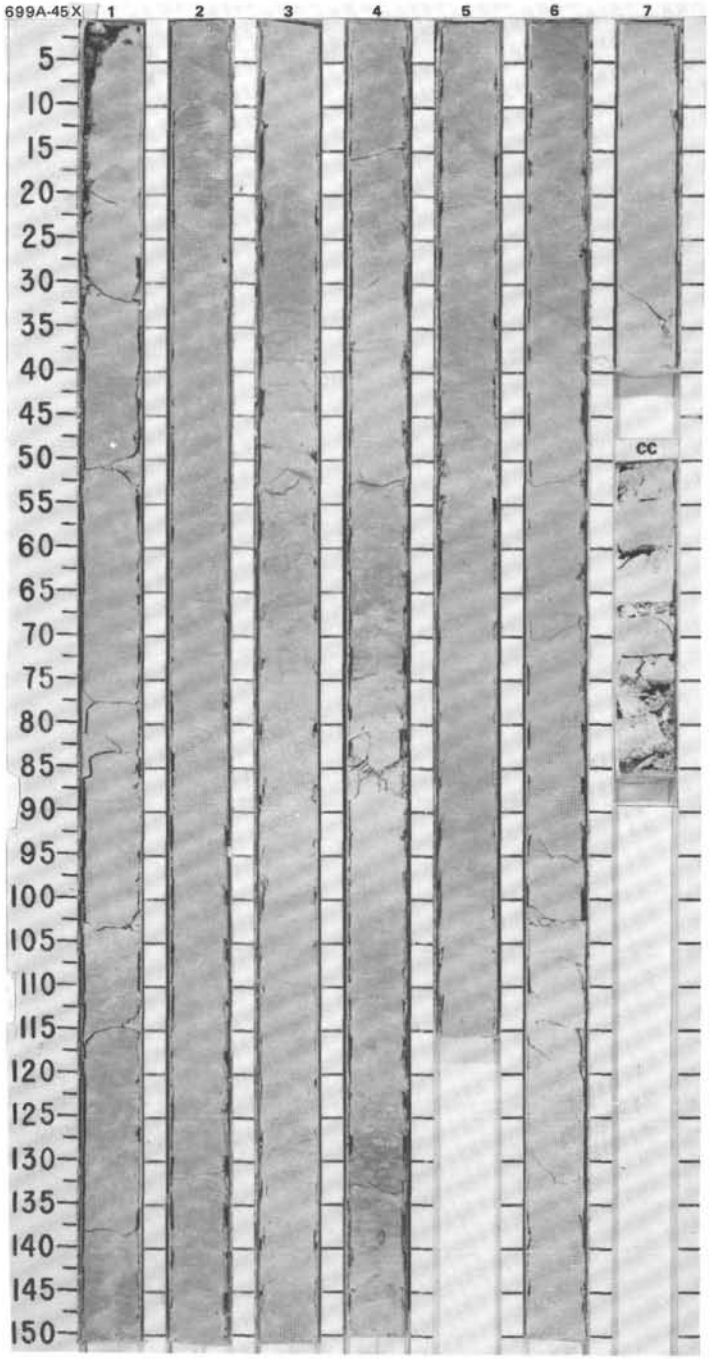

SITE 699 HOLE A CORE 47X CORED INTERVAL 4126.2-4135.6 mbsl; 430.1-439.6 mbsf

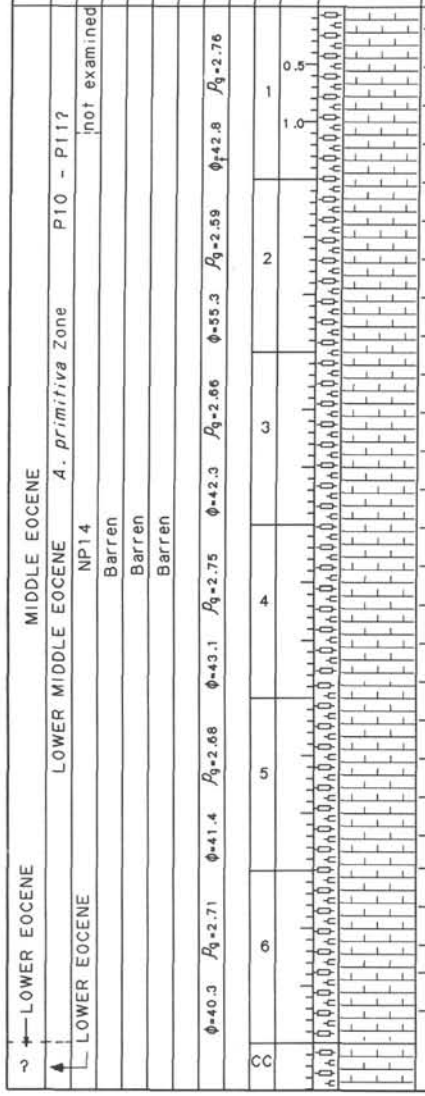

LITHOLOGIC DESCRIPTION

MICRITE-BEARING NANNOFOSSIL CHALK

Drilling disturbance: Moderately disturbed.

Major lithology: Micrite-bearing nannofossil chalk, pale yellow (2.5Y 7/4) to white (2.5Y 8/2). Bioturbated throughout, mainly *Planolites* and *Zoophycos*.

SMEAR SLIDE SUMMARY (%):

	2, 65 D	3, 68 D
COMPOSITION:		
Quartz	Tr	Tr
Calcite/dolomite	10	10
Foraminifers	Tr	Tr
Nannofossils	90	90

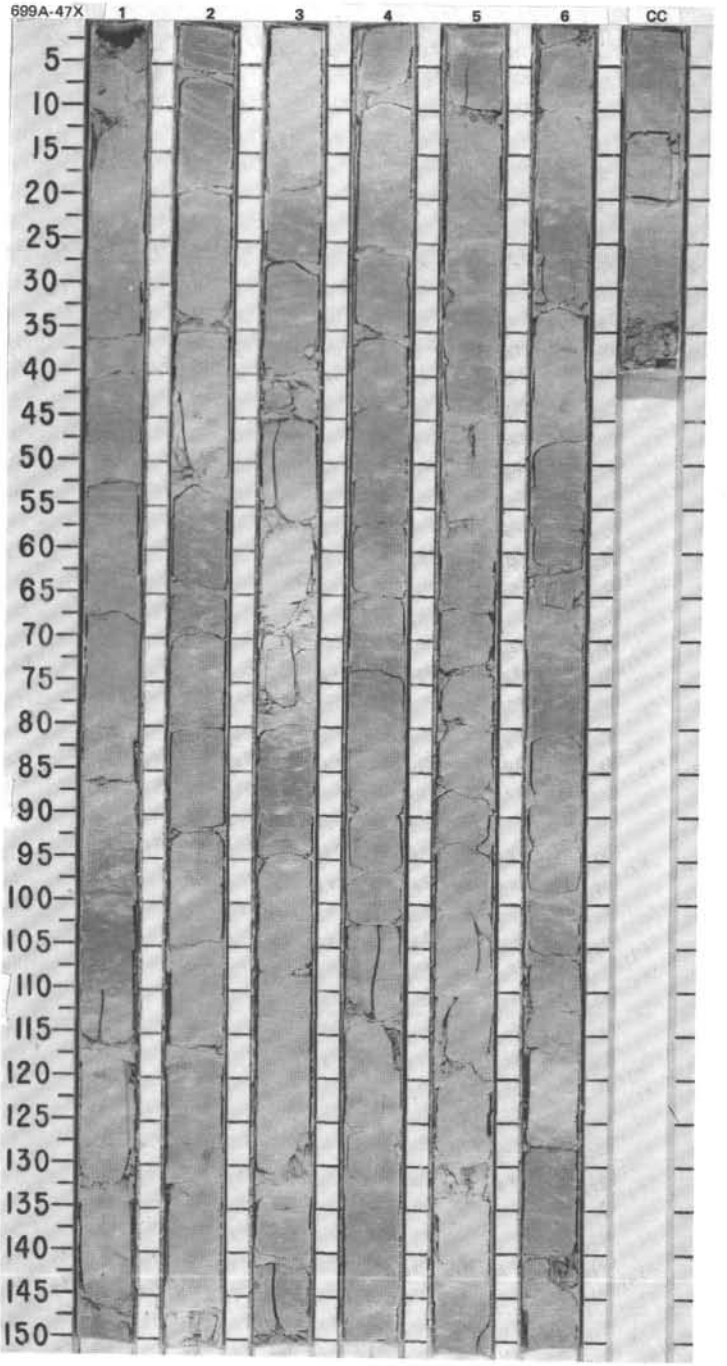

SITE 699 HOLE A CORE 48X CORED INTERVAL 4135.6-4155.1 mbsl; 439.6-449.1 mbsf

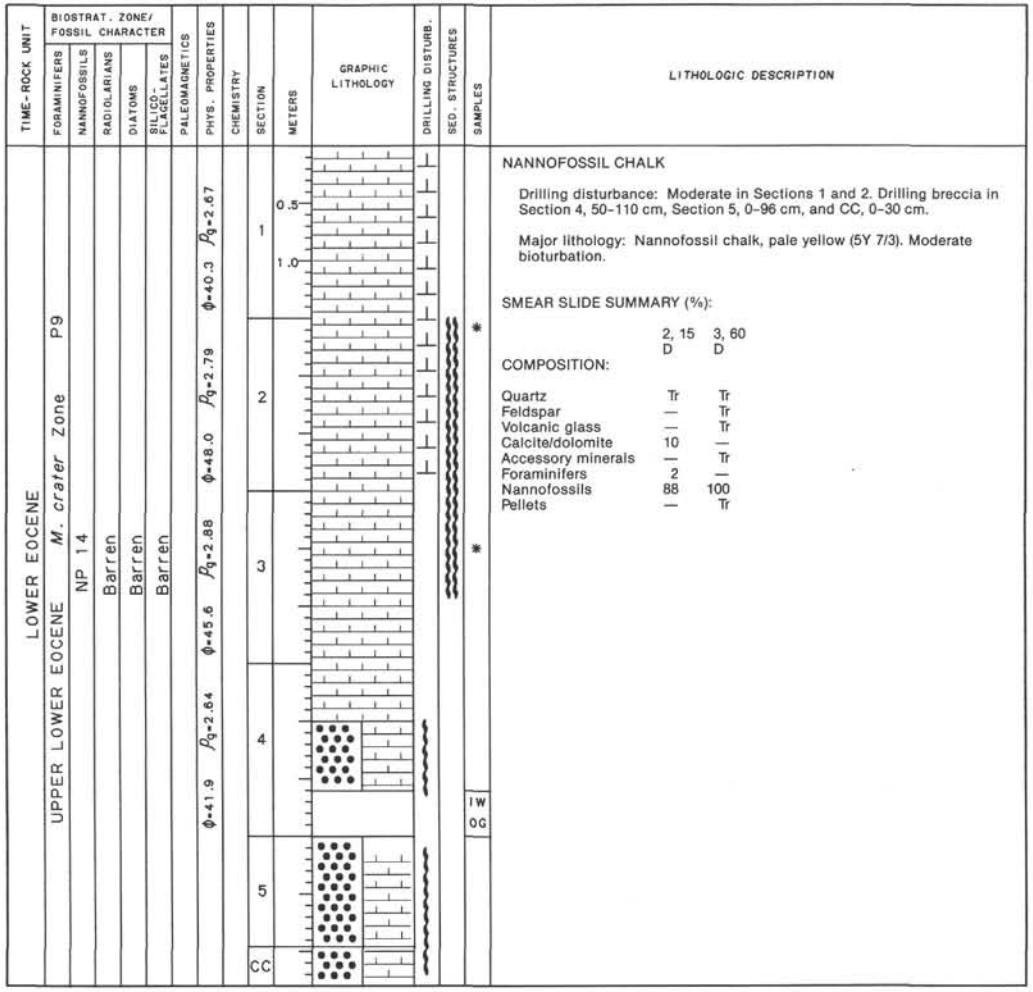

NANNOFOSSIL CHALK

Drilling disturbance: Moderate in Sections 1 and 2. Drilling breccia in Section 4, 50-110 cm, Section 5, 0-96 cm, and CC, 0-30 cm.

Major lithology: Nannofossil chalk, pale yellow (5Y 7/3). Moderate bioturbation.

SMEAR SLIDE SUMMARY (%):

	2, 15 D	3, 60 D
COMPOSITION:		
Quartz	Tr	Tr
Feldspar	—	Tr
Volcanic glass	—	Tr
Calcite/dolomite	10	—
Accessory minerals	—	Tr
Foraminifers	2	—
Nannofossils	88	100
Pellets	—	Tr

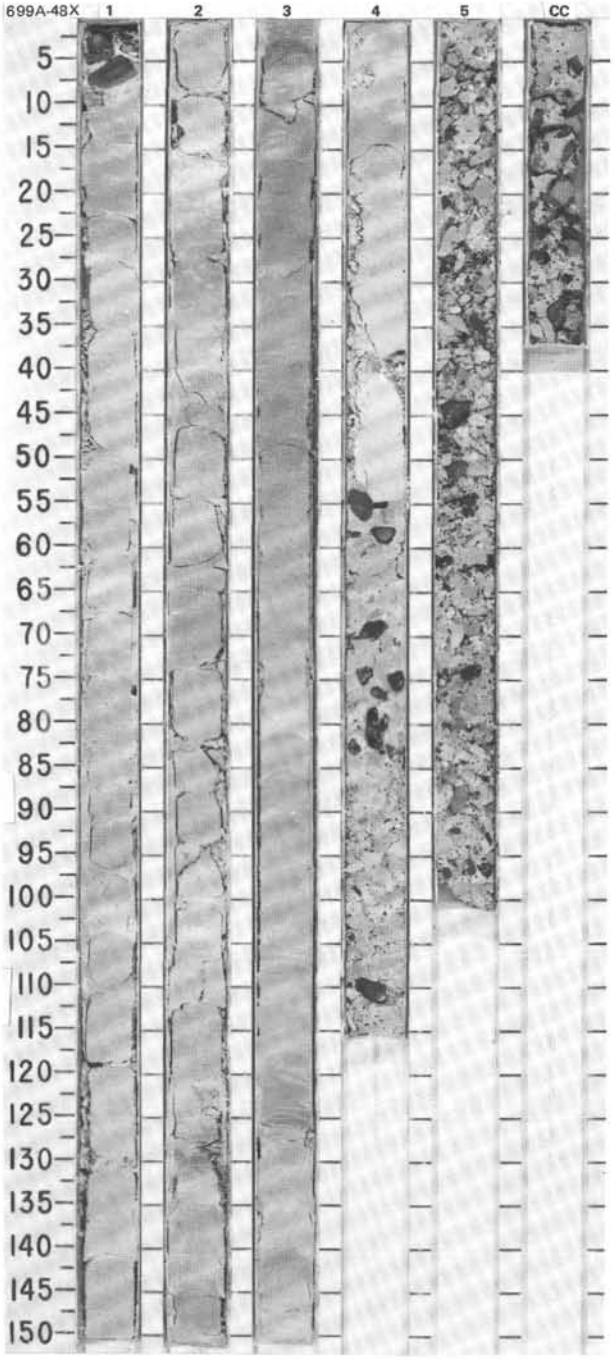

SITE 699 HOLE A CORE 49X CORED INTERVAL 4155.1-4164.1 mbsl; 449.1-458.6 mbsf

TIME-ROCK UNIT	BIOSTRAT. ZONE/ FOSSIL CHARACTER: FORAMINIFERS	NANNOFOSSILS	RADIOLARIANS	DIATOMS	SILICO-FLAGELLATES	PALEOMAGNETICS	PHYS. PROPERTIES	CHEMISTRY	SECTION	METERS	GRAPHIC LITHOLOGY	DRILLING DISTURB.	SED. STRUCTURES	SAMPLES
LOWER EOCENE	P9	NP 14	Barren	Barren	Barren	ϕ=42.7 ρ_g=2.64 ϕ=44.4 ρ_g=2.70 ϕ=39.9 ρ_g=2.77 ϕ=40.1 ρ_g=2.68 ϕ=39.6 ρ_g=2.69 ϕ=44.8 ρ_g=2.80			1	0.5 1.0	?		*
	M. crater Zone								2					
									3					
	UPPER LOWER EOCENE	not examined							4					
									5					
		NP 13							6					
									CC					

LITHOLOGIC DESCRIPTION

NANNOFOSSIL CHALK

Drilling disturbance: Moderate throughout. Gravel in Section 1, 0-10 cm, is due to downhole contamination.

Major lithology: Nannofossil chalk, pale yellow (2.5Y 7/4) to white (2.5Y 8/2). Moderately to highly bioturbated.

SMEAR SLIDE SUMMARY (%):

	1, 133 D
COMPOSITION:	
Cement	2
Nannofossils	98

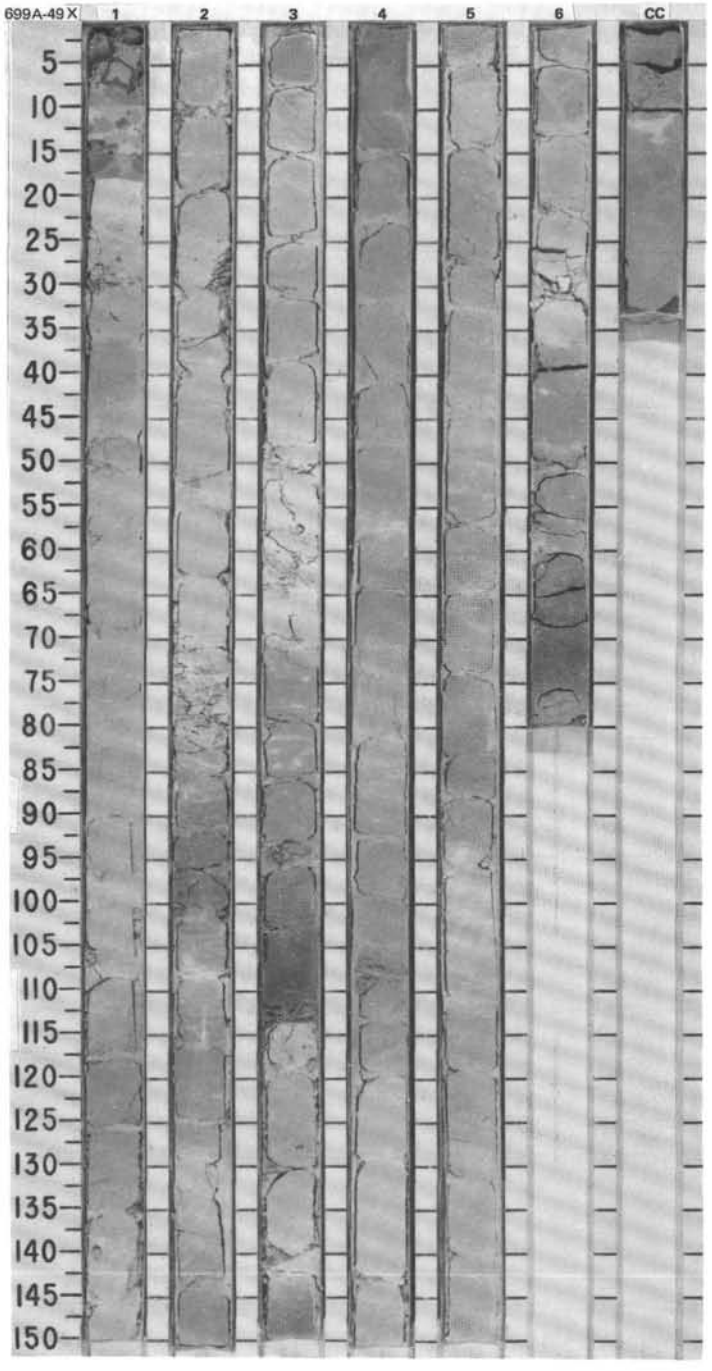

SITE 699 HOLE A CORE 50X CORED INTERVAL 4164.1-4173.6 mbsl; 458.6-468.1 mbsf

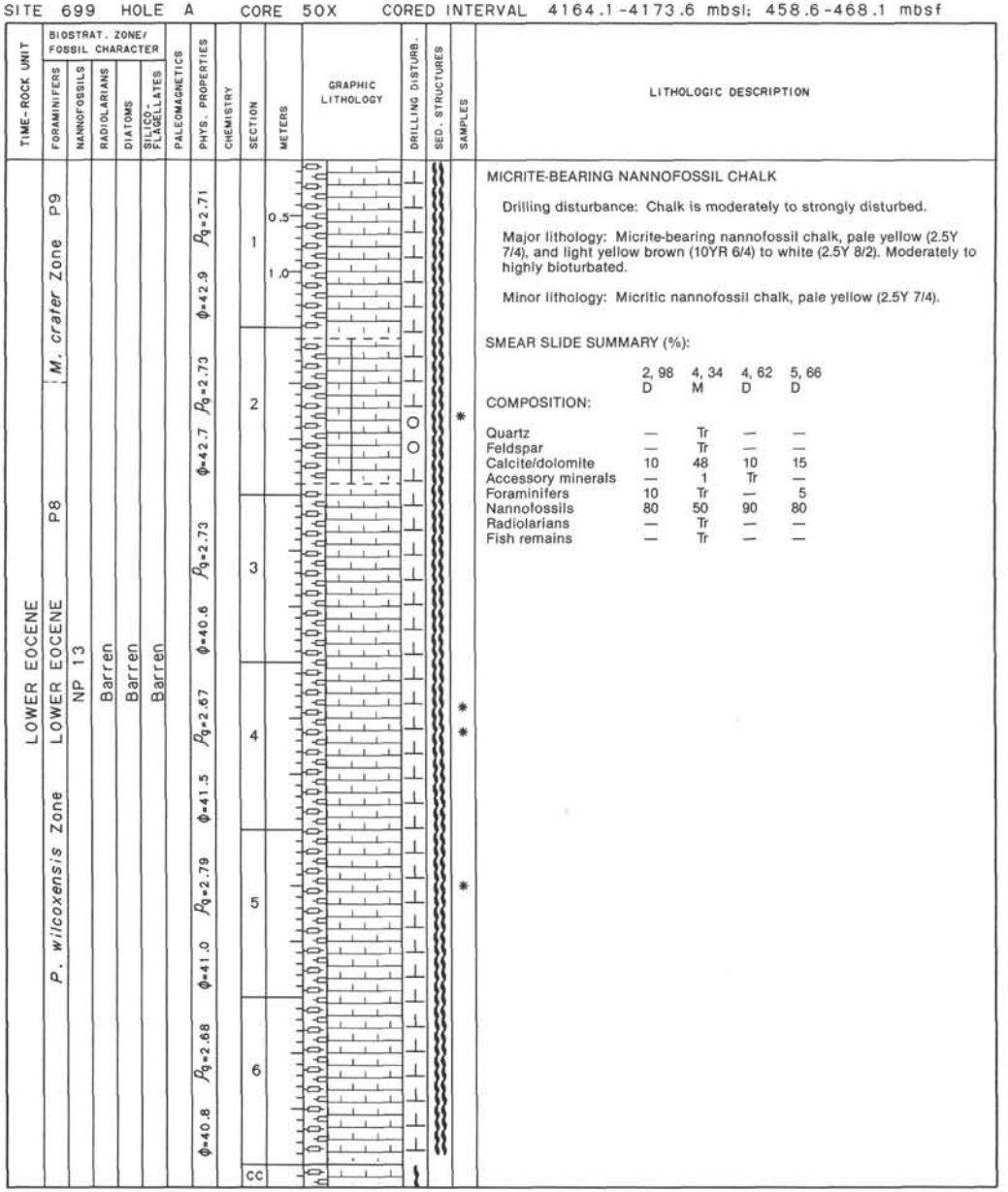

MICRITE-BEARING NANNOFOSSIL CHALK

Drilling disturbance: Chalk is moderately to strongly disturbed.

Major lithology: Micrite-bearing nannofossil chalk, pale yellow (2.5Y 7/4), and light yellow brown (10YR 6/4) to white (2.5Y 8/2). Moderately to highly bioturbated.

Minor lithology: Micritic nannofossil chalk, pale yellow (2.5Y 7/4).

SMEAR SLIDE SUMMARY (%):

	2, 98 D	4, 34 M	4, 62 D	5, 66 D
COMPOSITION:				
Quartz	—	Tr	—	—
Feldspar	—	Tr	—	—
Calcite/dolomite	10	48	10	15
Accessory minerals	—	1	Tr	—
Foraminifers	10	Tr	—	5
Nannofossils	80	50	90	80
Radiolarians	—	Tr	—	—
Fish remains	—	Tr	—	—

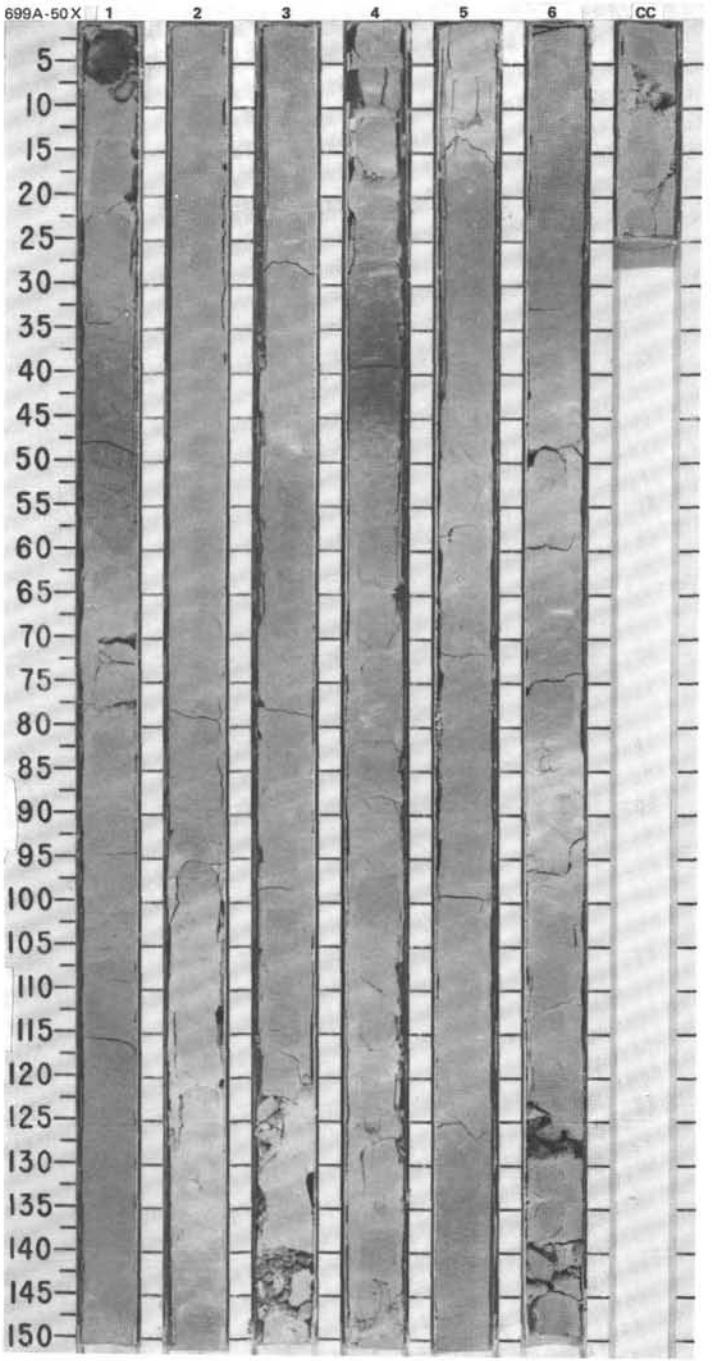

SITE 699 HOLE A CORE 51X CORED INTERVAL 4173.6-4183.1 mbsl; 468.1-477.6 mbsf

TIME-ROCK UNIT	BIOSTRAT. ZONE/ FOSSIL CHARACTER: FORAMINIFERS	NANNOFOSSILS	RADIOLARIANS	DIATOMS	SILICO-FLAGELLATES	PALEOMAGNETICS	PHYS. PROPERTIES	CHEMISTRY	SECTION	METERS	GRAPHIC LITHOLOGY	DRILLING DISTURB.	SED. STRUCTURES	SAMPLES	LITHOLOGIC DESCRIPTION
LOWER EOCENE	*P. wilcoxensis* Zone P8 LOWER EOCENE	NP 13	Barren	Barren	Barren				CC						NANNOFOSSIL CHALK Drilling disturbance: No recovery in main core. CC sediments mixed with pebbles from downhole contamination. Major lithology: Nannofossil chalk, pale yellow (2.5Y 7/4).

SITE 699 HOLE A CORE 52X CORED INTERVAL 4183.1-4192.6 mbsl; 477.6-487.1 mbsf

TIME-ROCK UNIT	BIOSTRAT. ZONE/ FOSSIL CHARACTER: FORAMINIFERS	NANNOFOSSILS	RADIOLARIANS	DIATOMS	SILICO-FLAGELLATES	PALEOMAGNETICS	PHYS. PROPERTIES	CHEMISTRY	SECTION	METERS	GRAPHIC LITHOLOGY	DRILLING DISTURB.	SED. STRUCTURES	SAMPLES	LITHOLOGIC DESCRIPTION
LOWER EOCENE	*P. wilcoxensis* Zone P8 LOWER EOCENE	NP 10-12	Barren	Barren	Barren				CC						NANNOFOSSIL CHALK Drilling disturbance: No recovery in main core. Major lithology: Nannofossil chalk, pale yellow (2.5Y 7/4), with gravel-sized pebbles from downhole contamination.

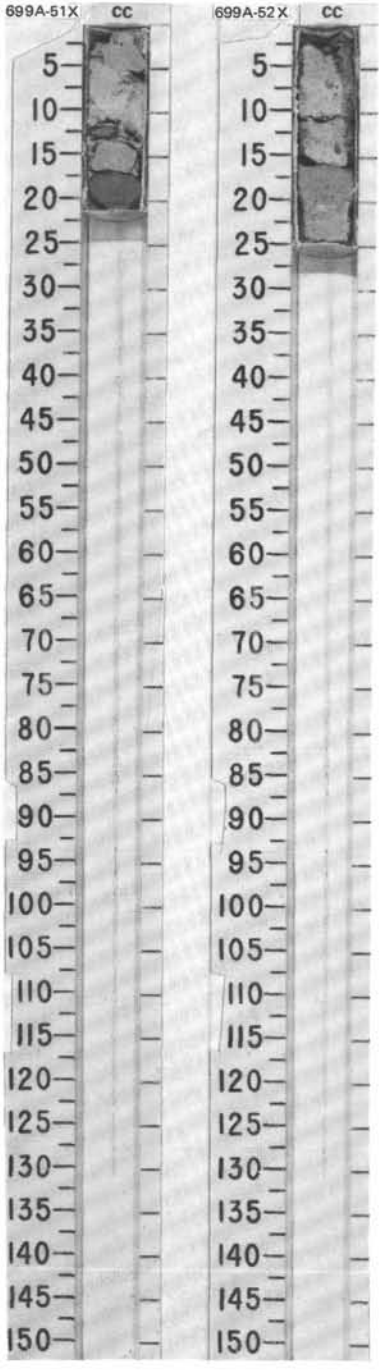

SITE 699 HOLE A CORE 53X CORED INTERVAL 4192.6-4202.1 mbsl; 487.1-496.6 mbsf

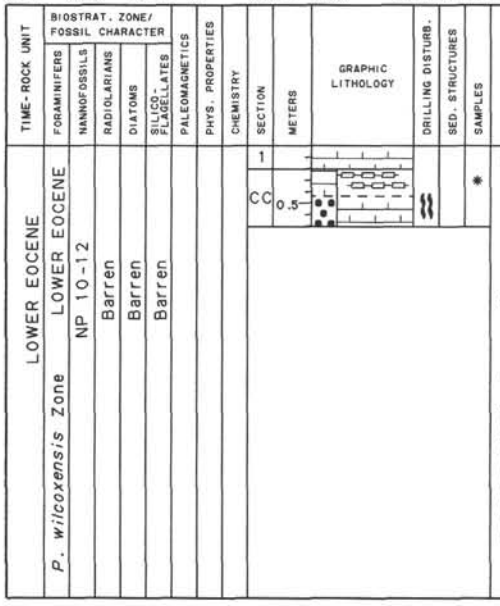

LITHOLOGIC DESCRIPTION

NANNOFOSSIL CHALK and MICRITIC NANNOFOSSIL CHALK

Drilling disturbance: Almost no core recovery in main core; drilling slurry in lower half of CC.

Major lithology: Nannofossil chalk, pale yellow (2.5Y 7/4), and micritic nannofossil chalk, light yellow brown (10YR 6/4).

SMEAR SLIDE SUMMARY (%):

	CC, 15 D
COMPOSITION:	
Quartz	Tr
Feldspar	Tr
Volcanic glass	Tr
Calcite/dolomite	80
Accessory minerals	Tr
Nannofossils	18
Diatoms	1
Fish remains	Tr
Pellets	Tr

SITE 699 HOLE A CORE 54X CORED INTERVAL 4202.1-4211.6 mbsl; 496.6-506.1 mbsf

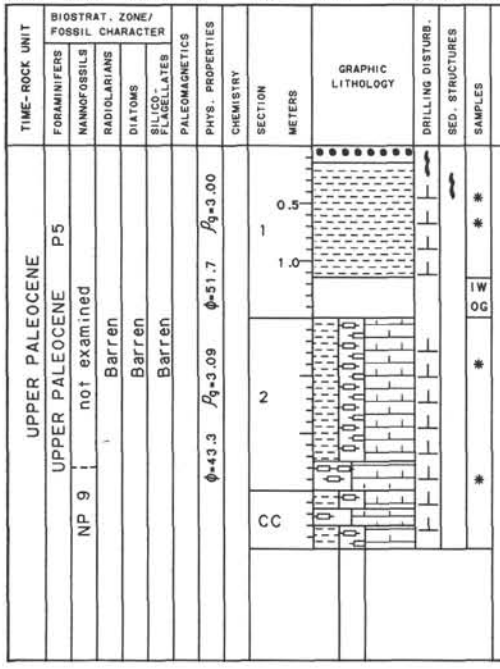

LITHOLOGIC DESCRIPTION

CLAYSTONE and CLAY-BEARING MICRITIC NANNOFOSSIL CHALK

Drilling disturbance: Moderate to strong at the top of Section 1, 0-30 cm.

Major lithology: Claystone, dark brown (7.5YR 4/4), containing laminae of zeolitic(?) claystone in Section 1. Clay-bearing micritic nannofossil chalk, pale brown (10YR 6/3), in Section 2. Little bioturbation.

Minor lithology: Zeolitic claystone(?), greenish gray (5GY 5/1), containing more carbonate components than the surrounding dark brown clay. Occurs as thin 0.5-5-cm laminae in the dark brown claystone in Section 1. Micritic nannofossil chalk, light gray (10YR 7/1), at the bottom of Section 2, 125-150 cm. Slightly bioturbated, *Planolites* and *Zoophycos*.

SMEAR SLIDE SUMMARY (%):

	1, 44 D	1, 56 M	2, 38 D	2, 144 D
COMPOSITION:				
Mica	5	Tr	—	—
Clay	85	80	10	5
Calcite/dolomite	5	7	42	42
Accessory minerals:				
Zeolites	1	10	—	—
Opaques	2	—	—	—
Foraminifers	—	—	Tr	5
Nannofossils	2	3	48	48

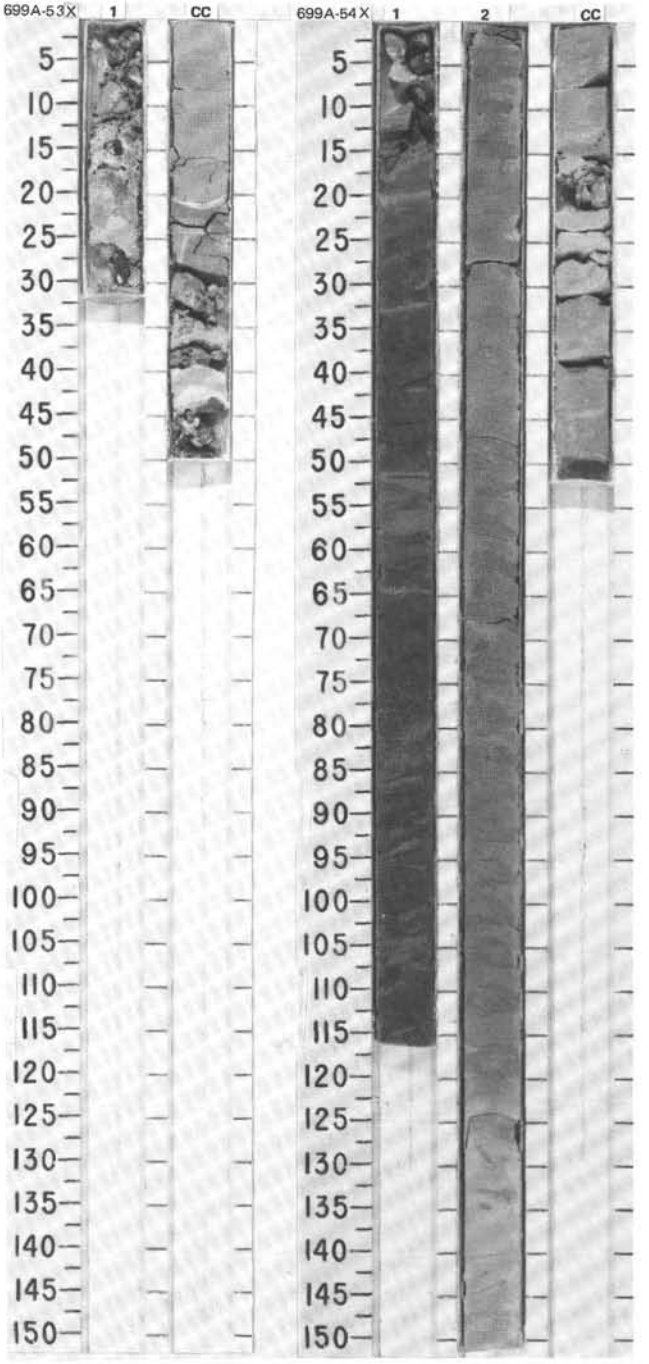

SITE 699 HOLE A CORE 55X CORED INTERVAL 4211.6-4214.1 mbsl; 506.1-508.6 mbsf

TIME-ROCK UNIT	BIOSTRAT. ZONE/ FOSSIL CHARACTER: FORAMINIFERS	NANNOFOSSILS	RADIOLARIANS	DIATOMS	SILICO-FLAGELLATES	PALEOMAGNETICS	PHYS. PROPERTIES	CHEMISTRY	SECTION	METERS	GRAPHIC LITHOLOGY	DRILLING DISTURB.	SED. STRUCTURES	SAMPLES	LITHOLOGIC DESCRIPTION
UPPER PALEOCENE	UPPER PALEOCENE P4 - P5	NP5-9	Barren	Barren	Barren				1	0.5, 1.0				*	CLAY-BEARING MICRITIC NANNOFOSSIL CHALK

Drilling disturbance: Badly disturbed.

Major lithology: Clay-bearing micritic nannofossil chalk, light gray (10YR 7/1). Drilling disturbance precludes the preservation of any structures, e. g., bioturbation.

SMEAR SLIDE SUMMARY (%):

	1, 87 D
COMPOSITION:	
Clay	10
Calcite/dolomite	40
Foraminifers	1
Nannofossils	49

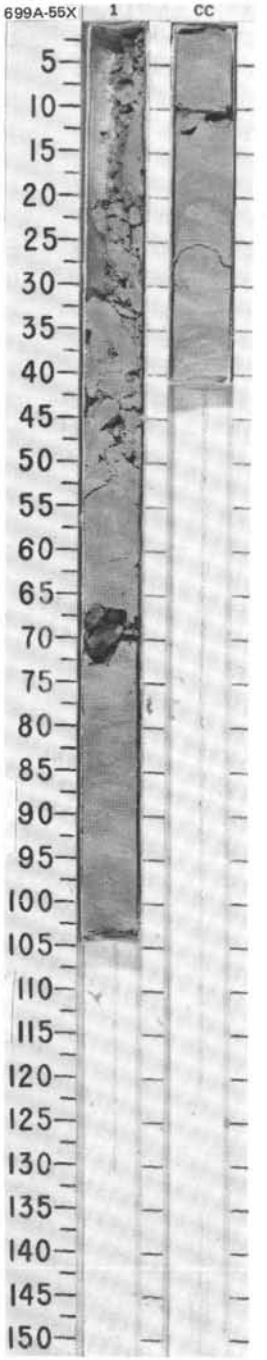

SITE 699 HOLE A CORE 56X CORED INTERVAL 4214.1-4223.6 mbsl; 508.6-518.1 mbsf

TIME-ROCK UNIT	BIOSTRAT. ZONE/ FOSSIL CHARACTER: FORAMINIFERS	NANNOFOSSILS	RADIOLARIANS	DIATOMS	SILICO-FLAGELLATES	PALEOMAGNETICS	PHYS. PROPERTIES	CHEMISTRY	SECTION	METERS	GRAPHIC LITHOLOGY	DRILLING DISTURB.	SED. STRUCTURES	SAMPLES
UPPER PALEOCENE	UPPER PALEOCENE P4	NP 8?	No CC sample	Barren	No CC sample				1, 2, 3, 4, 5, 6	0.5, 1.0	VOID			*

LITHOLOGIC DESCRIPTION

CLAY-BEARING NANNOFOSSIL MICRITIC CHALK

Drilling disturbance: Extensive brecciation and limited sediment recovery.

Major lithology: Clay-bearing nannofossil (coccoliths) micritic chalk, light gray (10YR 7/1), showing almost no structures because of drilling deformation. Faint remains of *Planolites* burrows at the top of Section 2.

Minor lithology: Clayey nannofossil micritic chalk, light brownish gray (5Y 6/2). Coccoliths only slightly outnumber discoasters. Volcanic sand in Section 6, 0-20 cm. Well-rounded grains of volcanic glass, very fine-grained basalt, fine-grained green grains of uncertain affinity, and hematite-rich particles. Sand is well sorted.

SMEAR SLIDE SUMMARY (%):
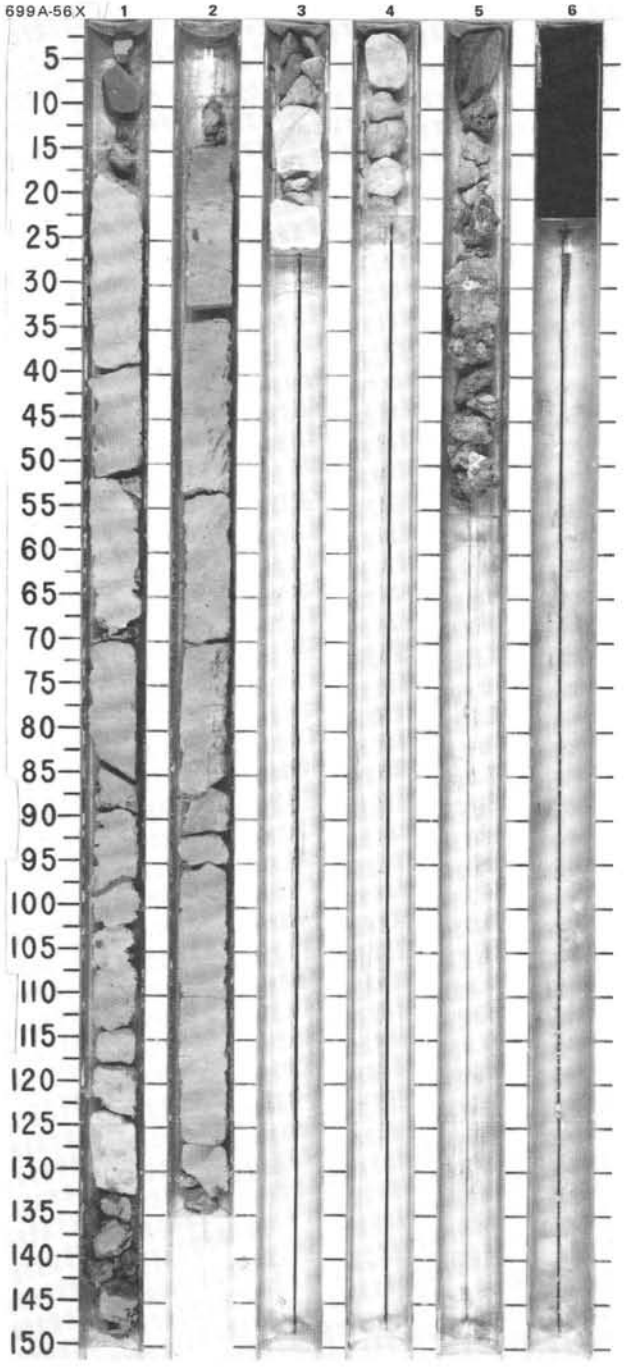
	1, 57 D	1, 144 M	3, 21 D	6, 10 D
COMPOSITION:				
Mica	Tr	5	—	—
Clay	20	5	30	—
Volcanic glass	—	—	—	100
Calcite/dolomite	39	54	40	—
Accessory minerals	Tr	—	—	—
Foraminifers	2	1	—	—
Nannofossils	39	40	30	—